APPLICATION OF MODAL TECHNIQUES TO MULTIPLY CONFIGURED GRATINGS

by

J. L. Adams, B.Sc. (Hons.), University of Tasmania

A thesis submitted in fulfilment of the requirements

for the degree of

Doctor of Philosophy

UNIVERSITY OF TASMANIA

HOBART

January, 1981.

Except as stated herein, this thesis contains no material which has been accepted for the award of any other degree or diploma in any university. To the best of my knowledge and belief, this thesis contains no copy or paraphrase of material published by another person, except when due reference is made in the text of the thesis.

J.L.Adams

Jennifer L. Adams,

January, 1981.

Any part of this thesis may be photocopied.

CONTENTS

SUMMARY

The main theme of this thesis is the development of new rigorous formalisms to describe the diffraction properties of multiply configured, perfectly conducting, gratings with simple groove geometries. This class of gratings is composed of singly or doubly periodic elements. The formalisms are derived using modal techniques which are particularly suited to solving the diffraction properties of these gratings. Considerable attention is paid to the far infrared properties of the gratings with the aim of describing their performance as interference filters used in this wavelength range.

The thesis contains a general review of the previous contributions to the theoretical study of diffraction gratings, including a review of investigations which have been undertaken into the properties of far infrared interferometers. This is followed by a discussion of a formalism describing the diffraction properties of lossless dielectric and finitely conducting gratings. This study represents one of the first generalisations of a modal formalism to structures which are other than perfectly conducting, and is a step towards the solution of the diffraction properties of capacitive or finitely conducting inductive grids.

The remainder of the thesis is concerned with perfectly conducting gratings having basically rectangular geometries. The structures considered are either singly periodic or doubly periodic. The double periodicity results either directly from the geometry of the element (as for example in the case of inductive grids) or is contrived by suitable arrangement of singly periodic elements.

The performance of singly periodic interference filters, composed

of two or more lamellar gratings, is then described. The first such structure to be considered is the double grating and the diffraction properties of this arrangement are described in detail. The associated analysis is performed by explicitly specifying the fields in each groove region by a modal expansion. The geometry of the double grating is then generalised to consider a grating composed of a stack of an arbitrary number of singly periodic elements, and the properties of this structure are analysed using a new rigorous multiple scattering technique.

These singly periodic gratings have application as Fabry-Perot interferometers only for radiation having a particular linear polarization. If the incident radiation is unpolarized it is necessary to use doubly periodic devices such as inductive grids. For this reason the performance of the double grid interferometer is considered, and a rigorous formalism for it is derived using an approach similar to that used for the double grating. The properties of multi-element grids are then analysed using a multiple scattering approach.

Interesting conservation properties for lossless singly and doubly periodic structures are presented and are related to the geometrical symmetry of the structure. These relations provide constraints on the scattering matrices of the diffraction system.

Finally, two formalisms are presented describing the diffraction properties of a structure which is doubly periodic by virtue of the positioning of its two singly periodic elements. This arrangement is termed the crossed lamellar transmission grating. The first formalism uses a modal expansion to describe the field within the grooves of each element, while the second employs a rigorous multiple scattering approach. In particular, it is demonstrated that this structure has application as a solar heat mirror.

ACKNOWLEDGEMENTS

I take this opportunity to express my gratitude to all the people who have given me support and friendship, while the investigations described in this thesis were being undertaken.

Firstly, I wish to thank my supervisor, Dr. M. D. Waterworth, University of Tasmania, for his ready support during my four years as a postgraduate student. His encouragement, willingness to discuss my progress and problems and his advice on the preparation of this thesis are very much appreciated.

I am fortunate to have had the opportunity to work in close association with both Dr. Ross McPhedran, University of Sydney, and Dr. Lindsay Botten, New South Wales Institute of Technology, throughout the duration of the study. Their great interest and enthusiasm have made it a stimulating experience working with them. Both Ross and Lindsay have shown unfailing readiness to discuss all aspects of these investigations and to suggest profitable avenues of study. Their suggestions on the preparation of this thesis are also very much appreciated. Finally, it has been their friendship that I will always remember with great pleasure.

The comradeship of Miss B. J. Brown, Mr. J. R. Andrewartha and Dr. I. J. Wilson, who were involved in diffraction grating research at the University of Tasmania, together with that of my other friends in the Physics Department, made my years at University very enjoyable.

During the last two years, I have worked for several months in the Department of Theoretical Physics, School of Physics, University of Sydney, and the School of Mathematical Sciences, the New South Wales Institute of Technology. The kindness and friendliness of all the people

I met at these institutions is greatly valued. In particular, the contributions to my investigations made by Dr. G. H. Derrick, University of Sydney, and Dr. M. S. Craig, the New South Wales Institute of Technology, are very much appreciated.

I also thank the University of Sydney and the New South Wales Institute of Technology for the provision of computing facilities, which permitted me, while in Sydney, to run my large computer programs.

Finally, I wish to thank my family for their continuing support and encouragement and in particular to thank my mother for typing this thesis.

I gratefully acknowledge the support of a Commonwealth Postgraduate Research Award throughout the duration of the studies.

CHAPTER 1

INTRODUCTION

1.1 PRELIMINARY COMMENTS

This thesis is chiefly concerned with the solution of the diffraction properties of multiply-configured gratings using modal techniques. These gratings are composed of one or more singly periodic or doubly periodic elements. Emphasis is placed on their application as far infrared interferometers and interference filters. Previous contributions in these two areas are reviewed in this chapter, together with an outline of the studies reported in this thesis.

It is only after the many years of research into singly periodic (classical) gratings and the development of successful theories describing the properties of these gratings that it is now possible to model doubly periodic structures. Thus it is appropriate to review firstly the earlier investigations into singly periodic gratings and this is performed in sections 1.2 and 1.3. Also it is important to discuss the advantages of using modal techniques in solving the problem of diffraction by multiply configured gratings in preference to using the other methods well-known to grating theorists (in particular, integral and differential methods). Only a brief precis of these latter techniques is given because a number of thorough review articles [1.1 - 1.4] and in particular an excellent and comprehensive text [1.5] on the electromagnetic theory of gratings have been published. For this reason, this chapter contains at most brief mention of many interesting associated studies of and controversies regarding the properties of diffraction gratings.

Section 1.4 is specifically devoted to the description of previous studies of the properties of far infrared interference filters. The use of the terms "grating" and "grid" concerning interference filters appears very confused in the literature. Thus, in order to make the classification used in this thesis perfectly clear, the following notation is specified: Gratings are singly periodic structures having arbitrary profiles, while grids are doubly periodic structures which may be of two types. Structures of the first type are called inductive grids and consist of apertures perforated periodically in a thin metal sheet, while those of the second type are called capacitive grids and are composed of a periodic array of isolated metallic shapes deposited in or on a supporting medium. More recently, the term "bi-grating" has been introduced (section 1.3) to describe generalised grids. These are doubly periodic structures whose profiles are specified by arbitrary functions.

1.2 A BRIEF HISTORICAL SURVEY AND DISCUSSION OF THEORETICAL APPROACHES APPLIED TO CLASSICAL GRATINGS

The evolution of grating theories from the ability to predict the dispersion properties of the instrument to the ability to solve the more difficult problem of determining the distribution of energy among the orders diffracted by a grating, has occurred over the last 160 years.

Fraunhofer, in 1821, first derived the constraint which determined the manner in which a grating disperses the incident radiation. This constraint, now called "the grating equation", is given by

$$\sin \phi_n = \sin \phi_0 + \frac{n\lambda}{d} .$$

Here ϕ_0 is the angle of incidence (measured from the grating normal), ϕ_n is the angle of diffraction (associated with the integer n), λ is

the wavelength of the incident radiation and d is the grating period.

However, it was many years after the discovery of the grating equation before any realistic attempts at determining the energy properties of gratings could be made. This only became possible with the advent of digital computers. Several major methods of determining these energy properties were developed and these are discussed in the following sections.

1.2.1 Scalar Theories

The many investigations undertaken into the properties of diffraction gratings using this technique have been reviewed [1.1, 1.2] and will not be discussed in detail here. In this method, the vectorial nature of light is neglected and consequently the differences in efficiency for a grating operated in different polarizations is not taken into account. Naturally, unless the wavelength to period ratio is very small ($\lambda/d \lesssim .1$), the diffraction efficiencies of a grating are greatly dependent on the polarization of the incident beam. The one useful feature of this method is that the diffraction efficiencies can be derived in a closed form and hence predictions, however unreliable, of the performance of gratings could be made before computers were available.

The necessity for an electromagnetic theory of gratings is obvious. Indeed, since the time of Fraunhofer it has been known that the energy properties of gratings are polarization dependent. Two fundamental polarizations of the incident field, namely P and S polarization, are defined for singly periodic diffraction gratings operated in classical mounts (that is, such that the wave vector lies in a plane perpendicular to that of the grating grooves). P polarization implies that the electric field vector of the incident wave is aligned with the grooves of

the grating, while S polarization designates the situation where the magnetic field vector is aligned with the grooves.

There are three basic criteria that the solution of the diffraction problem must satisfy. These are the outgoing wave conditions, the boundary conditions applying on the grating surface and the wave equation. Given that these conditions are satisfied, then the solution is unique. The outgoing wave (radiation) condition stipulates that at infinity the diffracted fields must consist purely of outgoing waves. In other words, it specifies a unique incident field.

The following sections consider the electromagnetic diffraction (or vector diffraction) theories which have been proposed.

1.2.2 Methods Based on the Rayleigh Expansion

In 1907, Lord Rayleigh [1.6] suggested that a single plane wave expansion (satisfying the Helmholtz equation and the radiation condition) could be used to describe the fields diffracted by a grating everywhere above the grating surface. This conjecture is now called the Rayleigh hypothesis and the plane wave expansion is termed the Rayleigh expansion.

Rayleigh's "dynamical theory of gratings" [1.6] was initially successful, in that it was able to predict some of the properties of the recently discovered S polarization Wood anomalies [1.7]. These Wood anomalies appear as rapid variations in the amplitudes of the diffracted propagating orders and were shown by Rayleigh to correspond to the passing on or off of a spectral order. (An order is said to pass on or off when its angle of diffraction reaches $\pm 90^{o}$). A second type of anomaly was later recognised by Hessel and Oliner [1.8] and was termed a "resonance anomaly". These anomalies appear as a resonant type of behaviour in the spectral amplitudes and are related to the complex

guided waves that the grating may support.

Again the review articles [1.2, 1.3] provide comprehensive discussions of the many theories, based on refinements of Rayleigh's method, which were proposed. Once digital computers became readily available and the Rayleigh expansion method could be adequately tested, it was found to be unsatisfactory with respect to the energy conservation criterion [1.9] as the groove depth increased and considerable controversy was generated over the validity of the method. Petit and Cadhilac [1.10], Nevière and Cadhilac [1.11], Nevière [1.12] and Millar [1.13] undertook theoretical studies of the region of validity of the Rayleigh hypothesis and it was concluded in general that the Rayleigh expansion is not a valid point-wise representation of the field everywhere, although it may give valid field representations if used in the least-squares sense.

Thus the method, although mathematically simple, is not reliable and the following physically and analytically sound techniques were subsequently developed.

1.2.3 Integral Formalisms

These rigorous theories express the diffraction problem for a grating in terms of an integral equation (or a system of coupled integral equations). In these formalisms, the fields above the grating surface are expressed in terms of integrals containing unknown functions which are characterised by their values at a finite number of points on the grating surface. The linear integral equation (or system of integral equations) is derived by applying the boundary conditions at the grating surface and is then solved numerically using either a Fourier series, iterative or more frequently a points-matching method. This latter method, which is the most reliable for the solution of diffraction grating problems,

replaces the linear integral equation by an infinite system of simultaneous linear equations (the Fredholm Alternative) which is truncated to enable a numerical solution to be obtained.

In the case of perfectly conducting gratings one unknown function, commonly related to the surface current density, is required and this results in a single integral equation. In early integral theories for finitely conducting gratings, two unknown functions, characterising both the field and its normal derivative at the grating surface, were chosen and a coupled system of linear integral equations were derived. However, as discussed later in this section a technique has been recently developed so that only one unknown function is required.

The first integral formalisms originated in the mid 1960's with the publication of papers by Petit and Cadhilac [1.14], Wirgin [1.15] and Uretsky [1.16] which described the diffraction of P polarized waves by perfectly conducting gratings. Subsequent papers by Petit [1.17 - 1.19] discussed the numerical treatment of the integral equation and presented the first numerical results using the formalism for P polarized radiation. Petit also presented an integral formalism for S polarized radiation.

Pavageau et al [1.20] reported the first successful integral solution to the diffraction of S polarized radiation by perfectly conducting gratings and the first numerical results obtained for this problem were later given in a paper published by Pavageau and Bousquet [1.21]. In 1971, Maystre and Petit [1.22] proposed an integral formalism for a perfectly conducting grating operated in a conical diffraction mount (that is, where the wave vector of the incident wave no longer lies in a plane perpendicular to the grooves).

One of the earliest integral formalisms for finitely conducting

gratings was described by Van den Berg [1.23] in 1971. This study resulted in a pair of coupled integral equations and consequently the method encountered numerical difficulties associated with the determination of the two unknown functions.

In 1972, Maystre [1.24] developed a fundamentally different integral formalism for describing the diffraction properties of finitely conducting gratings. This formalism, unlike earlier formalisms for finitely conducting gratings, involves only one equation in terms of one unknown, a fictitious surface current. The linking together of the field and its normal derivative in terms of one unknown function is a feature which all subsequent integral formalisms have utilized.

Following this, Maystre [1.25, 1.26] and Botten [1.27] have published integral formalisms for dielectric coated and multiprofile gratings. Botten [1.28] has also applied an integral treatment to the bi-metallic grating.

The integral theories have a wide range of application and can treat both finitely and perfectly conducting gratings having arbitrary profiles. Most importantly, these theories are rigorous and very general but are mathematically and numerically complex and so require the use of large digital computers.

1.2.4 Differential Formalisms

The differential method is based on the direct solution of the wave equation, with the diffraction properties of the grating being determined by the solution of a system of ordinary coupled differential equations. This system of second order differential equations is numerically integrated, often using Numerov's method. The technique was originally proposed by Petit [1.29] and subsequently the method has been developed so

that it is competative with (and complimentary to) the integral formalisms.

There are two main classes of differential formalisms in use. The first method applies to finitely conducting gratings and derives a set of ordinary differential equations by projecting the wave equation onto an orthogonal plane wave basis. This technique was developed by Cerutti-Maori et al [1.30] and Nevière et al [1.31] for finitely conducting gratings. Hutley et al [1.32] and Nevière et al [1.33] then applied this method to consider gratings conformally coated with dielectrics.

The second class of differential formalisms applies to perfectly conducting gratings. This method involves a conformal mapping of the grating profile onto a plane. The mapping preserves the outgoing wave condition and simplifies the boundary conditions, but at the expense of complicating the wave equation. The diffraction problem is solved by numerical integration of the modified wave equation. After the conformal mapping, the problem is equivalent to that of a perfectly conducting plane coated with a graded dielectric layer whose refractive index is periodic along the plane. This method was developed by Nevière and Cadilhac [1.34] and Nevière et al [1.35] to consider perfectly conducting gratings of arbitrary profile. Nevière et al [1.36] then applied the technique to dielectric coated perfectly conducting gratings.

The former, most general differential formalism can be applied to most grating problems [1.5]. However, numerical difficulties occur for highly reflecting gratings used in S polarized radiation. These difficulties are mainly due to the slow convergence of the Fourier series used to model the refractive index profiles of the gratings.

1.2.5 Modal Formalisms

Modal formalisms are intimately linked with waveguide theory since the technique involves the determination of waveguide modes to describe the fields within the grooves of the grating. These modes are eigenfunctions of a differential operator derived from the wave-equation (usually by separation of variables) and satisfy appropriate boundary conditions. The fields in the free-space regions exterior to the grating grooves are specified by Rayleigh (plane wave) expansions and the two series are matched at the grating-free space interfaces (that is, where the domains of convergence of the two expansions intersect) by utilizing the continuity conditions on the fields and applying the Method of Moments [1.37].

The earliest modal formalisms were derived for perfectly conducting, rectangular-profile gratings. Deriugin [1.38, 1.39] undertook one of the first investigations of the properties of these gratings using modal techniques and applied the approach to both polarization cases. Wirgin [1.40] in 1966, proposed a modal formalism for an irregular surface having rectangular grooves. This study was followed by the presentation by Wirgin and Deleuil [1.41] of a modal formalism for a perfectly conducting lamellar grating. In these investigations [1.40, 1.41], Green's theorem is applied to determine explicit expressions for the modes used in the description of the fields within the grating grooves. The latter authors commented upon the fact that the modal expansion for the groove region could not be expressed in the same form as the Rayleigh expansion, supporting Lippmann's proposition [1.42] of the non-rigorous nature of methods based on the Rayleigh hypothesis.

Subsequently, Maystre and Petit [1.43] detailed a modal formalism

describing the diffraction properties of a perfectly conducting lamellar grating. They derived a system of linear equations from the expression of the continuity conditions, after representing the lamellar profile by a Fourier series expansion. Roumiguieres et al [1.44] then generalised this study to take into account a lamellar grating surrounded by homogeneous dielectric layers.

Chen [1.45] in 1970 proposed a modal formalism for doubly periodic inductive grids (see section 1.3). By contrast with the approach of Maystre and Petit [1.43], the equations resulting from the application of the continuity conditions applying to the fields, are transformed into a system of linear equations by application of the Method of Moments [1.37]. To make this possible, the mode functions describing the fields within the grooves must form a complete orthogonal set over the groove region. This method is numerically preferable and is the type used in all modal formalisms presented in this thesis.

Jovićević and Sesnic [1.46] derived a modal formalism for a triangular profile grating where the modal fields are written as an expansion of Bessel functions of the first kind. The method, however, has been criticised [1.5] as not being rigorous in the case of asymmetrical profiles, but there is some debate as to whether the discrepancies observed in the tests of conservation of energy and reciprocity are due to programming errors or to a deficiency in the formalism.

More recently, Adams and Botten [1.47] have used the technique of Chen [1.45] to describe the diffraction properties of the double grating. Andrewartha et al [1.48] have developed a modal theory for perfectly conducting gratings having a semi-circular profile and have subsequently generalised the method to encompass perfectly conducting gratings of

arbitrary profiles [1.49]. Fox [1.50] has also considered the problem of diffraction by perfectly conducting gratings having arbitrary profiles and in particular discussed the unitary nature of the scattering matrix derived using this method.

Modal theories describing the diffraction properties of gratings which are other than perfectly conducting have only been proposed in recent years. In 1978, Knop [1.51] published a theory capable of describing the properties of lossless dielectric lamellar gratings. Botten et al [1.52, 1.53] then derived a modal formalism for both lossless dielectric and finitely conducting lamellar gratings using a substantially different approach to that of Knop (see section 2.2.2).

In summary, modal techniques are particularly suited to modelling the electromagnetic properties of diffraction gratings in that they provide a relatively easy means of solution compared with the integral and differential techniques and also give more physical insight into the relevant physical processes of the system. However, the advantages of the method are tempered by the difficulty of finding expressions for the modal fields in the groove regions. Consequently, this method has been until recently, restricted to relatively simple geometries. Nevertheless, it represents one of the few viable approaches for determining the diffraction of light by multiple gratings (and in particular, by doubly periodic diffracting structures). The numerical complexity of these diffraction problems is immense when solved using the other types of rigorous formalisms. A discussion of previous studies of doubly periodic structures is given in the following section.

1.3 RIGOROUS THEORETICAL STUDIES OF DOUBLY PERIODIC STRUCTURES

Theoretical interest in the rigorous diffraction properties of

doubly periodic structures has developed only over recent years following the mastering of the resolution of singly periodic diffraction problems. The interest in these structures gained impetus with the suggestion put forward by Horwitz [1.54] in 1974 that inductive grids have application as solar selective surfaces.

Chen [1.45, 1.55] proposed modal formalisms to describe the diffraction properties of perfectly conducting inductive grids having rectangular or circular apertures. The grids considered in these studies were assumed to be of infinitesimal thickness but Chen [1.56] later removed this restriction. The equations derived from applying the continuity conditions were reduced to a system of linear equations by application of the Method of Moments [1.37].

This theory was adapted in 1976 by McPhedran and Maystre [1.57] to study the diffraction properties of perfectly conducting rectangular-hole inductive grids of finite thickness. McPhedran and Botten [1.58] and Bliek et al [1.59] subsequently considered the diffraction of a plane wave by an inductive grid having circular apertures of finite depth, using a modal technique also based on the work of Chen [1.45]. These formalisms incorporated the possibility of the grid having dielectric plugs and sandwich films.

Adams et al [1.60] proposed a modal formalism to analyse a doubly periodic structure termed the crossed lamellar transmission grating. The author [1.61] also described the diffraction properties of a double grid composed of two rectangular-hole inductive grids using this technique.

More recently, interest has developed in the diffraction properties of doubly periodic reflection gratings. Maystre and Nevière [1.62] and Vincent [1.63] derived formalisms based on generalised differential

techniques to describe the properties of finitely conducting reflection bi-gratings of arbitrary profile. Derrick et al [1.64], however, proposed the most general formalism for this diffraction arrangement. This study uses a coordinate transformation to map the bi-grating surface onto a plane and a system of coupled integral equations is derived.

Wirgin [1.65] proposed an integral formalism describing the diffraction properties of a perfectly conducting bi-grating. The grating profiles along the two axes of periodicity were allowed to be arbitrary periodic functions. However, the enormous and unexplored computational difficulties associated with this formalism have made the method unattractive.

1.4 SURVEY OF PREVIOUS STUDIES REGARDING INTERFERENCE FILTERS AND FABRY-PEROT INTERFEROMETERS FOR THE FAR INFRARED

This section reviews the use in the far infrared of gratings and grids as filters and more particularly, as the reflecting elements in Fabry-Perot interferometers.

Fabry-Perot interferometers make use of the multiple reflections between two or more parallel, highly reflecting yet weakly absorbing films or elements. In order to obtain a practical Fabry-Perot interferometer for the far infrared, suitable reflectors for this region of the spectrum must be found. The necessary requirements (low absorptivity and high reflectivity) cannot be fulfilled simultaneously in the far infrared by the thin, homogeneous, conducting films or the multiple dielectric layers which are traditionally used for reflectors in the visible and ultra-violet regions of the spectrum. Such filters were found to be impractical for the far infrared because the dielectric films became too thick and the thin metal films too lossy.

However, the use of grids (or gratings) as the reflecting elements has enabled Fabry-Perot interferometers to be successfully constructed for the far infrared and sub-millimeter regions of the spectrum. Inductive grids having square symmetry can be used for unpolarized, normally incident radiation since they are polarization insensitive under these conditions. Although singly periodic gratings show strong polarization effects, they provide suitable alternative reflecting elements when used in long wavelength, P polarized radiation.

Many investigations have been undertaken over the last thirty years into the theoretical and experimental properties of grid (and grating) filters and interferometers. Excellent review articles by Genzel and Sakai [1.66] and Kneubühl [1.67] on contributions to this area of research have been published but some of the more significant contributions will be mentioned here with emphasis placed on the theoretical studies. The papers described here will, for the most part, be given in chronological order and consequently grid and grating studies will be intermixed.

Casey and Lewis [1.68] were among the first to introduce gratings as the reflecting elements for Fabry-Perot interferometers. Their suggestion on the use of double inductive grids and double gratings as interference filters for the microwave region [1.69] was further pursued in 1952 when they discussed the advantages of using double gratings as the reflectors in Fabry-Perot interferometers operated in P polarized, far-infrared radiation. Their theoretical study of the transmission properties of a parallel pair of wire gratings was performed by determining the currents induced in the wires of the grating. However, it was restricted to situations in which the wavelength far exceeded both the grating period and the diameter of the wires. The further restriction of

zero displacement of the wires in the top grating relative to those in the bottom grating was imposed.

Renk and Genzel [1.70] provided the first investigations into the optical properties of inductive grids and introduced these structures as the reflecting elements in Fabry-Perot interferometers. Subsequently Ulrich et al [1.71] theoretically and experimentally studied the properties of Fabry-Perot interferometers constructed from gratings and inductive grids. They investigated the grating problem using an equivalent circuit representation and qualitatively derived the optical properties of the grids from their results.

Ulrich [1.72] in 1967 introduced the capacitive grid, which was a complementary structure to the inductive grid, and developed a theory to describe this structure using a transmission line analogue. This approach applies to thin grids and radiation of wavelength longer than the grid period. Ulrich [1.73] demonstrated the use of capacitive grids as low pass transmission filters for the far infrared and investigated the use of both types of grid for far infrared multi-layer interference filters [1.74]. Many papers [1.75 - 1.78], mainly of an experimental nature, were published at this time. Adonina et al [1.79] produced a theoretical study of the diffraction properties of a double grating (i.e. a double array of rectangular bars) operated in long wavelength, normally incident radiation, using an equivalent electrical circuit representation. Saskena et al [1.80] also used this approach to study wire gratings.

During the early 1970's interest [1.81, 1.82] grew rapidly in the application of multi-element grid (and grating) stacks as interference filters for the far infrared. Multi-element structures are important since given enough elements, it should be possible to construct filters having nearly any desired characteristics. Also it has been found that

many elements are needed to give the required sharpness of cut-off to filter characteristics.

At this time Pradhan [1.83, 1.84] and Pradhan et al [1.85 - 1.87] published a series of papers concerned with the filtering properties of single and multi-element grids and gratings. Their analysis was performed using a multiple scattering technique for the zeroth diffracted orders. The treatment utilized values of the diffracted field amplitudes of the single elements obtained using non-rigorous methods (for example, the values given by Saskena et al [1.80] for the grating element). However, in this series of papers, the expressions derived for the multi-element structures (having up to six elements) were far too cumbersome and had little hope of being generalised to account for the properties of multi-element stacks with an arbitrary number of elements. In 1979, Botten [1.88] published an article generalising the work of Pradhan and Garg. A multiple scattering approach was used for the single specularly reflected and transmitted orders of a multi-element filter having an arbitrary number of elements and a recurrence relation was derived for the diffracted complex amplitudes of the structure. The transmission characteristics of a filter with an arbitrary number of elements could thus be written in closed form.

In 1972, one of the first rigorous descriptions of the diffraction properties of the double grating was presented by Blok and Mur [1.89]. They considered a pair of gratings of identical period having infinitesimally-thin metal prisms and solved the diffraction problem for the two fundamental polarizations using an integral equation technique. However, their interest was not in the interferometric nature of this structure and no pertinent results were given. Many experimentally oriented papers, describing the properties of interference filters and

grating interferometers for the far infrared [1.90 - 1.99] were presented in the following years.

This was the stage of the research in this field when many of the investigations reported in this thesis were undertaken. Adams and Botten [1.47] rigorously described the properties of a double grating interferometer composed of two perfectly conducting lamellar gratings and investigated the far infrared filtering characteristics of this structure. Botten et al [1.100] subsequently applied a multiple scattering treatment to the multi-element grating stack, which incorporated the interaction of all orders, both propagating and evanescent, between the elements of the grating. Adams [1.61] also proposed a modal formalism for a double inductive grid and discussed the application of this structure as a Fabry-Perot interferometer. Adams and Botten [1.101] then extended the geometry to encompass a multi-element inductive grid and determined the diffraction properties of this structure by applying a multiple scattering approach.

Whilst not an exhaustive survey of the literature pertaining to far infrared interferometry and filter design, this section does include the major contributions relevant to the work undertaken and reported in this thesis.

1.5 CONTENTS OF THE THESIS

In this thesis the application of modal formalisms to various diffraction problems are described. As discussed in section 1.2.5, modal methods have been almost exclusively applied to perfectly conducting structures. Indeed, the range of grating geometries associated with this method is particularly restricted. This thesis does not have as a primary goal the extension of the range of singly periodic geometries encompassed

by modal techniques. Nevertheless, the formalism [1.52, 1.53] presented in chapter 2, which describes the diffraction properties of finitely conducting and lossless dielectric lamellar gratings, is one of the first modal theories to remove the constraint of perfect conductivity. The contribution made by the author and co-workers L. C. Botten, M. S. Craig, R. C. McPhedran and J. R. Andrewartha, is in the prescription of the fields within the groove region since once these are found the solution is performed according to the well known Method of Moments [1.37]. The modes are eigenfunctions of a differential operator derived from the wave equation in that region.

In the case of a lossless dielectric grating the operator is self-adjoint and as a consequence its eigenvalues are real. This leads to a relatively simple solution of the diffraction problem. However, in the case of the finitely conducting lamellar grating, the problem is no longer self-adjoint and the eigenvalues lie in the complex plane. This necessitates the solution of the adjoint problem to obtain a complete set of eigenfunctions orthogonal to those of the physical problem and thus allow the Method of Moments to be applied.

Chapters 3 to 8 are concerned with perfectly conducting, multiply-configured gratings having rectangular geometries. The gratings are either singly periodic or doubly periodic. Modal techniques are used in the derivation of the formalisms describing the diffraction properties of these gratings.

Chapters 3 to 5 describe the properties of singly periodic interference filters composed of two or more lamellar transmission gratings. The author was fortunate to have worked closely with L. C. Botten, R. C. McPhedran and G. H. Derrick on many aspects of these investigations.

Chapter 3 discusses at length the properties of the double grating [1.47], which is a simple two element interferometer. The diffraction problem is analysed by explicitly specifying the fields in both the upper and lower arrays in terms of modal expansions. Rayleigh field expansions are used to describe the free space fields (in particular in region between the gratings). The interferometric characteristics of this structure are discussed in terms of the geometric parameters and those of the incident radiation. These long wavelength characteristics are elucidated by a simple multiple scattering approach (assuming that only the zeroth diffracted orders couple together the grating elements) used in conjunction with a monomodal approximation.

In chapter 4, a series of interesting conservation relations are presented, which apply to lossless, singly periodic structures and which are the subject of a paper [1.102]. Two techniques, namely an integral approach and the more powerful concept of time reversal, are applied in their derivation. The most compact forms of the relations exist when certain symmetries (left-right and/or up-down) are present in the grating geometry. Naturally the double grating is an ideal choice for the demonstration of these relations and numerical examples confirming the symmetry properties for this structure are presented.

The material presented in chapter 5 extends the analysis of chapter 3 and considers a grating composed of a stack of an arbitrary number of identical, up-down symmetric, singly periodic elements [1.100]. The method used in chapter 3 is too cumbersome for this geometry, and thus a rigorous multiple scattering technique is adopted and the properties of the stack are deduced from those of a single element. In this analysis, the interaction of all propagating and evanescent orders between the grating elements is taken into account. Also in this chapter, further

development of the conservation relations is presented. In particular, it is demonstrated that within the formalism, the unitarity and symmetry of the scattering matrices of each up-down, left-right symmetric element of the stack is assured. Furthermore, these properties are shown to be analytically preserved for the entire stack.

The gratings considered in chapters 3 and 5 are polarization dependent and consequently have application as Fabry-Perot interferometers only when operated in P polarized radiation. For effective interference filters in unpolarized incident radiation it is necessary to use doubly periodic devices, such as the structures described in chapters 6 and 7.

In chapter 6, the author applies an approach similar to that employed in chapter 3, to determine the diffraction properties of the double grid [1.61]. The interferometric properties of this structure are considered in detail and are shown to be very similar in general to those obtained for the double grating interferometer discussed in chapter 3.

Chapter 7 continues the theme of the previous chapter to consider multiple element inductive grids [1.101]. This study, conducted jointly with L. C. Botten, applies a multiple scattering approach similar to that used in chapter 5 and the properties of the stack are obtained from the knowledge of the diffraction properties of the individual grid elements. Furthermore, conservation properties analogous to those given in chapter 5 are developed, analytically constraining both the scattering matrices of the individual elements and those of the entire grid stack.

In chapter 8, a doubly periodic structure termed the crossed lamellar transmission grating is considered. This structure is composed of two singly periodic elements arranged so that the two axes of periodicity are inclined at an arbitrary (non-zero) angle to each other. Two

formalisms are presented to describe the diffraction properties of this grating. The first formalism uses a modal expansion to describe the fields within the grooves of each element and matches these expansions to Rayleigh expansions which describe the fields above, between and beneath the individual gratings. This represents an extension by the author of a study originally undertaken in collaboration with R. C. McPhedran and L. C. Botten [1.60]. The second formalism employs a rigorous multiple scattering approach similar to that used in chapter 5. When the two axes of periodicity are orthogonal, the crossed lamellar transmission grating is shown to behave in a similar manner to a single rectangular-hole, inductive grid [1.57] and once again it has a potential application as a solar selective surface. The array separation parameter, which is not a feature of the single inductive grid, determines to some extent the interference action between the arrays and thus may be used in optimising the transmissivity of the structure for this solar energy application.

Finally, two general comments regarding this thesis should be made. Firstly, in formalisms for doubly periodic structures described hereafter, TE/TM orthogonal vector modes are predominantly used in the prescription of the free-space and modal fields. TE (transverse electric) implies no electric field component parallel to the grating normal, while TM (transverse magnetic) implies no magnetic field component along this axis. It is advantageous to use this representation of the fields since under certain conditions (see section 6.3) no coupling occurs between the TE and TM fields. That is, a TE polarized incident wave is diffracted as TE polarized waves. Again, because of the linear nature of the problems considered in this thesis, the amplitudes of waves diffracted by a system illuminated in light of arbitrary polarization may be written very simply as a linear combination of the amplitudes corresponding to TE and TM

polarized incident waves. In these formalisms, the transverse resolute of a field is the decomposition of the field into its components in the plane perpendicular to the grating normal.

Secondly, the symbols used in the formalisms, particularly those describing doubly periodic structures, are very often reminiscent of the nomenclature used in FORTRAN programs and in fact, the notation was designed specifically with ease of programming in mind.

1.6 CONCLUDING REMARKS

The unifying features of this thesis are the use of modal techniques to solve the various diffraction problems and the application of these techniques to investigate the far infrared interferometric properties of different diffraction arrangements. The investigations described in the thesis are developed and concluded chapter by chapter since this is the manner in which the research was conducted.

Many of the investigations reported evolved naturally from studies in earlier chapters. For example, the research on the double grating was initially undertaken and this led to the author's interest in both the multi-element grating as well as the double grid and multi-element grid problems. The investigations of the symmetry constraints of lossless structures developed from interesting properties observed in the numerical results obtained from the double grating formalism. This initiated the search for a comprehensive series of these constraints for both singly periodic and doubly periodic structures.

When the author commenced this study, theoretical investigations of doubly periodic structures were few in number. Since that time, this area of research has grown rapidly and should continue to expand now that most of the singly periodic diffraction problems have been so thoroughly investigated.

REFERENCES

[1.1] PETIT (R.), MAYSTRE (D.). - Rev. Phys. Appl., 1972, 7, 427.

[1.2] McPHEDRAN (R.C.). - Ph. D. Thesis, University of Tasmania, 1973.

[1.3] MAYSTRE (D.). - Thèse No. AO9545, L'Université d'Aix-Marseille III, France, 1974.

[1.4] PETIT (R.). - Nouv. Rev. Opt., 1975, 6, 129.

[1.5] Ed. PETIT (R.). - Topics in Current Physics, Vol. 22, "Electromagnetic Theory of Gratings", Springer Verlag, Heidelberg, 1980.

[1.6] Lord RAYLEIGH. - Proc. R. Soc. A, 1907, 79, 399.

[1.7] WOOD (R.W.). - Philos. Mag., 1902, 4, 396.

[1.8] HESSEL (A.), OLINER (A.A.). - Appl. Opt., 1965, 4, 1275.

[1.9] PETIT (R.). - Rev. Opt., 1963, 42, 263.

[1.10] PETIT (R.), CADILHAC (M.). - C. R. Acad. Sci. (Paris), 1966, 262, 468.

[1.11] NEVIÈRE (M.), CADILHAC (M.). - Opt. Commun., 1970, 2, 235.

[1.12] NEVIÈRE (M.). - Opt. Commun., 1970, 2, 51.

[1.13] MILLAR (R.F.). - Radio Science, 1973, 8, 785.

[1.14] PETIT (R.), CADILHAC (M.). - C. R. Acad. Sci. Paris, 1964, 259, 2077.

[1.15] WIRGIN (A.). - Rev. Opt., 1964, 43, 451.

[1.16] URETSKY (J.L.). - Ann. Phys., 1965, 33, 400.

[1.17] PETIT (R.). - C. R. Acad. Sci. Paris, 1965, 260, 4454.

[1.18] PETIT (R.). - Appl. Opt., 1965, 4, 1551.

[1.19] PETIT (R.). - Rev. Opt., 1966, 45, 249.

[1.20] PAVAGEAU (J.), EIDO (R.), KOBEISSÉ (H.). - C. R. Acad. Sci. Paris, 1967, 264, 424.

[1.21] PAVAGEAU (J.), BOUSQUET (J.). - Opt. Acta, 1970, 17, 469.

[1.22] MAYSTRE (D.), PETIT (R.). - Opt. Commun., 1971, 4, 97.

[1.23] VAN DEN BERG (P.M.). - Thesis, Delft, 1971.

[1.24] MAYSTRE (D.). - Opt. Commun., 1972, 6, 50.

[1.25] MAYSTRE (D.). - J. Opt. Soc. Am., 1978, 68, 490.

[1.26] MAYSTRE (D.). - Opt. Commun., 1978, 26, 127.

[1.27] BOTTEN (L.C.). - Opt. Acta, 1978, 25, 481.

[1.28] BOTTEN (L.C.). - J. Optics (Paris), 1980, 11, 161.

[1.29] PETIT (R.). - Rev. Opt., 1966, 8, 353.

[1.30] CERUTTI-MAORI (G.), PETIT (R.), CADILHAC (M.). - C. R. Acad. Sci. Paris, 1969, B8, 1060.

[1.31] NEVIÈRE (M.), VINCENT (P.), PETIT (R.). - Nouv. Rev. Opt., 1974, 5, 65.

[1.32] HUTLEY (M.C.), VERRILL (J.P.), McPHEDRAN (R.C.), NEVIÈRE (M.), VINCENT (P.). - Nouv. Rev. Opt., 1975, 6, 87.

[1.33] NEVIÈRE (M.), MAYSTRE (D.), VINCENT (P.). - J. Optics (Paris), 1977, 8, 231.

[1.34] NEVIÈRE (M.), CADILHAC (M.). - Opt. Commun., 1971, 3, 379.

[1.35] NEVIÈRE (M.), CADILHAC (M.), PETIT (R.). - I.E.E.E. Trans., 1973, AP - 21, 37.

[1.36] NEVIÈRE (M.), CADILHAC (M.), PETIT (R.). - Opt. Commun., 1972, 6, 34.

[1.37] HARRINGTON (R.F.). - "Field Computation by Moment Methods", (London: Collier-Macmillan), 1968.

[1.38] DERIUGIN (L.N.). - Radiotekhnika, 1960, 15, 15.

[1.39] DERIUGIN (L.N.). - Radiotekhnika, 1960, 15, 9.

[1.40] WIRGIN (A.). - C. R. Acad. Sci. Paris, 1966, 262B, 870.

[1.41] WIRGIN (A.), DELEUIL (R.). - J. Opt. Soc. Am., 1969, 59, 1348.

[1.42] LIPPMANN (B.A.). - J. Opt. Soc. Am., 1953, 43, 408.

[1.43] MAYSTRE (D.), PETIT (R.), - Opt. Commun., 1972, 5, 90.

[1.44] ROUMIGUIERES (J.L.), MAYSTRE (D.), PETIT (R.), - Opt. Commun., 1973, 7, 402.

[1.45] CHEN (C.-C.). - I.E.E.E. Trans., 1970, MTT-18, 627.

[1.46] JOVICEVIC (S.), SESNIC (S.), - J. Opt. Soc. Am., 1972, 62, 865.

[1.47] ADAMS (J.L.), BOTTEN (L.C.), - J. Optics (Paris), 1979, 10, 109.

[1.48] ANDREWARTHA (J.R.), DERRICK (G.H.), McPHEDRAN (R.C.). - Opt. Acta, submitted.

[1.49] ANDREWARTHA (J.R.), DERRICK (G.H.), McPHEDRAN (R.C.). - Opt. Acta, submitted.

[1.50] FOX (J.R.). - Opt. Acta, 1980, 27, 289.

[1.51] KNOP (K.). - J. Opt. Soc. Am., 1978, 68, 1206.

[1.52] BOTTEN (L.C.), CRAIG (M.S.), McPHEDRAN (R.C.), ADAMS (J.L.), ANDREWARTHA (J.R.). - Opt. Acta, accepted.

[1.53] BOTTEN (L.C.), CRAIG (M.S.), McPHEDRAN (R.C.), ADAMS (J.L.), ANDREWARTHA (J.R.). - Opt. Acta, accepted.

[1.54] HORWITZ (C.M.). - Opt. Commun., 1974, 11, 210.

[1.55] CHEN (C.-C.), - I.E.E.E. Trans., 1971, MTT-19, 475.

[1.56] CHEN (C.-C.). - I.E.E.E. Trans., 1973, MTT-21, 1.

[1.57] McPHEDRAN (R.C.), MAYSTRE (D.). - Appl. Phys., 1977, 14, 1.

[1.58] McPHEDRAN (R.C.), BOTTEN (L.C.). - 1977, University of Sydney, Report SP77/5.

[1.59] BLIEK (P.), BOTTEN (L.C.), DELEUIL (R.), McPHEDRAN (R.C.), MAYSTRE (D.). - I.E.E.E., Trans. MTT, 1980, 28, 1119.

[1.60] ADAMS (J.L.), BOTTEN (L.C.), McPHEDRAN (R.C.), - J. Optics (Paris), 1978, 9, 91.

[1,61] ADAMS (J.L.). - J. Optics (Paris), accepted.

[1.62] MAYSTRE (D.), NEVIÈRE (M.). - J. Optics (Paris), 1978, 9, 301.

[1.63] VINCENT (P.). - Opt. Commun., 1978, 26, 293.

[1.64] DERRICK (G.H.), McPHEDRAN (R.C.), MAYSTRE (D.), NEVIÈRE (M.). - Appl. Phys., 1979, 18, 39.

[1.65] WIRGIN (A.). - Opt. Acta, 1979, 26, 801.

[1.66] GENZEL (L.), SAKAI (K.). - J. Opt. Soc. Am., 1977, 67, 871.

[1.67] KNEUBÜHL (F.). - Appl. Opt., 1969, 8, 505.

[1.68] CASEY (J.P.), LEWIS (E.A.). - J. Opt. Soc. Am., 1952, 42, 971.

[1.69] LEWIS (E.A.), CASEY (J.P.). - J. Opt. Soc. Am., 1951, 41, 360.

[1.70] RENK (K.F.), GENZEL (L.). - Appl. Opt., 1962, 1, 643.

[1.71] ULRICH (R.), RENK (K.F.), GENZEL (L.). - I.E.E.E., 1963, MTT-11, 363.

[1,72] ULRICH (R.). - Infrared Phys., 1967, 7, 65.

[1.73] ULRICH (R.). - Infrared Phys., 1967, 4, 37.

[1,74] ULRICH (R.). - Appl. Opt., 1968, 7, 1987.

[1.75] RAWCLIFFE (R.D.), RANDALL (C.M.). - Appl. Opt., 1967, 6, 1353.

[1.76] RESSLER (G.M.), MÖLLER (K.D.). - Appl. Opt., 1967, 6, 893.

[1.77] VARMA (S.P.), MÖLLER (K.D.). - Appl. Opt., 1969, 8, 1663.

[1.78] VARMA (S.P.), MÖLLER (K.D.). - Appl. Opt., 1969, 8, 2151.

[1.79] ADONINA (A.I.), KOMISSAROV (Y.S.), PAVLYUK (V.A.). - Radio Engineering and Electronic Physics, 1969, 14, 946.

[1.80] SASKENA (B.D.), PAWHA (D.R.), PRADHAN (M.M.), LAL (K.). - Infrared Phys., 1969, 9, 43.

[1.81] BELL (R.J.), ROMERO (H.V.). - Appl. Opt., 1970, 9, 2341.

[1.82] BELL (R.J.), ROMERO (H.V.), BLEA (J.M.). - Appl. Opt., 1970, 9, 2350.

[1.83] PRADHAN (M.M.). - Infrared Phys., 1970, 10, 199.

[1.84] PRADHAN (M.M.). - Infrared Phys., 1971, 11, 241.

[1.85] PRADHAN (M.M.), GERBAUX (X.), HADNI (A.). - Infrared Phys., 1972, 12, 263.

[1.86] PRADHAN (M.M.), GARG (R.K.). - Infrared Phys., 1976, 16, 449.

[1.87] PRADHAN (M.M.), GARG (R.K.). - Infrared Phys., 1977, 17, 253.

[1.88] BOTTEN (L.C.). - Infrared Phys., 1979, 19, 659.

[1.89] BLOK (H.), MUR (G.). - Appl. Sci. Res., 1972, 26, 389.

[1.90] ROMERO (H.V.), BLAIR (A.G.). - Appl. Opt., 1973, 12, 84.

[1.91] LECULLIER (J.-C.). - Nouv. Rev. Opt., 1974, 5, 313.

[1.92] HOLAH (G.D.), AUTON (J.P.). - Infrared Phys., 1974, 14, 217.

[1.93] KOMM (D.S.), BLANKEN (R.A.), BROSSIER (P.). - Appl. Opt., 1975, 14, 460.

[1.94] HOLAH (G.D.), MORRISON (N.). - J. Opt. Soc. Am., 1977, 67, 971.

[1.95] HENRY (R.L., TANNER (D.B.). - Infrared Phys., 1979, 19, 163.

[1.96] ARNAUD (J.A.), PELOW (F.A.). - Bell Syst. Tech. J., 1975, 54, 263.

[1.97] HOLAH (G.D.), DAVIS (B.), MORRISON (N.D.). - Infrared Phys., 1979, 19, 639.

[1.98] HOLAH (G.D.). - International Journal of Infrared and Millimeter Waves, 1980, 1, 225.

[1.99] HOLAH (G.D.). - International Journal of Infrared and Millimeter Waves, 1980, 1, 235.

[1.100] BOTTEN (L.C.), ADAMS (J.L.), DERRICK (G.H.). - J. Optics (Paris), submitted.

[1.101] ADAMS (J.L.), BOTTEN (L.C.), - J. Optics (Paris), to be submitted.

[1.102] BOTTEN (L.C.), ADAMS (J.L.), McPHEDRAN (R.C.), DERRICK (G.H.). - J. Optics (Paris), 1980, 11, 43.

CHAPTER 2

FINITELY CONDUCTING AND LOSSLESS DIELECTRIC LAMELLAR DIFFRACTION GRATINGS

2.1 INTRODUCTION

The investigations, to be discussed in this chapter, are the subject of papers submitted to Optica Acta [2.1, 2.2], and are concerned with the diffraction properties of both finitely conducting and lossless dielectric lamellar diffraction gratings. The theory is developed using a modal treatment similar to that employed in the solution of scattering problems associated with perfectly conducting lamellar gratings. The formalism is presented for the finitely conducting lamellar grating and the simplifications which arise when considering the lossless dielectric grating are clearly indicated. The lossless nature of the dielectric lamellar diffraction grating leads to an expression of the diffraction problem in a self-adjoint form. In contrast, the introduction of loss (or energy dissipation) in the grating material renders the finitely conducting lamellar diffraction problem non self-adjoint.

The areas of application of the two different types of gratings are extremely diverse and for this reason a review of previous investigations of these structures is given separately below. The studies of the properties of lossless dielectric diffraction gratings are covered first.

Recently, proposals [2.3, 2.4] have been made for the recording of colour images as surface relief structures, which are subsequently replicated by embossing in transparent plastic sheet. The recordings can then be read-out in conventional projection systems which transmit only the zeroth order diffracted beam. Knop [2.5] has suggested the use of square wave profile lossless dielectric (glass) gratings for providing

colour selectivity. Such structures can be produced having the required wavelength dependence in the zeroth order diffracted efficiency i.e. with transmission characteristics in the visible comparable with those of conventional colour filters.

Gratings used for such applications require small periods (wavelength to period ratios approximately unity) and under these conditions the scalar diffraction theories can no longer be rigorously applied. Knop [2.6] published a rigorous electromagnetic theory describing the diffraction properties of dielectric lamellar gratings. This analysis was based upon a technique previously applied by Burckhardt [2.7] who investigated the diffraction properties of a dielectric grating with sinusoidally-varying dielectric constant.

Knop's method involves the derivation of an eigenvalue equation constraining the eigenmodes describing the field in the groove region. The discontinuous function representing the square of the refractive index is specified in terms of a slowly convergent Fourier series. This, however, poses numerical difficulties as the refractive index transition becomes large, as can be seen from the experience of Nevière et al [2.8] when they applied their differential technique to similar situations. This differential method has been recently used [2.9] to verify the results given by Knop [2.6] and excellent agreement was found.

The motivations for studying the diffraction properties of finitely conducting lamellar gratings were entirely different. Firstly, the generalisation of existing modal methods to encompass finitely conducting structures may form the basis of a modal formalism for lossy inductive grids. Interest has developed in the problem of determining the diffraction properties of finitely conducting grids since the suggestion of Horwitz [2.10] that such structures could provide effective solar

selective surfaces.

Lamellar diffraction gratings also have application as masks in the fabrication of integrated circuits. With this in mind, Roumiguieres et al [2.11] conducted a study of the diffraction properties of perfectly conducting gratings encased in parallel dielectric layers. However, the masks used in photolithography are not well approximated by the assumption of infinite conductivity and it is thus important to derive a formalism which takes into account the lossy nature of the grating.

Finally, lamellar gratings are finding increasing application in the X ray region of the spectrum [2.12]. At these wavelengths the finite conductivity of the grating is very significant.

The method adopted in this chapter is a generalisation of the modal approach familiar in describing the diffraction properties of perfectly conducting lamellar gratings and thus retains the elegance of the classical treatments. The perfectly conducting lamellar grating has long attracted interest [2.13 - 2.16] since the surface profile of this structure is inherently simple and is well suited to a solution of the diffraction problem using a modal technique because the boundary conditions applying to the fields may be explicitly incorporated in the field expansions. The choice of the form of modes used in the description of the waveguide fields for the dielectric lamellar grating given in this chapter, was to some extent guided by the work of Marcuse [2.17]. A more detailed comparison of this method of solution and that of Knop's is included in section 2.2.2.1.

The diffraction problems were solved for the two fundamental polarizations P and S. Although a detailed description of the analysis for the former polarization is given in sections 2.2.1 - 2.2.3, only a review of the salient differences between the approaches for S and P

polarizations is provided in section 2.2.4.

Results of the numerical investigations undertaken for the lossless dielectric diffraction grating are presented in section 2.3.1. Included in this section are a curve for comparison with the results of Knop [2.6] and spectra obtained for gratings constructed from both weakly and strongly reflecting materials.

At the time of writing this thesis, the numerical algorithm for determining the complex roots of the eigenvalue equation associated with the finitely conducting lamellar grating was not sufficiently refined to make extensive calculations possible, and so only a limited number of results are presented for this structure (section 2.3.2). However, recently a more computationally reliable algorithm has been developed by Botten et al [2.29] so that the complex roots may now be determined for gratings constructed from highly conducting metals. The validity of the theory is confirmed using numerical results satisfying physical criteria such as reciprocity and conservation of energy. Results are presented indicating the adequacy of the formalism for dealing with extreme grating profiles, namely those having depths as large as several hundred times their period. Such problems are intractable by the widely used integral-formalisms of diffraction grating theory.

2.2 SOLUTION OF THE DIFFRACTION PROBLEM

2.2.1 Notation and Description of the Diffraction Arrangement

The grating configuration is illustrated in figure 2.1. A rectangular Cartesian coordinate system, with unit vectors $\hat{\underline{x}}$, $\hat{\underline{y}}$, $\hat{\underline{z}}$ along the OX, OY, OZ axes respectively, is introduced with the OZ axis aligned with the rectangular grooves of the grating. The origin of the coordinate system is taken to coincide with one vertical wall of the grating structure. The grating, of period d, groove width c and

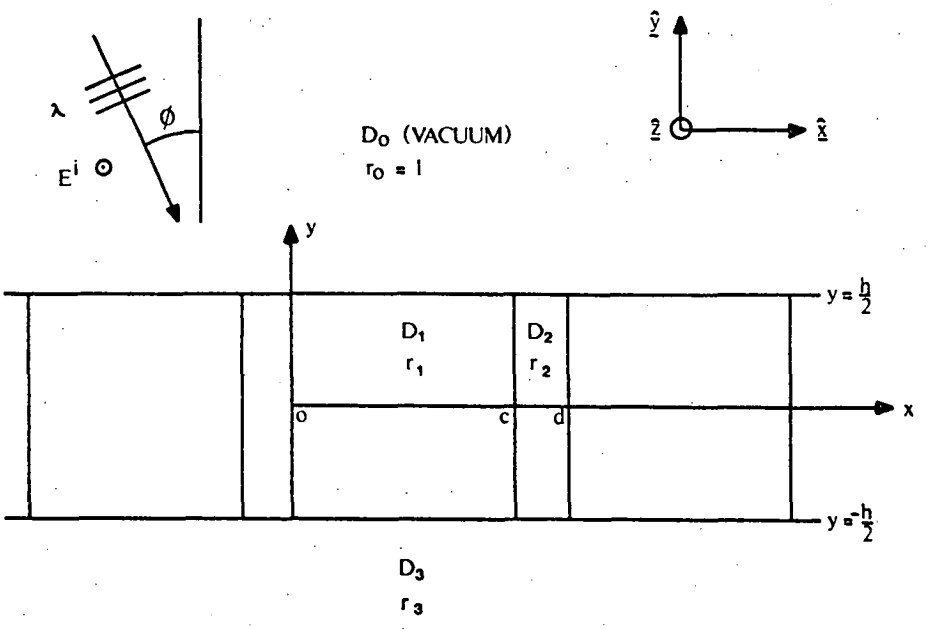

Figure 2.1 The geometry of the diffraction problem.

groove depth h, is assumed infinite in extent. The refractive indices r_i of the regions D_i $(i = 1,2,3)$ are assumed real for the lossless dielectric lamellar grating but may be complex for the lossy structure. The lower dielectric region D_3 is unbounded below and the region D_0 above the grating surface is taken (without loss of generality) to be free space $(r_0 = 1)$.

Consider a P polarized plane wave of free space wavelength λ, incident upon the grating at some angle ϕ. Then the incident electric field may be written

$$\underline{E}^i(x,y) = \exp[i(\alpha_0 x - \chi_0(y - h/2))]\hat{\underline{z}} \qquad (2.1)$$

where $\alpha_0 = k_0 \sin\phi$

$\chi_0 = k_0 \cos\phi$

$k_0 = 2\pi/\lambda$

and the time dependent term $\exp(-i\omega t)$ has been suppressed.

Now the incident field, upon interaction with the grating produces a diffracted field of the same polarization. The total field $\underline{E}$ is thus also of the same polarization and it must satisfy the Helmholtz equation in each region of space D_i, (see figure 2.1)

$$(\nabla^2 + k_i^2)\,\underline{E}(P_i) = 0 \qquad \text{for } P_i \text{ in region } D_i$$

where $k_i = k_0 r_i$ for $i = 0, 1, 2$ or 3

Since all fields have the same polarization, all vector dependence of the electric fields may be suppressed, remembering that they have non-zero components along the OZ axis only. The diffracted fields in the upper region D_0 and the lower region D_3 are composed of plane waves and thus the fields in regions D_0 and D_3 may be written as a series of outward going plane waves (Rayleigh expansions [2.18]). So the total electric

field is written

$$E(x,y) = \sum_{p=-\infty}^{\infty}[\exp(-i\chi_0(y-h/2))\,\delta_{p,0} + R_p\exp(i\chi_p(y-h/2))]\exp(i\alpha_p x)/\sqrt{d} \qquad \text{in } D_0 \qquad (2.2)$$

$$= \sum_{p=-\infty}^{\infty}[T_p\exp(-i\eta_p(y+h/2))]\exp(i\alpha_p x)/\sqrt{d} \qquad \text{in } D_3 \qquad (2.3)$$

where

$$\alpha_p = \alpha_0 + 2\pi p/d$$

$$\chi_p = \sqrt{k_0^2 - \alpha_p^2} \qquad \text{if} \quad |\alpha_p| \le k_0$$

$$= i\sqrt{\alpha_p^2 - k_0^2} \qquad \text{if} \quad |\alpha_p| > k_0$$

and $$\eta_p = \sqrt{k_3^2 - \alpha_p^2} \quad ,$$

where the imaginary part of η_p, $\mathrm{Im}(\eta_p)$ is chosen to be non-negative. The sets $\{R_p\}$ and $\{T_p\}$ are the reflection and transmission plane wave coefficients. If r_3 is complex then the transmitted waves decay exponentially in region D_3.

The basis of any modal method is that the field within the groove region is expanded in terms of waveguide modes. The Rayleigh fields are matched to the modal fields along the upper and lower grating surfaces (i.e. where the domains of convergence of the different field expansions overlap) and the resulting field equations are multiplied by orthogonal modal basis functions to extract a system of linear equations whose unknowns are the modal coefficients. Thus in order to apply the Method of Moments, an orthogonal set of modal functions is required.

2.2.2 Field Expansion in Groove Region for Finitely Conducting Lamellar Grating Operated in P Polarized Radiation

This section is devoted to the problem of determining a modal

expansion appropriate to the finitely conducting lamellar grating operated in P polarized radiation.

The aim is to determine a series expansion for the groove region, each term of which analytically satisfies the appropriate Helmholtz equation and the continuity and pseudo-periodicity conditions applying to the fields. The continuity conditions relating fields on the left and right hand sides of the interfaces are

$$\left.\begin{aligned} E(c^-,y) &= E(c^+,y) \quad ; \quad \frac{\partial E}{\partial x}(c^-,y) = \frac{\partial E}{\partial x}(c^+,y) \\ E(d^-,y) &= E(d^+,y) \quad ; \quad \frac{\partial E}{\partial x}(d^-,y) = \frac{\partial E}{\partial x}(d^+,y) \end{aligned}\right\} \tag{2.4}$$

The pseudo-periodicity conditions imply

$$\tau\, E(0^+,y) = E(d^+,y) \quad ; \quad \tau \frac{\partial E}{\partial x}(0^+,y) = \frac{\partial E}{\partial x}(d^+,y) \tag{2.5}$$

where $\tau = \exp(i\alpha_0 d)$ (2.6)

$\alpha_0 d$ representing the phase shift across one period associated with the incident wave.

2.2.2.1 *Comparison of Approaches*

At this stage it is appropriate to discuss the differences between the approach described in this thesis and that of Knop [2.6] and Burkhardt [2.7] who considered lossless dielectric gratings.

Firstly an outline of the approach to be used in this chapter is discussed. Each term of the modal expansion analytically satisfies the Helmholtz equation and continuity and pseudo-periodicity conditions. Solutions of the Helmholtz equation

$$\frac{\partial^2 u_n}{\partial x^2} + \frac{\partial^2 u_n}{\partial y^2} + k_0^2 r^2(x) u_n = 0$$

are determined and the pseudo-periodicity and continuity conditions are

applied to obtain the eigenvalue problem. In the above equation $r^2(x)$ is the square of the refractive index profile of the grating and $\{u_n\}$ are the eigenfunctions.

Since each eigenfunction involves only a single term, the eigenvalue problem involves the solution of only a single transcendental equation (for each eigenvalue). Then for the lossless dielectric lamellar grating, it can be shown that the eigenfunctions form an orthogonal set and thus the Method of Moments [2.19] may easily be applied to solve the diffraction problem. The infinite set of linear equations resulting from the application of this method are then truncated to obtain a numerical solution. In the case of the finitely conducting lamellar grating, the eigenfunctions $\{u_n\}$ do not form an orthogonal set. However, the eigenfunctions corresponding to the adjoint eigenvalue problem will be shown to be orthogonal to the eigenfunctions $\{u_n\}$ and again a Method of Moments solution can be applied.

Knop [2.5], however, uses a substantially different approach. Each individual eigenfunction of the wavefield is taken as a sum, each term of which automatically satisfies the pseudo-periodicity and continuity conditions but not the Helmholtz equation. Substitution of these eigenfunctions $\{u_n\}$ into the Helmholtz equation then yields the eigenvalue problem which involves an infinite set of homogeneous linear equations. These equations must be truncated to numerically obtain the values of the individual eigenvalues. However, the square of the refractive index is written in terms of a Fourier series and the dimension of the coefficient matrix of the linear equations appears highly dependent on the convergence of the Fourier series for $r^2(x)$. That is, for large refractive index discontinuities, when the Fourier series for the step function is slowly convergent, the matrix dimension needs to be large.

From this point on, the methods are essentially the same, in that Knop also applies the Method of Moments to solve the field problem.

In summary, the main difference between the approaches is that Knop introduces terms satisfying the boundary conditions and then satisfies the Helmholtz equation by using a series of these terms, whereas in the approach presented in this thesis, each eigenfunction individually satisfies the Helmholtz equation and is then constrained by the boundary conditions. Knop's modal expansion thus involves a double infinite sum whereas that used in this chapter is a single infinite sum.

The main advantage of Knop's method is that it is more easily generalised to solve the diffraction problems associated with different grating geometries - in particular for modulated dielectric surfaces. However, it does not appear well suited to the consideration of profiles having discontinuities. The approach discussed in this chapter is specific to this problem in that it only handles step function refractive index profiles, but it is a more elegant approach and as discussed, is less involved numerically.

2.2.2.2 *The Eigenvalue Problem*

Consider the determination of the eigenvalues associated with the eigenvalue problem. The Helmholtz equation in the groove region is given by

$$\frac{\partial^2 E}{\partial x^2} + \frac{\partial^2 E}{\partial y^2} + k_0^2 r^2(x) = 0 \qquad 0 \le x \le d \tag{2.7}$$

where

$$\left.\begin{aligned} r(x) &= r_1 \qquad 0 < x < c \\ &= r_2 \qquad c < x < d \end{aligned}\right\} \tag{2.8}$$

and E satisfies the continuity and pseudo-periodicity conditions specified in equations (2.4, 2.5). Assume a separable solution of the form

$$E(x,y) = u(x)\, v(y) \tag{2.9}$$

Then by introducing a separation constant μ , the following equations are obtained

$$u'' + (k^2 - \mu^2)\, u = 0 \tag{2.10}$$

$$v'' + \mu^2 v = 0 \tag{2.11}$$

where $''$ signifies d^2/dx^2.

If the following definition is introduced

$$S(x - c) = 0 \qquad \text{for } x < c$$

$$= 1 \qquad \text{for } x \geq c$$

then equation (2.10) may be rewritten as

$$u'' + \zeta^2\, S(x-c)\, u = -\beta^2 u \tag{2.12}$$

where

$$\left.\begin{aligned} \zeta^2 &= k_2^2 - k_1^2 \\ \beta^2 &= k_1^2 - \mu^2 \end{aligned}\right\} \tag{2.13}$$

and $k_i = k_0 r_i \qquad i = 1,2,3.$

Writing this in operator notation gives

$$Lu = -\beta^2 u \tag{2.14}$$

where

$$L = \frac{d^2}{dx^2} + \zeta^2\, S(x-c) \quad . \tag{2.15}$$

The problem is then to find eigenfunctions satisfying equation (2.14) and also the appropriate continuity conditions (u and u' continuous at $x = c$) and pseudo-periodicity constraints.

$$\left.\begin{aligned} \tau\, u(0^+) &= u(d^-) \\ \tau\, u'(0^+) &= u'(d^-) \end{aligned}\right\} \tag{2.16}$$

Here u' refers to $\frac{du}{dx}$ and τ has been defined in equation (2.6).

Let $\theta(x)$ and $\psi(x)$ be two linearly independent solutions of equation (2.14), which are continuous and continuously differentiable at $x = c$ and satisfy the following initial conditions:

$$\left.\begin{aligned} \theta(0) &= 1 & \psi(0) &= 0 \\ \theta'(0) &= 0 & \psi'(0) &= 1 \end{aligned}\right\} \qquad (2.17)$$

Then by applying the continuity and initial conditions, the following expressions may be obtained

$$\left.\begin{aligned} \theta(x) &= \cos(\beta x) && 0 < x < c \\ &= \cos(\beta c)\cos[\gamma(x-c)] - \frac{\beta}{\gamma}\sin(\beta c)\sin[\gamma(x-c)] && c < x < d \end{aligned}\right\} \qquad (2.18)$$

$$\left.\begin{aligned} \psi(x) &= \frac{1}{\beta}\sin(\beta x) && 0 < x < c \\ &= \frac{1}{\beta}\sin(\beta c)\cos[\gamma(x-c)] + \frac{1}{\gamma}\cos(\beta c)\sin[\gamma(x-c)] && c < x < d \end{aligned}\right\} \qquad (2.19)$$

where $\gamma^2 = \zeta^2 + \beta^2$. (2.20)

The solution of the eigenvalue equation (2.12), subject to the boundary conditions (u and u' continuous at x=c) is thus of the form

$$u(x) = \theta(x) + \omega\psi(x) \qquad (2.21)$$

where ω is found by applying the pseudo-periodicity constraints (equation (2.16)) as follows:

$$\left.\begin{aligned} \tau &= \theta(d^-) + \omega\psi(d^-) \\ \tau\omega &= \theta'(d^-) + \omega\psi'(d^-) \end{aligned}\right\} \qquad (2.22)$$

Thus

$$[\theta(d^-) - \tau]\,[\psi'(d^-) - \tau] - \psi(d^-)\theta'(d^-) = 0 \quad . \qquad (2.23)$$

This will provide a constraint on the eigenvalues (β^2). Since θ, ψ satisfy equation (2.12), it follows that

$$\frac{d}{dx}(\theta\psi' - \theta'\psi) = 0 \quad .$$

That is, the Wronskian

$$W(\theta,\psi) = \theta\psi' - \theta'\psi$$

is constant and so from equation (2.17), $\theta\psi' - \theta'\psi = 1$. Hence equation (2.23) may be simplified to

$$\tau[\theta(d^-) + \psi'(d^-)] = 1 + \tau^2$$

or $\theta(d^-) + \psi'(d^-) = 2\cos(\alpha_0 d)$ (2.24)

Substitution of equations (2.18), (2.19) into this equation yields the eigenvalue equation

$$\cos(\beta c)\cos(\gamma g) - \tfrac{1}{2}\left(\frac{\beta^2 + \gamma^2}{\beta\gamma}\right)\sin(\beta c)\sin(\gamma g) = \cos(\alpha_0 d) \quad (2.25)$$

where $g = d - c$ (2.26)

Note that when $\zeta = 0$, then $\beta = \gamma$ and so equation (2.25) degenerates to

$$\cos(\beta d) = \cos(\alpha_0 d)$$

i.e. $\beta = \alpha_0 + 2\pi p/d$ (for any integer p)

which is simply the classical grating equation.

Finally, the complete expression for the groove expansion is determined. For any eigenvalue β^2 satisfying equation (2.25) (i.e. those values of β chosen so that the system of equations (2.22) has a non-trivial solution) it follows that

$$\omega = \frac{\tau - \theta(d^-)}{\psi(d^-)} \quad (2.27)$$

Also the differential equation (2.11) constraining $v(y)$ has a solution of the form

$$v(y) = a\sin(\mu y) + b\cos(\mu y) \quad (2.28)$$

So the separable solution, equation (2.9), is given by

$$E(x,y) = [\theta(x) + \omega\psi(x)]\,[a\sin(\mu y) + b\cos(\mu y)] \quad (2.29)$$

2.2.2.3 *The Question of Self-Adjointness*

Now, for a lossless dielectric lamellar grating the operator L can be shown to be self-adjoint with respect to an inner product defined by

$$\langle f,g\rangle = \int_0^d \overline{f}(x)\, g(x)\, dx \quad (2.30)$$

where $f(x)$ and $g(x)$ are two functions from the space of functions satisfying the equations (2.4, 2.5, 2.7). Indeed, consider

$$\langle u,Lv\rangle - \langle Lu,v\rangle = \int_0^d \{\bar{u}[v'' + \zeta^2 S(x-c)v] - [\bar{u}'' + \zeta^2 S(x-c)\bar{u}]v\}\, dx$$

(since ζ^2 is real for a lossless structure)

$$= \int_0^d (v''\bar{u} - \bar{u}''v)\, dx$$

$$= 0 \quad \text{(by the pseudo-periodicity conditions (2.16).}$$

Thus, for the lossless dielectric grating, L is a self-adjoint operator and consequently has real eigenvalues (β^2) and the eigenfunctions corresponding to distinct eigenvalues are orthogonal. This means that the Method of Moments may readily be applied to this problem.

However, if the constraint of losslessness of the groove region is removed, then the term ζ^2 becomes complex and as shown below, the boundary value problem is no longer self-adjoint. Consequently, the eigenvalues of the differential operator are no longer constrained to be real, nor are the eigenfunctions corresponding to different eigenfunctions orthogonal. The aim, therefore, is to find a set of functions $\{u_j^+\}$ related to the set of eigenfunctions $\{u_j\}$ of the non-self adjoint problem by a biorthogonality relation

$$\begin{aligned} \langle u_j^+, u_i\rangle &= 0 \qquad \text{for } i \neq j \\ &\neq 0 \qquad \text{for } i = j \end{aligned} \tag{2.31}$$

where the inner product is defined by equation (2.30).

In order to obtain the functions $\{u_j^+\}$, an operator

$$L^+ = \frac{d^2}{dx^2} + \bar{\zeta}^2 S(x-c) \tag{2.32}$$

is introduced and the following eigenvalue problem is considered

$$L^+u^+ = -(\beta^+)^2 u^+ \tag{2.33}$$

subject to the constraints that u^+ and $\frac{du^+}{dx}$ be continuous at $x = c, d$ and pseudo-periodic between $x = 0$ and $x = d$.

The following discussion shows that L^+ is the adjoint of L

i.e. $$\langle u^+, Lu\rangle = \langle L^+u^+, u\rangle \tag{2.34}$$

where the eigenfunctions u^+ of L^+ are subject to the same boundary conditions as u.

Indeed consider

$$\langle u^+, Lu\rangle - \langle L^+u^+, u\rangle = \int_0^d \{[u'' + \zeta^2 S(x-c)u]\bar{u}^+ - u[(\bar{u}^+)'' + \zeta^2 S(x-c)\bar{u}^+]\}dx$$

$$= \int_0^d \{u''(\bar{u}^+) - u(\bar{u}^+)''\}dx$$

$$= 0 \quad \text{by the pseudo-periodicity conditions.}$$

2.2.2.4 *The Adjoint Problem*

In order to determine the form of the adjoint eigenfunctions, a process exactly similar to that described in section 2.2.2.2 is followed.

$\theta^+(x)$ and $\psi^+(x)$ are assumed to be two linearly independent solutions of equation (2.33), satisfying the initial conditions

$$\begin{aligned} \theta^+(0) &= 1 & \psi^+(0) &= 0 \\ \theta^{+\prime}(0) &= 0 & \psi^{+\prime}(0) &= 1 \end{aligned} \tag{2.35}$$

By applying the continuity and pseudo-periodicity conditions, the following expressions are obtained

$$\left.\begin{aligned} \theta^+(x) &= \cos(\beta^+x) && 0 < x < c \\ &= \cos(\beta^+c)\cos[\gamma^+(x-c)] - \frac{\beta^+}{\gamma^+}\sin(\beta^+c)\sin[\gamma^+(x-c)] && c < x < d \end{aligned}\right\} \tag{2.36}$$

$$\left.\begin{aligned} \psi^+(x) &= \frac{1}{\beta^+}\sin(\beta^+x) && 0 < x < c \\ &= \frac{1}{\beta^+}\sin(\beta^+c)\cos[\gamma^+(x-c)] + \frac{1}{\gamma^+}\cos(\beta^+c)\sin[\gamma^+(x-c)] && c < x < d \end{aligned}\right\} \tag{2.37}$$

where $\gamma^{+2} = \beta^{+2} + \bar{\zeta}^2$ (2.38)

Then by writing

$$u^+(x) = \theta^+(x) + \omega^+\psi^+(x) \tag{2.39}$$

and applying the pseudo-periodicity constraints, the eigenvalue equation constraining the values of β^+ so that ω^+ may be non trivial can be determined to be

$$\cos(\beta^+ c)\cos(\gamma^+ g) - \tfrac{1}{2}\frac{(\beta^{+2}+\gamma^{+2})}{\beta^+\gamma^+}\sin(\beta^+ c)\sin(\gamma^+ g) = \cos(\alpha_0 d) \tag{2.40}$$

Now this equation is exactly the same as equation (2.25), which constrains the eigenvalues (β^2) of the operator L, except that β^+ and γ^+ are related by $\bar{\zeta}$ (see equation (2.38)). Thus

$$\left.\begin{aligned} \beta^{+2} &= \bar{\beta}^2 \\ \gamma^{+2} &= \bar{\gamma}^2 \end{aligned}\right\} \tag{2.41}$$

and from equations (2.36), (2.37)

$$\theta^+(x) = \bar{\theta}(x) \quad ; \quad \psi^+(x) = \bar{\psi}(x) \tag{2.42}$$

Then for any eigenvalue $\bar{\beta}^2$ satisfying the eigenvalue equation (2.40), the following constraint on ω^+ can be determined:

$$\begin{aligned} \omega^+ &= \frac{\tau-\theta^+(d^-)}{\psi^+(d^-)} \\ &= \frac{\tau-\bar{\theta}(d^-)}{\bar{\psi}(d^-)} \end{aligned} \tag{2.43}$$

Thus the adjoint eigenfunctions have been specified. Now the eigenfunctions will be shown to satisfy the biorthogonality relation specified in equation (2.31).

Consider equation (2.34) which is written

$$\langle u_m^+, Lu_n\rangle = \langle L^+u_m^+, u_n\rangle$$

Using equations (2.14) and (2.33) this can be rewritten

$$-\beta_n^2 \langle u_m^+, u_n \rangle = -\overline{\beta}_m^{+2} \langle u_m^+, u_n \rangle \qquad \text{or}$$

$$-(\beta_n^2 - \beta_m^2)\langle u_m^+, u_n \rangle = 0 \qquad \text{using equation (2.41)}$$

That is,

$$\int_{0+}^{d-} u_n \overline{u_m^+}\, dx = \delta_{nm} \tag{2.44}$$

where the sets of eigenfunctions $\{u_n\}$ and $\{u_n^+\}$ have been renormalised according to

$$\langle u_n^+, u_n \rangle = 1 \tag{2.45}$$

Thus the sets $\{u_n\}$ and $\{u_n^+\}$ are indeed orthogonal with respect to the inner product defined by equation (2.30).

2.2.2.5 *Properties of the P Polarization Eigenvalue Problem*

This section is concerned with the properties of the eigenfunctions and eigenvalues associated with the differential operator L defined in equation (2.15). In particular, the following are discussed:

(i) constraints on the real or imaginary nature of β and γ for the lossless dielectric lamellar grating

(ii) the distribution of the eigenvalues (β^2) and

(iii) the completeness of the eigenfunctions.

(i) The eigenvalue problem associated with the lossless dielectric lamellar grating has been shown to be self-adjoint and the eigenvalues (β^2) to be real. Consider now the constraints on β and γ. Since β^2 and ζ^2 are purely real then so is γ^2. The possible values that β and γ may take are (remembering they must also satisfy equation (2.25))

(1) β real, γ real : $\gamma > \zeta$, $\beta > 0$

(2) β imaginary, γ real : $0 < \gamma < \zeta$, $0 < |\beta| < \zeta$

(3) β real, γ imaginary :

(4) β imaginary, γ imaginary :

Case (3) obviously cannot provide a possible combination of β and γ and by explicitly considering the eigenvalue equation (2.25) for case (4) it is found that it takes the following form

$$\cosh(|\beta|c)\cosh(|\gamma|g) + \tfrac{1}{2}\left[\frac{|\beta|^2 + |\gamma|^2}{|\beta||\gamma|}\right]\sinh(|\beta|c)\sinh(|\gamma|g) = \cos(\alpha_0 d)$$

Except when $|\beta| = |\gamma| = 0$, the left hand side of the above equation exceeds unity while the right hand side is less than unity and hence case (4) cannot furnish allowed β, γ values. The remaining two possible combinations, case (1) and case (2), are permissible.

(ii) Consider firstly the distribution of eigenvalues for the lossless dielectric lamellar grating problem. It may be shown [2.20] that $D(\beta^2) = \theta(d) + \psi'(d)$, taken as a function of β^2 always has behaviour of the type illustrated in figure 2.2. Firstly $D(\beta^2)$ is continuous. Secondly, $D(\beta^2) > 2$ for $\beta^2 <$ some number Ω. (It may be shown that $\Omega \geq -\zeta^2$). For $\beta^2 > \Omega$, $D(\beta^2)$ oscillates infinitely often; its maxima always being greater than 2 and its minima always being less than -2. $D(\beta^2)$ is always monotonic between values of β^2 where $D(\beta^2) = -2$ and $D(\beta^2) = 2$. Hence the eigenvalue equation (2.25) always has infinitely many discrete solutions ${\beta_1}^2, {\beta_2}^2, {\beta_3}^2 \ldots\ldots$ with ${\beta_n}^2 \to \infty$ as $n \to \infty$ (integer n). It may also be shown that provided $\zeta^2 \neq 0$, there is only one eigenfunction $u_m(x)$ corresponding to any eigenvalue ${\beta_m}^2$ (except possibly at certain isolated points if $\tau = \pm 1$).

Now consider what happens to the distribution of eigenvalues when a finitely conducting lamellar grating is considered. It may be shown that,

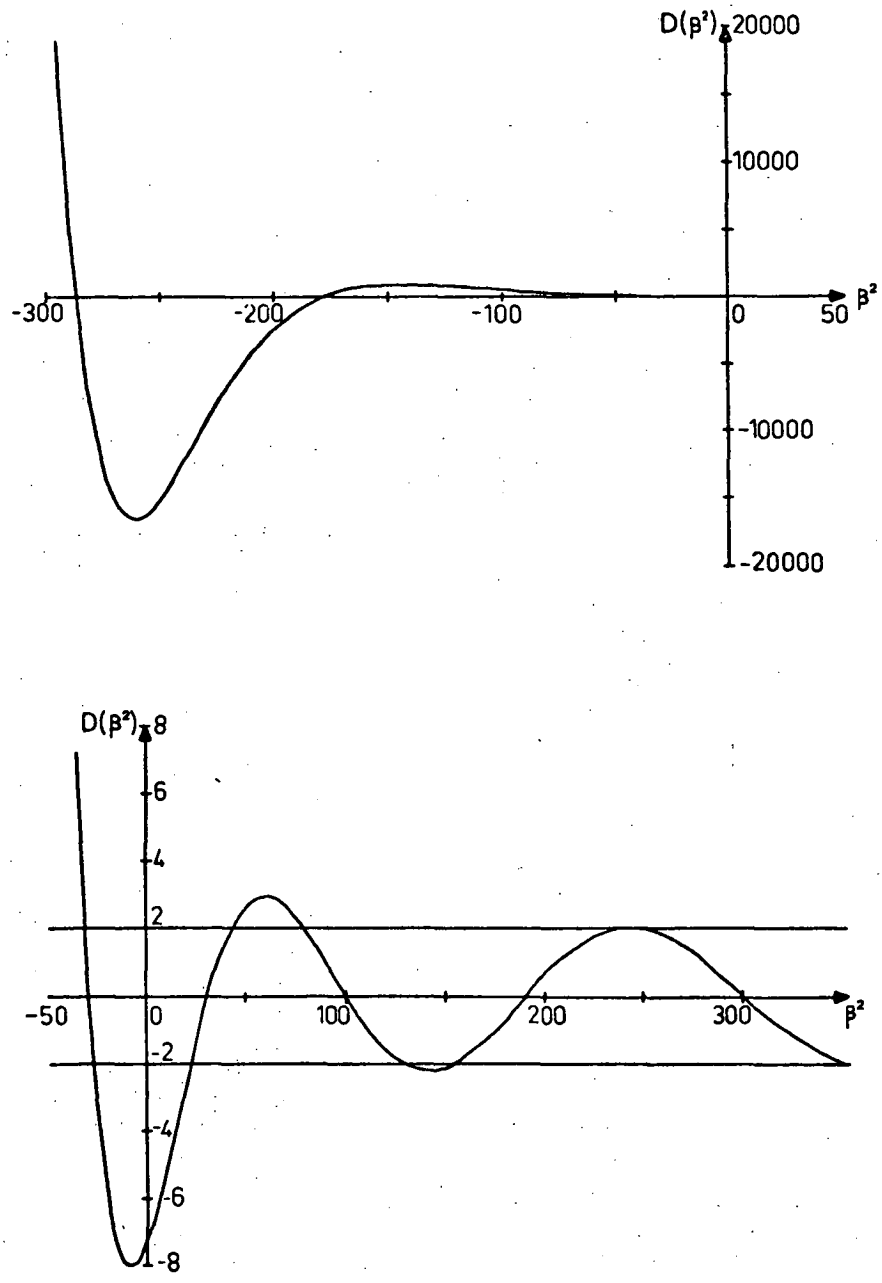

Figure 2.2 Plot of the function $D(\beta^2)$ for a lossless dielectric lamellar grating. The eigenvalues correspond to points where $D(\beta^2) = 2 \cos \alpha_0 d$. In the first case shown, at least three eigenvalues occur for $\beta^2 < 0$. In the second case only one eigenvalue occurs for $\beta^2 < 0$ while the first four eigenvalues for $\beta^2 > 0$ are shown.

as the imaginary part of a refractive index r_i ($i = 1$ or 2) is increased from zero, the eigenvalues β_n^2 move continuously away from their positions on the real axis into the complex plane (see figure 2.3), and that all the complex eigenvalues may be found by following the paths illustrated, starting from real eigenvalues. As the real part of the eigenvalues β_n^2 approaches infinity (that is as $n \to \infty$) the complex eigenvalues approach the real eigenvalues of the simpler problem, consisting of the differential equation (2.12), with $\zeta^2 = 0$ and the boundary conditions (2.4, 2.5). Further, the eigenfunctions $\{u_n\}$ approach the eigenfunctions of this simpler problem.

(iii) It may be shown using arguments similar to those in [2.21], chapter 12, that the eigenfunctions $\{u_n\}$ are complete in the sense that any continuous and piecewise differentiable function $f(x)$, satisfying the boundary conditions (2.4, 2.5), may be expanded as a linear combination of the $\{u_n\}$:

$$f(x) = \sum_{n=0}^{\infty} a_n u_n(x)$$

where $$a_n = \langle u_n^+, f \rangle$$

Thus it follows that the general solution for the total electric field E can be expressed in the form

$$E(x,y) = \sum_n [a_n \sin(\mu_n y) + b_n \cos(\mu_n y)] \, u_n(x) \qquad (2.46)$$

The following section describes the matching of the plane wave field to this solution at $y = \pm h/2$.

2.2.3 Solution of the P Polarization Diffraction Problem for the Finitely Conducting Lamellar Grating

The following sections are concerned with the solution of the

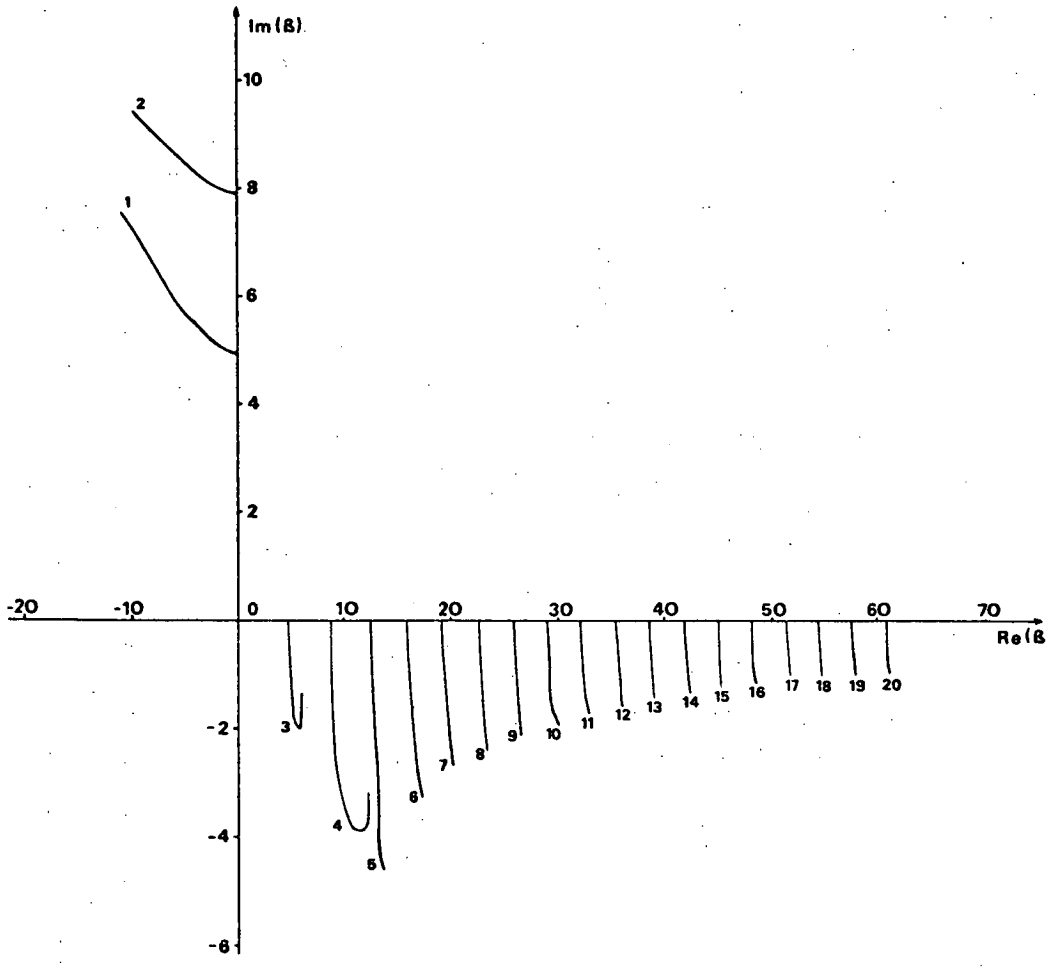

Figure 2.3 Evolution of the first 20 complex eigenvalues β_p with increasing imaginary part of r_2 from 0.0 to 1.0, for a finitely conducting lamellar grating operated in P polarized radiation, having the following specifications: d = 1.0, c = 0.4, h = 0.1, r_1 = 1.0, r_2 = 1.5+i1.0, r_3 = 1.0, λ = 0.8, ϕ = 11.5°.

diffraction problem for the finitely conducting lamellar grating, but simplifications which arise when considering the lossless dielectric lamellar grating will be indicated throughout.

2.2.3.1 *Application of the Method of Moments*

Consider the continuity of the electric field at $y=h/2$. This can be written

$$\sum_p [R_p + \delta_{p0}] e_p(x) = \sum_m (a_m^* + b_m^*)\, u_m(x) \qquad 0 \le x \le d \qquad (2.47)$$

where $$e_p(x) = \frac{1}{\sqrt{d}} \exp(i\alpha_p x)$$

$$a_m^* = a_m \sin(\mu_m h/2)$$

$$b_m^* = b_m \cos(\mu_m h/2)$$

and the $u_m(x)$ are normalised according to section 2.2.2.4.

This equation is multiplied throughout by $\bar{u}_n^+(x)$ and integrated over the interval $[0,d)$ to make use of the biorthogonality relation (2.31). The following system of equations is then obtained

$$a_n^* + b_n^* = \sum_p [R_p + \delta_{p0}]\, \bar{K}_{pn} \qquad \text{for } n=1, 2, \ldots \qquad (2.48)$$

where $$K_{pn} = \int_0^d \bar{e}_p(x)\, u_n^+(x)\, dx \qquad (2.49)$$

It is noted that for the self-adjoint problem corresponding to the lossless dielectric structure, $u_n^+(x) = u_n(x)$ and the set $\{u_n\}$ is orthonormal.

Equation (2.48) may be rewritten in more concise matrix notation as follows

$$a^* + b^* = K^H (R + F) \qquad (2.50)$$

where $a^* = [a_n^*]$, $b^* = [b_n^*]$, $K = [K_{pn}]$, $R = [R_p]$, F is a vector whose entries are $F_p = \delta_{p0}$ and the superscript H is used to denote the Hermitian conjugate of a matrix.

Similarly, continuity of the field at $y = -h/2$, projected onto the adjoint modal basis gives

$$-a^* + b^* = K^H T \tag{2.51}$$

where $T = [T_p]$.

Now applying the continuity of the normal derivative of E, $\frac{\partial E}{\partial y}$, at $y=h/2$ gives rise to the equation

$$\sum_p i\chi_p[R_p - \delta_{p0}]e_p(x) = \sum_m (D_{1m}a_m^* + D_{2m}b_m^*)\, u_m(x) \quad \text{for } 0 \le x \le d \tag{2.52}$$

where $D_{1m} = \mu_m \cot(\mu_m h/2)$

$D_{2m} = -\mu_m \tan(\mu_m h/2)$.

The Method of Moments is then applied by multiplying throughout equation (2.52) by $\bar{e}_q(x)$ (for some integer q) and integrating over the interval $[0,d]$ to derive

$$i\chi_q [R_q - \delta_{q0}] = \sum_m (D_{1m}a_m^* + D_{2m}b_m^*)\, J_{qm} \quad q=0, \pm1, \pm2... \tag{2.53}$$

where $J_{qm} = \int_0^d \bar{e}_q(x)\, u_m(x)\, dx$

This procedure is followed without change for the lossless dielectric problem.

Equations (2.53), when expressed in matrix notation, reduce to

$$R = F - i\chi^{-1} J(D_1 a^* + D_2 b^*) \tag{2.54}$$

where $\chi = \text{diag}\,(\chi_p)$; $D_1 = \text{diag}\,(D_{1m})$; $D_2 = \text{diag}\,(D_{2m})$ and $J = [J_{qm}]$.

Similarly by projecting the continuity of $\frac{\partial E}{\partial y}$ at $y = -h/2$ onto the plane wave basis, the following equation is obtained

$$T = in^{-1}J(D_1 a^* - D_2 b^*) \tag{2.55}$$

where $\eta = \text{diag}(\eta_p)$

By substituting equations (2.54) and (2.55) into equations (2.50) and (2.51), the following coupled pair of linear equations, relating the unknown modal coefficients $\{a_m^*\}$ and $\{b_m^*\}$ can be obtained:

$$\begin{bmatrix} iK^H \chi^{-1} JD_1 + I & iK^H \chi^{-1} JD_2 + I \\ -iK^H \eta^{-1} JD_1 - I & iK^H \eta^{-1} JD_2 + I \end{bmatrix} \begin{bmatrix} a^* \\ b^* \end{bmatrix} = 2 \begin{bmatrix} K^H F \\ 0 \end{bmatrix} \tag{2.56}$$

Here I denotes the identity matrix of the appropriate dimension.

The system of equations (2.56) may readily be solved numerically using standard elimination techniques after truncation of the matrices of infinite dimension. The Rayleigh field amplitudes may then be obtained using the reconstruction equations (2.54) and (2.55).

2.2.3.2 *Conservation of Energy - Calculation of Efficiencies*

The conservation of energy criterion can be shown to hold analytically (independently of truncation errors) for the modal formalism describing the properties of the lossless dielectric lamellar grating. Consequently, it can provide no test on the numerical accuracy of this formalism. However, this is not the case for the finitely conducting lamellar grating formalism for which the energy balance between the incident, reflected and transmitted fields is dependent on truncation errors, i.e. the errors introduced when the infinite modal (2.46) or Rayleigh (2.2, 2.3) series are truncated to a finite sum in the numerical solution. Thus the energy conservation criterion can provide

an excellent check on the convergence and accuracy of this formalism.

Two important results can be shown [2.2] for the finitely conducting lamellar grating. To describe these the following definitions are introduced:

The total flux of energy crossing a surface $x \in [0,d]$, y constant is

$$P(y) = \int_0^d [E \frac{\partial \overline{E}}{\partial y} - \overline{E} \frac{\partial E}{\partial y}] \, dx \tag{2.57}$$

Within the dissipative grating region $(-h/2 < y < h/2)$ the ohmic loss Q is given by

$$Q = \iint_{D_1 U D_2} \text{div}[E \, \text{grad}\overline{E} - \overline{E} \, \text{grad}E] \, dA \tag{2.58}$$

where the area integral is over the grating region $0 \leq x \leq d$, $-h/2 \leq y \leq h/2$.

Then it can be shown [2.2] that

(a) the ohmic loss Q in the groove region is both physically and analytically equal to the difference in the flux of energy crossing the surfaces at $y = (h/2)^-$ and $y = (-h/2)^+$

i.e. $Q = P[(h/2)^-] - P[(-h/2)^+]$

and

(b) the flux of energy crossing the surface $y = (h/2)^+$ is not analytically equal to that crossing the surface $y = (h/2)^-$ i.e. the quantity $P[(h/2)^+] - P[(h/2)^-]$ is dependent upon the truncation errors arising in the numerical calculations. Similar remarks obviously will apply at the lower grating surface $y = -h/2$. Thus by comparing the energy fluxes crossing the surfaces $y = (h/2)^+$ and $y = (h/2)^-$ the extent of the truncation errors in the numerical results can be estimated.

2.2.4 The Formulation of the S Polarization Problem for a Finitely Conducting Lamellar Grating

The fields for this problem are described in terms of a scalar magnetic field $H(x,y)$, since the magnetic field vector has a component only along the OZ axis. The differences occurring between this and the earlier problem arise because of the different boundary conditions applying to this polarization. These are that H and $\frac{1}{r^2}\frac{\partial H}{\partial n}$ be continuous at each interface and also be pseudo-periodic. Here $\frac{\partial H}{\partial n}$ signifies the derivative of H taken normal to the surface.

2.2.4.1 *The S Polarization Eigenvalue Problem*

Since k is a function of x in the groove region, the wave equation appropriate to this polarization may be written

$$\frac{\partial}{\partial x}\left(\frac{1}{k^2}\frac{\partial H}{\partial x}\right) + \frac{\partial}{\partial y}\left(\frac{1}{k^2}\frac{\partial H}{\partial y}\right) + H = 0 \qquad (2.59)$$

where $k^2 = k_0^2\, r^2(x)$

and $r(x)$ has been defined in equation (2.8).

This may be rewritten as

$$\frac{\partial^2 H}{\partial x^2} + \frac{\partial^2 H}{\partial y^2} + k^2 H = \frac{1}{k^2}\frac{\partial H}{\partial x}\,\zeta^2\,\delta(x-c) \qquad (2.60)$$

where $\delta(x)$ denotes the Dirac delta distribution and ζ^2 is defined in equation (2.13).

Equation (2.60) is an inhomogeneous Helmholtz equation and has the same form as the Helmholtz equation derived for the P polarization problem, equation (2.7), but with a distributive term on the right hand side. This distributive term behaves in the same manner as the discontinuity in the normal derivative of H at the surface of discontinuity $(x = c)$.

The essential changes to the eigenvalue problem will now be outlined. Again a separable solution of the wave equation is assumed of the form

$$H(x,y) = u(x)\, v(y) \tag{2.61}$$

Substitution of this into equation (2.59) yields

$$k^2[\frac{1}{k^2} u']' + \zeta^2 S(x-c)\, u = -\beta^2 u \tag{2.62}$$

$$v'' + \mu^2 v = 0 \tag{2.63}$$

where the separation constant

$$\mu^2 = k_1^2 - \beta^2$$

has been introduced.

Equation (2.62) may be written in operator notation

$$Lu = -\beta^2 u \tag{2.64}$$

where

$$L = k^2 \frac{d}{dx} (\frac{1}{k^2} \frac{d}{dx}) + \zeta^2 S(x-c). \tag{2.65}$$

The boundary conditions for this problem may be explicitly written:

$$\left.\begin{aligned} u(c^-) = u(c^+) \quad ; \quad \frac{1}{r_1^2} u'(c^-) = \frac{1}{r_2^2} u'(c^+) \\ u(d^-) = u(d^+) \quad ; \quad \frac{1}{r_2^2} u'(d^-) = \frac{1}{r_1^2} u'(d^+) \end{aligned}\right\} \tag{2.66}$$

while the pseudo-periodicity conditions are

$$\tau u(0^+) = u(d^+) \quad ; \quad \frac{1}{r_1^2} \tau u'(0^+) = \frac{1}{r_2^2} u'(d^+) \tag{2.67}$$

Two functions $\theta(x)$, $\psi(x)$ are again introduced which are linearly independent solutions of equation (2.62), satisfying the same continuity and pseudo-periodicity conditions given in equations (2.66), (2.67) for u and obeying the initial conditions specified in equation (2.17). Then

$$\left.\begin{aligned}\theta(x) &= \cos(\beta x). && \text{for} \quad 0<x<c\\ &= \cos(\beta c)\cos[\gamma(x-c)] - \frac{r_2^2}{r_1^2}\frac{\beta}{\gamma}\sin(\beta c)\sin[\gamma(x-c)] && c<x<d\end{aligned}\right\} \quad (2.68)$$

$$\left.\begin{aligned}\psi(x) &= \frac{1}{\beta}\sin(\beta x) && \text{for} \quad 0<x<c\\ &= \frac{1}{\beta}\sin(\beta c)\cos[\gamma(x-c)] + \frac{r_2^2}{r_1^2}\frac{1}{\gamma}\cos(\beta c)\sin[\gamma(x-c)] && c<x<d\end{aligned}\right\} \quad (2.69)$$

where $\gamma^2 = \beta^2 + \zeta^2$ (2.70)

Then $u(x)$ can be written in terms of the basis functions θ, ψ

$$u(x) = \theta(x) + \omega\psi(x)$$

where, by applying the pseudo-periodicity constraints (2.67), it follows that

$$\omega = \frac{\psi(d^-)}{\tau - \theta(d^-)}$$

subject to the non-linear eigenvalue equation

$$\cos(\beta c)\cos(\gamma g) - \tfrac{1}{2}\left(\frac{r_2^2}{r_1^2}\frac{\beta}{\gamma} + \frac{r_1^2}{r_2^2}\frac{\gamma}{\beta}\right)\sin(\beta c)\sin(\gamma g) = \cos(\alpha_0 d) \quad (2.71)$$

This eigenvalue equation has properties similar to those discussed in section 2.2.2.5.

In the groove region $D_1 \cup D_2$, the field H is given by an expansion involving terms of the form

$$u(x)v(y) = [\theta(x) + \omega\psi(x)][a\sin(\mu y) + b\cos(\mu y)] \quad (2.72)$$

The following inner product of two functions $f(x)$ and $g(x)$, defined with respect to a weighting distribution $\frac{1}{k^2(x)}$, is introduced.

$$\langle f, g\rangle = \int_0^d \frac{1}{k^2(x)}\,\bar{f}(x)g(x)dx \quad (2.73)$$

It can be shown that the operator L defined by equation (2.65) is

self-adjoint with respect to the inner product (2.73) only for the lossless dielectric lamellar structure. Since the operator L corresponding to the finitely conducting lamellar grating is non self-adjoint, its eigenfunctions $\{u_j\}$ do not form an orthogonal set. It is therefore necessary to find a set of functions $\{u_j^+\}$ which are orthogonal to the $\{u_j\}$ in order that the field problem can be solved using the Method of Moments.

As in section 2.2.2.3, an operator

$$L^+ = \bar{k}^2 \frac{d}{dx}\left(\frac{1}{\bar{k}^2}\frac{d}{dx}\right) + \bar{\zeta}^2 S(x-c) \tag{2.74}$$

is introduced and the following eigenvalue problem is considered

$$L^+u^+ = -(\beta^+)^2 u^+ \tag{2.75}$$

subject to the following continuity and pseudo-periodicity conditions

$$\left.\begin{aligned} u^+(c^-) &= u^+(c^+) \quad ; \quad \frac{1}{\bar{r}_1^2} u^{+\prime}(c^-) = \frac{1}{\bar{r}_2^2} u^{+\prime}(c^+) \\ u^+(d^-) &= u^+(d^+) \quad ; \quad \frac{1}{\bar{r}_2^2} u^{+\prime}(d^-) = \frac{1}{\bar{r}_1^2} u^{+\prime}(d^+) \\ \tau u^+(0^+) &= u^+(d^+) \quad ; \quad \frac{1}{\bar{r}_1^2} \tau u^{+\prime}(0^+) = \frac{1}{\bar{r}_1^2} u^{+\prime}(d^+) \end{aligned}\right\} \tag{2.76}$$

Then L^+ can be shown, using an analysis similar to that described in section 2.2.2.3, to be the adjoint of the operator L, with respect to the inner product defined by equation (2.73). That is

$$\langle u^+, Lu\rangle = \langle L^+u^+, u\rangle \tag{2.77}$$

Note that the adjoint boundary conditions (2.76) differ from those given in equations (2.66, 2.67), the latter corresponding to the physical problem.

2.2.4.2 *The Adjoint Problem*

The solution of the eigenvalue problem given in equations (2.75), (2.76) proceeds in an exactly analogous manner to that described in

section 2.2.2.4.

The eigenfunctions $u^+(x)$ are written in terms of two linearly independent solutions, $\theta^+(x)$ and $\psi^+(x)$, of equation (2.75).

$$u^+(x) = \theta^+(x) + \omega^+\psi^+(x)$$

where $\theta^+(x)$ and $\psi^+(x)$ satisfy the initial conditions given in equation (2.35) and the boundary conditions specified in equation (2.76). These functions may be written explicitly as:

$$\left.\begin{aligned} \theta^+(x) &= \cos(\beta^+x) && 0<x<c \\ &= \cos(\beta^+c)\cos[\gamma^+(x-c)] - \frac{\bar{r}_2^{\,2}}{\bar{r}_1^{\,2}}\frac{\beta^+}{\gamma^+}\sin(\beta^+c)\sin[\gamma^+(x-c)] && c<x<d \end{aligned}\right\} \quad (2.78)$$

$$\left.\begin{aligned} \psi^+(x) &= \frac{1}{\beta^+}\sin(\beta^+x) && 0<x<c \\ &= \frac{1}{\beta^+}\sin(\beta^+c)\cos[\gamma^+(x-c)] + \frac{\bar{r}_2^{\,2}}{\bar{r}_1^{\,2}}\frac{1}{\gamma^+}\cos(\beta^+c)\sin[\gamma^+(x-c)] && c<x<d \end{aligned}\right\} \quad (2.79)$$

where $(\gamma^+)^2 = \bar{\zeta}^2 + (\beta^+)^2$ (2.80)

The pseudo-periodicity constraints may be used to obtain

$$\omega^+ = \frac{\tau - \theta^+(d^-)}{\psi^+(d^-)} \quad (2.81)$$

They also lead to the non-linear eigenvalue equation for the adjoint problem

$$\cos(\beta^+c)\cos(\gamma^+g) - \tfrac{1}{2}\left(\frac{\bar{r}_2^{\,2}}{\bar{r}_1^{\,2}}\frac{\beta^+}{\gamma^+} + \frac{\bar{r}_1^{\,2}}{\bar{r}_2^{\,2}}\frac{\gamma^+}{\beta^+}\right)\sin(\beta^+c)\sin(\gamma^+g) = \cos(\alpha_0 d) \quad (2.82)$$

Since (2.80, 2.82) are exactly the same as (2.70, 2.71), it follows that

$$\left.\begin{aligned} (\beta^+)^2 &= \bar{\beta}^2 \\ (\gamma^+)^2 &= \bar{\gamma}^2 \end{aligned}\right\} \quad (2.83)$$

and thus

$$\left.\begin{aligned} \theta^{+}(x) &= \bar{\theta}(x) \\ \psi^{+}(x) &= \bar{\psi}(x) \end{aligned}\right\} \qquad (2.84)$$

2.2.4.3 *Properties of the S Polarization Eigenvalue Problem*

Firstly, following a process exactly similar to that given at the end of section 2.2.2.3, the eigenfunctions $\{u_n\}$ may be shown to be orthogonal to their adjoint functions $\{u_n^{+}\}$ and they may be renormalised according to equation (2.45).

Secondly, the eigenvalue equation (2.71) can be shown to have properties similar to those discussed in section 2.2.2.5 (ii).

Finally, the eigenfunctions may be shown to form a complete set using an extension of the methods described in [2.21] (see section 2.2.2.4 (iii)) and so it is possible to express the field within the groove region $(D_1 \cup D_2)$ as the sum of eigenfunctions

$$H(x,y) = \sum_m [a_m \sin(\mu_m y) + b_m \cos(\mu_m y)]\, u_m(x) \qquad (2.85)$$

2.2.4.4 *Solution of the S Polarization Diffraction Problem*

This proceeds in exactly the same manner as for the P polarization problem, by applying the Method of Moments. The magnetic fields in free space (D_0) and in region D_3 are given by Rayleigh expansions having the same form as those introduced in section 2.2.1. These fields are matched to the modal field described by equation (2.85) at the surfaces $y = h/2$, $y = -h/2$. Thus the analysis described in section 2.2.3 is unaltered except that the inner products must be redefined

$$K_{pn} = \int_0^d \frac{1}{\overline{\overline{k^2(x)}}}\, \bar{e}_p(x)\, u_n^{+}(x)\, dx \qquad (2.86)$$

$$J_{qm} = \int_0^d \frac{1}{k^2(x)}\, \bar{e}_q(x)\, u_m(x)\, dx \qquad (2.87)$$

and the matrices χ and η must be redefined as

$$\chi = \text{diag}\ (\chi_p/k_0^2)$$

$$\eta = \text{diag}\ (\eta_p/k_3^2)$$

2.2.4.5 *The Conservation of Energy Criterion*

The discussion given in section 2.2.3.2 can be repeated here and the same conclusions may be drawn:

(a) $Q = P[(h/2)^-] - P[(-h/2)^+]$ both physically and analytically and

(b) $P[(h/2)^+] - P[(h/2)^-]$ is not analytically zero.

Here of course, $P(y)$ and Q must be redefined as

$$P(y) = \int_0^d (\overline{H} \frac{1}{\nu^2} \frac{\partial H}{\partial y} - H \frac{1}{\overline{\nu^2}} \frac{\partial \overline{H}}{\partial y})\ dx$$

$$Q = \iint_{D_1 \cup D_2} \text{div}[\overline{H} \frac{1}{r^2(x)} \text{grad } H - H \frac{1}{\overline{r^2(x)}} \text{grad } \overline{H}]\ dA$$

where

$$\nu(x,y) = 1 \quad \text{for} \quad y > h/2$$

$$= r(x) \quad \text{for} \quad -h/2 < y < h/2$$

$$= r_3 \quad \text{for} \quad y < -h/2$$

2.3 CONFIRMATIONS OF THE THEORY AND APPLICATIONS

This section will be subdivided into two parts in order to discuss the two different types of lamellar gratings separately.

2.3.1 Numerical Results Pertaining to the Lossless Dielectric Lamellar Grating

The conservation of energy criterion can be shown to be analytically satisfied by the lossless dielectric lamellar grating formalism, independently of truncation errors. Thus this test can not serve as a check on the convergence properties of the formalism. However, the

formalism was rigorously tested using the Reciprocity Theorem and a series of symmetry constraints [2.22]. An example confirming the Reciprocity Theorem is contained in table 2.1 while sample results demonstrating the symmetry properties associated with the Littrow mount are given in tables 2.2 to 2.4. The formalism was also compared with the results published by Knop [2.6]. Figure 2.4 illustrates one comparison curve which was obtained using the formalism described in section 2.2. The S polarization formalism was also tested for the case where the grating degenerates to a dielectric slab ($r_1 = r_2$) and the radiation is incident at the Brewster angle. Under these conditions, total transmission of the incident energy occurs as required.

Further verification of the convergence properties of the formalism was obtained in the region of strong diffraction anomalies, not only for weakly reflecting materials (such as glass), but also for the case of a strongly reflecting material (having a refractive index of 5.0). The change in energy diffracted as the number of modes was increased was observed and the numerical accuracy of field matching was determined. These results were satisfied to much better than 1% for all points on the curves given in figures 2.4 - 2.10.

Figures 2.5 and 2.6 show spectra obtained for a glass reflection grating operated in normally incident radiation. The solid curves designate the total energy transmitted through the grating while the broken curves show the energy transmitted by the zeroth diffracted order. Two observations may be made immediately. The grating is more strongly diffracting (i.e. disperses more energy) for P polarization than for S polarization. Also the diffraction anomalies are much stronger for the former polarization. Note that for refraction gratings, Wood anomalies occur at differing wavelengths in air and in the substrate. The position

Table 2.1 Confirmation of the Reciprocity Theorem for a Lossless Dielectric Lamellar Grating

Grating parameters : $d = 1.0$, $c = 0.5$, $h = 0.2$

Problem 1 : $\lambda/d = 0.8$, $\phi = 0^{\circ}$, $r_1 = 1.0$, $r_2 = 1.5$, $r_3 = 2.0$

Problem 2 : Return -1 order in reflection
$\lambda/d = 0.8$, $\phi = 53.1301^{\circ}$, $r_1 = 1.0$, $r_2 = 1.5$, $r_3 = 2.0$

Problem 3 : Return -1 order in transmission
$\lambda/d = 0.4$, $\phi = 23.5782^{\circ}$, $r_1 = 0.5$, $r_2 = 0.75$, $r_3 = 0.5$

The parameters for this latter run are taken so that the incident wave appears to be returned from beneath the grating in the new problem. For the physical problem, it is equivalent to $\lambda/d = 0.4$, $\phi = 23.5782^{\circ}$, $r_1 = 1.0$, $r_2 = 1.5$, $r_3 = 2.0$.

Method Parameters : P polarization - 10 modes
S polarization - 12 modes
Number of Rayleigh orders = 17

		P Polarization	S Polarization
Run 1	Φ^R_{-1}	(0.04249,-105.04)	(0.02325, 86.85)
	Φ^T_{-1}	(0.08213,-115.48)	(0.04580,-123.18)
	E.T.	0.9106	0.9384
Run 2	Φ^R_{-1}	(0.04249,-105.04)	(0.02325, 86.86)
	E.T.	0.9501	0.9531
Run 3	Φ^T_{-1}	(0.08213,-115.48)	(0.04581,-123.18)
	E.T.	0.9266	0.9140

$\Phi^R_p = (\rho^R_p, \arg(R_p))$ where ρ^R_p is the efficiency of the p^{th} reflected order and $\arg(R_p)$ is the phase of the p^{th} reflected order. E.T. specifies the total energy transmitted by the grating.

Table 2.2 Confirmation of Symmetry Properties for a Lossless Dielectric Lamellar Grating Operated in a -1 Order Littrow Mount

The properties to be shown in this table rely on the lossless structure being left-right (LR) symmetric. The following results apply to a -1 order Littrow mount.

$$X = \mathrm{Re}\left(R_0\bar{R}_{-1} + T_0\sqrt{\frac{\eta_0'}{\chi_0}}\,\bar{T}_{-1}\sqrt{\frac{\eta_{-1}}{\chi_0}}\right) = 0 \qquad \text{(P polarization)}$$

$$X = \mathrm{Re}\left(R_0\bar{R}_{-1} + T_0\sqrt{\frac{\eta_0}{\chi_0 r_3^2}}\,\bar{T}_{-1}\sqrt{\frac{\eta_{-1}}{\chi_0 r_3^2}}\right) = 0 \qquad \text{(S polarization)}$$

Grating Parameters : $d = 1.0$, $c = 0.8$, $h = 0.2$

$r_1 = 1.0$, $r_2 = 1.5$, $r_3 = 2.0$

Incidence Parameters : P polarization - $\lambda/d = 1.5$, $\phi = 48.5904^{\circ}$

S polarization - $\lambda/d = 1.6$, $\phi = 53.1301^{\circ}$

Method Parameters : P polarization - 12 modes, 21 Rayleigh orders

S polarization - 8 modes, 15 Rayleigh orders

	P polarization	S polarization
$(\lvert R_0\rvert^2, \arg(R_0))$	0.1695 , -150.95	0.2021×10^{-1}, 47.54
$(\lvert T_0\rvert^2, \arg(T_0))$	0.2918 , -22.41	0.1269×10^{1} , -21.67
$(\lvert R_{-1}\rvert^2, \arg(R_{-1}))$	0.3809×10^{-2}, -130.38	0.9678×10^{-2}, 99.41
$(\lvert T_{-1}\rvert^2, \arg(T_{-1}))$	0.3120×10^{-2}, -128.74	0.1315×10^{-2}, 84.41
X	-7.04×10^{-6}	-4.42×10^{-6}

Table 2.3 Confirmation of the Littrow Constraints Associated with the Rayleigh Field Quantities of a Lossless Dielectric Grating

The properties are applicable to a lossless LR, UD (up-down) symmetric structure operated in a -1 order Littrow mount and are given by equations (4.7-9) of §4.2 and (4.21-22, 4.43-46) of §4.3 of this thesis.

Also, for example $\Theta_p^R = (|R_p|, \arg(R_p))$.

Grating parameters : $d = 1.0$, $c/d = 0.5$, $h/d = 0.2$

$r_1 = 1.0 \quad r_2 = 1.5, \quad r_3 = 1.0$

Incidence parameters: $\lambda/d = 1.2, \quad \phi = 36.8699^\circ$

Method parameters : P polarization - 10 modes, 17 Rayleigh orders

S polarization - 8 modes, 15 Rayleigh orders

	P polarization	S polarization
Θ_0^R	$(.2001\times10^{-1}, 107.48)$	$(.4844\times10^{-3}, -76.11)$
Θ_0^T	(.9401 , 9.20)	(.9914 , 6.27)
Θ_{-1}^R	$(.1737\times10^{-1}, -71.25)$	$(.6912\times10^{-2}, 96.80)$
Θ_{-1}^T	$(.2247\times10^{-1}, -73.43)$	$(.1223\times10^{-2}, -80.74)$
Θ_1^R	$(.7083\times10^{-2}, -171.41)$	$(.8670\times10^{-2}, 131.09)$
Θ_1^T	$(.7942\times10^{-2}, -158.39)$	$(.7998\times10^{-2}, -120.19)$
Θ_{-2}^R	$(.4455\times10^{-2}, 12.29)$	$(.5216\times10^{-2}, -126.54)$
Θ_{-2}^T	$(.5155\times10^{-2}, 25.40)$	$(.6078\times10^{-2}, 139.16)$
$\mathrm{Re}(R_0\bar{R}_{-1}+T_0\bar{T}_{-1})$	5.05×10^{-6}	4.37×10^{-7}
$\mathrm{Re}(R_0\bar{T}_{-1}+R_{-1}\bar{T}_0)$	-7.50×10^{-7}	1.32×10^{-6}
$\mathrm{Re}(R_0\bar{T}_0+R_{-1}\bar{T}_{-1})$	1.02×10^{-5}	1.07×10^{-6}
$\frac{1}{2}\arg(A_0+A_{-1})$	0.62	3.89
$\frac{1}{2}\arg(A_0-A_{-1})$	16.97	1.13
$\frac{1}{2}\arg(B_0+B_{-1})$	90.03	90.73
$\frac{1}{2}\arg(B_0-B_{-1})$	91.12	97.16
$\arg(A_1+A_{-2})+(\pi)$	0.62	3.89
$\arg(A_1-A_{-2})+(\pi)$	16.97	1.11
$\arg(B_1+B_{-2})+(\pi)$	90.07	90.36
$\arg(B_1-B_{-2})+(\pi)$	91.12	97.16

Table 2.4 Confirmation of the Symmetry Properties Associated with the Modal Field Quantities of a Lossless Dielectric Lamellar Grating Operated in a -1 Order Littrow Mount

The properties to be tested are given by equations (4.49) of § 4.3.2 of this thesis. The following data was obtained for the grating configuration specified in table 2.3.

	m	X-Symm.	$\arg(a_m)+(\pi)$	$\arg(b_m)+(\pi)$
P polarization	1	odd	1.12	106.97
	2	even	90.04	0.61
	3	odd	1.12	106.97
	4	even	90.04	0.61
	5	even	90.03	0.61
	6	odd	1.12	106.97
	7	even	90.03	0.61
	8	odd	1.12	106.97
S polarization	1	odd	7.16	91.13
	2	even	90.37	3.89
	3	even	90.38	3.89
	4	odd	7.16	91.13
	5	odd	7.14	91.13
	6	even	90.36	3.89
	7	odd	7.16	91.13
	8	even	89.16	3.89

These tables must be used in conjunction with the following data obtained from the results given in table 2.3.

	P polarization	S polarization
$\frac{1}{2}\arg(R^+-T^+)$	90.04	90.37
$\frac{1}{2}\arg(R^++T^+)$	0.62	3.89
$\frac{1}{2}\arg(R^--T^-)$	91.12	97.16
$\frac{1}{2}\arg(R^-+T^-)$	16.97	1.13

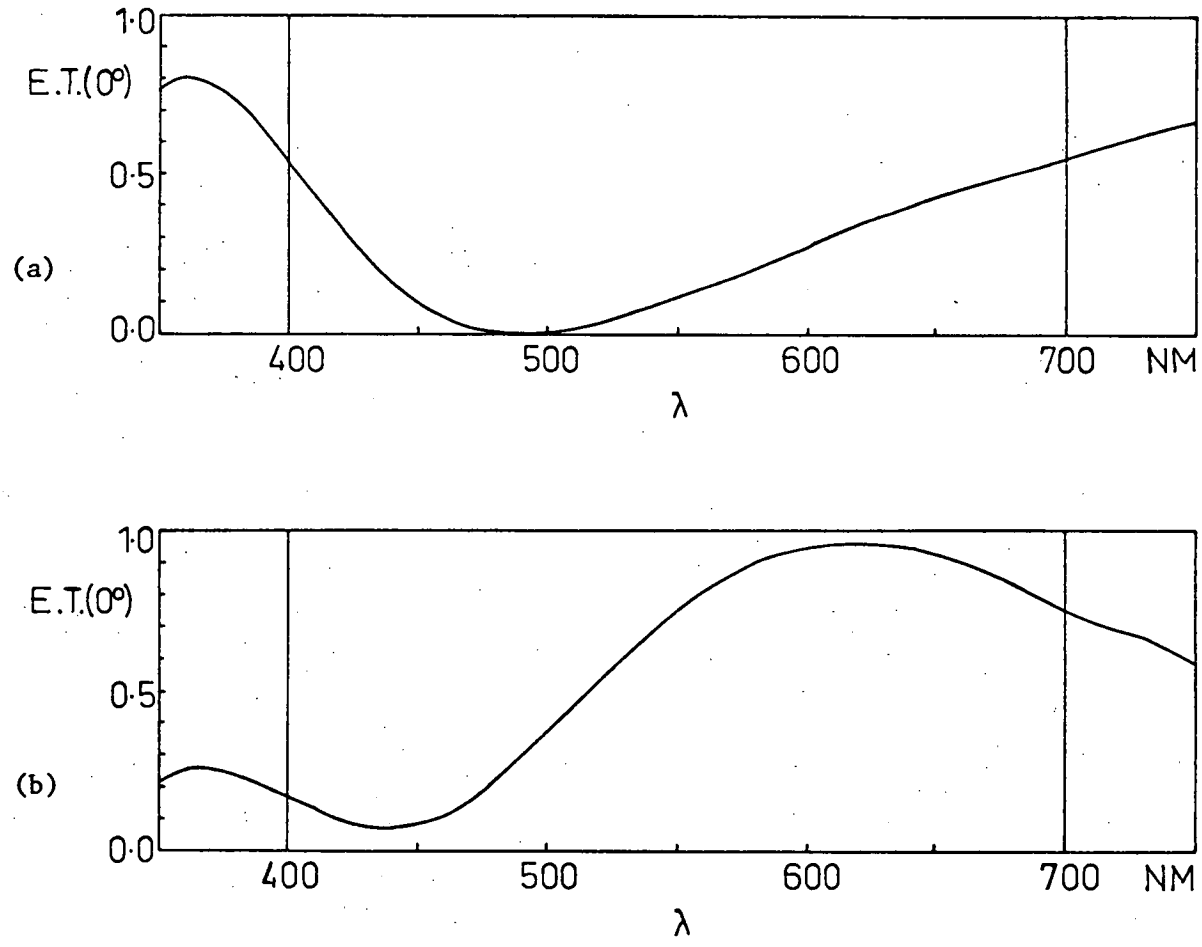

Figure 2.4 The energy transmitted by the zeroth diffracted order as a function of wavelength for the grating configuration considered by Knop [2.6], operated in S polarized normally incident radiation.
Grating parameters: d = 1.4μ, h = 1.56μ, $r_2 = r_3 = 1.5$
(a) c = 1.26μ
(b) c = 0.98μ

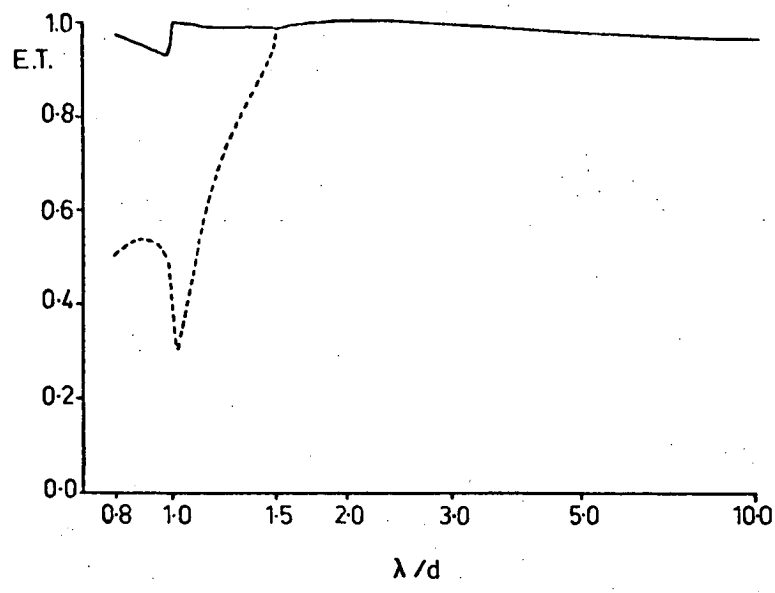

Figure 2.5 The total transmitted energy (solid line) and the energy transmitted by the zeroth order (broken line) are shown as a function of normalised wavelength (λ/d) for normally incident light ($\phi = 0^{o}$). The grating parameters are: $c/d = 0.6$, $h/d = 0.4$, $r_1 = 1.0$, $r_2 = r_3 = 1.5$. P polarized light.

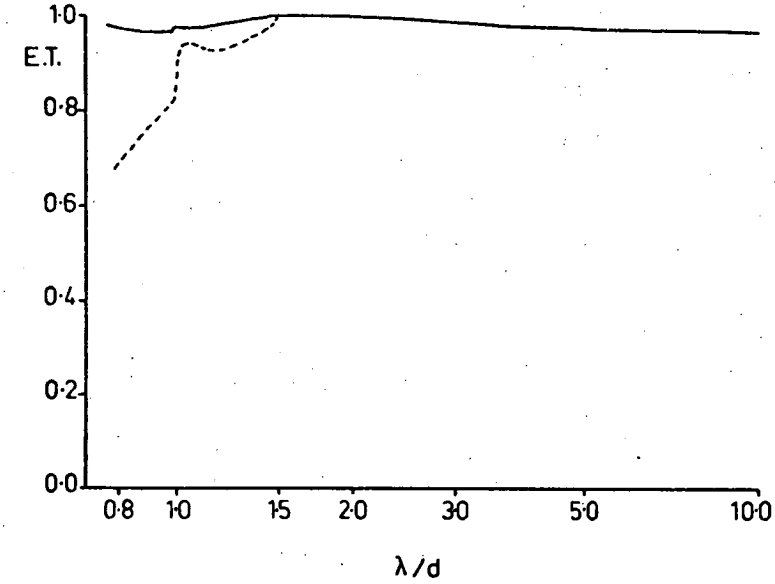

Figure 2.6 As for figure 2.5, but with S polarized light.

of the anomaly corresponding to the p^{th} order in air is given by the wavelength

$$\left.\begin{aligned} \lambda_R &= d(+1 - \sin\phi)/p && \text{for all } p > 0 \\ &= d(+1 + \sin\phi)/(-p) && \text{for all } p < 0 \end{aligned}\right\} \qquad (2.88)$$

while for the p^{th} order in the dielectric medium of refractive index r_3, the Rayleigh wavelength is

$$\left.\begin{aligned} \lambda_R' &= d(+ r_3 - \sin\phi)/p && \text{for all } p > 0 \\ &= d(+ r_3 + \sin\phi)/(-p) && \text{for all } p < 0 \end{aligned}\right\} \qquad (2.89)$$

It is also interesting to note that as the wavelength increases the energy transmitted in both polarizations tends to 96% - just the value given by Fresnel's equations for a refractive index of 1.5.

Figures 2.7, 2.8 show the performance of a glass ($r_2 = 1.5$) transmission grating operated in both P and S polarized radiation. In contrast with the previous figures the anomaly in the S polarization curve is sharper than is the P polarization anomaly. This is generally the case for diffraction gratings. At long wavelengths the incident wave no longer "sees" the grating and 100% of the incident energy is transmitted.

Figures 2.9 and 2.10 show spectra for a high refractive index ($r_2 = 5.0$) transmission grating. The striking feature of these curves is the large number of resonance anomalies that are present. These anomalies are of the type discussed by Hessel and Oliner [2.23] and are related to the leaky guided waves which the grating may support. In their description, the grating is viewed as being analogous to a multi-mode resonant cavity. After a propagating wave has passed off it becomes an evanescent wave which may resonate as its wave number approaches that of a complex guided wave supportable by the grating. This peak of intensity in the evanescent order causes a corresponding change in the

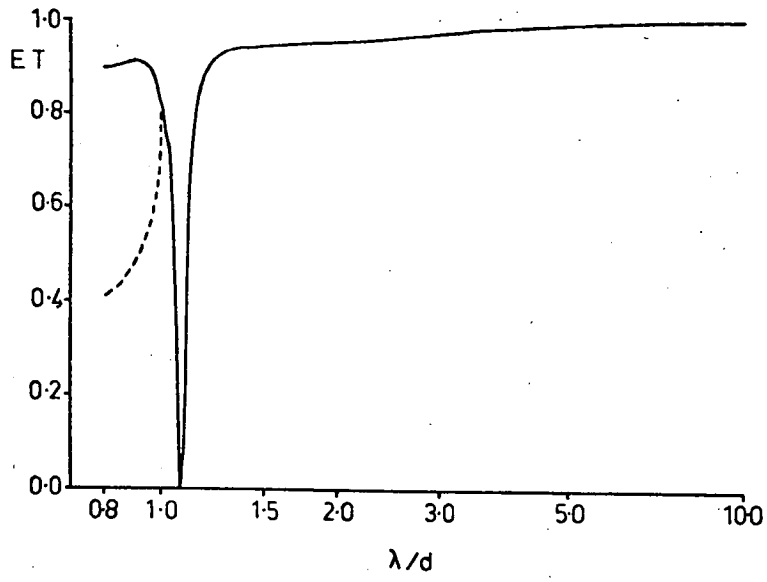

Figure 2.7 As for figure 2.5, but with $r_2 = 1.5$, $r_3 = 1.0$.

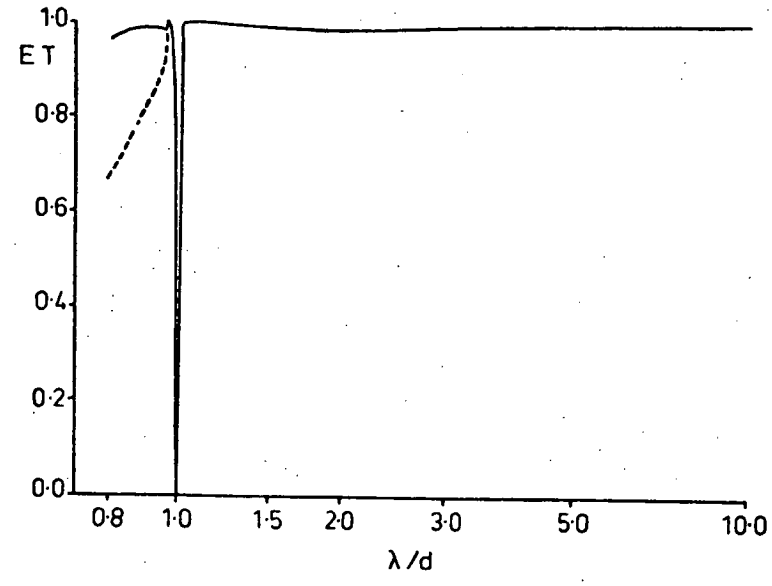

Figure 2.8 As for figure 2.6, but with $r_2 = 1.5$, $r_3 = 1.0$.

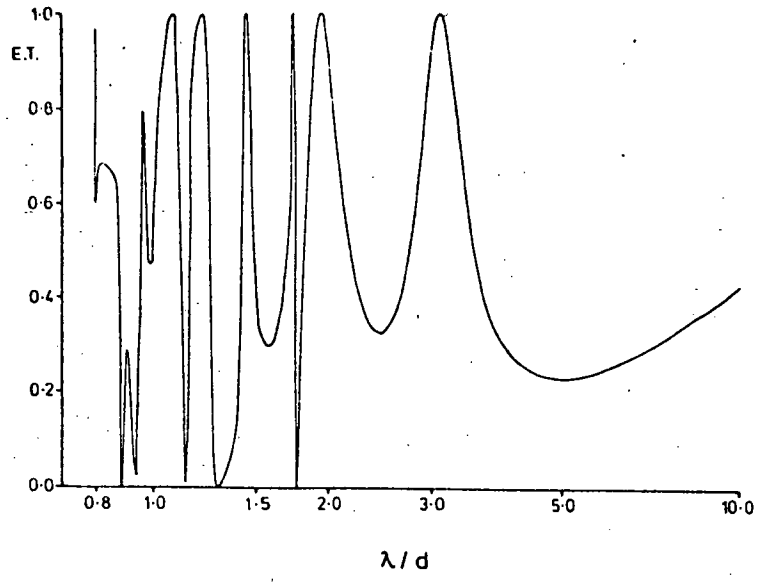

Figure 2.9 As for figure 2.5, but with $r_2 = 5.0$, $r_3 = 1.0$. (To simplify the figure, the zeroth -order energy transmission curve has been omitted).

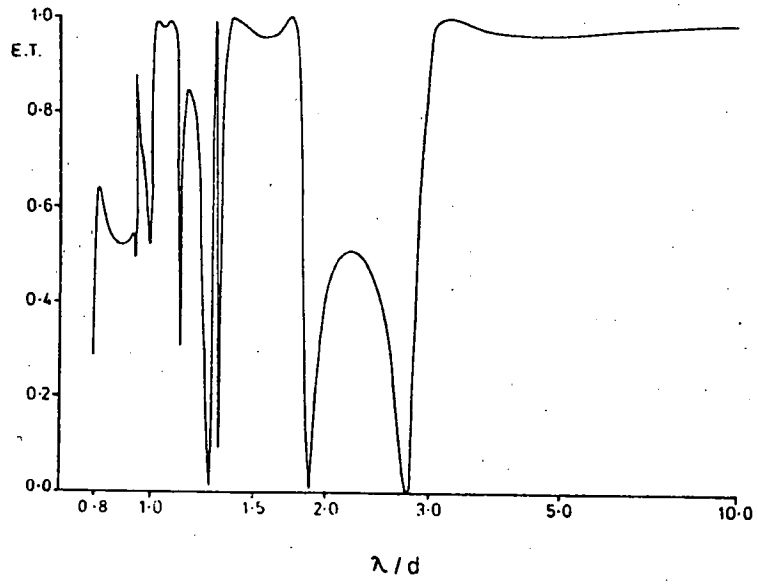

Figure 2.10 As for figure 2.9, but with S polarized light.

intensities of the propagating orders. The high Q-factor of the resonances in these figures is due to the large value of the refractive index of the dielectric and the consequent high reflectance of the groove walls. The high refractive index also permits the grating to support a large number of "propagating" modes (those for which μ_m is real) which may resonate in the vicinity of their cut-off wavelengths.

2.3.2 Numerical Investigations Concerning the Finitely Conducting Lamellar Grating

Any numerical implementation of the finitely conducting lamellar grating formalism must involve the solution of the complex, non-linear equations (2.25, 2.71) for the two fundamental polarization cases. The problem of solving such equations poses substantial numerical difficulties, as it is essential to find a complete set of roots with modulus smaller than a specified tolerance. The use of an incomplete set of eigenvalues and modes leads to intolerable numerical errors.

The numerical method initially used to determine the complex roots is based on a generalisation [2.24] to complex numbers of the standard numerical technique "Regula Falsi" [2.25]. It has proved adequate in the case where the modulus of the complex refractive index is not too large. However, when this modulus does become large, the computation times become excessive and in some cases the algorithm does not find a complete set of eigenvalues. An alternative algorithm was subsequently developed by Botten et al [2.29], based on the argument principle of complex variable theory.

The numerical implementation of the finitely conducting lamellar grating formalism has been tested using various criteria. Firstly, the numerical results obtained for structures having either purely real or purely imaginary refractive indices have been shown to agree with results

obtained from the lossless dielectric lamellar grating formalism. Secondly, the criteria of conservation of energy and the Reciprocity Theorem have been used to confirm the numerical results. A typical result of such a verification for a grating whose modulus of complex refractive index is small, is given in table 2.5. In this table the following notations are adopted for brevity:

$$\Phi_p^R = (\rho_p^R, \arg(R_p)) \quad ,$$

where ρ_p^R is the efficiency of the p^{th} reflected order, and the $\arg(R_p)$ is the phase of the p^{th} reflected order;

E.R. is the total reflected energy,

E.T. is the total transmitted energy, and

E.D. = 1 - E.R. - E.T. .

From table 2.5, it can be seen that the numerical results are in excellent accord with the Reciprocity Theorem, whether the returned order be reflected or transmitted. The agreement is slightly less satisfactory for the S polarization results than for the P polarization results. This feature is also evident in the criterion of conservation of energy (as can be seen by comparing E.D. with Q for each problem). It is a general situation in diffraction grating theory that in corresponding S and P polarization calculations, the results of numerical errors are more evident for the former than for the latter.

The results presented in table 2.6 provide confirmation of the Reciprocity Theorem and conservation of energy criterion for a finitely conducting grating, whose modulus of complex refractive index is large.

One characteristic of the present formalism is that the convergence of the modal expansions it employs grows more rapid as the ratio of groove depth to period becomes large. This characteristic has been

Table 2.5 Reciprocity Results for a Finitely Conducting Lamellar Grating

Grating parameters : $d = 1.0000$, $c = 0.4001$, $h = 0.1000$, $r_1 = 1.0$, $r_2 = 1.5 + i1.0$, $r_3 = 1.0$.

Wavelength : $\lambda = 0.80$.

Incident parameters : Problem 1 - $\phi = 11.50^\circ$, Problem 2 - $\phi = 36.91518^\circ$ Problem 3 - $\phi = -87.96276^\circ$.

Method parameters : Number of modes = 20 , Number of Rayleigh orders = 51 .

Problem	Quantity	P Polarization	S Polarization
1	$\Phi^R_{\bar{T}^1}$	$(2.8529\times10^{-2},\ 92.7502^\circ)$	$(1.6772\times10^{-2},\ -78.6682^\circ)$
	$\Phi^{\bar{T}^1}_{\bar{R}^1}$	$(3.8574\times10^{-2},\ 96.3899^\circ)$	$(2.1372\times10^{-2},\ 117.5688^\circ)$
	$\Phi^{\bar{R}^1}_0$	$(6.2128\times10^{-2},\ -139.1595^\circ)$	$(9.5755\times10^{-2},\ 32.6897^\circ)$
	Φ^T_0	$(4.6913\times10^{-1},\ 44.8301^\circ)$	$(3.9939\times10^{-1},\ 50.8365^\circ)$
	Φ^R_1	$(4.6011\times10^{-3},\ -61.1899^\circ)$	$(1.2779\times10^{-3},\ 120.5751^\circ)$
	Φ^T_1	$(5.4894\times10^{-3},\ -59.6281^\circ)$	$(3.6226\times10^{-3},\ -46.2306^\circ)$
	E.R.	0.09526	0.11381
	E.T.	0.51319	0.42438
	E.D.	0.39155	0.46181
	Q	0.39156	0.46047
2	$\Phi^R_{\bar{T}^1}$	$(2.8529\times10^{-2},\ 92.7501^\circ)$	$(1.6772\times10^{-2},\ -78.6671^\circ)$
	$\Phi^{\bar{T}^1}_{-1}$	$(3.8574\times10^{-2},\ 96.3899^\circ)$	$(2.1372\times10^{-2},\ 117.5694^\circ)$
	E.R.	0.16745	0.06755
	E.T.	0.37027	0.43902
	E.D.	0.46229	0.49343
	Q	0.46229	0.49184
3	Φ^R_1	$(4.6012\times10^{-3},\ -61.1899^\circ)$	$(1.2800\times10^{-3},\ 120.5788^\circ)$
	Φ^T_1	$(5.4894\times10^{-3},\ -59.6281^\circ)$	$(3.6223\times10^{-3},\ -46.2321^\circ)$
	E.R.	0.89431	0.82541
	E.T.	0.00993	0.02269
	E.D.	0.09575	0.15190
	Q	0.09575	0.15151

Table 2.6 Reciprocity Results for an Aluminium Grating Operated in S Polarized Radiation

Grating parameters : $d = 1.0000$, $c = 0.9001$, $h = 0.1000$, $r_1 = 1.0$, $r_2 = 1.8 + i7.12$, $r_3 = 1.0$

Wavelength : $\lambda = 0.75$

Incident parameters : Problem 1 - $\phi = 11.5^{\circ}$
2 - $\phi = 33.41039^{\circ}$

Method parameters : Number of modes = 22
Number of Rayleigh orders = 29.

Quantity	Problem 1	Problem 2
Φ^R_{-1}	$(0.1261\times10^{-1}, -103.04^{\circ})$	$(0.1261\times10^{-1}, -103.04^{\circ})$
Φ^T_{-1}	$(0.2071\times10^{-2}, 106.56^{\circ})$	$(0.2069\times10^{-2}, 106.56^{\circ})$
E.R.	0.0268	0.0504
E.T.	0.9567	0.9285
E.D.	0.0165	0.0211
Q	0.0101	0.0137

Table 2.7 Results for a Finitely Conducting Lamellar Grating with Large h/d

Grating parameters : $d = 0.0040$, $c = 0.0024$, $h = 0.8000$, $h/d = 200$, $r_1 = 1.0$, $r_2 = 2.7 + i0.5$, $r_3 = 2.7 + i0.5$.

Incidence parameters : $\lambda = 0.80$, $\phi = 0^0$.

Method parameters : Number of modes = 3,
Number of Rayleigh orders = 31.

Quantity	P Polarization	S Polarization
a_1^*	3.1734×10^{-1}	6.5833×10^{-1}
b_1^*	3.7891×10^{-1}	6.4689×10^{-1}
a_2^*	1.1223×10^{-5}	3.5221×10^{-9}
b_2^*	1.3451×10^{-5}	4.2734×10^{-9}
a_3^*	5.0528×10^{-9}	1.0174×10^{-3}
b_3^*	6.0571×10^{-9}	1.0678×10^{-3}
E.R.	0.10043	0.04284
E.T.	0.02295	0.71290
E.D.	0.87663	0.24426
Q	0.87663	0.24416

exploited previously in discussions of inductive grids [2.26, 2.27], and is well exemplified by the modal amplitudes given (for a relatively extreme case) in table 2.7. The formalism is here shown to provide results of good accuracy for a grating with a groove depth to period ratio of two hundred. When a similar calculation was attempted with the most powerful existing integral equation formalism [2.28], adequate accuracy was achievable only for values of this ratio substantially smaller than five.

It is noted that the good accuracy of the numerical results in table 2.7 is obtained with a very small number of modes used in the calculations. In fact, the accuracy of these results has been seen to be not significantly reduced if only the first mode is used in field expansions inside the grating groove region.

2.4 CONCLUSIONS

A new modal formalism has been described for determining the diffraction properties of both finitely conducting and lossless dielectric lamellar diffraction gratings. This represents the generalisation of the classical modal formalism for perfectly conducting lamellar gratings.

The lossy nature of the finitely conducting lamellar grating makes it necessary to consider not only the boundary value problem associated with the physical structure, but also that associated with the adjoint structure. The problem is much simplified in the case of a lossless dielectric lamellar grating where the diffraction problem can be expressed in a self-adjoint form. Nevertheless, both formalisms retain the elegance of the modal formalism widely used in the description of the diffraction properties of perfectly conducting lamellar gratings.

REFERENCES

[2.1] BOTTEN (L.C.), CRAIG (M.S.), McPHEDRAN (R.C.), ADAMS (J.L.), ANDREWARTHA (J.R.). - Opt. Acta, accepted.

[2.2] BOTTEN (L.C.), CRAIG (M.S.), McPHEDRAN (R.C.), ADAMS (J.L.), ANDREWARTHA (J.R.). - Opt. Acta, accepted.

[2.3] GALE (M.T.). - Phys. Bull., 1978, 29, 553.

[2.4] KNOP (K.). - Opt. Commun., 1976, 18, 298.

[2.5] KNOP (K.). - Appl. Opt., 1978, 17, 3598.

[2.6] KNOP (K.). - J. Opt. Soc. Am., 1978, 68, 1206.

[2.7] BURCKHARDT (C.B.). - J. Opt. Soc. Am., 1966, 56, 1502.

[2.8] NEVIÈRE (M.), VINCENT (P.), PETIT (R.). - Nouv. Rev. Opt., 1974, 5, 65.

[2.9] PETIT (R.). - Topics in Current Physics, Vol 22,"Electromagnetic Theory of Gratings", Springer-Verlag, Heidelberg, 1980.

[2.10] HORWITZ (C.M.). - Opt. Commun., 1974, 11, 210.

[2.11] ROUMIGUIERES (J.L.), MAYSTRE (D.), PETIT (R.). - Opt. Commun., 1973, 7, 4.

[2.12] FRANKS (A.), LINDSAY (V.), BENNET (J.M.), SPEER (R.J.), TURNER (D.), HUNT (D.J.). - Philos. Trans. R. Soc., Ser.A, 1975, 277, 503.

[2.13] DERIUGIN (L.N.). - Radiotekhnika, 1960, 15, 15.

[2.14] DERIUGIN (L.N.). - Radiotekhnika, 1960, 15, 9.

[2.15] WIRGIN (A.), DELEUIL (R.). - J. Opt. Soc. Am., 1969, 59, 1348.

[2.16] MAYSTRE (D.), PETIT (R.). - Opt. Commun., 1972, 5, 90.

[2.17] MARCUSE (D.). - J. Opt. Soc. Am., 1974, 64, 794.

[2.18] Lord RAYLEIGH. - Proc. Roy. Soc. A, 1907, 79, 399.

[2.19] HARRINGTON (R.F.). - "Field Computation by Moment Methods", (London: Collier - Macmillan), 1968.

[2.20] EASTHAM (M.S.P.). - "The Spectral Theory of Periodic Differential Equations" (Edinburgh: Scottish Academic Press), 1973.

[2.21] CODDINGTON (E.A.), LEVINSON (N.). - "Theory of Ordinary Differential Equations" (London: McGraw-Hill), 1955.

[2.22] BOTTEN (L.C.), ADAMS (J.L.), McPHEDRAN (R.C.), DERRICK (G.H.). - J. Optics (Paris), 1980, 11, 43.

[2.23] HESSEL (A.), OLINER (A.A.). - Appl. Opt., 1965, 4, 1275.

[2.24] CLAYTON (E.), DERRICK (G.H.). - Aust. J. Phys., 1977, 30, 15.

[2.25] HAMMING (R.W.). - "Numerical Methods for Scientists and Engineers" (New York : McGraw-Hill), 1973, p 64-67.

[2.26] CHEN (C.- C.). - I.E.E.E. Trans. MTT-19, 1971, 475.

[2.27] McPHEDRAN (R.C.), MAYSTRE (D.). - Appl. Phys., 1977, 14, 1.

[2.28] MAYSTRE (D.). - J. Opt. Soc. Am., 1978, 68, 490.

[2.29] BOTTEN (L.C.), CRAIG (M.S.), McPHEDRAN (R.C.). - private communication.

CHAPTER 3

DIFFRACTION PROPERTIES OF DOUBLE GRATINGS AND THEIR APPLICATION AS FABRY-PEROT INTERFEROMETERS

3.1 INTRODUCTION

In this chapter, the diffraction properties of a double grating are discussed. This structure is composed of two singly periodic, perfectly conducting, lamellar transmission gratings lying in closely spaced, separated parallel planes and arranged so that the two axes of periodicity are mutually parallel.

These investigations, which are the subject of a paper [3.1] published in the Journal of Optics (Paris), were motivated by the widespread use of multi-element gratings as the reflecting elements in Fabry-Perot interferometers and as interference filters in the far infrared. Many theoretical and experimental studies, which are reviewed in chapter 1 of this thesis, have been undertaken to describe the interferometric properties of multi-element gratings. However, most of the theoretical investigations so far have been based on scalar-optics descriptions of individual grating (or grid) elements. There were several exceptions to this description which should be mentioned.

One of the earliest rigorous theories describing diffraction by a double grating was presented by Blok and Mur [3.2] in 1972. Their analysis was performed for the two fundamental polarizations using an integral equation technique and was limited to gratings having infinitesimally thin arrays of identical period. However, few numerical results were presented and the interferometric nature of the grating was not examined. Since the study reported in this chapter was completed,

investigations of the interferometric properties of filters composed of an arbitrary number of gratings have been undertaken by Botten [3.3] and Botten et al [3.4].

In this chapter, the diffraction of a plane wave, incident at an arbitrary angle, by a double grating is considered. The analysis is more general than that presented by Blok and Mur, since gratings having finite thickness arrays of different periods are considered. The only necessary condition that must be added is that the ratio of the two periods is a rational number.

The diffraction problem is formulated in two different ways, each by applying the Method of Moments. The first method involves the solution of the diffraction problem for the two fundamental types of polarization, P and S. The Rayleigh field amplitudes so derived are then combined using the method of Petit and Maystre [3.7] to determine the Rayleigh field amplitudes for the conical diffraction problem. The second formalism employs a method similar to that described in chapter 8 of this thesis, where the behaviour of the four field components defining the problem is explicitly considered. This latter method is detailed in [3.5] but is not included here for the sake of brevity.

The interferometric aspects of the double grating are discussed in section 3.3.2. Attention is focussed mainly on the performance of the structure in P polarized radiation since the operation of high resolution interferometers relies upon the use of highly reflecting elements. This study has confirmed the application of double gratings in long wavelength Fabry-Perot interferometers and also theoretically examines the individual effects of the design parameters. It is shown that a double grating, composed of identical lamellar arrays having deep

grooves and relatively narrow apertures, can produce an interferometer with very high finesse. If the incident radiation is unpolarized, it is necessary to construct the interferometer from polarization independent filters such as doubly periodic inductive grids. Investigations into the diffraction properties of the double grid are described in chapter 6 of this thesis.

Section 3.3.3 discusses the operation of the double grating in S polarized radiation. Although this configuration is not applicable as an interferometer, an analysis of the features of the S polarization spectra is included for completeness and again the individual effects of the grating parameters are determined.

3.2 THEORETICAL FORMALISMS

3.2.1 Definition of the Diffraction Problem

Consider a plane wave incident with an oblique wave vector $\underline{k}$ (i.e. in conical diffraction) upon the double grating depicted in figure 3.1a. A rectangular Cartesian coordinate system, with unit vectors $\hat{\underline{x}}$, $\hat{\underline{y}}$ and $\hat{\underline{z}}$ is chosen so that the OY axis is orthogonal to the grating surface and the array grooves are aligned with the OZ axis. The upper and lower surfaces of the arrays are taken to lie at $y = s + \frac{1}{2}h$, $s - \frac{1}{2}h$, $-s + \frac{1}{2}h'$ and $-s - \frac{1}{2}h'$. The apertures in the upper array are of width c and spaced periodically along OX with period d. The lower array has periodicity d' along OX, aperture width c' and is displaced in the X-direction by an amount δx relative to the upper array (see figure 3.1a).

The overall period d_T of the grating structure is the "lowest common multiple" of d and d'. It is worth noting that if the ratio d'/d is irrational then the structure is aperiodic (i.e. the grating

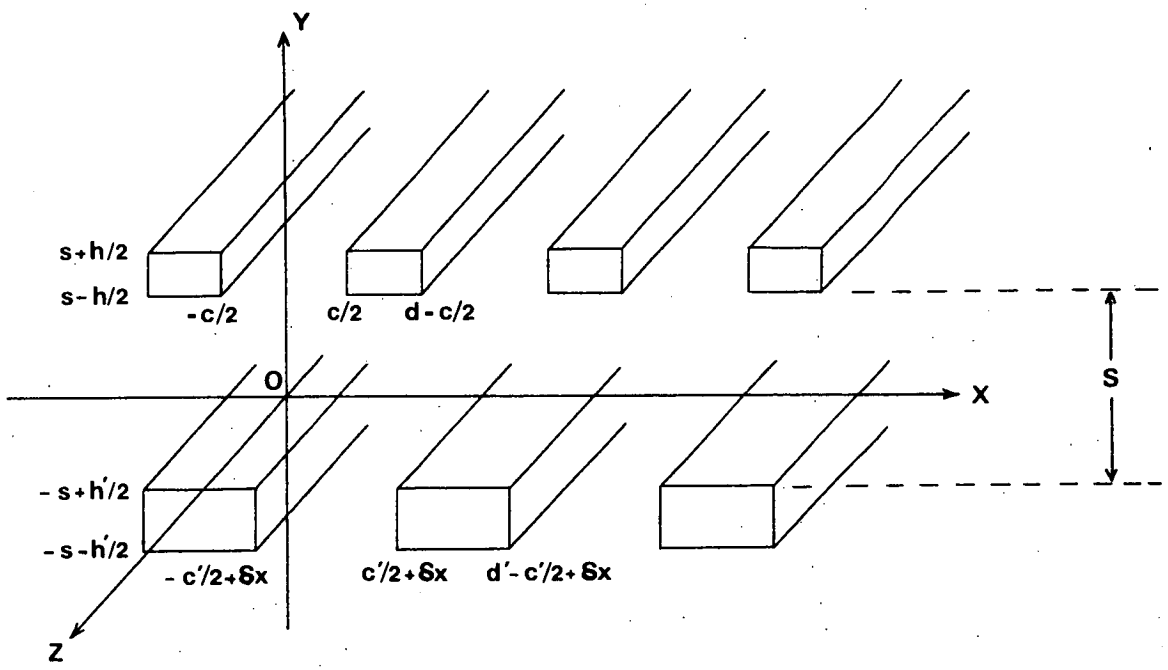

Figure 3.1a The geometry of the double grating.

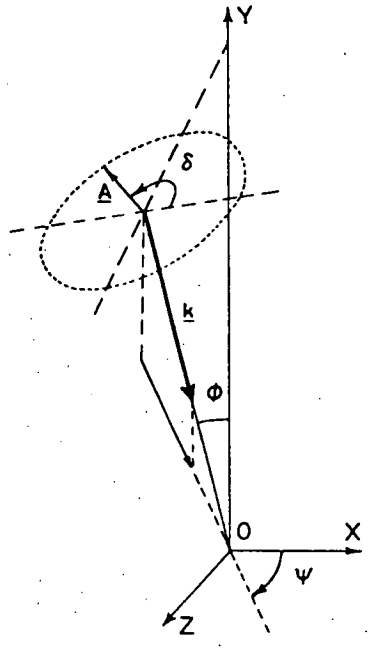

Figure 3.1b Specification of the incident field.

period is infinite) and an unlimited number of "real" orders can propagate giving rise to a continuous spectrum of plane waves.

The geometry of the incident field for the conical diffraction problem is defined as follows: The wave vector $\underline{k}$ of the incident wave strikes the grating in a direction specified by the angles ϕ and ψ (see figure 3.1b). ϕ is the angle between $\underline{k}$ and the OY axis, while ψ is the angle between the projection of $\underline{k}$ onto the XOZ plane and the OX axis. Thus if α_0, β_0 and γ_0 represent the direction cosines of the incident beam and $k = 2\pi/\lambda$ is the wave number of the incident wave, then

$$\underline{k} = (\alpha_0, -\beta_0, \gamma_0)$$

and

$$\left.\begin{aligned} \alpha_0 &= k \sin\phi \cos\psi \\ \beta_0 &= k \cos\phi \\ \gamma_0 &= k \sin\phi \sin\psi \end{aligned}\right\} \qquad (3.1)$$

Throughout the following analysis, the time varying term $\exp(-i\omega t)$ in all field representations is suppressed. Then the electric and magnetic field vectors of the incident wave can be written respectively

$$\underline{E}^i = \underline{A}\{\exp[i\ (\alpha_0 x - \beta_0 y + \gamma_0 z)]\}/\sqrt{d_T} \qquad (3.2)$$

$$\underline{H}^i = \underline{B}\{\exp[i\ (\alpha_0 x - \beta_0 y + \gamma_0 z)]\}/\sqrt{d_T} \qquad (3.3)$$

The polarization of the incident wave is defined by introducing an angle δ such that when $\delta = 90^\circ$ the vector amplitude of the incident electric field $\underline{A}$ lies in the plane of incidence, and when $\delta = 0^\circ$, $\underline{A}$ is orthogonal to the plane of incidence.

By normalising the moduli of the vector amplitudes $\underline{A}$ and $\underline{B}$, the following expressions are obtained for the Cartesian components of the incident fields:

$$\left.\begin{aligned} A_x &= \sin\psi\cos\delta + \sin\delta\cos\phi\cos\psi \\ A_y &= \sin\delta\sin\phi \\ A_z &= \cos\phi\sin\psi\sin\delta - \cos\delta\cos\psi \end{aligned}\right\} \qquad (3.4)$$

and

$$\left.\begin{aligned} B_x &= ik(\cos\delta\cos\phi\cos\psi - \sin\delta\sin\psi) \\ B_y &= ik(\cos\delta\sin\phi) \\ B_z &= ik(\cos\delta\cos\phi\sin\psi + \sin\delta\cos\psi) \end{aligned}\right\} \qquad (3.5)$$

In deriving expressions for B_x, B_y and B_z, a constant multiplying factor $(\frac{1}{i\omega\mu_0})$ has been suppressed.

3.2.2 Outline of the Theoretical Approach

The diffraction problem is solved by determining the diffraction properties of the double grating operated in a classical mount in both P and S polarized radiation and then applying Petit and Maystre's theorem of conical diffraction [3.6, 3.7]. These authors showed that the efficiency of a perfectly conducting grating operated in a conical diffraction mount can be derived from the efficiencies of the same grating operated in the two fundamental polarizations (with the wavevectors lying in the XOY plane).

For this reason the following subsections discuss the diffraction properties of the double grating operated in each fundamental polarization. A complete description of the formalism appropriate to the diffraction of a P polarized plane wave (whose wavevector lies in the XOY plane, $\psi=0^\circ$) by the double grating is presented and modifications required when considering S polarized radiation are indicated in the following section (3.2.4).

3.2.3 Solution of the P Polarization Diffraction Problem

In this case the component of the electric vector $\underline{E}$ is aligned

with the grooves i.e. $\underline{E} = E_z(x,y)\ \hat{z}$.

The incident field can now be written as

$$\underline{E}^i(x,y) = \frac{1}{\sqrt{d_T}} \exp[i(\alpha_0' x - \beta_0' y)]\ \hat{z} \tag{3.6}$$

where

$$\left.\begin{aligned} \alpha_0' &= k \sin\phi \\ \beta_0' &= k \cos\phi \end{aligned}\right\} \quad . \tag{3.7}$$

Diffracted plane wave fields propagating above, below and between the arrays are produced when the field is incident upon the grating. It may be shown that the reflected fields can be written as the superposition of plane wave terms of the form

$$P_p(x,y) = \exp[i(\alpha_p' x + \beta_p' y)]/\sqrt{d_T} \tag{3.8}$$

where $$\alpha_p' = \alpha_0' + 2\pi p/d_T \quad , \tag{3.9}$$

$$\left.\begin{aligned} \beta_p' &= \sqrt{k^2 - \alpha_p'^2} \qquad \text{if} \quad \alpha_p'^2 \le k^2 \\ &= i\sqrt{\alpha_p'^2 - k^2} \qquad \text{otherwise} \end{aligned}\right\} \quad . \tag{3.10}$$

Correspondingly, the transmitted field expansion is composed of terms of the form

$$\hat{P}_p(x,y) = \exp[i(\alpha_p' x - \beta_p' y)]/\sqrt{d_T} \ . \tag{3.11}$$

In the region between each of the two arrays, the field must be expanded using both upward (equation (3.8)) and downward (equation (3.11)) going plane waves.

Since the diffracted fields have the same polarization as the incident field, all non-trivial field components may be expanded in terms of the scalar field quantity representing the z (non-zero) component of the electric field (E_z).

3.2.3.1 *Boundary Conditions and Specification of the Field Expansions*

Although Rayleigh expansions are used to describe the fields in all semi-infinite free space regions, they are not valid descriptions of the field excited within the grooves (3.8, 3.9). Instead, the fields in the apertures are specified by superposition of waveguide modes and the fields within the different regions are matched by applying conditions of continuity on all grating surfaces. The continuity conditions to be applied to the problem are that E_z and its normal derivative $\frac{\partial E_z}{\partial y}$ be continuous across aperture-free space interfaces and that E_z be zero on metal walls.

The fields in the different free space regions are written in terms of the following Rayleigh expansions

$$E_z(x,y) = \frac{1}{\sqrt{d_T}}\exp[i(\alpha_0' x - \beta_0' y)] + \sum_{p=-\infty}^{\infty} C_p P_p(x,y) \quad \text{if} \quad y > s + \frac{h}{2} \tag{3.12}$$

$$= \sum_{p=-\infty}^{\infty} [C_p^{+} P_p(x,y) + C_p^{-} \hat{P}_p(x,y)] \quad \text{if} \quad -s + \frac{h'}{2} < y < s - \frac{h}{2} \tag{3.13}$$

$$= \sum_{p=-\infty}^{\infty} \hat{C}_p \hat{P}_p(x,y) \quad \text{if} \quad y \quad -s - \frac{h'}{2} \tag{3.14}$$

In order to characterise the modal expansions, the following definitions are made.

$$\left.\begin{aligned} N &= \frac{d_T}{d} - 1 \\ N' &= \frac{d_T}{d'} - 1 \end{aligned}\right\} \tag{3.15}$$

$$\Delta = \{\text{integer } \ell \mid 0 \leq \ell \leq N\}$$

and $$\Delta' = \{\text{integer } \ell \mid 0 \leq \ell \leq N'\}$$

Note that there are (N+1) grooves in the upper array and (N'+1) grooves

in the lower array for each period d_T of the double grating. The appropriate forms of the mode structure corresponding to the field component E_z for the upper and lower grooves are then given by the functions $U_m^{\ell}(x)$ and $L_m^{\ell'}(x)$ respectively which are defined as follows:

$$U_m^{\ell}(x) = \sqrt{\frac{2}{c}} \sin\left[\frac{m\pi}{c}\left(x + \frac{c}{2} - \ell d\right)\right] \tag{3.16}$$

and

$$L_m^{\ell'}(x) = \sqrt{\frac{2}{c'}} \sin\frac{m\pi}{c'}\left(x + \frac{c'}{2} - \delta x - \ell' d'\right)] \tag{3.17}$$

where $\ell \in \Delta$ and $\ell' \in \Delta'$.

Each of the functions introduced above satisfies the appropriate boundary conditions on the aperture walls. These modal functions may be derived by following the work of Wirgin [3.10].

The electric field in the upper grooves can then be written

$$E_z(x,y) = \sum_{m=1}^{\infty} \left[c_m^{\ell} \sin(\mu_m(y-s)) + d_m^{\ell} \cos(\mu_m(y-s))\right] U_m^{\ell}(x) \tag{3.18}$$

for $x \in \left[\ell d - \frac{c}{2},\ (\ell + 1)d - \frac{c}{2}\right]$ and $\ell \in \Delta$.

In order that each mode satisfies the Helmholtz equation,

$$\mu_m = \sqrt{k^2 - \left(\frac{m\pi}{c}\right)^2}$$

The field in the lower grooves is specified by the waveguide modal expansion

$$E_z(x,y) = \sum_{m=1}^{\infty} \left[\hat{c}_m^{\ell} \sin(\hat{\mu}_m(y + s)) + \hat{d}_m^{\ell} \cos(\hat{\mu}_m(y + s))\right] L_m^{\ell}(x) \tag{3.19}$$

for $x \in \left[\ell d' - \frac{c'}{2} + \delta x,\ (\ell+1)d' - \frac{c'}{2} + \delta x\right]$ and $\ell \in \Delta'$

where $\hat{\mu}_m = \sqrt{k^2 - (\frac{m\pi}{c'})^2}$

3.2.3.2 *Solution of the Diffraction Problem*

The continuity conditions are applied across the surfaces $y = s + \frac{h}{2}$, $s - \frac{h}{2}$, $-s + \frac{h'}{2}$, $-s - \frac{h'}{2}$ and the resulting equations are solved using the Method of Moments.

Consider the continuity of the electric field at $y = s + \frac{h}{2}$. This can be written

$$\sum_p [C_p Y_p(s+\tfrac{h}{2}) + Y_0^{-1}(s+\tfrac{h}{2})\delta_{p0}]\, P_p(x,0) = \sum_{m=1}^{\infty} [c_m^{\ell *} + d_m^{\ell *}]\, U_m^{\ell}(x)$$

$$\text{if } x \in [\ell d - \tfrac{c}{2},\ (\ell+1)d - \tfrac{c}{2}]$$

$$= 0 \quad \text{otherwise} \qquad (3.20)$$

where $Y_p(y) = \exp(i\beta_p' y)$,

$$c_m^{\ell *} = c_m^{\ell} \sin(\mu_m \tfrac{h}{2}) \ ,$$

and $$d_m^{\ell *} = d_m^{\ell} \cos(\mu_m \tfrac{h}{2}) \ .$$

Using the Method of Moments, this equation is multiplied by $\overline{R}_q(x,0)$ (where the bar denotes complex conjugation) and integrated over the period $x \in [-\frac{c}{2}\ ,\ d_T - \frac{c}{2}]$. The orthogonality properties of the plane wave terms can be written

$$\int_0^{d_T} P_p(x,0)\overline{P}_q(x,0)dx = \delta_{pq} \qquad (3.21)$$

and thus

$$C_q Y_q(s+\tfrac{h}{2}) + Y_0^{-1}(s+\tfrac{h}{2})\ \delta_{q0} = \sum_{m=1}^{\infty} \sum_{\ell=0}^{N} [c_m^{\ell *} + d_m^{\ell *}]\, J_{qm}^{\ell} \qquad (3.22)$$

where the modal inner product J_{qm}^{ℓ}, defined by

$$J_{qm}^{\ell} = \sqrt{\frac{2}{cd_T}} \int_{\ell d-c/2}^{\ell d+c/2} \sin[\frac{m\pi}{c}(x + \frac{c}{2} - \ell d)] \exp[-i\alpha_q' x]\, dx \qquad (3.23)$$

can be evaluated analytically.

A similar analysis for the continuity of E_z at $y = s - \frac{h}{2}$ yields

$$C_q^+ Y_q(s - \tfrac{h}{2}) + C_q^- Y_q^{-1}(s - \tfrac{h}{2}) = \sum_{m=1}^{\infty} \sum_{\ell=0}^{N} [-c_m^{\ell *} + d_m^{\ell *}]\, J_{qm}^{\ell} \qquad (3.24)$$

The continuity of E_z at $y = -s + \frac{h'}{2}$ can be written

$$\sum_p [C_p^+ Y_p(-s + \tfrac{h'}{2}) + C_p^- Y_p^{-1}(-s + \tfrac{h'}{2})]\, P_p(x,0) = \sum_{m=1}^{\infty} [\hat{c}_m^{\ell *} + \hat{d}_m^{\ell *}]\, L_m^{\ell}(x)$$

$$\text{if } x \in [\ell d' + \delta x - \tfrac{c'}{2}, (\ell+1)d' - \tfrac{c'}{2} + \delta x]$$

$$= 0 \quad \text{otherwise} . \qquad (3.25)$$

Here $\hat{c}_m^{\ell *} = \hat{c}_m^{\ell} \sin(\hat{\mu}_m \frac{h'}{2})$,

and $\hat{d}_m^{\ell *} = \hat{d}_m^{\ell} \cos(\hat{\mu}_m \frac{h'}{2})$.

This equation is multiplied throughout by $\overline{R}_q(x,0)$ and integrated over the region $x \in [\delta x - \frac{c'}{2}, d_T + \delta x - \frac{c'}{2}]$ to give the following equation

$$C_q^+ Y_q(-s + \tfrac{h'}{2}) + C_q^- Y_q^{-1}(-s + \tfrac{h'}{2}) = \sum_{m=1}^{\infty} \sum_{\ell=0}^{N'} [\hat{c}_m^{\ell *} + \hat{d}_m^{\ell *}]\, K_{qm}^{\ell} \qquad (3.26)$$

where the following inner product has been introduced:

$$K_{qm}^{\ell} = \sqrt{\frac{2}{c'd_T}} \int_{\delta x+\ell d'-c'/2}^{\delta x+\ell d'+c'/2} \sin[\frac{m\pi}{c'}(x + \frac{c'}{2} - \delta x - \ell d')] \exp[-i\alpha_q' x]\, dx \qquad (3.27)$$

Similarly, by applying the continuity of E_z at $y = -s - \frac{h'}{2}$, the following equation is obtained

$$\hat{C}_q \, Y_q^{-1}(-s - \tfrac{h'}{2}) = \sum_{m=1}^{\infty} \sum_{\ell=0}^{N'} [-\hat{c}_m^{\ell *} + \hat{d}_m^{\ell *}] \, K_{qm}^{\ell} \tag{3.28}$$

The continuity of $\frac{\partial E_z}{\partial y}$ is now applied at all free space-aperture interfaces. At $y = s + \frac{h}{2}$

$$\sum_p \{ i\beta'_p [C_p Y_p(s+\tfrac{h}{2}) - Y_0^{-1}(s+\tfrac{h}{2})\delta_{p0}] \, P_p(x,0)\} = \sum_{m=1}^{\infty} [D_{1m} c_m^{L*} + D_{2m} d_m^{L*}] \, U_m^L(x)$$

$$\text{if } x \in [Ld - \tfrac{c}{2}, \, Ld + \tfrac{c}{2}]$$

$$\text{and for each } L \in \Delta \tag{3.29}$$

where $D_{1m} = \mu_m \cot(\mu_m \frac{h}{2})$

and $D_{2m} = -\mu_m \tan(\mu_m \frac{h}{2})$.

Multiplying both sides of this equation by $\bar{U}_M^L(x,z)$ and integrating over the aperture $x \in [Ld - \frac{c}{2}, \, Ld + \frac{c}{2}]$ yields

$$\sum_p \{ i\beta'_p [C_p Y_p(s+\tfrac{h}{2}) - Y_0^{-1}(s+\tfrac{h}{2})\delta_{p0}] \, \bar{J}_{pM}^L \} = D_{1M} c_M^{L*} + D_{2M} d_M^{L*} \tag{3.30}$$

where $M \in [1, \infty)$, $L \in \Delta$,

and the following orthonormality of the modal basis has been used:

$$\int_{Ld-c/2}^{Ld+c/2} U_m^{\ell}(x) \, \bar{U}_M^L(x) \, dx = \delta_{mM} \tag{3.31}$$

Similarly by applying the continuity of $\frac{\partial E_z}{\partial y}$ at $y = s - \frac{h}{2}$, the following equation is obtained

$$\sum_p \{i\beta_p'[C_p^+ Y_p(s - \tfrac{h}{2}) - C_p^- Y_p^{-1}(s - \tfrac{h}{2})]\ \bar{J}_{pM}^L\} = D_{1M} c_M^{L*} - D_{2M} d_M^{L*} \qquad (3.32)$$

$$M \in [1, \infty) \quad , \quad L \in \Delta$$

The Method of Moments is applied to the equations derived from consideration of the continuity of $\frac{\partial E_z}{\partial y}$ at $y = -s + \frac{h'}{2}$, $y = -s - \frac{h'}{2}$, by multiplying by $\bar{L}_M^L(x)$ and integrating over the aperture $x \in [Ld' + \delta x - \frac{c'}{2}$, $Ld' + \delta x + \frac{c'}{2}]$. Here $M \in [1, \infty)$, $L \in \Delta'$. The following equations are obtained using this procedure.

$$\sum_p \{i\beta_p'[C_p^+ Y_p(-s + \tfrac{h'}{2}) - C_p^- Y_p^{-1}(-s + \tfrac{h'}{2})]\ \bar{K}_{pM}^L\} = D_{3M} \hat{c}_M^{L*} + D_{4M} \hat{d}_M^{L*} \qquad (3.33)$$

$$\sum_p \{-i\beta_p' \hat{C}_p Y_p^{-1}(-s - \tfrac{h'}{2})\ \bar{K}_{pM}^L\} = D_{3M} \hat{c}_M^{L*} - D_{4M} \hat{d}_M^{L*} \qquad (3.34)$$

where $D_{3m} = \hat{\mu}_m \cot(\hat{\mu}_m \frac{h'}{2})$,

and $D_{4m} = -\hat{\mu}_m \tan(\hat{\mu}_m \frac{h'}{2})$.

Thus, four electric and four magnetic field equations linking the eight sets of unknown Rayleigh and modal coefficients have been derived. Following some elementary but tedious manipulation, four independent matrix equations in the four infinite sets of modal coefficients can be derived. These are

$$\sum_{m=1}^{\infty} \sum_{\ell=0}^{N} \{c_m^{\ell*}[\sum_p i\beta_p' J_{pm}^{\ell} \bar{J}_{pM}^L - D_{1m}\delta_{mM}\delta_{\ell L}] + d_m^{\ell*}[\sum_p i\beta_p' J_{pm}^{\ell} \bar{J}_{pM}^L - D_{2m}\delta_{mM}\delta_{\ell L}]\}$$

$$= 2i\beta_0' Y_0^{-1}(s+\tfrac{h}{2})\ \bar{J}_{0M}^L \qquad L \in \Delta \qquad (3.35)$$

$$\sum_{m=1}^{\infty}\sum_{\ell=0}^{N}\{-c_m^{\ell *}[\sum_p H_p J_{pm}^{\ell}\bar{J}_{pM}^{L} + D_{1m}\delta_{mM}\delta_{\ell L}] + d_m^{\ell *}[\sum_p H_p J_{pm}^{\ell}\bar{J}_{pM}^{L} + D_{2m}\delta_{mM}\delta_{\ell L}]\}$$

$$- \sum_{m=1}^{\infty}\sum_{\ell=0}^{N'}\{\hat{c}_m^{\ell *}[\sum_p G_p K_{pm}^{\ell}\bar{J}_{pM}^{L}] - \hat{d}_m^{\ell *}[\sum_p G_p K_{pm}^{\ell}\bar{J}_{pM}^{L}]\} = 0 \qquad L \in \Delta \qquad (3.36)$$

where $$G_p = \frac{\beta'_p}{\sin(\beta'_p S)} ,$$

$$H_p = \beta'_p \cot(\beta'_p S) ,$$

and $$S = 2s - \frac{h}{2} - \frac{h'}{2} .$$

$$\sum_{m=1}^{\infty}\sum_{\ell=0}^{N}\{-c_m^{\ell *}[\sum_p G_p J_{pm}^{\ell}\bar{K}_{pM}^{L}] + d_m^{\ell *}[\sum_p G_p J_{pm}^{\ell}\bar{K}_{pM}^{L}]\}$$

$$+ \sum_{m=1}^{\infty}\sum_{\ell=0}^{N'}\{-\hat{c}_m^{\ell *}[\sum_p H_p K_{pm}^{\ell}\bar{K}_{pM}^{L} + D_{3m}\delta_{mM}\delta_{\ell L}] - \hat{d}_m^{\ell *}[\sum_p H_p K_{pm}^{\ell}\bar{K}_{pM}^{L} + D_{4m}\delta_{mM}\delta_{\ell L}]\}$$

$$= 0 \qquad L \in \Delta' \qquad (3.37)$$

and

$$\sum_{m=1}^{\infty}\sum_{\ell=0}^{N'}\{\hat{c}_m^{\ell *}[\sum_p i\beta'_p K_{pm}^{\ell}\bar{K}_{pM}^{L} - D_{3m}\delta_{mM}\delta_{\ell L}] - \hat{d}_m^{\ell *}[\sum_p i\beta'_p K_{pm}^{\ell}\bar{K}_{pM}^{L} - D_{4m}\delta_{mM}\delta_{\ell L}]\}$$

$$= 0 \qquad L \in \Delta' \qquad (3.38)$$

In the above equations, $M \in [1, \infty)$. Once equations (3.35 - 3.38) are solved, the Rayleigh coefficients can be reconstructed using equations (3.22, 3.28) and the efficiencies in reflection and transmission evaluated.

3.2.4 Solution of the S Polarization Diffraction Problem

In this case, the component of the magnetic vector $\underline{H}$ is aligned with the grooves

$$\underline{H}(x,y,z) = H_z(x,y)\hat{\underline{z}} \qquad \text{only} \tag{3.39}$$

The non-trivial fields for this problem may be derived from the scalar field quantity H_z.

The differences occurring between the solution of the S polarization diffraction problem and that given in the previous section for a P polarized wave field arise because of the different boundary conditions which apply to the two polarizations. The continuity conditions applicable to the S polarization problem are that

(1) H_z is continuous across groove-free space interfaces, and

(2) $\frac{\partial H_z}{\partial y}$ is continuous across groove-free space interfaces and equal to zero on metal surfaces.

The free space magnetic fields are specified by the Rayleigh expansions (3.12 - 14) but with the Rayleigh coefficients $\{C_p\}$, $\{C_p^+\}$. $\{C_p^-\}$ and $\{\hat{C}_p\}$ replaced by $\{D_p\}$, $\{D_p^+\}$, $\{D_p^-\}$ and $\{\hat{D}_p\}$ respectively.

For this polarization, the mode functions corresponding to the field component H_z in the upper and lower grooves are given respectively by

$$U_m^{\ell}(x) = \sqrt{\frac{2}{c}} \cos\left[\frac{m\pi}{c}(x + \frac{c}{2} - \ell d)\right]$$

and $$L_m^{\ell}(x) = \sqrt{\frac{2}{c'}} \cos\left[\frac{m\pi}{c'}(x + \frac{c'}{2} - \delta x - \ell' d')\right]$$

where $\ell \in \Delta$ and $\ell' \in \Delta'$.

The fields in the groove regions are then specified by the modal expansions (3.18) and (3.19) but the modal coefficients are denoted by $\{a_m^{\ell}\}$, $\{b_m^{\ell}\}$,

$\{\hat{a}_m^{\ell}\}$ and $\{\hat{b}_m^{\ell}\}$.

The diffraction problem is solved in a similar manner to the method given in section 3.2.3.2. In contrast to the P polarization analysis, however, the Method of Moments is applied to equations derived from consideration of the continuity of the field component H_z, by multiplying throughout by the conjugate of a modal basis function. Equations derived from consideration of the continuity of $\frac{\partial H_z}{\partial y}$ are projected onto the plane wave basis.

Using this treatment, four matrix equations are again derived in the four infinite sets of unknown modal coefficients. These may be solved using standard elimination techniques and the Rayleigh field coefficients for the reflected and transmitted magnetic fields are reconstructed. The efficiencies in reflection and transmission may then be evaluated.

3.2.5 Solution of the Diffraction Problem for Arbitrary Incidence Parameters

In this section, Petit and Maystre's theorem of conical diffraction [3.6] is applied. This method requires that the Rayleigh field amplitudes corresponding to the field diffracted by the grating operated in the two fundamental polarizations, P and S, be determined before combining these amplitudes to solve the diffraction problem for arbitrary incidence parameters.

As discussed in section 3.2.1, the incident fields $\underline{E}^i$ and $\underline{H}^i$ associated with the arbitrary incidence diffraction problem propagate in the direction of the wave vector $\underline{k}$ whose direction cosines are $(\alpha_0, -\beta_0, \gamma_0)$. The basis of the method is to project the wave vector $\underline{k}$ onto the XOY plane and to solve the P and S polarization diffraction problems associated with the modulus $\tilde{k}$ and direction cosines $\tilde{\alpha}_0$ and $\tilde{\beta}_0$ of this projection.

An understanding of this theorem is most clearly gained by describing the direction of the incident wave by new angles θ, ζ, introduced by Maystre and defined in the accompanying diagram.

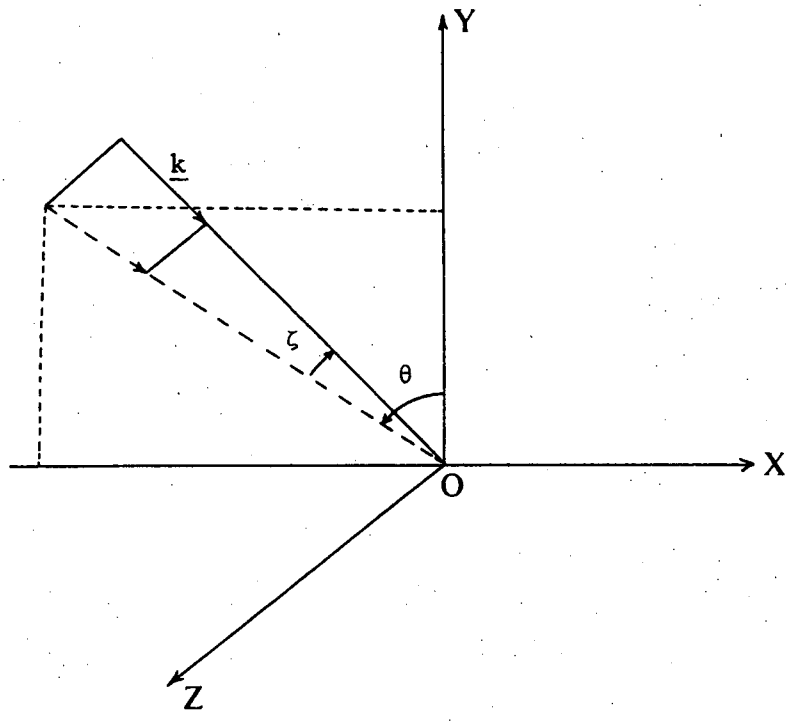

Relations between the angles θ, ζ and ϕ, ψ may readily be obtained. In this notation

$$\left.\begin{aligned} \alpha_0 &= k \sin\theta \cos\zeta \quad , \\ \beta_0 &= k \cos\theta \cos\zeta \quad , \\ \text{and} \qquad \gamma_0 &= k \sin\zeta \quad . \end{aligned}\right\} \tag{3.40}$$

The modulus of the projected wave vector is then given by

$$\tilde{k} = k \cos\zeta = \sqrt{k^2 - \gamma_0^2} \tag{3.41}$$

while the projected direction sines of the incident field

$$\tilde{\alpha}_0 = \tilde{k} \sin\theta \quad , \quad \tilde{\beta}_0 = \tilde{k} \cos\theta \tag{3.42}$$

are unchanged from α_0 and β_0.

Using the work of Petit and Maystre [3.7], the following expressions for the electric and magnetic field components may be derived for $y > s + \frac{h}{2}$:

$$E_x = -\sum_{p=-\infty}^{\infty} \frac{1}{\tilde{k}^2} [(\alpha_0 A_y + \beta_0 A_x)\beta_p D_p + \gamma_0 A_z \alpha_p C_p] \tilde{P}_p(x,y,z) \tag{3.43}$$

$$E_z = \sum_{p=-\infty}^{\infty} A_z C_p \tilde{P}_p(x,y,z) \tag{3.44}$$

$$H_x = \sum_{p=-\infty}^{\infty} \frac{1}{\tilde{k}^2 \omega \mu_0} [k^2 \beta_p A_z C_p - \gamma_0 \alpha_p (\alpha_0 A_y + \beta_0 A_x) D_p] \tilde{P}_p(x,y,z) \tag{3.45}$$

and

$$H_z = \sum_{p=-\infty}^{\infty} \frac{1}{\omega \mu_0} (\alpha_0 A_y + \beta_0 A_x) D_p \tilde{P}_p(x,y,z) \quad . \tag{3.46}$$

In these equations $\{C_p\}$ and $\{D_p\}$ are the Rayleigh field coefficients of the reflected fields corresponding to the classical P and S polarization diffraction problems respectively discussed in sections 3.2.3 and 3.2.4. These problems are solved for a wavelength $\tilde{\lambda} = \frac{\lambda}{\cos\zeta}$ and direction cosines $\tilde{\alpha}_0$ and $\tilde{\beta}_0$. Also,

$$\left.\begin{aligned} \alpha_p &= \alpha_0 + \frac{2\pi p}{d_T} \\ \tilde{\beta}_p &= \sqrt{\tilde{k}^2 - \alpha_p^2} = \sqrt{k^2 - \alpha_p^2 - \gamma_0^2} \quad \text{if } |\alpha_p| < \tilde{k} \\ &= i\sqrt{\alpha_p^2 - \tilde{k}^2} = i\sqrt{\alpha_p^2 + \gamma_0^2 - k^2} \quad \text{otherwise} \end{aligned}\right\} \tag{3.47}$$

$$\tilde{P}_p(x,y,z) = \exp[i(\alpha_p x + \beta_p y + \gamma_0 z)]/\sqrt{d_T} \tag{3.48}$$

and A_x, A_y, A_z are defined in equation (3.4).

The fields in the region $y < -s - \frac{h'}{2}$ are given by exactly analogous expressions to (3.43 - 3.46) except that β_p is replaced by $-\beta_p$, $\{C_p\}$, $\{D_p\}$ are replaced by $\{\hat{C}_p\}$, $\{\hat{D}_p\}$ respectively, and $\tilde{P}_p$ is replaced by $\hat{P}_p$ where

$$\hat{\tilde{P}}_p(x,y,z) = \exp[i(\alpha_p x - \beta_p y + \gamma_0 z)] / \sqrt{d_T} \tag{3.49}$$

At this stage, it is worth commenting on the origin of the name "conical diffraction". The diffracted plane waves propagate in directions specified by the direction cosines α_p, β_p, γ_0. That is, the grating conserves momentum parallel to the OZ axis, and changes momentum in the OX direction by multiples of $\frac{2\pi}{d_T}$. Thus the diffracted wave vectors lie on the surface of a cone whose axis is parallel to the grooves.

Finally, the energy conservation criterion can be written as

$$\beta_0 = \sum_{p\in\Omega_r} \frac{\beta_p}{\tilde{k}^2} \{[(\alpha_0 A_y + \beta_0 A_x)^2 |D_p|^2 + A_z^2 |C_p|^2] + [(\alpha_0 A_y + \beta_0 A_x)^2 |\hat{D}_p|^2 + A_z^2 |\hat{C}_p|^2]\} \tag{3.50}$$

where $\Omega_r = \{p | \mathrm{Im}(\beta_p) = 0\}$

The problem of conical diffraction by a double grating has been reduced to the two separate diffraction problems corresponding to the two fundamental states of polarization for the double grating, in the classical mounting. Each of these problems involves solving a set of four matrix equations of infinite dimension (in the unknown modal coefficients) which are truncated in order to obtain a solution.

3.3 DISCUSSION OF THE LONG WAVELENGTH PROPERTIES OF THE DOUBLE GRATING

3.3.1 Introduction

The main reason for studying the double grating was to investigate the possible application of the structure as a Fabry-Perot interferometer. Since this type of interferometer relies upon highly reflecting elements substantially displaced from one another so as to produce a multiplicity of interference orders, the double grating is only useful in this context when used in P polarized incident radiation. For long wavelength radiation of this polarization the double grating elements are highly reflecting. Thus the following section discussing the Fabry-Perot aspects of the double grating considers operation in P polarized radiation only. However, the multiple scattering approach used in this section to locate and explain the resonances can also be beneficially applied to predict features of the curves obtained for a double grating used in S polarized radiation. Section 3.3.2 is therefore devoted to analysing the features of spectra for double gratings operated in S polarized radiation, using the multiple scattering technique.

Extensive numerical tests have been performed on the formalism and table 3.1 includes results of one such test carried out using the Reciprocity Theorem. Further verification of the method is provided in chapter 4 where the double grating formalism is thoroughly tested using a series of symmetry properties.

3.3.2 The Double Grating as a Fabry-Perot Interferometer (P Polarized Radiation)

A typical spectrum for a double grating interferometer composed of two identical lamellar arrays is presented in figure 3.2a. This curve was computed using the double grating formalism described in section 3.2. As discussed in section 3.3.1, a multiple scattering approach was adopted

Table 3.1 Confirmation of the Reciprocity Theorem

Reciprocity results for a double grating specified by $d'/d = 1.5$, $c/d = 0.8$, $c'/d = 0.9$, $\delta x/d = 0.3$, $S/d = 0.6$, $h/d = h'/d = 0.3$ used in P polarized radiation of wavelength $\lambda/d = 1.65$.

Problem 1 was characterised by $\phi = 20.4873^{\circ}$. The +1 order was returned to give the second diffraction problem ($\phi = -64.1624^{\circ}$) while the -1 order was returned to form the third problem ($\phi = 11.5389^{\circ}$). In each case, 7 waveguide modes and 15 Rayleigh orders were used to characterise the wave fields.

	Order p	Efficiency (p)	Phase (p)	Total Energy Transmitted
Problem 1	1	0.03386	14.49100	0.50557
	-1	0.00722	-77.35114	
Problem 2	1	0.03447	14.39083	0.03495
Problem 3	-1	0.00720	-77.49372	0.43898

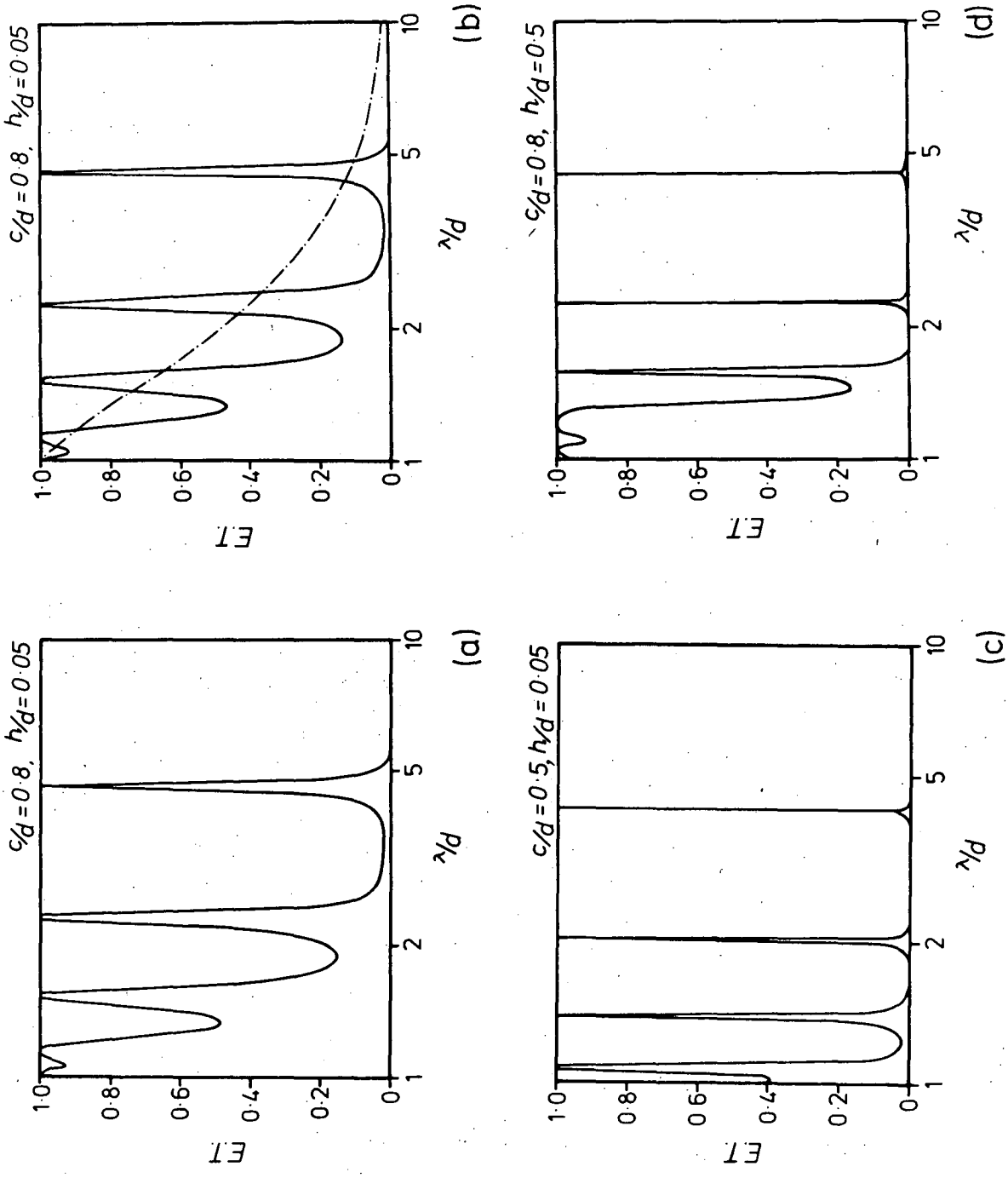

Figure 3.2 Normal incidence wavelength spectra for a double grating composed of a pair of identical lamellar arrays separated by S/d = 2.0 and aligned such that δx/d = 0.0, operated in P polarized radiation.

in order to explain the features of this curve. In this treatment, the double grating is thought of as being composed of two single lamellar transmission gratings ($d = d'$) coupled together by the multiple reflections of the zeroth order beam between the two arrays. Naturally, such a treatment requires that the wavelength of the incident radiation be longer than the grating period (so that the only propagating order is the zeroth order) and that the separation of the two arrays be large enough so that there is no evanescent coupling between them. That is, the zeroth order provides the only significant coupling mechanism between the gratings. This treatment is generalised in chapter 5 to allow for multi-element grating arrangements with small array separations and small wavelength to period ratios by incorporating the interaction of all real and evanescent waves between the arrays.

Let the complex zeroth order reflection and transmission coefficients of each lamellar array be R_0 and T_0 respectively. Then if a unit amplitude plane wave is incident at an angle ϕ upon the double grating, the total transmitted amplitude of the grating (whose phase origin is shown in figure 3.1) is given by the infinite geometric series

$$\tau = T_0^2[1 + R_0^2 \exp(2i\chi) + R_0^4 \exp(4i\chi) + \ldots]$$

$$= \frac{T_0^2}{1 - R_0^2 \exp(2i\chi)} \tag{3.51}$$

where $$\chi = \beta_0'(S + h) \tag{3.52}$$

is the phase difference between successive emergent beams and β_0' is defined in equation (3.7). Hence it follows from equation (3.51) that the total transmitted intensity of the double grating is

$$|\tau|^2 = \frac{1}{1 + f \sin^2\xi} \tag{3.53}$$

where $$\xi = \chi + \arg(R_0) \tag{3.54}$$

and the term f, known as the finesse of the interferometer, is defined by

$$f = \frac{4|R_0|^2}{(1 - |R_0|^2)^2} \tag{3.55}$$

By determining the value of R_0 using the computer program for solving the diffraction properties of a single lamellar transmission grating and using equation (3.53), the reconstruction of the P polarized transmittance is possible. Such a reconstruction was performed and the resulting spectrum is depicted by the solid curve in figure 3.2b (the dotted curve in this figure represents the transmission properties of the single lamellar array). Comparison of this curve with figure 3.2a shows the excellent agreement between the rigorous theory and the reconstruction procedure.

It follows from equation (3.53) that for normally incident radiation, resonance maxima occur when

$$\frac{2\pi}{\lambda}(S + h) + \arg(R_0) = \ell\pi \tag{3.56}$$

where ℓ is an integer specifying the order of interference ($\ell = 1,2,3...$). This equation demonstrates that the phase term $\arg(R_0)$, (a quantity dependent on both the groove geometry and the incidence parameters) is capable of displacing the resonance maxima from their geometrically obtained positions, given by

$$\lambda_{max} = \frac{2S}{\ell} \qquad (\ell = 1,2.....) \tag{3.57}$$

Further inspection of the curves in figures 3.2a and 3.2b reveals the improved resolution of the interferometer at long wavelengths. This can be directly attributed to the increasing reflectivity of each lamellar array with increasing wavelength as demonstrated by the dotted curve in figure 3.2b, which describes the transmittance of a single lamellar grating. This rise in reflectivity increases the finesse and consequently reduces the resonance half-widths. It is also interesting to note that the positions of the interference maxima approach their geometrically obtained limit, given by equation (3.57), as the wavelength increases. In order to explain this property, a monomodal treatment was adopted and applied to the single lamellar problem. This model, which has been discussed previously by Chen [3.11] and McPhedran and Maystre [3.12], is based upon the observation that the bulk of the incident energy is channelled into the fundamental mode, i.e. the mode having the lowest spatial frequency (m=1). This technique when applied to a single lamellar array yields the following expressions for the reflected and transmitted amplitudes:

$$R_0 = \exp(-i\beta_0' h)\left\{ -1 + \frac{2i\beta_0' |K_0|^2 [\mu_1 \cos(\mu_1 h) - P \sin(\mu_1 h)]}{[2\mu_1 P \cos(\mu_1 h) - (P^2-\mu_1^2)\sin(\mu_1 h)]} \right\} \tag{3.58}$$

and

$$T_0 = \frac{2i\mu_1\beta_0' |K_0|^2 \exp(-i\beta_0' h)}{[2\mu_1 P \cos(\mu_1 h) - (P^2-\mu_1^2) \sin(\mu_1 h)]} \tag{3.59}$$

where

$$P = \sum_p i\beta_p' |K_p|^2 \tag{3.60}$$

and

$$K_p = \sqrt{\frac{2}{cd}} \int_{-c/2}^{c/2} \exp(-i\alpha_p' x) \sin\left[\frac{\pi}{c}(x + \frac{c}{2})\right] dx \qquad (3.61)$$

Using these results, it can be shown that for normally incident radiation $|T_o|$ must approach zero with increasing wavelength and

$$R_0 \to -\exp(-i\beta_0' h) \qquad \text{i.e.} \quad \arg(R_0) \to \pi - \beta_0' h \ ,$$

from which it can be shown that

$$\xi \to \pi + \beta_0' S \ , \qquad (3.62)$$

The interference maxima are then situated at the geometrical positions given by equation (3.57).

The grating parameters, the aperture width c and groove depth h, will now be considered in relation to their effects on the performance of the interferometer. Figures 3.2a - 3.2d, showing the transmission spectra of several double gratings operated in normally incident radiation, demonstrate an enhanced resolution with both decreasing aperture width and increasing groove depth. It is noted that it is the parameter c which appears to govern the positions of the interference maxima. These observations may be readily understood by further pursuing the monomodal treatment.

Consider firstly the effect of the aperture width. It can be shown, using equation (3.59), that for normally incident radiation and small values of c, $|T_0|$ approaches zero, thereby improving the finesse of the instrument. Once again

$$\arg(R_0) \to \pi - \beta_0' h$$

which moves the interference maxima to their geometrical positions.

Now consider the dependence of these spectra on groove depth. Consider in particular wavelengths in excess of twice the aperture width, so that every mode is evanescent. In this case, the denominator of equation (3.59) can be written

$$i[2|\mu_1|(P\cosh(|\mu_1|h)) - (P^2 + |\mu_1|^2)\sinh(|\mu_1|h)]$$

$$\simeq -\frac{i}{2}[(P-|\mu_1|)^2\exp(|\mu_1|h)] \quad \text{if} \quad h \quad \text{is sufficiently large.}$$

It is the presence of the exponential term that leads to an enhanced finesse. It is also evident from the above expression that the phase of T_0 (and hence of R_0) is, for large groove depths, largely determined by the term $(P - |\mu_1|)^2$. This term is dependent only on the incidence parameters and the aperture width. Hence

$$\arg(T_0) = \frac{3\pi}{2} - \beta_o'h - \chi'$$

where
$$\chi' = \arg[(P - |\mu_1|)^2] \quad . \tag{3.63}$$

Now since
$$\arg(R_0) = \arg(T_0) - \frac{\pi}{2} \qquad \text{(see [3.13])} \tag{3.64}$$

hence
$$\xi = \pi + \beta_0'S - \chi' \quad . \tag{3.65}$$

This shows that for large groove depths the positions of the interference maxima are essentially independent of the groove depth and are determined solely by the aperture width.

Finally, the effects of oblique incidence on the performance of the structure will be briefly discussed. Figure 3.3 depicts angle of incidence spectra for three double gratings of varying groove depth and aperture width. An immediate observation is that these curves exhibit the

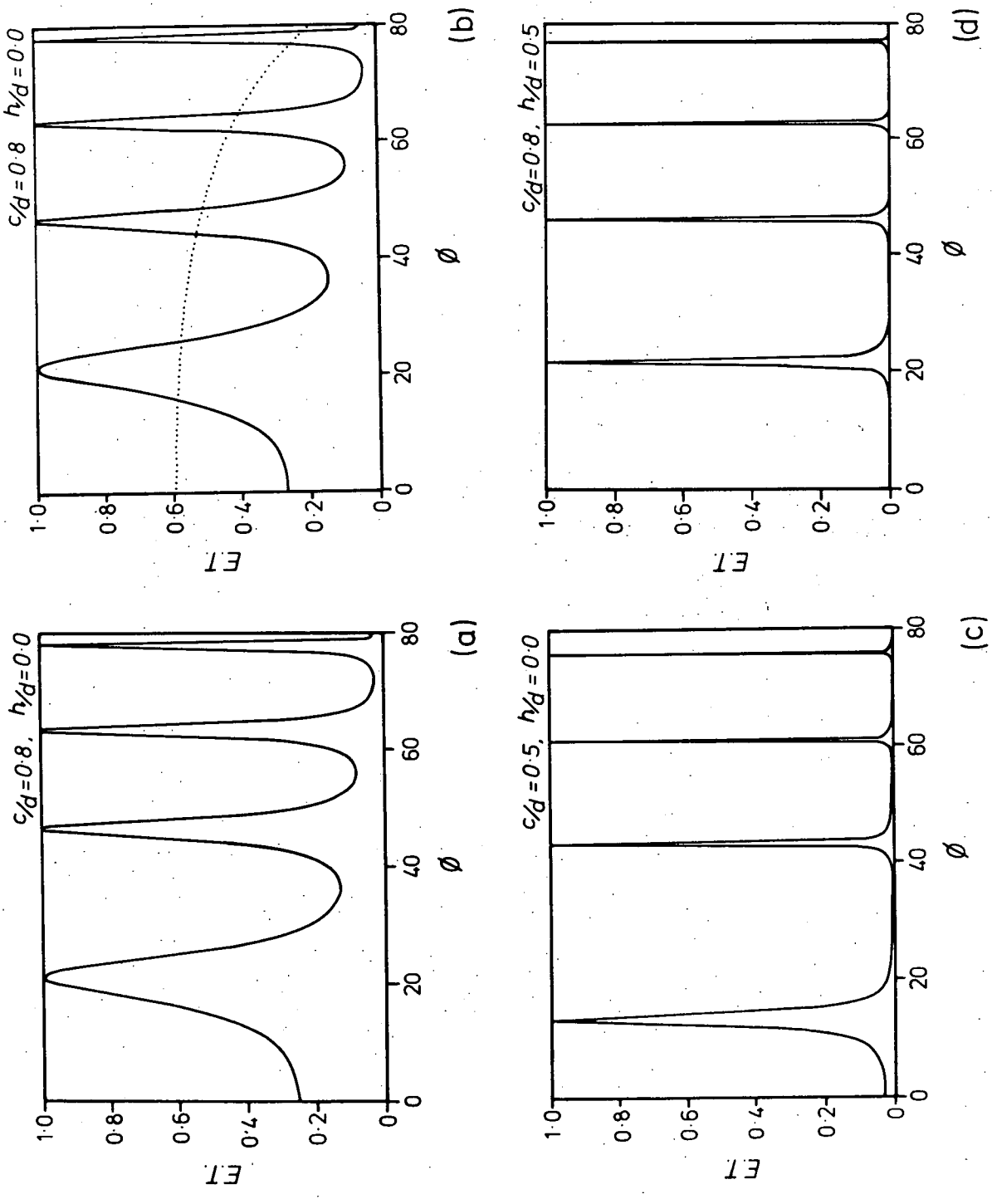

Figure 3.3 Angle of incidence spectra for a double grating characterised by the parameters d'/d = 1.0, S/d = 4.0, δx/d = 0.0, operated in P polarized radiation of wavelength λ/d = 2.0. The dashed curve shows the transmission properties of a single lamellar array and the solid curve accompanying this was obtained by the reconstruction procedure.

same aperture width and groove depth dependence as seen in the wavelength spectra. Inspection of these curves also shows the finesse to be increasing as the angle of incidence becomes more oblique. In order to explain this, consider equations (3.58) and (3.59). The numerator of both equations contains the term $\beta_0' = k\cos\phi$ which tends to zero as ϕ tends to $\pm 90^\circ$. Hence $|T_0|$ tends to zero, so increasing the finesse of the interferometer, and $\arg(R_0)$ tends to π. Thus the resonance maxima approach their geometrical positions given by

$$\phi_{max} = \text{arc}\cos\left(\frac{\ell\lambda}{2S}\right) \tag{3.66}$$

as the obliquity of the angle of incidence increases.

3.3.3 Analysis of the Performance of the Double Grating in S Polarized Incident Radiation

As suggested in section 3.3.1, the double grating is not useful as a long wavelength Fabry-Perot interferometer operated in S polarized incident radiation, since generally the reflectivity of the structure is low for radiation of this polarization and wavelength. That is, the transmittance of the grating approaches zero as the wavelength increases. Nevertheless, the method of analysis presented in section 3.3.2 affords some explanation of the features occurring in the S polarization spectra of the double grating and so once more a multiple scattering approach is adopted.

As before, the assumptions made are that the separation of the two identical arrays ($d=d'$) of the double grating be sufficiently large so that no evanescent coupling occurs between the arrays and that the wavelength be long enough so that the zeroth orders are the sole propagating waves. Then the grating can be analysed in terms of two

single lamellar arrays and the diffraction problem solved by summation of all multiple reflections of the zeroth order waves. If R_0 and T_0 represent the zeroth order reflection and transmission coefficients of each of the lamellar arrays, then as discussed in section 3.3.2, the total transmitted intensity of the double grating is again given by equation (3.53).

Figure 3.4a shows the S polarization transmittance of a double grating, computed using the rigorous theory described in section 3.2.4, while the solid curve in figure 3.4b depicts the S polarization transmission properties of the double grating obtained using equation (3.53) and the computer program for solving the diffraction problem of a single lamellar transmission grating (dashed curve). The excellent agreement between these curves again confirms the validity of the approach. This is also demonstrated by the remaining curves in figure 3.4 which show transmission spectra of double gratings, obtained by using the rigorous formalism (3.4c and 3.4e) or the reconstruction procedure (3.4d and 3.4f).

These spectra show that the finesse decreases as the wavelength increases. This is due to the increasing transmittance of each lamellar array under these conditions, as shown by the broken curve in figure 3.4b, depicting the S polarization transmittance of the single lamellar array. This behaviour is in contrast with the phenomena observed in the P polarization spectra, where the finesse increased with increasing wavelength due to an increased reflectance of each lamellar array.

It is also interesting to note by comparing figure 3.2c (P polarization) and figure 3.4e (S polarization) that the P polarization resonance maxima correspond to the S polarization resonance minima. To explain this feature a monomodal treatment (see section 3.3.2) is again applied, where for this polarization it is assumed that the majority of

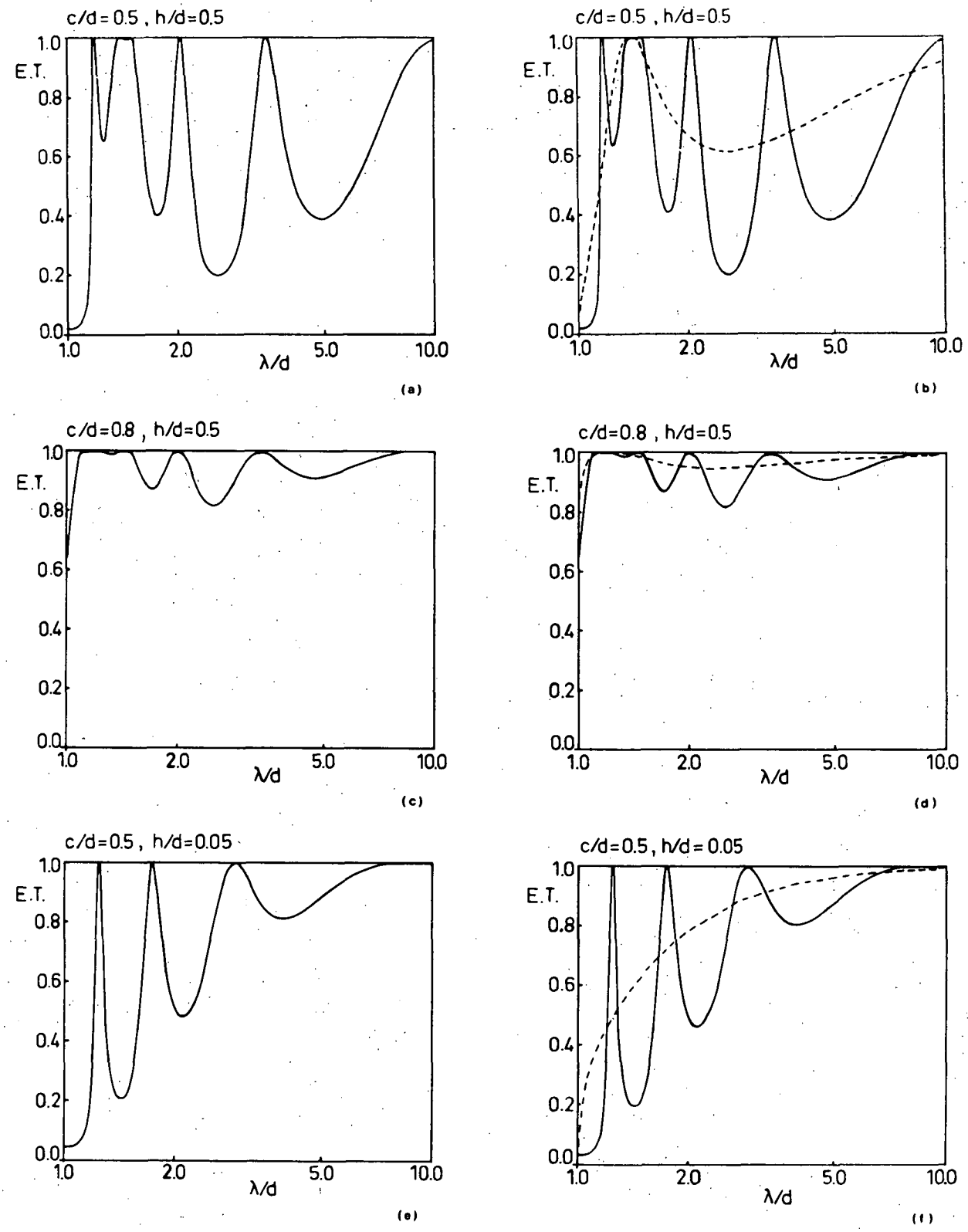

Figure 3.4 Wavelength spectra for a double grating composed of identical lamellar arrays separated by S/d = 2.0, with zero relative displacement (δx/d = 0.0) operated in normally incident, S polarized radiation. All figures incorporating both broken and solid curves depict the transmission properties of each single lamellar array and the properties of the double grating obtained from the reconstruction process, respectively.

energy incident upon the grating is carried by the m=0 mode. Applying this treatment to the single lamellar array operated in S polarized radiation yields the following expressions for R_0 and T_0:

$$R_0 = \exp(-i\beta_0' h)\left\{1 - \frac{2i\mu_0|J_0|^2[\cos(\mu_0 h) - \mu_0 P'\sin(\mu_0 h)]}{\beta_0'[(1 - \mu_0^2 P'^2)\sin(\mu_0 h) + 2\mu_0 P'\cos(\mu_0 h)]}\right\} \tag{3.67}$$

and

$$T_0 = \exp(-i\beta_0' h)\left\{\frac{2i\mu_0|J_0|^2}{\beta_0'[2\mu_0 P'\cos(\mu_0 h) + (1 - \mu_0^2 P'^2)\sin(\mu_0 h)]}\right\} \tag{3.68}$$

where

$$P' = \sum_{p=-\infty}^{\infty} \frac{i|J_p|^2}{\beta_p'}$$

and

$$J_p = \sqrt{\frac{1}{cd}} \int_{-c/2}^{c/2} \exp(-i\alpha_p' x)\, dx \tag{3.70}$$

Using these equations, it can be shown that for normally incident radiation

$$\lim_{\lambda \to \infty} |R_0| = 0 \tag{3.71}$$

and $$\arg(R_0) \to -\beta_0' h - \frac{\pi}{2} \quad \text{as} \quad \lambda \to \infty \tag{3.72}$$

Thus the finesse decreases as the wavelength increases. This is observed numerically as shown by figure 3.4a.

Equations (3.54) and (3.72) imply that for normally incident radiation, the positions of the S polarization resonance maxima and

minima as $\lambda \to \infty$ are given by

$$\lambda_{max} = \frac{2S}{(\ell+\frac{1}{2})} \qquad \ell = 0, 1, \ldots \tag{3.73}$$

$$\lambda_{min} = \frac{2S}{(\ell+1)} \tag{3.74}$$

respectively. By comparing equation (3.74) with equation (3.57), it is seen that the positions of the S polarization resonance minima approach the positions of the P polarization maxima (which are the geometrical positions) as the wavelength increases.

Consider briefly the effects of aperture width and groove depth on the spectra, for normally incident radiation. It can be shown by considering equation (3.68) that (for h sufficiently large that $\sin(\mu_0 h)$ be non-negligible) $|T_0| \to 0$ as $c \to 0$, thus improving the finesse of the double grating, and that $\arg(T_0) \to \pi/2 - \beta_0' h$. Using equation (3.64) it follows that $\arg(R_0) \to -\beta_0' h$ as $c \to 0$. This implies that

$$\lambda_{max} \to \frac{2S}{\ell} \quad \text{as} \quad c \to 0 \qquad \ell = 1, 2, \ldots ,$$

which is the geometrical position.

This result depends upon the value of the groove depth and consequently this effect would only be seen for large h. Figures 3.4a and 3.4c confirm these results and show that as the aperture width decreases the finesse of the structure increases and a slight movement of the resonance towards the geometrical positions occurs.

Consider now the effect of the groove depth. In this case the dominant (m=0) mode is always non-evanescent. This is one of the fundamental reasons for the differing long wavelength behaviour of the grating operated in P and S polarized radiation. The dominant mode

(m=1) for P polarized radiation becomes evanescent as the wavelength increases. The following results may be derived from equation (3.68):

$$|T_0| \to 1 \qquad \text{as} \quad h \to 0 \ , \ \lambda \to \infty$$

which causes a decrease in the finesse of the structure.

Also

$$\arg(T_0) \to -\beta_0' h \qquad \text{as} \quad h \to 0 \ , \ \lambda \to \infty$$

which, using equation (3.64), implies

$$\arg(R_0) \to -\beta_0' h - \frac{\pi}{2} \ .$$

Thus the resonance minima are moved towards the position of the P polarization resonance maxima. Comparison of figures 3.4e and 3.2c confirms these predictions for long wavelengths.

Finally, the effects on non-normal incidence will be discussed. It can be shown that $|T_0| \to 0$ and $\arg(R_0) \to -\beta_0' h$ as $\phi \to 90^\circ$ $(c,h > 0)$, which implies that as the angle of incidence becomes more oblique, the finesse of the double grating increases and the resonance maxima approach the geometrical positions. This property can be seen in figures 3.5a-d.

It is to be noted that the aperture width dependence observed in these curves is the same as that in the wavelength spectra. In determining the groove depth dependence of the angle of incidence spectra, it can be shown for oblique incidence that $|T_0| \to 1$ and $\arg(R_0) \to -\beta_0' h - \frac{\pi}{2}$ as $h \to 0$ $(\phi \to 90^\circ)$. This again causes a decrease in finesse and a movement of the resonance minima to the positions of the P polarization resonance maxima.

3.3.4 Validity of the Multiple Scattering Approach

The multiple scattering treatment has been thoroughly tested and

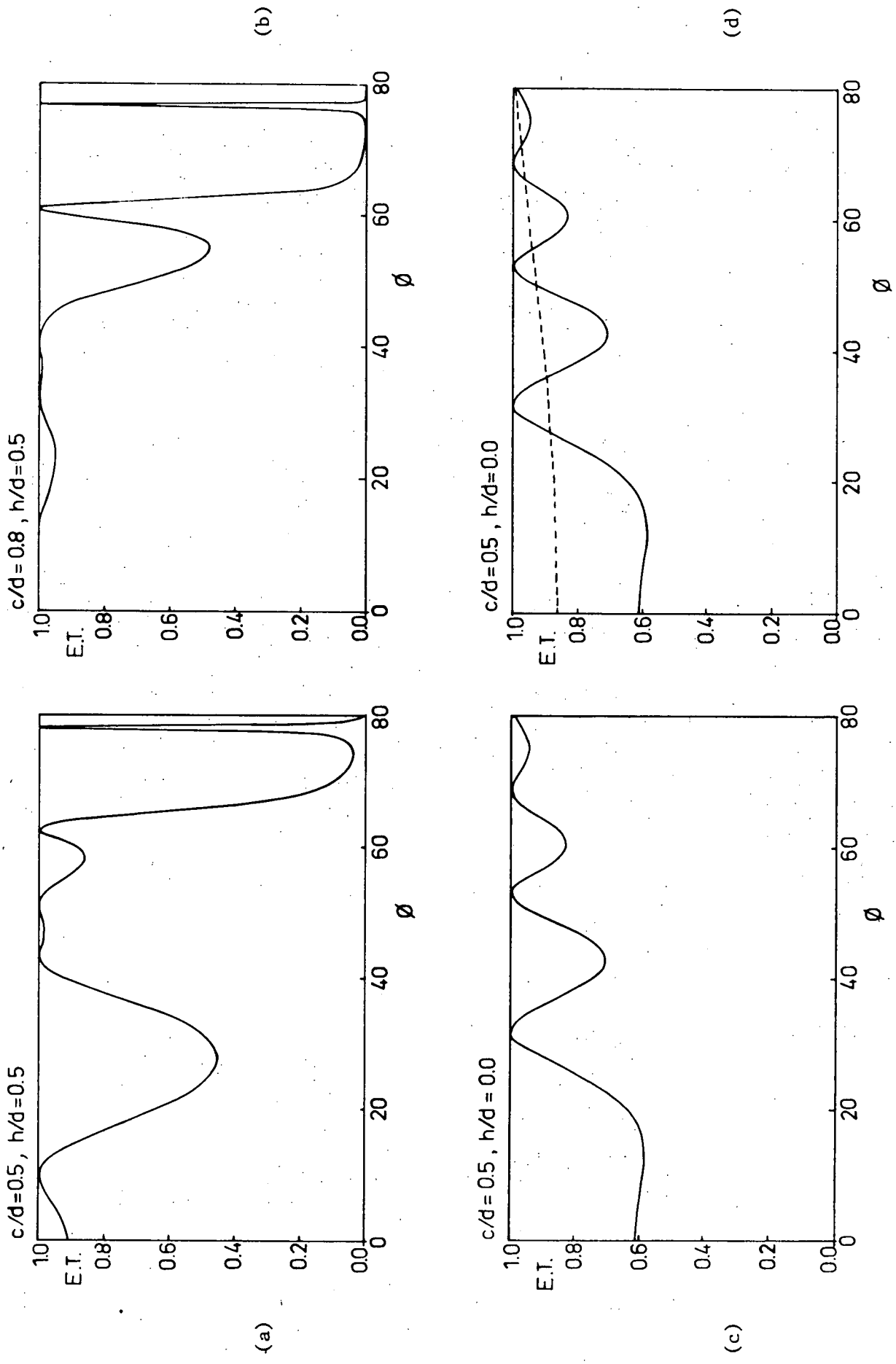

Figure 3.5 Transmission properties of double gratings characterised by the parameters $d'/d = 1.0$, $S/d = 4.0$, $\delta x/d = 0.0$, operated in S polarized radiation of wavelength $\lambda/d = 2.0$.

found to be valid for normalised separations of $S/d \gtrsim 0.5$. Smaller separations lead to a significant coupling of the two arrays by the evanescent field. This may be demonstrated by consideration of the array phasing parameter δx. The multiple scattering approach predicts no dependence upon δx, and for large array separations ($S/d \gtrsim 0.5$) this prediction is in agreement with the numerical results obtained from the rigorous theory. However, for separations $S/d \lesssim 0.5$ the evanescent coupling becomes quite noticeable and a marked dependence upon δx is observed. This is illustrated by figure 3.6, which shows the effects of array phasing on the transmission properties of a double grating with an array separation of $S/d = 0.02$. It is interesting to note that when $\delta x = 0.5$, total blocking of P polarized radiation occurs whereas there is a substantial leakage occurring for S polarised radiation. It is thought that this may be attributed to the directions of current flow appropriate to the two polarizations.

3.4 CONCLUSIONS

A rigorous theoretical formalism, capable of describing the diffraction of radiation with arbitrary incidence parameters by a perfectly conducting double grating, has been presented.

In addition to confirming the applicability of this structure as a Fabry-Perot interferometer (operated in P polarized radiation), these studies have also clarified the individual effects of the basic design parameters. It was demonstrated that the finesse of the interferometer is influenced by both the mark-space ratio and groove depth, whereas only the aperture width plays a dominant role in the determination of the location of the interference resonances.

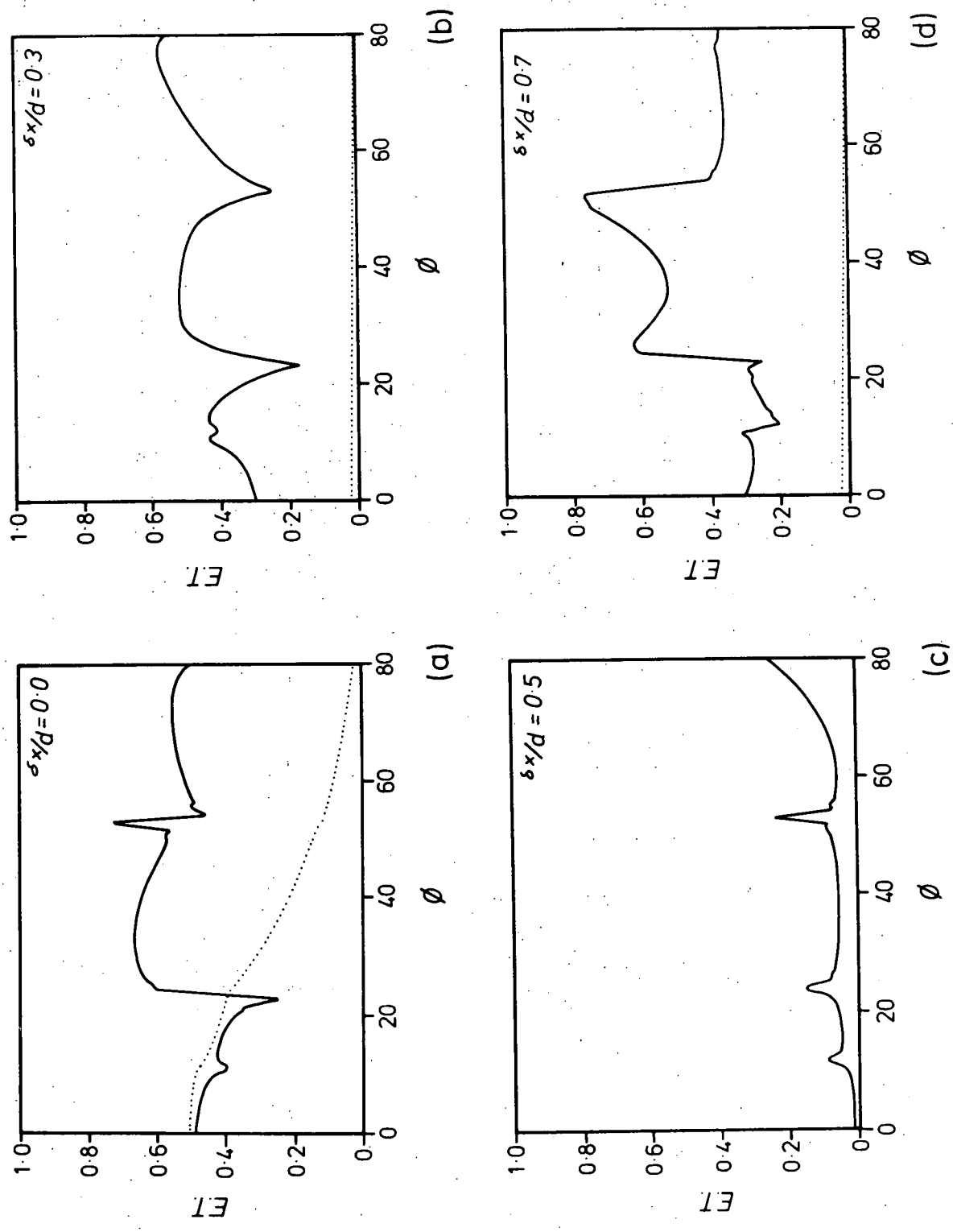

Figure 3.6 Demonstration of the effect of the array displacement parameter on gratings with small separations. The grating was composed of identical lamellar arrays specified by c/d = 0.5, h/d = 0.4, separated by S/d = 0.02 and operated in both P polarized (broken curve) and S polarized (solid curve) radiation of wavelength λ/d = 0.6.

If the incident radiation is unpolarized, it is essential that the interferometer be constructed from elements which are polarization independent. An analysis of the properties of such a structure, composed of an identical pair of doubly periodic inductive grids [3.14], is given in chapters 6 and 7.

Investigations into the performance of the double grating in S polarized radiation, although not relevant to Fabry-Perot interferometers, were also described. Again the effects of the grating parameters on the wavelength and angle of incidence spectra were determined.

REFERENCES

[3.1] ADAMS (J.L.), BOTTEN (L.C.). - J. Optics (Paris), 1979, 10, 109.

[3.2] BLOK (H.), MUR (G.). - Appl. Sci. Res., 1972, 26, 389.

[3.3] BOTTEN (L.C.). - Infrared Phys., 1979, 19, 659.

[3.4] BOTTEN (L.C.), ADAMS (J.L.), DERRICK (G.H.). - J.Optics (Paris), submitted; Chapter 5 this thesis.

[3.5] ADAMS (J.L.), BOTTEN (L.C.). - University of Tasmania Research Report, D.G.R.G. 78/2.

[3.6] MAYSTRE (D.). - Thèse No. A09545, 1974, L'Université d'Aix-Marseille III, France.

[3.7] PETIT (R.), MAYSTRE (D.). - Rev. Phys. Appl., 1972, 7, 427.

[3.8] NEVIÈRE (M.), CADILHAC (M.). - Opt. Commun., 1970, 2, 235.

[3.9] PETIT (R.). - Rev. Opt., 1966, 45, 249.

[3.10] WIRGIN (A.). - C. R. Acad. Sci. Paris, 1966, 262B, 870.

[3.11] CHEN (C.-C.). - I.E.E.E. Trans. MTT - 21, 1973, 1, 1.

[3.12] McPHEDRAN (R.C.), MAYSTRE (D.). - Appl. Phys., 1977, 14, 1.

[3.13] BOTTEN (L.C.), ADAMS (J.L.), McPHEDRAN (R.C.), DERRICK (G.H.). - J. Optics (Paris), 1980, 11, 43.

[3.14] ADAMS (J.L.). - J. Optics (Paris), accepted.

CHAPTER 4

SYMMETRY PROPERTIES OF LOSSLESS DIFFRACTION GRATINGS

4.1 INTRODUCTION

Many of the 'conservation theorems' found in nuclear scattering theory have analogues in electromagnetic theory, and in particular diffraction grating theory. Amongst these properties are energy conservation and reciprocity which are distinguished by their independence of either the geometry or the conductivity of the structure. In contrast, the constraints [4.1] which are derived in this chapter apply only to lossless structures.

During the past decade, authors such as Petit [4.2] and Van den Berg [4.3], who were concerned with integral formalisms for diffraction gratings, presented clear discussions of the concept of energy conservation and demonstrated that their theories obeyed this criterion to high precision. Although conservation of energy represents an actual physical test of the validity and convergence properties of the integral and differential formalisms, the same remarks do not apply to modal formalisms. This was shown by Amitay and Galindo [4.4] and later by McPhedran and Maystre [4.5] who demonstrated that conservation of energy was analytically satisfied, independently of any truncation errors.

The Reciprocity Theorem, however, does not share this problem since it provides a physical test to all integral, differential and modal formalisms. Early investigations concerning the Reciprocity Theorem were undertaken by Uretsky [4.6] and Petit [4.7] with a view to establishing a statement of the result appropriate to perfectly conducting gratings. In 1974, Maystre and McPhedran [4.8] generalised this property to include

finitely conducting reflection gratings. Nevière and Vincent [4.9] further extended the theorem to account for the reciprocity property consequent upon the return of a transmitted order. Subsequently, McPhedran and Maystre [4.5] discovered the form of the Reciprocity Theorem appropriate to doubly periodic structures.

The properties to be derived in this chapter using the principle of time reversal, rely upon the perfect conductivity of the grating and the most compact forms of these relations exist when certain symmetries (left-right and/or up-down) are present in the grating geometry. Relations of this form have already been determined by McPhedran and Maystre [4.5], Botten[4.10] and Adams et al [4.11] using a variety of methods.

A brief review of some of these properties derived using conventional integral techniques [4.12] is provided in section 4.2 and this approach is extended to derive further relations. A detailed description of the derivation of the conservation relations using the concept of time reversibility is then provided in section 4.3. Specific properties of this type were originally derived solely for a left-right, up-down symmetric double grating as a means of checking the numerical implementation of the formalism which is described in chapter 3. Once the significance and usefulness of the properties were discovered, the analysis was more closely investigated so that as many singly periodic, lossless structures as possible could be encompassed in the treatment. The derivations are restricted to the two important cases:

(a) the long wavelength formulation (for which only the zeroth orders are propagating) and

(b) the first order Littrow mount (for which only the zeroth and first orders are propagating).

It is the field symmetry associated with these two mounts that facilitates

the derivation of concise analytic forms of the conservation relations using the principle of time reversibility. Particular reference is made throughout to the double grating with the constraints derived being illustrated by numerical results obtained from the formalism [4.13] for this structure.

The conservation relations presented in this chapter are derived in a thoroughly general manner. Some of the results are well known but others are new. The existence of such a catalogue of analytic tests will be of great value in the future development of grating formalisms, and also to users of existing numerical implementations.

A further series of new conservation relations constraining the scattering matrices of singly periodic diffraction gratings are described in chapter 5.

4.2 A REVIEW OF SOME CONSERVATION THEOREMS DERIVED USING INTEGRAL TECHNIQUES

The relations to be derived in this section depend upon both the symmetry and the lossless nature of the structure and the importance of both of these properties applying cannot be stressed too heavily. The symmetry properties and physical constraints required for the derivation of the conservation relations in this and all subsequent sections will be recalled using the notations

(a) LR - left-right symmetry,

(b) UD - up-down symmetry,

(c) RT - Reciprocity Theorem, and

(d) CE - conservation of energy.

The discussions in this section refer to a P polarized wave field but an exactly analogous analysis may be used for S polarized radiation.

4.2.1 Relations for a First Order Littrow Mount

Botten [4.10] has proposed a constraint relating the phases and efficiencies of the reflected and transmitted orders excited by a lossless left-right symmetric transmission grating used in a first order Littrow mount with only two propagating orders. The proof contained in this article is repeated in order to permit the derivation of two further properties.

Consider a P polarized plane wave I of wavelength $\lambda = 2\pi/k$ incident upon the structure shown in figure 4.1. In the semi-infinite free space regions (D_u and D_ℓ), the field may be expressed in terms of the following Rayleigh expansions:

$$E_u(x,y) = \sum_{p=-\infty}^{\infty} [\delta_{p0}\exp(-i\beta_0 y) + R_p\exp(i\beta_p y)]\exp(i\alpha_p x) \quad \text{in } D_u \tag{4.1}$$

and

$$E_\ell(x,y) = \sum_{p=-\infty}^{\infty} [T_p\exp(-i\beta_p y)]\exp(i\alpha_p x) \quad \text{in } D_\ell \tag{4.2}$$

Here $\alpha_p = -\alpha_{-1-p} = (p + \tfrac{1}{2})K$, a constraint imposed by the $(-1)^{th}$ order Littrow configuration, and $K = 2\pi/d$. Also

$$\beta_p = \sqrt{k^2 - \alpha_p^2} \quad \text{if} \quad |\alpha_p| \leq k$$

$$= i\sqrt{\alpha_p^2 - k^2} \quad \text{if} \quad |\alpha_p| > k$$

If a second incident wave I' is returned along the path of the original zeroth order reflected wave, a corresponding wave field given by

$$E'_u(x,y) = \sum_{p=-\infty}^{\infty} [\delta_{p0}\exp(-i\beta'_0 y) + R'_p\exp(i\beta'_p y)]\exp(i\alpha'_p x) \quad \text{in } D_u \tag{4.3}$$

and

$$E'_\ell(x,y) = \sum_{p=-\infty}^{\infty} [T'_p\exp(-i\beta'_p y)]\exp(i\alpha'_p x) \quad \text{in } D_\ell \tag{4.4}$$

is established. In this case $\alpha'_p = -\alpha_{-p} = (p - \tfrac{1}{2})K$.

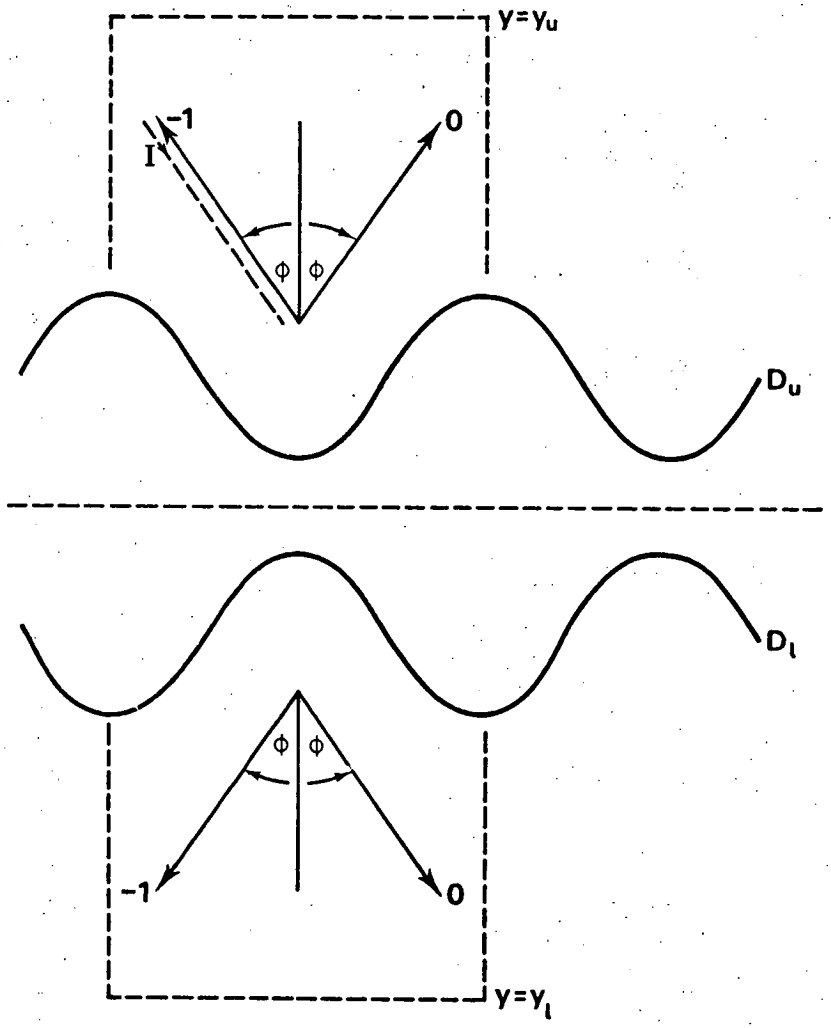

Figure 4.1 Integral derivation of the conservation relations for a first order Littrow configuration.

Now if E^T denotes the superposition of these two fields, i.e. $E^T = E + E'$, then it may be shown (using a simple application of Green's Theorem) that for lossless gratings

$$\int_0^d F(x,y_u)dx = \int_0^d F(x,y_\ell)dx \tag{4.5}$$

where $$F(x,y) = E^T \frac{\partial \bar{E}^T}{\partial y} - \bar{E}^T \frac{\partial E^T}{\partial y}$$

(Here the bar denotes complex conjugation).

If the symmetry relations $R'_p = R_{-p}$ and $T'_p = T_{-p}$ (consequent upon the left-right symmetry of the structure) are now applied and equation (4.5) is explicitly integrated using the field expansions given in equations (4.1 - 4.4), it follows that

$$|R_0 + R_{-1}|^2 + |T_0 + T_{-1}|^2 = 1 \tag{4.6}$$

From the constraint imposed by conservation of energy, namely

$$|R_0|^2 + |R_{-1}|^2 + |T_0|^2 + |T_{-1}|^2 = 1$$

equation (4.6) may be reduced to the form

$$\mathrm{Re}(R_0\bar{R}_{-1} + T_0\bar{T}_{-1}) = 0 \qquad \text{(LR)} \tag{4.7}$$

Numerical evidence of this property is given in [4.10]. It has already been shown [4.11] that, for the case of modal formalisms, this constraint is analytically satisfied provided that the set of Rayleigh orders used in

the numerical algorithm is symmetrically truncated about the propagating orders.

If the further constraint of up-down symmetry is now imposed, it is possible to derive two additional conservation relations. Consider a wave returned along the path traversed by the original zeroth order transmitted wave so that the following wave fields

$$E'_u(x,y) = \sum_{p=-\infty}^{\infty} [T'_p \exp(i\beta'_p y)]\exp(i\alpha'_p x) \qquad \text{in } D_u,$$

and

$$E'_\ell(x,y) = \sum_{p=-\infty}^{\infty} [\delta_{p0}\exp(i\beta'_0 y) + R'_p\exp(-i\beta'_p y)]\exp(i\alpha'_p x) \qquad \text{in } D_\ell$$

are established. On substituting these expressions into (4.5) and noting the field symmetry given by $R'_p = R_{-p}$ and $T'_p = T_{-p}$, one derives

$$\mathrm{Re}(R_0\overline{T}_{-1} + R_{-1}\overline{T}_0) = 0 \qquad \text{(LR, UD)} \tag{4.8}$$

The final conservation relation appropriate to this mount,

$$\mathrm{Re}(R_0\overline{T}_0 + R_{-1}\overline{T}_{-1}) = 0 \qquad \text{(UD)} \tag{4.9}$$

may be similarly derived, this time by returning a wave along the path of the original $(-1)^{th}$ order transmitted wave. However, its derivation requires that only up-down symmetry is invoked.

These properties have been verified numerically, sample evidence of which can be found in table 4.1a.

Table 4.1a Confirmation of the Littrow Field Constraints for a -1 Order Littrow Mount

These results were obtained for an UD, LR symmetric double grating [4.13] composed of two identical lamellar arrays specified by $c/d = 0.8$, $h/d = 0.4$. The arrays were separated by $S/d = 0.6$ and were arranged with zero relative displacement ($\delta x/d = 0$). The grating, operated in a -1 order Littrow mount, was illuminated by P polarized radiation of wavelength $\lambda/d = 1.2001$. The fields were specified by 4 waveguide modes and 10 Rayleigh orders. The Rayleigh orders were symmetrically chosen [4.11] about the Littrow order $\{p|-1-n \le p \le n \text{ for } n \ge 0\}$ so the Littrow constraints are satisfied analytically. In the following, $\Phi_p^R = (\rho_p^R, \arg(R_p))$ where ρ_p^R and $\arg(R_p)$ denote respectively the efficiency and phase of the p^{th} reflected order. A superscript T refers to transmitted orders.

$$\Phi_0^R = (0.1315478654, -134.37053299^\circ)$$

$$\Phi_{-1}^R = (0.4061970027, 44.642000892^\circ)$$

$$\Phi_0^T = (0.2323407636, -46.65716855^\circ)$$

$$\Phi_{-1}^T = (0.2299143685, -46.66589318^\circ)$$

Using these results, it follows that

$$\mathrm{Re}[R_0\bar{R}_{-1} + T_0\bar{T}_{-1}] = 4.9\times10^{-10}$$

$$\mathrm{Re}[R_0\bar{T}_{-1} + R_{-1}\bar{T}_0] = 2.2\times10^{-8}$$

$$\mathrm{Re}[R_0\bar{T}_0 + R_{-1}\bar{T}_{-1}] = 2.2\times10^{-8} \quad .$$

4.2.2 Constraints for Long Wavelength Radiation

This section discusses the constraints which may be derived using an integral technique, for a lossless grating operated in radiation whose wavelength is sufficiently long so that only the zeroth order reflected and transmitted waves are propagating.

Consider then a long wavelength plane wave I incident at some angle ϕ upon a lossless grating possessing LR symmetry. Let the resulting reflected and transmitted propagating waves have complex amplitudes R_0 and T_0 respectively, as shown in figure 4.2a. A second incident wave I' is returned from below the grating (also at an angle ϕ to the normal). Let the resulting zeroth order reflection and transmission complex amplitudes be R_0' and T_0' respectively.

Conservation of energy for this field distribution may be expressed in the form

$$|R_0 + T_0'|^2 + |R_0' + T_0|^2 = 2 \qquad \text{(CE)} \qquad (4.10)$$

However, from LR symmetry and the Reciprocity Theorem,

$$T_0' = T_0 \qquad \text{(LR, RT)}$$

and

$$|R_0'| = |R_0| \qquad \text{(CE)}$$

With these constraints, some simple manipulation reduces equation (4.10) to the form

$$\mathrm{Re}(R_0\overline{T}_0 + R_0'\overline{T}_0) = 0 \qquad \text{(LR)} \qquad (4.11)$$

or

$$\tfrac{1}{2}\,[\arg(R_0) + \arg(R_0')] - \arg(T_0) = \frac{\pi}{2} + (\pi) \qquad (4.12)$$

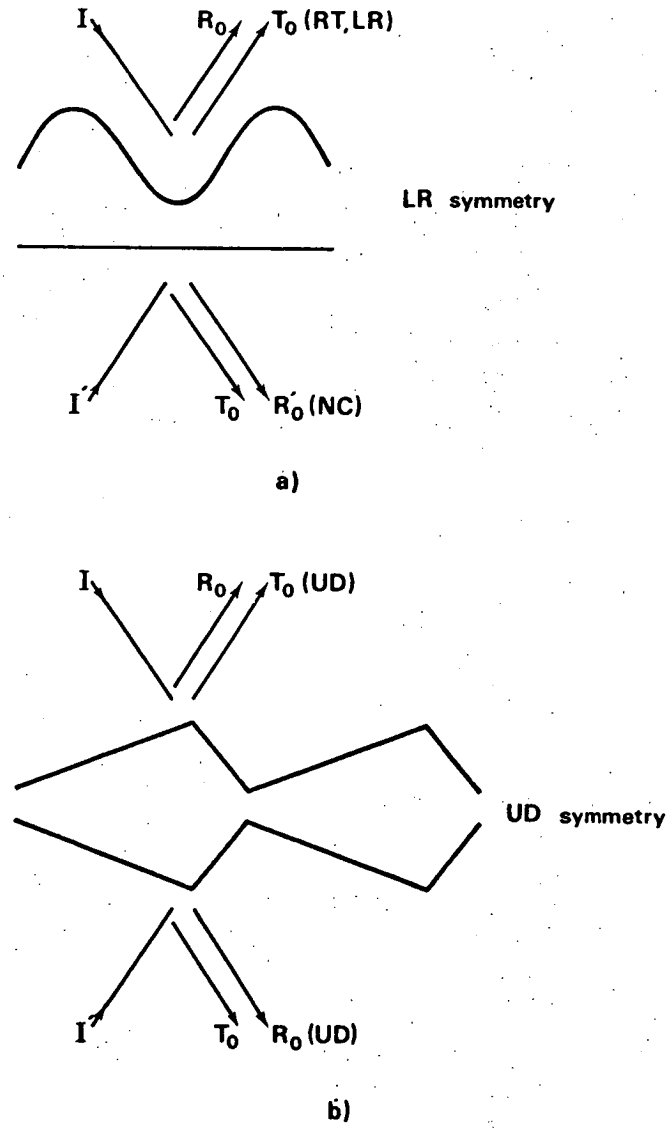

Figure 4.2 Integral derivation of constraints appropriate to the long wavelength case.

Here (π) denotes an arbitrary additive multiple of π.

Note that in the case of normal incidence, the Reciprocity Theorem alone will constrain $T_0' = T_0$ so that under these conditions it is not necessary to impose the constraint of LR symmetry to derive equations (4.11, 4.12).

For structures possessing UD-symmetry only (such as that shown in figure 4.2b), $R_0 = R_0'$ and $T_0 = T_0'$ and these constraints together with the conservation of energy criterion (4.10) lead to the simpler result

$$\arg(R_0) - \arg(T_0) = \pi/2 + (\pi) \qquad \text{(UD)} \qquad (4.13)$$

Numerical confirmation of these results is given in table 4.1b.

4.3 TIME REVERSIBILITY AND ITS APPLICATION TO CONSERVATION THEOREMS

The concept of time reversibility provides a means of establishing conservation relations for lossless structures, which, as the following sections demonstrate, is more powerful than the integral techniques. Grivet [4.14] has given a lucid discussion of this concept. In the context of this thesis the following principle is sufficient: the field distribution in the lossless system is unmodified if the directions of all wave vectors are reversed and the conjugates of all complex amplitudes are taken.

The application of the principle of time reversal is now considered in the following situations:

(1) a lossless, symmetric structure operated in long wavelength radiation such that only the zeroth orders in reflection and transmission are propagating (section 4.3.1),

(2) a lossless "asymmetric" structure formed by displacing relative to one another the grooves of a two element LR, UD symmetric grating, operated in normally incident, long wavelength radiation (section 4.3.1.4), and

Table 4.1b

Numerical Evidence of the Long Wavelength Rayleigh Phase Properties for LR Symmetric Structures (non-normal incidence) and Asymmetric Structures (normal incidence).

Pol.	m	Symmetry	$\arg(R_0)^\circ$	$\arg(T_0)^\circ$	$\arg(R_0')^\circ$	X
P	20	LR	-175.622	-108.078	139.947	90.241
S	20	LR	-55.534	-159.809	-83.448	90.319
P	30	LR	-176.541	-108.634	139.523	90.125
S	30	LR	-56.199	-160.152	-83.693	90.205
P	20	NC	-62.609	173.474	-130.248	90.098
S	20	NC	115.541	173.696	51.907	90.028
P	30	NC	-62.667	173.485	-130.220	90.071
S	30	NC	115.105	173.488	51.877	90.003

These results were obtained for the following structures:

(a) The optical arrangement shown in figure 4.2a. The sine profile is defined by a depth of 0.18 μm. and period of 1.0 μm. and is placed 0.20 μm. beneath the planar surface. The refractive index of the dielectric grating is taken to be 3.1 (LR)

(b) A triangular profile of blaze angle 10° and period 1 μm., 0.21 μm. above a planar surface. Again the refractive index of the grating is chosen to be 3.1 (NC)

$X = \frac{1}{2}[\arg(R_0) + \arg(R_0')] - \arg(T_0) + (\pi)$.

Note that the original data were obtained from the numerical solution of a Fredholm integral equation of the first kind (using a points matching technique) and thus the final results are non-analytic.

m denotes the number of sampling points per period.

(3) a lossless symmetric grating operated in a first order Littrow mount (section 4.3.2).

Note that analyses presented in all subsequent sections assume the radiation to be P polarized but the same derivations and relations apply to the orthogonal polarization.

4.3.1 The Long Wavelength Case

Consider a plane wave I incident upon the lossless structure shown in figure 4.3 at some angle ϕ such that there are only two plane wave output energy channels, R_0 and T_0 (state 1). Upon application of time reversibility there are now two input channels $\overline{R}_0$ and $\overline{T}_0$ and a single output channel $\overline{I}$ (state 2).

Initially the far field behaviour is discussed and LR symmetry is invoked. State 2 of figure 4.3 is regarded as the superposition of states 2a and 2b, and thus the following equations are obtained.

$$|R_0|^2 + |T_0|^2 = 1 \qquad \text{(LR)} \qquad (4.14)$$

$$\overline{R}_0 T_0 + \overline{T}_0 R_0' = 0 \qquad \text{(LR)} \qquad (4.15)$$

Since UD symmetry has not been assumed, then R_0' is not constrained (NC) to be equal to R_0, but their moduli are equal (CE). The result expressed in equation (4.12) is derived from (4.15).

The uniqueness condition [4.15] is now invoked in order to extend these far field results to all space. Here the assertion is that if two fields diffracted by the same structure exhibit the same far field behaviour, then their difference has zero far field and is zero everywhere in space. In the upper and lower free space regions D_u and D_ℓ, field distributions $E_u(x,y)$ and $E_\ell(x,y)$ are defined to be excited by the incident plane wave I. Time reversal then implies that the fields

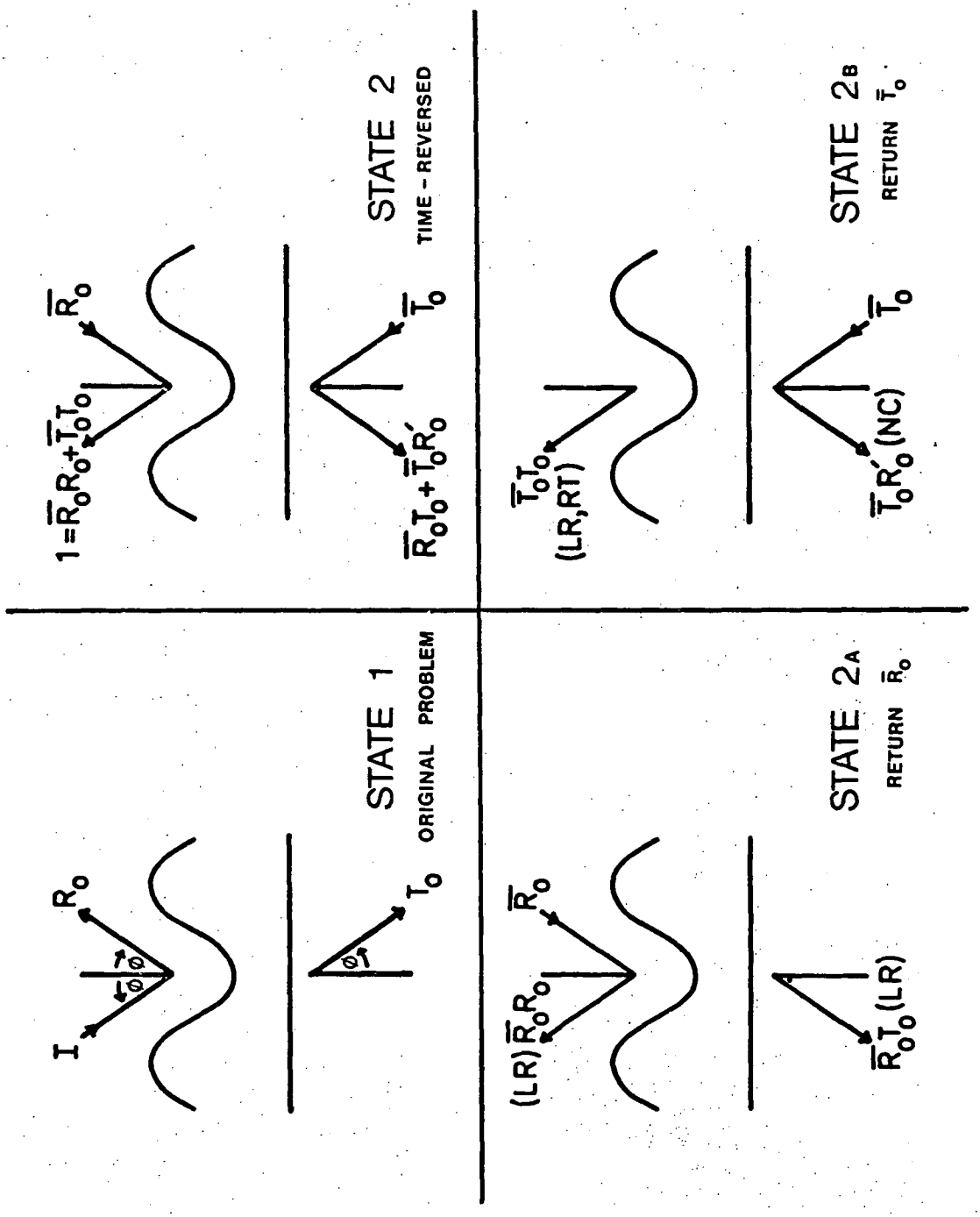

Figure 4.3 Time reversal treatment of the long wavelength problem.

in D_u and D_ℓ excited by the incident fields $\bar{R}_0$ and $\bar{T}_0$ of state 2 are given by $\bar{E}_u(x,y)$ and $\bar{E}_\ell(x,y)$ respectively.

In D_u, an incident field $\bar{R}_0$ gives rise to a wave field $\bar{R}_0 E_u(-x,y)$ because of LR symmetry. In order to be able to relate fields corresponding to an incident wave in D_ℓ to those applying to the initial situation, the additional assumption of UD symmetry must be invoked. Thus the form of this field corresponding to an incident wave of amplitude $\bar{T}_0$ in D_ℓ is $\bar{T}_0 E_\ell(-x,-y)$. Hence, for all UD, LR symmetric structures,

$$\bar{E}_u(x,y) = \bar{R}_0 E_u(-x,y) + \bar{T}_0 E_\ell(-x,-y) \quad . \tag{4.16}$$

In order to express the time reversed field $\bar{E}_\ell(x,y)$ in medium D_ℓ as a linear superposition of E_u and E_ℓ, both LR and UD symmetry must again be imposed and it follows that

$$\bar{E}_\ell(x,y) = \bar{T}_0 E_u(-x,-y) + \bar{R}_0 E_\ell(-x,y) \tag{4.17}$$

Equations (4.16) and (4.17) are the most general form of the constraints on the lossless symmetric system.

In the following sections specific field representations (appropriate to their various regions of convergence) will be applied in order to extract a number of explicit conservation relations.

4.3.1.1 *Application to Rayleigh Fields*

For those regions of D_u and D_ℓ not lying within the grooves of the grating, the fields E_u and E_ℓ may be expressed in terms of Rayleigh series. On substituting expressions (4.1) and (4.2) into (4.17) and equating the coefficients of like plane waves, it can be seen that

(a) the contribution from the real order term ($p = 0$) yields

$\bar{R}_0 T_0 + \bar{T}_0 R_0 = 0$, and

(b) the evanescent order terms ($p \neq 0$) give rise to

$$\bar{T}_p = \bar{R}_0 T_p + \bar{T}_0 R_p \quad . \tag{4.18}$$

Similarly, from equation (4.16),

(a) $|R_0|^2 + |T_0|^2 = 1$ from the zeroth order term, and

(b) $\bar{R}_p = \bar{R}_0 R_p + \bar{T}_0 T_p$ from the evanescent order contributions.

The significance of the real order terms, discussed in section 4.2.2, may be readily seen from an inspection of figure 4.3. Now consider the evanescent order contributions. These properties (which cannot be extracted from the integral treatment) may be readily summarised in the form

$$\arg(A_p) = \tfrac{1}{2} \arg(A_0) + (\pi) \qquad (p \neq 0) \tag{4.19}$$

$$\arg(B_p) = \tfrac{1}{2} \arg(B_0) + (\pi) \qquad (p \neq 0) \tag{4.20}$$

where

$$A_p = R_p + T_p \tag{4.21}$$

$$B_p = R_p - T_p \tag{4.22}$$

Numerical evidence of these relations obtained using the double grating formalism [4.12] is presented in table 4.2a.

4.3.1.2 *Application to Modal Formalisms*

The importance of the general field constraints (equations (4.16) and (4.17)) to modal formalisms will now be discussed. Only those formalisms for which it is possible to expand the groove fields in terms

Table 4.2a

Demonstration of the Long Wavelength Phase Constraint for the Rayleigh Fields

Order p	$\lvert R_p \rvert$	$\arg(R_p)^o$	$\lvert T_p \rvert$	$\arg(T_p)^o$	$\arg(A_p)^o$	$\arg(B_p)^o$
0(real)	0.93946	26.1651	0.34265	116.1651	46.2035	6.1267
-1(evan)	4.50734	-164.1307	1.47349	-134.2479	-156.8983	-176.9367
+1(evan)	6.9267×10^{1}	-164.8529	1.8683×10^{1}	-126.0298	-156.8983	-176.9367
-2(evan)	2.4431×10^{1}	5.0619	1.9763×10^{1}	-179.4075	23.1017	3.0633
+2(evan)	2.5723×10^{3}	14.8127	6.3213×10^{2}	59.0216	23.1017	3.0633
-3(evan)	3.3958×10^{3}	17.6967	1.6579×10^{3}	34.2265	23.1017	3.0633
+3(evan)	8.4597×10^{4}	-165.0203	2.1782×10^{4}	-123.6189	-156.8983	-176.9367

These results were obtained for a double grating composed of two identical lamellar arrays specified by $c/d = 0.8$, $h/d = 0.4$ with zero relative displacement ($\delta x/d = 0$), separated by $S/d = 0.6$. The grating was operated in P polarized radiation of wavelength $\lambda/d = 1.8$ and incident at $\phi = 35^o$. The run was performed with 6 waveguide modes in each array and 9 Rayleigh orders. These results confirm equations (4.19) and (4.20).

Notice also that these results show $|R_0|^2 + |T_0|^2 = 1$, $\arg(T_0) - \arg(R_0) = \pi/2$.

of separable modes will be considered. The following classification of the modes can then be made because of the assumed LR and UD symmetries of the structure.

(a) LR symmetric and antisymmetric modes, namely

$$\left.\begin{aligned} E_m^x(x) &= E_m^x(-x) \\ \text{and} \quad O_m^x(x) &= -O_m^x(-x) \end{aligned}\right\} \tag{4.23}$$

(b) UD symmetric and antisymmetric modes

$$\left.\begin{aligned} E_m^y(y) &= E_m^y(-y) \\ \text{and} \quad O_m^y(y) &= -O_m^y(-y) \end{aligned}\right\} \tag{4.24}$$

Naturally in making such definitions it is essential to select the axes of the coordinate system to be coincident with the axes of symmetry of the physical system. Furthermore, since the structure is assumed lossless, the diffraction problem may be expressed in a self-adjoint form and it is possible, without loss of generality to take all modal functions to be real. Also as a consequence of the self-adjoint nature of the problem, no coupling terms arise between different modes. Hence, it is possible to speak unambiguously of the "energy flux" carried by a mode".

Since the next section derives the property of "detailed balance of modal fluxes" which relies upon the analysis of a structure having two systems of grooves, this arrangement will be considered here. Obviously relations for a single array will follow similarly.

Using the definitions (4.23, 4.24), the field in the upper grooves may now be written as

$$E_u(x,y) = \sum_{m=1}^{\infty} [a_m^E O_m^y(y') + b_m^E E_m^y(y')]E_m^x(x) + \sum_{m=1}^{\infty} [a_m^O O_m^y(y') + b_m^O E_m^y(y')]O_m^x(x)$$

(4.25)

where $y' = y - s$, s representing the displacement of the axis of groove symmetry from the axis of grating symmetry. In a similar manner the field in the lower set of grooves is specified by

$$E_\ell(x,y) = \sum_{m=1}^{\infty} [\hat{a}_m^E O_m^y(y'') + \hat{b}_m^E E_m^y(y'')]E_m^x(x) + \sum_{m=1}^{\infty} [\hat{a}_m^O O_m^y(y'') + \hat{b}_m^O E_m^y(y'')]O_m^x(x)$$

(4.26)

where $y'' = y + s$.

On substituting these expansions into equation (4.17) and equating the coefficients of like modal terms, the following relations are obtained.

$$\left.\begin{aligned} \bar{\hat{a}}_m^E &= \bar{R}_0 \hat{a}_m^E - \bar{T}_0 a_m^E \\ \bar{\hat{b}}_m^E &= \bar{R}_0 \hat{b}_m^E + \bar{T}_0 b_m^E \end{aligned}\right\} \qquad (4.27)$$

Equation (4.16) yields a further set of relations

$$\left.\begin{aligned} \bar{a}_m^E &= \bar{R}_0 a_m^E - \bar{T}_0 \hat{a}_m^E \\ \bar{b}_m^E &= \bar{R}_0 b_m^E + \bar{T}_0 \hat{b}_m^E \end{aligned}\right\} \qquad (4.28)$$

Analogous relations linking the x anti-symmetric modal coefficients may be found. After some elementary manipulation, the information contained in equations (4.27) and (4.28) may be summarised by equations of

the form

$$\arg(a_m^E + \hat{a}_m^E) = \tfrac{1}{2}\arg(B_0) + (\pi) \tag{4.29}$$

$$\arg(a_m^E - \hat{a}_m^E) = \tfrac{1}{2}\arg(A_0) + (\pi) \tag{4.30}$$

The results expressed in these two equations are the analogues (for single periodicity) of the common modal phase property established by McPhedran and Maystre [4.5]. Numerical confirmation of these properties for a LR, UD symmetric double grating is presented in table 4.2b.

Although these properties may not appear to be of fundamental importance, they do enable a rather startling phenomenon, which is referred to herein as the detailed energy balance of the mode structure in the upper and lower arrays of grooves, to be explained.

4.3.1.3 *Detailed Balance of Modal Fluxes*

Before commencing the mathematical analysis of this phenomenon, the result will be accurately defined. In each of the upper and lower arrays of grooves, it is possible to calculate a set of modal energy fluxes $\{F_m^{E/O}\}$ and $\{\hat{F}_m^{E/O}\}$ respectively. Here the 'E' and the 'O' refer to the LR symmetric and antisymmetric modes respectively. If the structure possesses both LR and UD symmetry, then the flux of each mode is array invariant,

i.e. $$F_m^{E/O} = \hat{F}_m^{E/O} \qquad \text{for all } m \tag{4.31}$$

This flux invariance may be shown to be equivalent to

$$\mathrm{Im}(a_m \bar{b}_m)\big|_{E/O} = \mathrm{Im}(\hat{a}_m \bar{\hat{b}}_m)\big|_{E/O} \quad . \tag{4.32}$$

Consider now the derivation of this property for the even LR

Table 4.2b

Results confirming the modal field phase constraints applying to the long wavelength formulation and the 'detailed balance' of modal fluxes.

m	x-symmetry	$\arg(a_m+\hat{a}_m)^o$	$\arg(a_m-\hat{a}_m)^o$	F_m	$\hat{F}_m$	$\arg(a_m+\hat{a}_m)^o - \frac{1}{2}\arg(B_0)^o$	$\arg(a_m-\hat{a}_m)^o - \frac{1}{2}\arg(A_0)^o$
1	E	-176.937	-156.898	0.11686	0.11686	180	180
2	O	93.063	113.102	0.46449×10^{-3}	0.46449×10^{-3}	90	90
3	E	-176.937	-156.898	0.80501×10^{-4}	0.80501×10^{-4}	180	180
4	O	93.063	113.102	0.30167×10^{-5}	0.30167×10^{-5}	90	90
5	E	-176.937	-156.898	0.11184×10^{-5}	0.11184×10^{-5}	180	180
6	O	93.063	113.102	0.63581×10^{-7}	0.63581×10^{-7}	90	90

These results were obtained using the diffracting arrangement described in table 4.2a and 6 waveguide modes in each array and 9 Rayleigh orders to specify the fields. The values of $\arg(A_0)$ and $\arg(B_0)$ given in table 4.2a were also used.

symmetric modes. The information contained in equations (4.27) and (4.28) is best summarised in the following matrix notation

$$\overline{A} = \overline{M}A \; ; \quad \overline{B} = \overline{M}B$$

where

$$A = \begin{bmatrix} a_m^E \\ -\hat{a}_m^E \end{bmatrix} \qquad B = \begin{bmatrix} b_m^E \\ \hat{b}_m^E \end{bmatrix}$$

and

$$M = \begin{bmatrix} R_0 & T_0 \\ T_0 & R_0 \end{bmatrix}$$

At this point it should be noted that M is a unitary matrix. To derive equation (4.32) consider the product

$$\begin{aligned} A^T\overline{B} &= \overline{A^T}\, M^T\, \overline{M}\, B \\ &= \overline{A^T}\, I\, B \\ &= \overline{A^T}\, B \end{aligned} \quad ,$$

i.e.

$$\mathrm{Im}(a_m^E \overline{b}_m^E - \hat{a}_m^E \overline{\hat{b}}_m^E) = 0 \quad .$$

Of course an identical result can be derived for the LR antisymmetric modes. Numerical examples of these properties (pertaining to the double grating) are presented in table 4.2b.

4.3.1.4 *An Asymmetric Arrangement of the Upper and Lower Arrays of Symmetric Grooves*

In this section the discussion centres on the conservation relations associated with an asymmetric structure constructed by displacing (relative to one another) the upper and lower arrays of the

previously discussed UD, LR symmetric grating.

Consider long wavelength radiation incident upon the structure shown in figure 4.4. Now invoking the principle of time reversibility, incident fields are returned as the waves $\overline{R}_0$ and $\overline{T}_0$. If the point $(\frac{\delta x}{2},0)$ is taken to be the phase origin, it becomes evident that the wave returned along the channel $\overline{T}_0$ is incident upon a structure almost identical to that which diffracted the original incident wave. (In fact, it is exactly the same except for the transformation $x \to -x$).

However, from an inspection of the accompanying diagram, it is clear that the same remarks do not apply to a wave returned along the path $\overline{R}_0$. Only for normally incident radiation can both $\overline{R}_0$ and $\overline{T}_0$ be incident upon a structure that is essentially the same to both waves.

Hence for normally incident radiation, the general conservation relations for the system can be written

$$\overline{E}_u(x,y) = \overline{R}_0 E_u(x,y) + \overline{T}_0 E_\ell(-x,-y) \tag{4.33}$$

$$\overline{E}_\ell(x,y) = \overline{T}_0 E_u(-x,-y) + \overline{R}_0 E_\ell(x,y) \tag{4.34}$$

Upon substituting the Rayleigh expansions (equations (4.1) and (4.2)) into expressions (4.33) and (4.34), the following constraints can be derived.

$$\left.\begin{aligned} &\text{(a) for the real order } (p = 0) \quad |R_0|^2 + |T_0|^2 = 1, \\ &\qquad\qquad\qquad\qquad\qquad\qquad \mathrm{Re}(R_0\overline{T}_0) = 0, \end{aligned}\right\} \tag{4.35}$$

and (b) for the evanescent orders $(p \neq 0)$

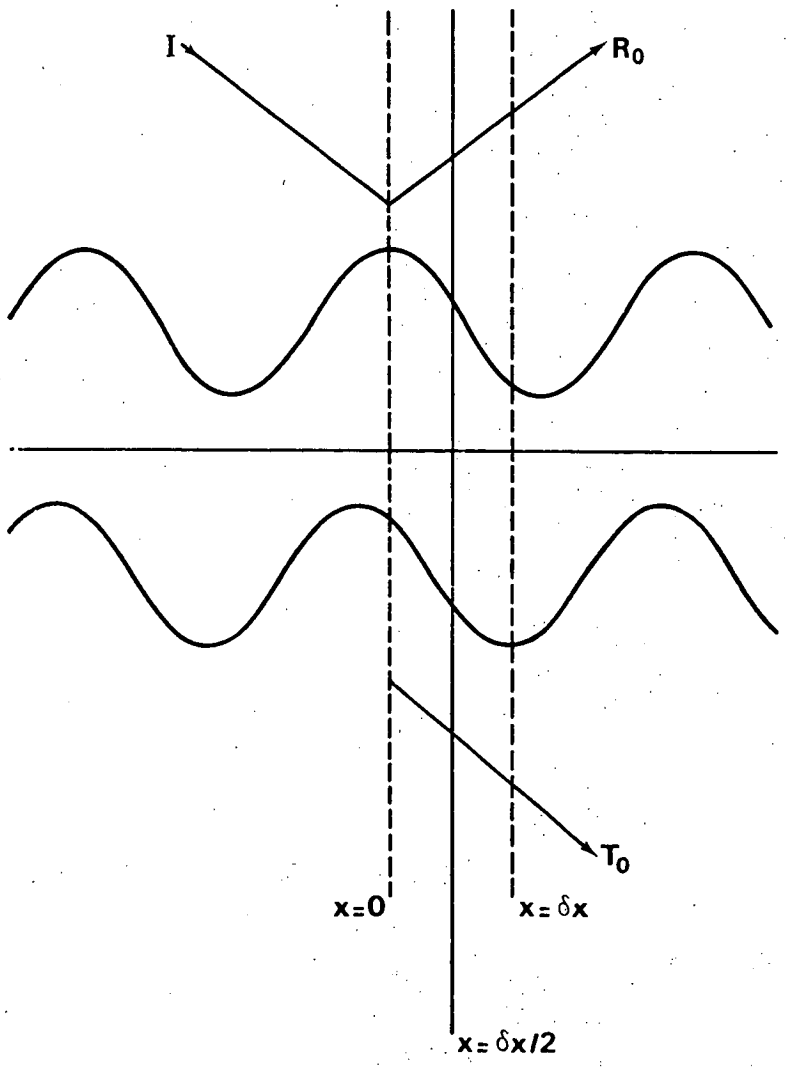

Figure 4.4 The asymmetric structure of section 4.3.1.4.

$$\left.\begin{aligned} \overline{R}_p &= \overline{R}_0 R_{-p} + \overline{T}_0 T_p \quad , \\ \overline{T}_p &= \overline{T}_0 R_p + \overline{R}_0 T_{-p} \quad . \end{aligned}\right\} \tag{4.36}$$

(It is to be noted that when $\delta x = 0$ equations (4.36) revert to their earlier form discussed in section 4.3.1.1). Once again these evanescent order properties may be summarised in the concise notation

$$\arg(A_p + A_{-p}) = \tfrac{1}{2} \arg(A_0) + (\pi) \tag{4.37}$$

$$\arg(A_p - A_{-p}) = \tfrac{1}{2} \arg(B_0) - \pi/2 + (\pi) \tag{4.38}$$

$$\arg(B_p + B_{-p}) = \tfrac{1}{2} \arg(B_0) + (\pi) \tag{4.39}$$

$$\arg(B_p - B_{-p}) = \tfrac{1}{2} \arg(A_0) - \pi/2 + (\pi) \tag{4.40}$$

using the definitions for A_p and B_p given in equations (4.21, 4.22). Sample numerical results confirming these assertions for the double grating are given in table 4.3a.

Constraints on the modal quantities may also be established [4.16] using a treatment analogous to that discussed in section 4.3.1.2. The detailed modal flux balance which is observed numerically (table 4.3b) may be readily verified from these relations.

4.3.2 The First Order Littrow Configuration

In general it is not possible to apply the time reversal (or any other) treatment to devise further conservation relations (relying only upon a knowledge of the original diffraction problem) for arbitrary wavelength and angle of incidence combinations. However, the angular symmetry of the field distribution associated with the first order Littrow mount (when only the first and zeroth orders are propagating) is

Table 4.3a

An example to verify the phase properties pertaining to the Rayleigh field quantities of an asymmetric double grating.

Order p	$\|R_p\|$	$\arg(R_p)^o$	$\|T_p\|$	$\arg(T_p)^o$	$\arg(A_p+A_{-p})^o$	$\arg(A_p-A_{-p})^o$	$\arg(B_p+B_{-p})^o$	$\arg(B_p-B_{-p})^o$
0(real)	0.59047	-89.8986	0.80706	-179.8986	-143.7085	-	-36.0887	-
-1(evan)	7.79043	-180.0250	1.5254×10^1	-6.7296	-71.8543	-108.0444	161.9556	18.1457
+1(evan)	7.90892	-108.2162	1.5315×10^1	-78.4082				
-2(evan)	2.4889×10^2	-88.5381	2.5600×10^2	-126.8985	-71.8543	71.9556	-18.0444	-161.8543
+2(evan)	2.4510×10^2	54.7156	2.5231×10^2	88.5983				
-3(evan)	5.8188×10^3	28.8298	3.0083×10^3	-211.4406	-71.8543	-108.0444	-18.0444	-161.8543
+3(evan)	5.7507×10^3	243.2105	2.8744×10^3	-65.9814				

Results obtained from the computer program for a double grating consisting of two identical lamellar arrays specified by the parameters $c/d = 0.8$, $h/d = 0.4$, separated by $S/d = 0.6$ and with a relative displacement $\delta x/d = 0.2$. The grating was operated in normally incident P polarized radiation of wavelength $\lambda/d = 1.8$ and 6 modes in each array and 9 Rayleigh orders were used to describe the fields. The above phases have been modified so that the phase origin lies at the axis of symmetry of the grating $x = \delta x/2$. These results confirm equations (4.37), (4.38), (4.39) and (4.40).

Table 4.3b

Numerical confirmation of the modal phase properties and 'detailed balance' of the modal fluxes for the asymmetric double grating.

m	x-symmetry	$\arg(a_m + \hat{a}_m)^\circ$	$\arg(a_m - \hat{a}_m)^\circ$	F_m	$\hat{F}_m$
1	E	161.956	108.146	.65049	.65049
2	O	108.146	161.956	$.41429\times10^{-11}$	$.41437\times10^{-11}$
3	E	161.956	108.146	$.85137\times10^{-3}$	$.85137\times10^{-3}$
4	O	108.146	161.956	$-.41003\times10^{-11}$	$-.41004\times10^{-11}$
5	E	161.956	108.146	$.11529\times10^{-4}$	$.11529\times10^{-4}$
6	O	108.146	161.956	$-.42576\times10^{-13}$	$-.42571\times10^{-13}$

These results are applicable to the diffracting arrangement specified in table 4.3a and were obtained from the computer program using 6 modes in each array and 9 Rayleigh orders. Again the phase origin was taken to be at $x = \delta x/2$. The above results, together with those presented in table 4.3a, can be used to verify the following properties:

$$\arg(a_m^E + \hat{a}_m^E) = \tfrac{1}{2}\arg(R_0 - T_0) + (\pi)$$

$$\arg(a_m^E - \hat{a}_m^E) = \tfrac{1}{2}\arg(R_0 + T_0) + (\pi)$$

$$\arg(a_m^O + \hat{a}_m^O) = \tfrac{1}{2}\arg(R_0 + T_0) + (\pi)$$

$$\arg(a_m^O - \hat{a}_m^O) = \tfrac{1}{2}\arg(R_0 - T_0) + (\pi)$$

sufficient to permit the elegant derivation of a further set of analytic constraints.

Consider a plane wave I incident upon the symmetric structure shown in figure 4.5. Upon applying the principle of time reversibility, there are now four input energy channels ($\overline{R}_0$, $\overline{R}_{-1}$, $\overline{T}_0$ and $\overline{T}_{-1}$) and a single outgoing energy channel ($\overline{I}$). States 2(a) to 2(d) of the accompanying diagram show a detailed examination of the return of these various waves together with a legend illustrating the minimum number of symmetry constraints that need to be applied in order to derive the propagating diffracted wave amplitudes. An inspection of state 2 reveals that the conservation relations derived using this treatment are identical to those discussed in section 4.2.1.

However, in order to be able to construct general field constraints of a similar form to those in equations (4.16) and (4.17), both UD and LR symmetries need to be invoked. For this particular mount the following relations are derived:

$$\overline{E}_u(x,y) = \overline{R}_{-1}E_u(x,y) + \overline{R}_0E_u(-x,y) + \overline{T}_{-1}E_\ell(x,-y) + \overline{T}_0E_\ell(-x,-y) \tag{4.41}$$

and

$$\overline{E}_\ell(x,y) = \overline{T}_{-1}E_u(x,-y) + \overline{T}_0E_u(-x,-y) + \overline{R}_{-1}E_\ell(x,y) + \overline{R}_0E_\ell(-x,y) \; . \tag{4.42}$$

After substituting the Rayleigh expansions (4.1) and (4.2) into equations (4.41) and (4.42) and equating the coefficients of like plane waves, the evanescent order contributions ($p \neq 0, -1$) are found to be of the form

$$\overline{R}_{-1-p} = \overline{R}_{-1}R_p + \overline{R}_0R_{-1-p} + \overline{T}_{-1}T_p + \overline{T}_0T_{-1-p}$$

and

$$\overline{T}_{-1-p} = \overline{T}_{-1}R_p + \overline{T}_0R_{-1-p} + \overline{R}_{-1}T_p + \overline{R}_0T_{-1-p} \; .$$

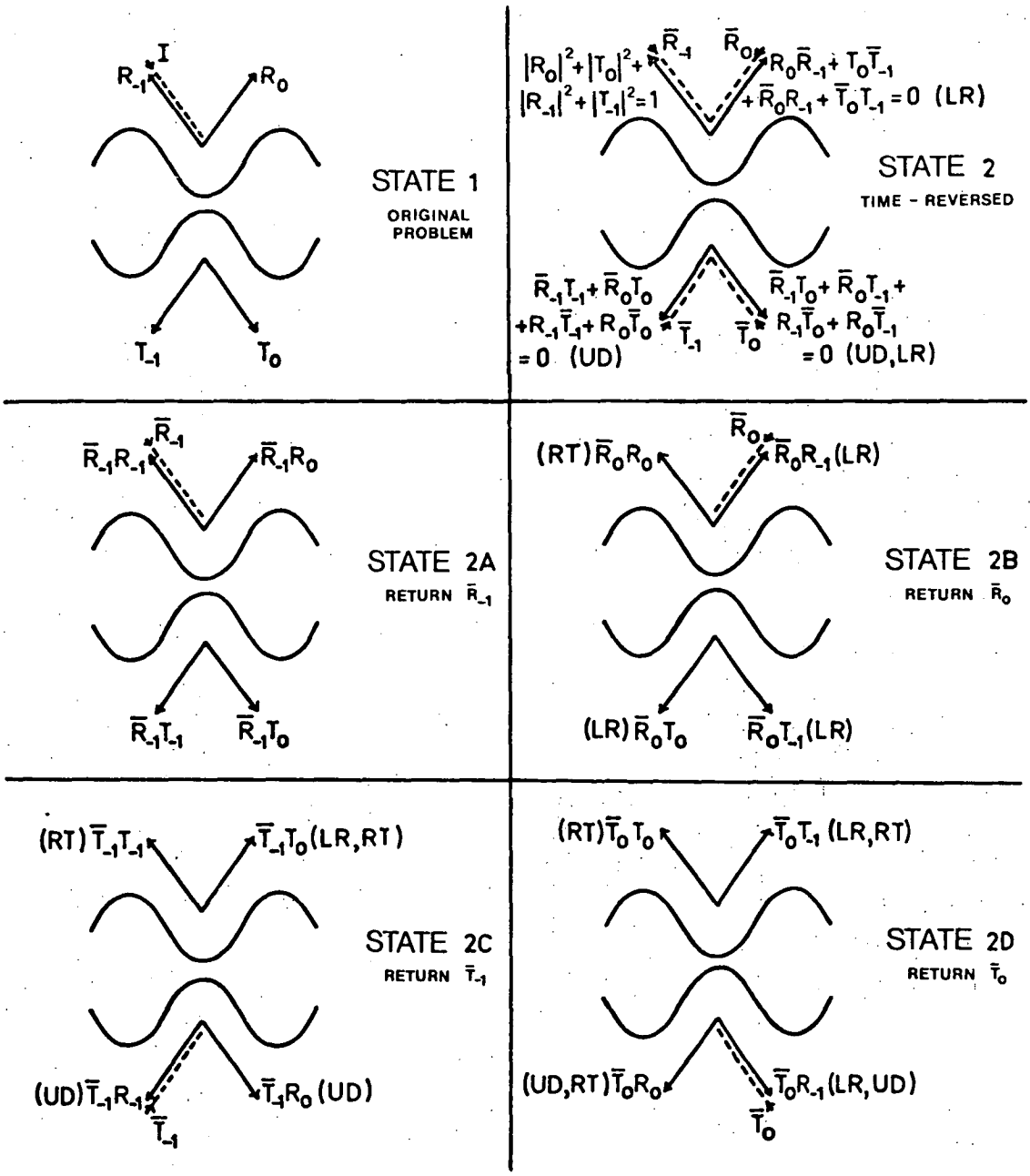

Figure 4.5 Time reversal treatment of the $(-1)^{th}$ order Littrow configuration.

These may be summarised as follows:

$$\arg(A_p + A_{-1-p}) = \tfrac{1}{2}\arg(A_0 + A_{-1}) + (\pi) \tag{4.43}$$

$$\arg(A_p - A_{-1-p}) = \tfrac{1}{2}\arg(A_0 - A_{-1}) + (\pi) \tag{4.44}$$

$$\arg(B_p + B_{-1-p}) = \tfrac{1}{2}\arg(B_0 + B_{-1}) + (\pi) \tag{4.45}$$

$$\arg(B_p - B_{-1-p}) = \tfrac{1}{2}\arg(B_0 - B_{-1}) + (\pi) \tag{4.46}$$

where A_p and B_p are defined in equations (4.21, 4.22).

If the general modal expansions, discussed in section 4.3.1.2, are also applied to equations (4.41) and (4.42), the following modal coefficient constraints are derived:

$$\left.\begin{aligned}
\bar{\hat{a}}_m^E &= \bar{R}^\dagger\, \hat{a}_m^E - \bar{T}^\dagger\, a_m^E \\
\bar{a}_m^E &= \bar{R}^\dagger\, a_m^E - \bar{T}^\dagger\, \hat{a}_m^E \\
\bar{\hat{b}}_m^E &= \bar{R}^\dagger\, \hat{b}_m^E + \bar{T}^\dagger\, b_m^E \\
\bar{b}_m^E &= \bar{R}^\dagger\, b_m^E + \bar{T}^\dagger\, \hat{b}_m^E
\end{aligned}\right\} \tag{4.47}$$

where

$$\left.\begin{aligned}
R^\dagger &= R_0 + R_{-1} \\
T^\dagger &= T_0 + T_{-1}
\end{aligned}\right\} \tag{4.48}$$

Then for example, these equations are written in the following summarised form:

$$\left.\begin{aligned}
\arg(a_m^E - \hat{a}_m^E) &= \tfrac{1}{2}\arg(R^\dagger + T^\dagger) + (\pi) \\
\arg(a_m^E + \hat{a}_m^E) &= \tfrac{1}{2}\arg(R^\dagger - T^\dagger) + (\pi)
\end{aligned}\right\} \tag{4.49}$$

A further set of relations applying to the LR antisymmetric modes may also be deduced.

Note that these expressions are identical in form to those presented in equations (4.27) and (4.28). It is this feature together with the result

$$|R^{\dagger}|^2 + |T^{\dagger}|^2 = |R_0|^2 + |R_{-1}|^2 + |T_0|^2 + |T_{-1}|^2 + 2\mathrm{Re}(R_0\bar{R}_{-1} + T_0\bar{T}_{-1}) = 1$$

that ensures the detailed balance of the modal fluxes for the UD, LR symmetric grating operated in this configuration. Numerical confirmation of these results is presented in tables 4.4.

4.4 CONCLUSIONS

A series of conservation relations for lossless, symmetric singly periodic diffraction gratings, derived by direct consideration of the field symmetry associated with the structure, have been presented. Until now, the consideration of symmetry in diffraction grating studies has been much neglected. However, as indicated by the results in this chapter, its application can yield a number of interesting field constraints of value to those involved in the testing of grating theories.

Relations have been derived not only for the propagating orders but also for the evanescent orders and the groove modes. In particular, the relations appropriate to the modal coefficients enable a fascinating property which we term the detailed balance of mode fluxes to be identified.

With the existence of such constraints having been established, it may well be possible to use these to some advantage in designing more efficient theories and algorithms. At first sight, it would appear that such algorithms would be of insufficient generality to be useful. However, it is stressed that the mountings considered here are the most interesting to users of gratings as spectrographic instruments (the Littrow mount) and as filters (the long wavelength mount).

Table 4.4a

Results demonstrating the phase properties for the evanescent Rayleigh orders applicable to a -1 order Littrow mount.

Order p	$\|R_p\|$	$\arg(R_p)^\circ$	$\|T_p\|$	$\arg(T_p)^\circ$	$\arg(A_p+A_{-1-p})^\circ$	$\arg(A_p-A_{-1-p})^\circ$	$\arg(B_p+B_{-1-p})^\circ$	$\arg(B_p-B_{-1-p})^\circ$
0(real)	0.36278	-133.3856	0.48212	-46.6548	-30.7135	-134.1289	117.3904	-134.4416
-1(real)	0.63729	45.2026	0.47939	-46.6683				
+1(evan)	5.1611×10^{1}	142.6262	1.9706×10^{1}	112.9256	164.6433	112.9356	-121.3048	112.7792
-2(evan)	5.0217×10^{1}	-97.8241	1.8974×10^{1}	112.5656				
+2(evan)	2.3965×10^{3}	-24.2412	1.2765×10^{3}	-53.9954	-15.3567	-67.0644	58.6952	-67.2208
-3(evan)	2.0336×10^{3}	59.5136	1.2710×10^{3}	-54.1249				

Results obtained for a diffracting arrangement identical to that used in table 4.2a, using 6 waveguide modes to describe the field in each array and 15 Rayleigh orders to specify the free space fields. These results confirm equations (4.43), (4.44), (4.45) and (4.46).

Table 4.4b

Demonstration of the modal phase properties and 'detailed balance' of modal fluxes for a (-1) order Littrow mount.

m	x-symmetry	$\arg(a_m+\hat{a}_m)^o$	$\arg(a_m-\hat{a}_m)^o$	F_m	$\hat{F}_m$
1	E	-121.305	164.643	.46221	.46221
2	O	22.779	22.936	$.37136\times10^{-5}$	$.37136\times10^{-5}$
3	E	-121.305	164.643	$.43104\times10^{-4}$	$.43104\times10^{-4}$
4	O	22.779	22.936	$.10264\times10^{-7}$	$.10264\times10^{-7}$
5	E	-121.305	164.643	$.70754\times10^{-6}$	$.70754\times10^{-6}$
6	O	22.779	22.936	$.12906\times10^{-9}$	$.12905\times10^{-9}$

Results obtained from the computer program for the diffracting geometry described in table 4.2a using 6 waveguide modes in each array and 15 Rayleigh orders. These results, together with those given in table 4.4a, demonstrate the following properties:

$$\arg(a_m^E - \hat{a}_m^E) = \tfrac{1}{2}\arg(R^{\dagger} + T^{\dagger}) + (\pi)$$

$$\arg(a_m^E + \hat{a}_m^E) = \tfrac{1}{2}\arg(R^{\dagger} - T^{\dagger}) + (\pi)$$

$$\arg(a_m^O + \hat{a}_m^O) = \tfrac{1}{2}\arg(R^{-} - T^{-}) + \pi/2 + (\pi)$$

$$\arg(a_m^O - \hat{a}_m^O) = \tfrac{1}{2}\arg(R^{-} + T^{-}) + \pi/2 + (\pi)$$

where $R^{-} = R_0 - R_{-1}$

and $T^{-} = T_0 - T_{-1}$

REFERENCES

[4.1] BOTTEN (L.C.), ADAMS (J.L,), McPHEDRAN (R.C.), DERRICK (G.H.). - J. Optics (Paris), 1980, 11, 43.

[4.2] PETIT (R.). - Rev. Opt., 1966, 45, 249.

[4.3] VAN DEN BERG (P.M.). - Thesis, Delft University of Technology, Delft, The Netherlands, 1971.

[4.4] AMITAY (N.), GALINDO (V.). - I.E.E.E. Trans. AP-17, 1969, 17, 747.

[4.5] McPHEDRAN (R.C.), MAYSTRE (D.). - Appl. Phys., 1977, 14, 1.

[4.6] URETSKY (J.L.). - Ann. Phys., 1965, 33, 400.

[4.7] PETIT (R.). - Opt. Acta, 1967, 14, 301.

[4.8] MAYSTRE (D.), McPHEDRAN (R.C.). - Opt. Commun., 1974, 12, 164.

[4.9] NEVIÈRE (M.), VINCENT (P.). - Opt. Acta, 1976, 23, 557.

[4.10] BOTTEN (L.C.). - Opt. Acta, 1978, 25, 481.

[4.11] ADAMS (J.L.), BOTTEN (L.C.), McPHEDRAN (R.C.). - J. Optics (Paris), 1978, 2, 78.

[4.12] BOTTEN (L.C.). - Thesis, University of Tasmania, Hobart, Tasmania, 1978.

[4.13] ADAMS (J.L.), BOTTEN (L.C.). - J. Optics (Paris), 1979, 10, 109.

[4.14] GRIVET (P.). - in "Proceedings of the Symposium on Modern Optics", Polytechnic Institute of Brooklyn, Polytechnic Press, New York, 1967.

[4.15] JONES (D.S.). - "Theory of Electromagnetism", Pergamon Press, New York, 1964, pp 56,-57, 562-566.

[4.16] ADAMS (J.L.), BOTTEN (L.C.). - University of Tasmania, Report DGRG 78/3.

CHAPTER 5

THE MULTI-ELEMENT GRATING

5.1 INTRODUCTION

In this chapter, the results of a study [5.1] of the diffraction properties of multi-element gratings are presented. These gratings are composed of an arbitrary number of identical, up-down symmetric, singly periodic transmission gratings lying in spatially separated parallel planes.

The formalism presented in section 5.2.2 is derived using a rigorous multiple scattering approach, which takes into account the interaction of all diffracted orders (both propagating and evanescent) between the individual elements of the grating stack. This treatment leads to the derivation of a matrix recurrence relation for the scattering matrices (and hence the complex amplitudes of the diffracted waves) of the multi-element grating.

The study reported in this chapter represents a generalisation of the earlier work of Botten [5.2], which describes a theoretical formalism for the far infrared transmission characteristics of multi-element grating interference filters. This formalism was developed by adopting a multiple scattering approach for the zeroth order diffracted waves. Consequently, the wavelength of the incident radiation was assumed to be longer than the grating period and the separation of the individual elements was assumed to be sufficiently large so that the zeroth order provided the only means of interaction between them. Using this analysis, a non-linear first order recurrence relation for the zeroth order diffracted amplitudes was derived. This equation was linearised and solved using

standard techniques.

Several new relations constraining the scattering matrices of the individual up-down symmetric, lossless elements of the multi-element grating are derived and presented in section 5.2.4. The relations are comprehensive in that they constrain the complex amplitudes of both propagating and evanescent orders diffracted by the grating for plane waves incident not only in the propagating order channels but also in the evanescent order channels. The conservation relations are shown to constrain the "physical" submatrix of the scattering matrix to be unitary, in accordance with the investigation of Uretsky [5.3]. The "physical" submatrix contains the elements of the scattering matrix corresponding to the propagating orders produced by waves incident in the propagating order channels. If the elements of the grating are also left-right symmetric then the scattering matrices are symmetric. Furthermore, the conservation relations are shown to hold analytically, independently of errors introduced by truncating the field expansions in the numerical calculation of the properties of a single lamellar transmission grating element. The multi-element grating containing an arbitrary number of elements is then shown in section 5.2.5 to possess the same conservation properties as the individual elements. Several studies [5.3 - 5.6] of this type have been undertaken previously and the properties derived here are a generalisation of those presented in chapter 4 of this thesis.

Multi-element interference filters are used extensively in the far infrared and many studies, which are reviewed in chapter 1, aimed at predicting the characteristics of filters composed of either grating or grid elements, have been published. However, most of these analyses rely upon the explanation of the characteristics of individual grating or grid

elements in terms of scalar theories.

The study reported in chapter 3 rigorously describes the diffraction properties of the double grating (a two-element lamellar grating) and discusses its use as a Fabry-Perot interferometer. The analysis in chapter 3 explicitly specifies the field in both groove regions and the three free space regions. The appropriate continuity conditions and the Method of Moments are applied to relate these fields. Consequently, the technique is not easily adapted to solve the more general problem. The study reported in this chapter encompasses the results described in chapter 3 and in the papers [5.2, 5.8]. The large number of elements in the grating enables quite varied filtering characteristics to be obtained and sample numerical results of the diffraction properties of multi-element lamellar transmission gratings are presented in section 5.3.

5.2 THE THEORETICAL ANALYSIS

5.2.1 Concepts and Nomenclature

The structure to be considered is composed of $(n + 1)$ (integer n, $n > 0$) identical, up-down symmetric singly periodic transmission gratings having period $d = 2\pi/K$ and separated from one another by a constant distance t as shown in figure 5.1. Also shown is the rectangular Cartesian coordinate system which is introduced with the OY axis normal to the elements in the multi-element grating stack and the OZ axis aligned with the grooves of the grating.

A plane wave of wavelength $\lambda = 2\pi/k$ is assumed to be incident upon the structure at some angle ϕ to the grating normal. The wavevector of this wave is taken to lie in the XOY plane and the two fundamental polarizations of the incident wave are considered. A discrete

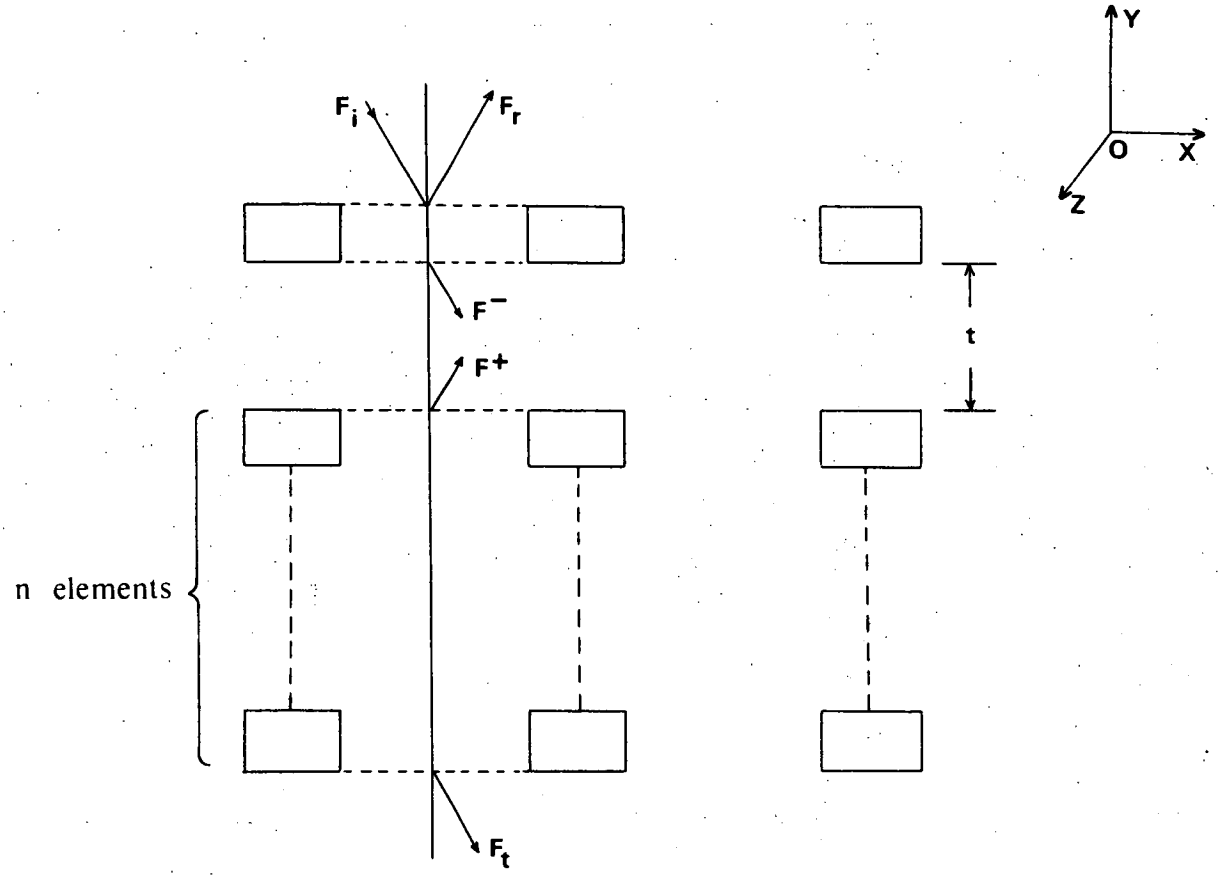

Figure 5.1 A side view of the (n + 1) -element grating and description of the notation used in the multiple scattering analysis.

set of diffracted plane waves is established, propagating in free space regions with direction sines α_r/k and direction cosines β_r/k. Here

$$\alpha_r = \alpha_0 + rK \qquad \text{(integer } r,\ -\infty < r < \infty\text{)} \tag{5.1}$$

$$\alpha_0 = k \sin \phi \quad , \tag{5.2}$$

$$\text{and} \quad \left.\begin{aligned} \beta_r &= \sqrt{k^2 - \alpha_r^2} && \text{if } |\alpha_r| \le k \\ &= i\sqrt{\alpha_r^2 - k^2} && \text{if } |\alpha_r| > k \end{aligned}\right\} \quad . \tag{5.3}$$

The fields in the free space regions are then specified by the summation of plane wave terms of the form

$$\left.\begin{aligned} &\exp[i(\alpha_r x + \beta_r y)] && \text{for upward going waves} \\ \text{and} \quad &\exp[i(\alpha_r x - \beta_r y)] && \text{for downward going waves} \end{aligned}\right\} \tag{5.4}$$

In order to derive the recurrence relation for the reflection and transmission scattering matrices describing the properties of the multi-element grating, it is necessary to regard the $(n + 1)$-element grating as a composite structure consisting of a single grating displaced from the remaining n-element stack (see figure 5.1). Before proceeding further, it is essential to note that the set of direction sines for the problem is closed. To explain this concept, a wave incident upon the single grating with direction sine α_0/k is considered. This wave is diffracted into a set of reflected and transmitted waves with direction sines constrained within the set $W = \{\alpha_p/k\}$. Each of these transmitted waves will be scattered by the n-element stack into a further series of orders whose direction sines are also elements of W, this process being

repeated ad infinitum for all subsequent reflections and transmissions.

In order to perform the multiple scattering analysis, the interaction between the individual elements of the grating and plane waves incident not only in the zeroth channel (i.e. with direction sine α_0/k) but also in any channel p (with direction sine α_p/k) must be characterised. This is most readily achieved by describing the scattering properties of each element of the stack by the reflection and transmission scattering matrices R_1 and T_1, where for example, the elements of R_1 are designated by R_{pq}. In this notation $R_{pq}/\sqrt{\beta_p}$ is the complex amplitude of the wave reflected into the p^{th} channel from an incident wave of complex amplitude $1/\sqrt{\beta_q}$ in the channel q. The apparently arbitrary scaling factors (i.e. $1/\sqrt{\beta_p}$) are introduced since their inclusion normalizes the diffraction problem with respect to the energy conservation properties. This is demonstrated in the sections discussing the inherent properties of the scattering matrices. Similar definitions apply to the elements of the matrix T_1 and to those of the scattering matrices R_n and T_n of the n-element stack. The phase origin of the complex amplitudes constituting the elements of R_1 is taken to be the upper surface of the single grating element while that for the elements of T_1 is the lower surface of this component. Correspondingly, the phase origins of the elements of R_n and T_n are the upper and lower surfaces respectively of the remaining n-element stack.

Following these preliminary definitions, the recurrence relations constraining the scattering matrices of the multi-element grating will be derived and the properties of the stack will be inferred from those of the single element.

5.2.2 Derivation of a Recurrence Relation

The complex amplitudes of the various channels of the incident

field are represented by the entries of a column vector F_i. These amplitudes have phase origins at the upper surface of the single element of the grating stack. In a similar manner, the overall reflected and transmitted fields are represented by F_r and F_t respectively (with phase origin at the upper surface of the single grating element and lower surface of the remaining elements of the grating stack respectively). The upward and downward scattered fields shown in figure 5.1 are represented by F^+ and F^-.

The diagonal matrix $P = \text{diag}\,(\exp(i\beta_p t))$ is introduced to describe the propagation of the set of plane waves across the region between successive elements of the grating. Then the field F^+ propagating upwards from the upper surface of the n-element stack becomes the field PF^+ at the lower surface of the single grating as shown in figure 5.1. Correspondingly F^-, representing a downward propagating field whose phase origin is at the lower surface of the single grating, becomes the field PF^- at the upper interface of the grating stack.

The scattering of the inward going fields F_i and PF^+ at the single grating is considered firstly. F_i will produce a reflected component R_1F_i and a transmitted component T_1F_i. By virtue of the up-down symmetry of the single grating, the other inward coming field PF^+ (see figure 5.1) produces an upward going transmitted field T_1PF^+ and a downward going reflected field R_1PF^+. Thus, it follows from the principle of linear superposition that

$$F_r = R_1F_i + T_1PF^+ \tag{5.5}$$

$$F^- = T_1F_i + R_1PF^+ \tag{5.6}$$

In an analogous manner, it also follows from consideration of the fields incident on the remaining n-elements of the grating stack that

$$F^{+} = R_n P F^{-} \tag{5.7}$$

$$F_t = T_n P F^{-} \tag{5.8}$$

By eliminating F^{+} and F^{-} from equations (5.5) - (5.8) it can be shown that

$$F_r = R_{n+1} F_i \tag{5.9}$$

$$F_t = T_{n+1} F_i \tag{5.10}$$

where $$R_{n+1} = R_1 + T_1 P R_n P (I - R_1 P R_n P)^{-1} T_1 \tag{5.11}$$

and $$T_{n+1} = T_n P (I - R_1 P R_n P)^{-1} T_1 \tag{5.12}$$

denote the reflection and transmission scattering matrices of the (n+1)-element grating. Here I denotes the identity matrix of appropriate dimension. Equations (5.11) and (5.12) may be stated more concisely in the form

$$A_{n+1} = A_1 + B_1 A_n (I - A_1 A_n)^{-1} B_1 \tag{5.13}$$

and $$B_{n+1} = B_n (I - A_1 A_n)^{-1} B_1 \tag{5.14}$$

where $A_k = R_k P$ and $B_k = T_k P$ $\quad k = 1, 2, \ldots n+1$

Equations (5.13) and (5.14) are the fundamental recurrence relations from which the scattering properties of a grating containing an arbitrary number of components can be deduced. It is noted that similar recurrence

relations can be derived by considering the (n+1)-element grating stack as being composed of an n-element structure placed above the remaining single element. The two derivations are equally valid.

Botten [5.2], when considering the properties of a multi-element grating stack whose elements were coupled only by the zeroth order diffracted waves, was able to linearize the non-linear recurrence relation for the diffracted amplitudes of the stack by a sequence of substitutions. This approach may also be used to linearize equations (5.13 - 14). However, this procedure is of no obvious benefit for this problem since the matrices referenced in equations (5.13 - 14) do not necessarily commute, thus inhibiting an elegant analytic solution. The linearized recurrence relation may be solved but only by introducing a large eigenvalue problem. Overall, the computational efficiency of the problem is markedly reduced by employing this linearization approach.

The multiple scattering technique may now be easily extended to consider a multi-element grating having arbitrary separations and arbitrary x-displacements of the elements composing it. The separation of the single grating and the remaining n-element grating stack is designated by t_n and the displacement of the stack relative to the single grating is denoted by δx_n. This parameter denotes the lateral distance between corresponding features of the upper grating in the n-element stack and the single grating. Naturally, the following matrices must also be introduced

$$P_n = \text{diag}\,(\exp(i\beta_p t_n))$$

and $$X_n = \text{diag}\,(\exp(i\alpha_p \delta x_n)) \quad .$$

The reflection and transmission scattering matrices associated with

the generalised (n+1)-element grating are then easily shown to be given by the following expressions, analogous to those given in equations (5.11, 5.12).

$$R_{n+1} = R_1 + T_1 P_n X_n^{-1} R_n P_n X_n (I - R_1 P_n X_n^{-1} R_n P_n X_n)^{-1} T_1 \qquad (5.15)$$

and $$T_{n+1} = X_n^{-1} T_n P_n X_n (I - R_1 P_n X_n^{-1} R_n P_n X_n)^{-1} T_1 \qquad (5.16)$$

5.2.3 Scattering Matrices for a Single Lamellar Transmission Grating

The reflection and transmission scattering matrices for a perfectly conducting single lamellar transmission grating are now derived explicitly to enable the properties of a multi-element lamellar grating to be determined. The motivations for choosing the components of the multi-element grating stack to be perfectly conducting lamellar transmission gratings were;

(a) that the theory describing the diffraction properties of this grating is well known [5.9, 5.10],

(b) that the structure is lossless and

(c) that the structure possesses both up-down and left-right symmetries. (The importance of this latter constraint will become evident in sections 5.2.4 - 5).

Also the grating is considered to be operated in P polarized radiation but the analysis may be easily applied to the other fundamental polarization. The derivation of the diffraction properties of the lamellar transmission grating presented in this section is based on the formalism developed for this structure by Maystre and Petit [5.10].

The geometry of the structure considered in this section is shown in figure 5.2. A plane P polarized wave is assumed to be incident in

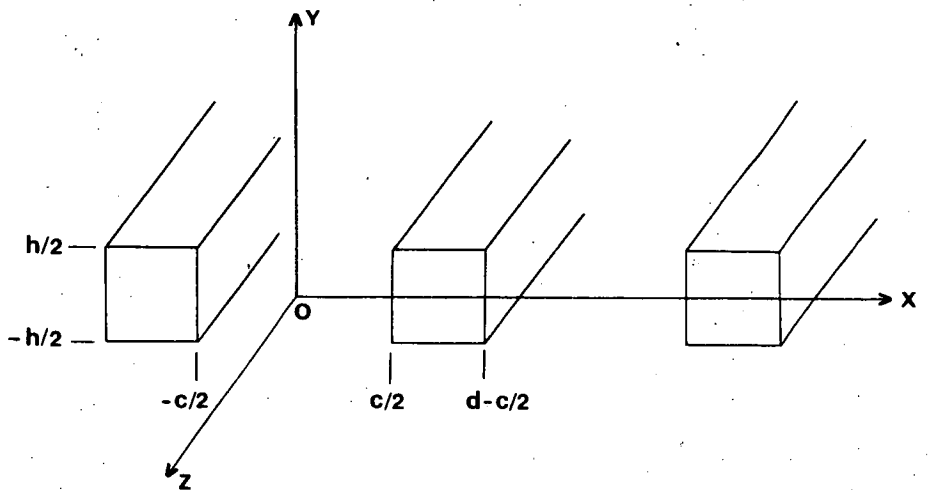

Figure 5.2 The geometry of the individual lamellar transmission gratings.

channel q (that is, with direction sine α_q/k). Since the radiation is P polarized, the electric field component along the OZ axis and its normal derivative are the only non-zero components of the diffracted fields. Consequently, all vector dependence of the fields may be suppressed.

The electric field in the free space region $y \geq h/2$ is given by the Rayleigh expansion

$$E(x,y) = \sum_{p=-\infty}^{\infty} \frac{1}{\sqrt{\beta_p}} [R_{pq} \exp(i\beta_p(y-h/2)) + \delta_{pq} \exp(-i\beta_q(y-h/2))] e_p(x) \tag{5.17}$$

where $$e_p(x) = \frac{1}{\sqrt{d}} \exp(i\alpha_p x) \tag{5.18}$$

and α_p, β_p have been defined in equations (5.1) and (5.3). Similarly for $y \leq -h/2$

$$E(x,y) = \sum_{p=-\infty}^{\infty} \frac{1}{\sqrt{\beta_p}} [T_{pq} \exp(-i\beta_p(y+h/2))] e_p(x) \tag{5.19}$$

while the field within the apertures ($|x| \leq c/2$, $|y| \leq h/2$) is given by

$$E(x,y) = \sum_{m=1}^{\infty} [b_{1;mq} \cos(\mu_m y) + b_{2;mq} \sin(\mu_m y)] N_m(x) \tag{5.20}$$

with $$N_m(x) = \sqrt{\frac{2}{c}} \sin[\frac{m\pi}{c}(x + c/2)]$$

and $$\mu_m = \sqrt{k^2 - (\frac{m\pi}{c})^2} \quad .$$

The boundary conditions applying to this polarization are

(a) $E = 0$ on the metal surfaces and is continuous across the aperture-free space interfaces, and

(b) $\frac{\partial E}{\partial y}$ is continuous across the aperture-free space boundaries.

The continuity of the electric field at $y = h/2$ is projected onto the orthogonal plane wave basis and the following equation is obtained

$$R_{pq} + \delta_{pq} = \sqrt{\beta_p} \sum_m [b_{1;mq}\cos(\mu_m h/2) + b_{2;mq}\sin(\mu_m h/2)]L_{pm} \tag{5.21}$$

where $$L_{pm} = \int_{-c/2}^{c/2} \bar{e}_p(x)N_m(x) \tag{5.22}$$

Similarly at $y = -h/2$, the projection of the field continuity onto the plane wave basis yields

$$T_{pq} = \sqrt{\beta_p} \sum_m [b_{1;mq}\cos(\mu_m h/2) - b_{2;mq}\sin(\mu_m h/2)]L_{pm} \tag{5.23}$$

At this stage, the up-down symmetry of the lamellar transmission grating is exploited to decouple the field problem into its y-symmetric and y-antisymmetric parts. The derivation of the scattering matrices for the y-symmetric problem is considered firstly. Adding equations (5.21) and (5.23) yields

$$S_{1;pq} + \delta_{pq} = 2\sqrt{\beta_p} \sum_m L_{pm} b^*_{1;mq} \tag{5.24}$$

where $S_{1;pq} = R_{pq} + T_{pq}$

and $b^*_{1;mq} = b_{1;mq}\cos(\mu_m h/2)$.

The continuity of the normal derivative of the electric field at $y = h/2$ is now considered. The expression of this continuity is projected onto the orthogonal waveguide modal basis and the following equation is obtained

$$\sum_{p=-\infty}^{\infty} i\sqrt{\beta_p}\,[R_{pq} - \delta_{pq}]\bar{L}_{pn} = -\mu_n[b_{1;nq}\sin(\mu_n h/2) - b_{2;nq}\cos(\mu_n h/2)] \tag{5.25}$$

The following equation may be derived similarly from the continuity of $\frac{\partial E}{\partial y}$ at $y = -h/2$:

$$\sum_{p=-\infty}^{\infty} -i\sqrt{\beta_p}\,T_{pq}\bar{L}_{pn} = \mu_n[b_{1;nq}\sin(\mu_n h/2) + b_{2;nq}\cos(\mu_n h/2)] \tag{5.26}$$

Equations (5.25) and (5.26) imply

$$\sum_{p=-\infty}^{\infty} i\sqrt{\beta_p}\,(S_{1;pq} - \delta_{pq})\bar{L}_{pn} = -2\mu_n b^*_{1;nq}\tan(\mu_n h/2) \tag{5.27}$$

Substitution of equations (5.24) in (5.27) leads to the relation

$$\sum_m [M_{nm} + iD_{1;nm}\delta_{nm}]b^*_{1;mq} = V_{nq} \tag{5.28}$$

where

$$M_{nm} = \sum_p \beta_p L_{pm}\bar{L}_{pn} \tag{5.29}$$

$$D_{1;nm} = -\mu_m \tan(\mu_m h/2) \tag{5.30}$$

and

$$V_{nq} = \sqrt{\beta_q}\,\bar{L}_{qn} \tag{5.31}$$

Definitions (5.29, 5.31) are best summarised by using the following matrix notation

$$M = L^H \beta L \quad ,$$

$$D_1 = \text{diag}\,(D_{1;nm}) \quad ,$$

and

$$V = L^H \beta^{\frac{1}{2}} \quad .$$

where $\beta = \text{diag}\ (\beta_p)$

and $L = [L_{pn}]$

At this stage it is worth noting that the elements of the diagonal matrix D_1 are purely real.

Using this matrix notation, equation (5.28) becomes

$$(M + iD_1)b_1^* = V \tag{5.32}$$

where $b_1^* = [b^*_{1;mq}]$. Similarly equation (5.24) may be rewritten as

$$S_1 = -I + 2\beta^{\frac{1}{2}}Lb_1^* \tag{5.33}$$

$$= -I + 2\beta^{\frac{1}{2}}L(M + iD_1)^{-1}L^H\beta^{\frac{1}{2}} \tag{5.34}$$

where $S_1 = [S_{1;pq}]$.

The numerical treatment involves solving the system of linear equations (5.32) for the modal coefficients $\{b^*_{1;mq}\}$ and then reconstructing the scattering matrix elements $S_{1;pq}$ using equation (5.33).

The y-antisymmetric problem follows in a precisely analogous manner. The system of linear equations corresponding to those presented in equation (5.32) now reads

$$(M + iD_2)b_2^* = V \tag{5.35}$$

while the analogous version of the reconstruction equation (5.34) is given by

$$S_2 = -I + 2\beta^{\frac{1}{2}}L(M + iD_2)^{-1}L^H\beta^{\frac{1}{2}} \tag{5.36}$$

Here $S_{2;pq} = R_{pq} - T_{pq}$

$$b^{*}_{2;nq} = b_{2;nq}\sin(\mu_n h/2)$$

and $$D_2 = \text{diag}\,(\mu_m \cot(\mu_m h/2))$$

It is stressed that the physical significance of the matrices S_1 and S_2 is that

$$S_1 = R_1 + T_1 \tag{5.37}$$

$$S_2 = R_1 - T_1 \tag{5.38}$$

where R_1 and T_1 are the reflection and transmission scattering matrices of the single lamellar transmission grating element, using the notation introduced earlier in section 5.2.2.

5.2.4. Properties of the Scattering Matrices of the Single Grating

5.2.4.1 *Introductory Comments*

The two most important constraints upon any electromagnetic scattering system are those imposed by conservation of energy and reciprocity. A review of these properties is given in section 4.1 of this thesis and so they will not be discussed in detail here. These constraints are not the only conservation properties which apply to lossless systems. Several new constraints of this type are described in chapter 4 of this thesis and were derived by applying the principle of time reversal. It should be noted that in deriving the scattering matrices for this problem, the orders were not returned according to the principle of time reversal. However, the assumed up-down symmetry of each grating ensures that the single element diffracting system is directly equivalent to the arrangement considered under time reversal.

As discussed in section 5.2.1, the apparently arbitrary scaling factors $1/\sqrt{\beta_p}$ used in the prescription of the plane wave fields are introduced since they normalise the diffraction problem and thus simplify the mathematical representation of the laws of conservation of energy and reciprocity. For the lossless system considered here, conservation of energy is then given by

$$\sum_{p\epsilon\Omega_r} [|R_{pq}|^2 + |T_{pq}|^2] = 1 \qquad q \in \Omega_r \tag{5.39}$$

where $\Omega_r = \{p | \mathrm{Im}(\beta_p) = 0\}$ is the set of propagating orders. Also the Reciprocity Theorem may be written

$$R_{pq} = R'_{qp} \qquad \text{and} \qquad T_{pq} = T'_{qp} \tag{5.40}$$

where the primed quantities refer to the diffraction problem consequent upon the return of a diffracted order of the original problem.

The same simplifying influence is observed in the symmetry constraints which are derived in this section. These constraints are summarised by the equation

$$S^H I_r S = I_r + iS^H I_e - iI_e S \tag{5.41}$$

where S represents either S_1 or S_2 given in equations (5.37) and (5.38) and I_r and I_e are matrices whose elements are defined respectively by

$$(I_r)_{pq} = \epsilon_p \delta_{pq} \tag{5.42}$$

where $\epsilon_p = 1$ if $\beta_p^2 \geq 0$

$= 0$ if $\beta_p^2 < 0$

and $(I_e)_{pq} = (1 - \epsilon_p)\delta_{pq}$ (5.43)

Throughout this chapter the superscript H denotes the Hermitian conjugate of a matrix.

In addition, if the structure is also assumed to be left-right symmetric, then this feature together with the Reciprocity Theorem, constrains R_1 and T_1 to be symmetric matrices. That is, equations (5.40) may be rewritten for a left-right symmetric element as

$$R_{pq} = R_{qp} \quad , \qquad T_{pq} = T_{qp} \quad .$$

The conservation properties specified in equation (5.41) are derived in the following section for a lossless single element grating whose profile is constrained only by the requirement of up-down symmetry. These constraints, as well as the symmetric nature of the scattering matrices of an up-down, left-right symmetric structure are then shown in section 5.2.4.3 to hold analytically within the lamellar grating formalism.

5.2.4.2 *General Derivation of the Conservation Properties*

This section is concerned with the derivation of the conservation properties associated with a general lossless up-down symmetric, single-element structure. The derivation assumes a P polarized wave field but it applies equally well to S polarized radiation.

If D denotes a column vector whose entries $\{D_p\}$ represent the complex amplitudes of the various channels (specified by direction sines α_p/k) of the diffracted field and F denotes the corresponding vector describing the incident field, then

$$D = SF \tag{5.44}$$

where S denotes the scattering matrix of the system.

In free space regions, the field distribution is specified in terms of a plane wave expansion which may be written in the form

$$E(x,y) = \sum_{p\in\Omega_r} \frac{1}{\sqrt{\beta_p}} [F_p \exp(-i\beta_p y) + D_p \exp(i\beta_p y)]\exp(i\alpha_p x)$$

$$+ \sum_{p\in\Omega_e} \frac{1}{\sqrt{i}\sqrt{|\beta_p|}} [F_p \exp(|\beta_p|y) + D_p \exp(-|\beta_p|y)]\exp(i\alpha_p x) \quad (5.45)$$

where α_p and β_p are defined in equations (5.1) and (5.3) and

$$\Omega_r = \{p \,|\, \mathrm{Im}(\beta_p) = 0\} \quad , \quad (5.46)$$

$$\Omega_e = \{p \,|\, \mathrm{Re}(\beta_p) = 0\} \quad . \quad (5.47)$$

represent the sets of propagating and evanescent orders respectively.

The conservation of energy criterion provides the constraint

$$\mathrm{Im}\left[\int_0^d E \frac{\partial \bar{E}}{\partial y} dx\right] = 0 \quad (5.48)$$

where the bar denotes complex conjugation.

Using equation (5.45), this implies

$$\mathrm{Im}\{ \sum_{p\in\Omega_r} i[F_p \exp(-i\beta_p y) + D_p \exp(i\beta_p y)][-\bar{D}_p \exp(-i\beta_p y) + \bar{F}_p \exp(i\beta_p y)]$$

$$+ \sum_{p\in\Omega_e} [F_p \exp(|\beta_p|y) + D_p \exp(-|\beta_p|y)][\bar{F}_p \exp(|\beta_p|y) - \bar{D}_p \exp(-|\beta_p|y)]\}$$

$$= 0 \quad .$$

Following some elementary manipulation this may be reduced to

$$\sum_{p\in\Omega_r} [|F_p|^2 - |D_p|^2] + i \sum_{p\in\Omega_e} [\bar{D}_p F_p - D_p \bar{F}_p] = 0$$

or

$$\sum_{p\in\Omega_r} |D_p|^2 = \sum_{p\in\Omega_r} |F_p|^2 + i \sum_{p\in\Omega_e} [\bar{D}_p F_p - D_p \bar{F}_p] \quad (5.49)$$

This equation demonstrates that the total energy diffracted by the system is equal to the sum of the energy entering the system through the propagating order channels and the energy coupled in through the evanescent order channels.

Equation (5.49) can be rewritten

$$D^H I_r D = F^H I_r F + iD^H I_e F - iF^H I_e D \tag{5.50}$$

or using (5.44)

$$S^H I_r S = I_r + iS^H I_e - iI_e S \tag{5.51}$$

which is the relation introduced in section 5.2.4.1. This expression is the fundamental equation constraining the conservative properties of the system. The following conservation relations can be obtained by pre- and post-multiplying equation (5.51) by the matrices I_r or I_e and noting the relations $I_r I_r = I_r$, $I_e I_e = I_e$, $I_r I_e = 0$:

$$I_r S^H I_r S I_r = I_r \tag{5.52}$$

$$I_r S^H I_r S I_e = iI_r S^H I_e \tag{5.53}$$

$$I_e S^H I_r S I_r = -iI_e S I_r \tag{5.54}$$

$$I_e S^H I_r S I_e = iI_e S^H I_e - iI_e S I_e \tag{5.55}$$

The significance of each of the results expressed in equations (5.52) to (5.55) is now discussed.

Equation (5.52) expresses the well-known property [5.3, 5.6] of the unitarity of the submatrix S_r of the scattering matrix S. Here S_r

contains the elements of S corresponding to the propagating orders. That is, the elements $(S_r)_{pq}$ such that $p,q \in \Omega_r$. Alternatively, this equation constrains the partitioned matrix

$$\begin{bmatrix} R_r & T_r \\ T_r & R_r \end{bmatrix}$$

to be unitary. Again R_r and T_r are submatrices of R_l and T_l respectively, such that $p,q \in \Omega_r$. The conservation of energy property is also assured by this equation.

The results expressed by equations (5.53) to (5.55) have not, to the author's knowledge, been presented before. These equations are of great interest in that they provide constraints on the evanescent orders of the diffraction problem.

Equation (5.53) is a generalised description of the conservation properties previously derived [5.7] using the time reversal technique and constrains the evanescent orders produced by the return of propagating orders. The final two relations given in equations (5.54) and (5.55) cannot be obtained from the time reversal treatment. They provide constraints on the propagating and evanescent orders respectively, diffracted by the grating when waves are incident in the evanescent order channels.

Thus the conservation properties derived from the time reversal treatment have been generalised so that all the complex amplitudes of fields diffracted by single element lossless up-down symmetric structures operated in any angle of incidence and wavelength configuration are now constrained. Equation (5.51) is therefore a very powerful result which provides a comprehensive check on the numerical results of singly

periodic grating formalisms.

5.2.4.3 *Derivation of the Conservation Properties for the Lamellar Transmission Grating*

In this section, the analyticity of the conservation relation (5.51) is investigated for the lamellar grating formalism (described in section 5.2.3).

The scattering matrix S_1 is considered. From equation (5.34), S_1 is given by

$$S_1 = -I + 2\beta^{\frac{1}{2}} L (M + iD_1)^{-1} L^H \beta^{\frac{1}{2}}$$

$$= -I + 2\beta^{\frac{1}{2}} L J^{-1} L^H \beta^{\frac{1}{2}}$$

where $$J = (M + iD_1) = L^H \beta L + iD_1 \tag{5.56}$$

Consider

$$S_1^H I_r S_1 = (I + S_1^H) I_r (I + S_1) - I_r - S_1^H I_r - I_r S_1$$

$$= 4(\bar{\beta})^{\frac{1}{2}} L (J^{-1})^H L^H (\bar{\beta})^{\frac{1}{2}} I_r \beta^{\frac{1}{2}} L J^{-1} L^H \beta^{\frac{1}{2}} - I_r - S_1^H I_r - I_r S \quad . \tag{5.57}$$

To progress further the following relation must be shown

$$J + J^H = 2L^H I_r \beta I_r L \tag{5.58}$$

To establish this result, consider

$$(J + J^H)_{nm} = J_{nm} + \bar{J}_{mn}$$

$$= \sum_{p \epsilon \Omega_r} \beta_p L_{pm} \bar{L}_{pn} + i \sum_{p \epsilon \Omega_e} |\beta_p| L_{pm} \bar{L}_{pn} + iD_{1;nm}$$

$$+ \sum_{p \epsilon \Omega_r} \beta_p \bar{L}_{pn} L_{pm} - i \sum_{p \epsilon \Omega_e} |\beta_p| \bar{L}_{pn} L_{pm} - iD_{1;nm} \quad ,$$

since $D_{l;nm}$ is purely real,

$$= 2 \sum_{p\epsilon\Omega_r} \beta_p L_{pm} \bar{L}_{pn}$$

$$= 2(L^H I_r \beta I_r L)_{nm}$$

confirming equation (5.58).

So equation (5.57) becomes

$$S_l^H I_r S_l = 2(\bar{\beta})^{\frac{1}{2}} L(J^{-1})^H (J + J^H) J^{-1} L^H \beta^{\frac{1}{2}} - I_r - S_l^H I_r - I_r S_l \qquad (5.59)$$

If it is noted that

$$\beta_p^{\frac{1}{2}} = \frac{1 + i}{\sqrt{2}} |\beta_p| \qquad \text{for } p\epsilon\Omega_e$$

then it follows that

$$(\bar{\beta})^{\frac{1}{2}} = (I_r + I_e)(\bar{\beta})^{\frac{1}{2}} = I_r \beta^{\frac{1}{2}} - iI_e \beta^{\frac{1}{2}}$$

Using this result, equation (5.59) may be rewritten, after much tedious manipulation, as follows

$$S_l^H I_r S_l = 2(I_r \beta^{\frac{1}{2}} L J^{-1} L^H \beta^{\frac{1}{2}})^H + 2(-iI_e \beta^{\frac{1}{2}} L J^{-1} L^H \beta^{\frac{1}{2}})^H + 2(I_r \beta^{\frac{1}{2}} L J^{-1} L^H \beta^{\frac{1}{2}})$$

$$+ 2(-iI_e \beta^{\frac{1}{2}} L J^{-1} L^H \beta^{\frac{1}{2}}) - I_r - S_l^H I_r - I_r S_l$$

$$= (I_r (I + S_l))^H + (-iI_e (I + S_l))^H + I_r (I + S_l) - iI_e (I + S_l)$$

$$- I_r - S_l^H I_r - I_r S_l$$

$$= I_r + iS_l^H I_e - iI_e S_l \quad .$$

Since at no stage in this analysis was it necessary to introduce any matrix properties dependent upon the completeness of the plane wave and modal bases, the above derivation ensures that the conservation properties are analytically constrained by the lamellar grating formalism. Naturally, a similar analysis may be used to derive this result for the scattering matrix S_2.

Thus the conservation properties provide a useful test on the numerical implementation of the lamellar grating formalism. They do not, however, give any indication of the accuracy of the numerical results, since they are satisfied analytically.

5.2.4.4 *Symmetry*

The scattering matrices associated with the single lamellar grating (which is an up-down, left-right symmetric structure) will be shown to be symmetric in this section.

Firstly, the scattering matrix defined by equation (5.34),

$$S_1 = -I + 2\beta^{\frac{1}{2}} L J^{-1} L^H \beta^{\frac{1}{2}} \tag{5.60}$$

where $$J = L^H \beta L + iD_1 \quad , \tag{5.61}$$

is considered and it is noted that a necessary and sufficient condition for the symmetry of S_1 must be the symmetry of $LJ^{-1}L^H$.

In order to prove this, it is sufficient to demonstrate that

$$(L^H \beta L)_{nm} = (-1)^{n+m} (L^H \beta L)_{mn} \tag{5.62}$$

The following two elements of the matrix $L^H \beta L$ are examined

$$(L^H \beta L)_{nm} = \sum_p \bar{L}_{pn} \beta_p L_{pm}$$

and $$(L^H \beta L)_{mn} = \sum_p \bar{L}_{pm} \beta_p L_{pn} \quad .$$

The nature of the elements of the matrix L, which are the modal inner products L_{pm}, are now considered. Since the structure under consideration is left-right symmetric, the modes can only be either purely symmetric or purely anti-symmetric functions of x. For the case of the lamellar grating the purely symmetric modes are denoted by m an odd integer. It therefore follows that the inner product L_{pm} (equation (5.22)) is purely real in the case of purely symmetric modes and purely imaginary for purely anti-symmetric modes. Clearly then

$$(L^H \beta L)_{nm} = (-1)^{n+m} (L^H \beta L)_{mn} \quad .$$

Since D_1 is a diagonal matrix, then from equation (5.61)

$$(J)_{nm} = (-1)^{n+m} (J)_{mn} \quad .$$

By denoting $A = J^{-1}$, it has been proven [5.11] that

$$A_{nm} = (-1)^{n+m} A_{mn} \tag{5.63}$$

Now $$(LAL^H)_{pq} = \sum_{n,m} L_{pn} A_{nm} \bar{L}_{qm}$$

while $$(LAL^H)_{qp} = \sum_{n,m} \bar{L}_{pn} A_{mn} L_{qm}$$

$$= \sum_{n,m} \bar{L}_{pn} (-1)^{n+m} A_{nm} L_{qm}$$

$$= (LAL^H)_{pq}$$

This establishes the result.

In a similar manner the matrix S_2 defined in equation (5.36), may be shown to be symmetric. Clearly then, R_1 and T_1 must also be symmetric matrices.

In summary, the left-right symmetry of the lamellar transmission grating and reciprocity are sufficient conditions to constrain the scattering matrices of this structure to be symmetric. The proof given in this section relies nowhere upon the summation limits (that is, the completeness of the bases) and therefore holds analytically independently of truncation errors.

The conservation and symmetry properties of the scattering matrices determined for the single lamellar transmission grating have been confirmed numerically and a sample result is given in table 5.1.

5.2.5 Properties of the Scattering Matrices of the Multi-element Grating

In this section the unitarity of the scattering matrices of an aligned ($\delta x_n = 0$ for all n), evenly spaced ($t_n = t$ for all n) multi-element grating is established by the process of mathematical induction. The symmetry of the scattering matrices of an aligned, evenly spaced left-right symmetric multi-element grating is also established using this process.

5.2.5.1 *Unitarity and Conservation Properties*

The results to be derived by mathematical induction are summarised by the following equations :

$$A_k^H I_r A_k + B_k^H I_r B_k = I_r + iA_k^H I_e P - iP^H I_e A_k \qquad (5.64)$$

and $$A_k^H I_r B_k + B_k^H I_r A_k = iB_k^H I_e P - iP^H I_e B_k \qquad (5.65)$$

By noting that $A_k = R_k P$ and $B_k = T_k P$ and upon addition or subtraction, this pair of equations are easily shown to be equivalent to equation (5.51), the general conservation constraint, for the k-element grating stack.

Array R_1

-2 -2 3.13775E-02 1.47182E+02	-1 -2 1.11113E-01-1.97855E+01	0 -2 4.78288E-02 1.49161E+02	1 -2 1.54219E-02-1.26666E+02
-2 -1 1.11113E-01-1.97855E+01	-1 -1 4.95273E-01-1.42231E+02	0 -1 1.83988E-01 3.56523E+01	1 -1 1.27450E-01 1.41544E+02
-2 0 4.78288E-02 1.49161E+02	-1 0 1.83998E-01 3.56523E+01	0 0 6.05617E-02-1.36910E+02	1 0 9.65375E-02 1.11432E+01
-2 1 1.54219E-02-1.26666E+02	-1 1 1.27450E-01 1.41544E+02	0 1 9.65375E-02 1.11432E+01	1 1 2.29572E-01 1.60446E+02

Array T_1

-2 -2 3.20105E-02 2.27960E+01	-1 -2 2.61543E-02-1.37016E+00	0 -2 6.90830E-03 1.50360E+02	1 -2 1.38175E-02-1.39967E+02
-2 -1 2.61543E-02-1.37016E+00	-1 -1 7.27614E-02 1.31023E+01	0 -1 2.47977E-01 7.17866E+01	1 -1 6.30106E-02 1.45024E+02
-2 0 6.90830E-03 1.50360E+02	-1 0 2.47977E-01 7.17866E+01	0 0 5.07473E-01 5.33410E+01	1 0 3.37312E-02 5.22113E-01
-2 1 1.38175E-02-1.39967E+02	-1 1 6.30106E-02 1.45024E+02	0 1 3.37312E-02 5.22113E+01	1 1 5.67975E-02 3.37693E+01

Array Z_1

-2 -2 4.00355E-22 0.	-1 -2 1.08826E-22 0.	0 -2 5.62493E-23 0.	1 -2 8.27181E-23 0.
-2 -1 1.08826E-22 0.	-1 -1 8.47033E-22 0.	0 -1 3.34181E-22 0.	1 -1 2.64698E-23 0.
-2 0 5.62483E-23 0.	-1 0 3.34181E-22 0.	0 0 1.90582E-21 0.	1 0 4.79765E-22 0.
-2 1 8.27181E-23 0.	-1 1 2.64698E-23 0.	0 1 4.79765E-22 0.	1 1 1.32349E-23 0.

Array Z_2

-2 -2 2.98612E-22 0.	-1 -2 3.30872E-24 0.	0 -2 2.19720E-23 0.	1 -2 6.72084E-24 0.
-2 -1 3.30872E-24 0.	-1 -1 0. 0.	0 -1 2.61079E-23 0.	1 -1 4.65289E-25 0.
-2 0 2.19720E-23 0.	-1 0 2.61079E-23 0.	0 0 8.47033E-22 0.	1 0 1.65436E-23 0.
-2 1 6.72084E-24 0.	-1 1 4.65289E-25 0.	0 1 1.65436E-23 0.	1 1 2.06795E-25 0.

Table 5.1 Confirmation of the conservation and symmetry properties for a 1-element grating.
Grating parameters: $c/d = 0.8$, $h/d = 0.2$.
Incidence parameters: $\lambda/d = 0.9501$, $\phi = 10^\circ$, P polarization
Here the array Z_j is defined by $Z_j = S^H_j I_r S_j - I_r - iS^H_j I_e + iI_e S_j$ for $j=1,2$ where $S_1 = R_1 + T_1$, $S_2 = R_2 - T_2$
Note that the two integers designate the diffracted and incident channels associated with the matrix element.

Equations (5.64) and (5.65) have been shown to hold for $k = 1$ in section 5.2.4.3. Assume equations (5.64) and (5.65) hold for $k = n$ and consider firstly

$$A_{n+1}^H I_r A_{n+1} + B_{n+1}^H I_r B_{n+1}$$

$$= [A_1^H + B_1^H(I - A_n^H A_1^H)^{-1} A_n^H B_1^H]\, I_r\, [A_1 + B_1 A_n (I - A_1 A_n)^{-1} B_1]$$

$$+ B_1^H (I - A_n^H A_1^H)^{-1} B_n^H I_r B_n (I - A_1 A_n)^{-1} B_1$$

using equations (5.13) and (5.14) .

This equation upon expansion and use of equations (5.64) and (5.65) for $k = n$, may be rewritten

$$A_{n+1}^H I_r A_{n+1} + B_{n+1}^H I_r B_{n+1}$$

$$= I_r + i[A_1^H + B_1^H(I - A_n^H A_1^H)^{-1} A_n^H B_1^H]\, I_e P$$

$$- iP^H I_e [A_1 + B_1 A_n (I - A_1 A_n)^{-1} B_1] + \Lambda$$

where

$$\Lambda = B_1^H [-I_r + iI_e P A_n (I - A_1 A_n)^{-1} - I_r A_1 A_n (I - A_1 A_n)^{-1}$$

$$- i(I - A_n^H A_1^H)^{-1} A_n^H P^H I_e - (I - A_n^H A_1^H)^{-1} A_n^H A_1^H I_r$$

$$+ (I - A_n^H A_1^H)^{-1} A_n^H B_1^H I_r B_1 A_n (I - A_1 A_n)^{-1}$$

$$+ (I - A_n^H A_1^H)^{-1} B_n^H I_r B_n (I - A_1 A_n)^{-1}]\, B_1 \quad .$$

Thus

$$A_{n+1}^H I_r A_{n+1} + B_{n+1}^H I_r B_{n+1} = I_r + iA_{n+1}^H I_e P - iP^H I_e A_{n+1} + \Lambda \qquad (5.66)$$

After much manipulation it can be shown that

$$\Lambda = B_1^H(I - A_n^H A_1^H)^{-1}[iI_e PA_n - iP^H I_e A_n + iA_n^H I_e P - iA_n^H P^H I_e](I - A_1 A_n)^{-1} B_1$$

$$= 0$$

thus confirming equation (5.64) for $k = n + 1$.

To establish equation (5.65) for all k it is necessary to introduce alternate expressions for A_k and B_k analogous to equations (5.13) and (5.14). These are derived by considering the $(n + 1)$-element grating as an n-element grating stack placed above a single array and can be written

$$A_{n+1} = A_n + B_n A_1 (I - A_n A_1)^{-1} B_n \tag{5.67}$$

$$B_{n+1} = B_1 (I - A_n A_1)^{-1} B_n \tag{5.68}$$

Consider

$$A_{n+1}^H I_r B_{n+1} + B_{n+1}^H I_r A_{n+1}$$

$$= [A_n^H + B_n^H (I - A_1^H A_n^H)^{-1} A_1^H B_n^H]\, I_r\, [B_n (I - A_1 A_n)^{-1} B_1]$$

$$+ [B_n^H (I - A_1^H A_n^H)^{-1} B_1^H]\, I_r\, [A_1 + B_1 A_n (I - A_1 A_n)^{-1} B_1]$$

using equations (5.67) and (5.68). This equation may be expanded, using equations (5.64) and (5.65) to yield

$$A_{n+1}^H I_r B_{n+1} + B_{n+1}^H I_r A_{n+1} = iB_{n+1}^H I_e P - iP^H I_e B_{n+1} + \Lambda' . \tag{5.69}$$

where

$$\Lambda' = B_n^H (I - A_1^H A_n^H)^{-1}[-(iP^H I_e + A_1^H I_r)(I - A_1 A_n) + (I - A_1^H A_n^H)(iI_e P - I_r A_n)$$

$$+ A_1^H B_n^H I_r B_n + B_1^H I_r B_1 A_n](I - A_1 A_n)^{-1} B_1 \quad .$$

Again it can be shown following elementary manipulation that $\Lambda' = 0$ and consequently equation (5.65) is satisfied for $k = n + 1$, and thus for all k.

From these results it is clear that the multi-element grating containing an arbitrary number of elements possesses the same conservation properties as the individual elements. Furthermore, this result is independent of truncation errors introduced in the numerical treatment of the problem.

5.2.5.2 *Symmetry*

In this section the scattering matrices of a left-right symmetric multi-element grating are shown to be symmetric. The proof follows by induction. R_k and T_k are assumed to be symmetric matrices for $1 \leq k \leq n$.

From equation (5.11)

$$R_{n+1}^T = R_1^T + T_1^T(I - P^T R_n^T P^T R_1^T)^{-1} P^T R_n^T P^T T_1^T$$

$$= R_1 + T_1(I - PR_nPR_1)^{-1}PR_nPT_1$$

$$= R_1 + T_1PR_nP(I - R_1PR_nP)^{-1}T_1$$

$$= R_{n+1}$$

Thus R_{n+1} is a symmetric matrix. In a similar manner, from equation (5.12)

$$T_{n+1}^T = T_1^T(I - P^T R_n^T P^T R_1^T)^{-1} P^T T_n^T$$

$$= T_1(I - PR_nPR_1)^{-1}PT_n$$

$$= T_1P(I - R_nPR_1P)^{-1}T_n$$

$$= T_{n+1} \qquad \text{using equation (5.68)}$$

confirming that T_{n+1} is a symmetric matrix.

The computer program describing the diffraction properties of multi-element lamellar transmission gratings has been used to confirm numerically the unitarity and symmetry properties of the scattering matrices of gratings with up to six elements. Sample numerical results are given in table 5.2.

Thus, not only are the conservation and symmetry properties invaluable for testing the numerical solution of single element diffraction problems but they also provide the same function for the entire multi-element grating stack.

5.3 LONG WAVELENGTH FILTERING CHARACTERISTICS OF MULTI-ELEMENT LAMELLAR TRANSMISSION GRATINGS

In this section, the long wavelength transmission characteristics of an aligned multi-element lamellar transmission grating are briefly discussed. These results are obtained numerically using the formalism described in section 5.2.

The spectra depicted in figures 5.3 and 5.4 correspond to a multi-element lamellar transmission grating operated in P polarized radiation. Figure 5.3 shows the low pass filtering characteristics of a grating with up to six elements separated by a constant distance $t = t_n$ (n = 1,2 ....5). The increasing steepness of the edge between the passband and stopband regions with increasing number of elements is evident from these figures. The edge of the passband also moves to longer wavelengths and the depth of modulation in the passband increases as the number of elements increases. These phenomena have been observed by Ulrich [5.12] and Holah [5.13] while investigating multi-element metallic mesh (inductive grid) filters.

Array R_6

-2 -2 6.40710E-02 1.48383E+02	-1 -2 1.32350E-01 2.18987E+01	0 -2 1.02819E-01 9.84162E+01	1 -2 5.92823E-03-8.25645E+01
-2 -1 1.32350E-01 2.18987E+01	-1 -1 1.05053E-03-1.88710E+00	0 -1 8.98359E-01 2.86021E+01	1 -1 5.17169E-02 1.68269E+02
-2 0 1.02819E-01 9.84162E+01	-1 0 8.98359E-01 2.86021E+01	0 0 6.02840E-03 1.60767E+02	1 0 3.16251E-02-3.92135E+01
-2 1 5.92823E-03-8.25645E+01	-1 1 5.17169E-02 1.68269E+02	0 1 3.16251E-02-3.92135E+01	1 1 3.27978E-01 1.72683E+02

Array T_6

-2 -2 3.83042E-03 1.18429E+02	-1 -2 2.33064E-02 6.72342E+01	0 -2 6.91830E-03 4.36460E+01	1 -2 3.26322E-03-4.75443E+01
-2 -1 2.33064E-02 6.72342E+01	-1 -1 8.37873E-02 9.50149E+00	0 -1 1.68032E-02-6.56909E+01	1 -1 3.49257E-02-1.04025E+02
-2 0 6.91830E-03 4.36460E+01	-1 0 1.68032E-02-6.56909E+01	0 0 7.88094E-02-1.34191E+02	1 0 2.76157E-02-1.23587E+02
-2 1 3.26322E-03-4.75443E+01	-1 1 3.49257E-02-1.04025E+02	0 1 2.76157E-02-1.23587E+02	1 1 2.16881E-03 1.74333E+02

Array Z_1

-2 -2 1.96174E-20 0.	-1 -2 8.38993E-20 0.	0 -2 3.54199E-20 0.	1 -2 1.81972E-20 0.
-2 -1 8.38993E-20 0.	-1 -1 5.94829E-19 0.	0 -1 2.65696E-19 0.	1 -1 9.97712E-20 0.
-2 0 3.54199E-20 0.	-1 0 2.65696E-19 0.	0 0 2.74439E-19 0.	1 0 5.43367E-20 0.
-2 1 1.81972E-20 0.	-1 1 9.97712E-20 0.	0 1 5.43367E-20 0.	1 1 2.78530E-20 0.

Array Z_2

-2 -2 2.78264E-21 0.	-1 -2 5.23197E-21 0.	0 -2 6.29174E-23 0.	1 -2 1.31031E-21 0.
-2 -1 5.23197E-21 0.	-1 -1 4.76456E-20 0.	0 -1 2.45760E-20 0.	1 -1 1.28709E-21 0.
-2 0 6.29174E-23 0.	-1 0 2.45760E-20 0.	0 0 1.02491E-19 0.	1 0 4.56981E-21 0.
-2 1 1.31031E-21 0.	-1 1 1.28709E-21 0.	0 1 4.56981E-21 0.	1 1 2.92843E-21 0.

Table 5.2 Confirmation of the conservation and symmetry properties for 6-element grating. The grating elements are those given in table 5.1, and are separated by $t_i/d = 0.5$ (for $i = 1$ to 5).
The array Z_j is defined in table 5.1, but $S_1=R_6+T_6$, $S_2=R_6-T_6$

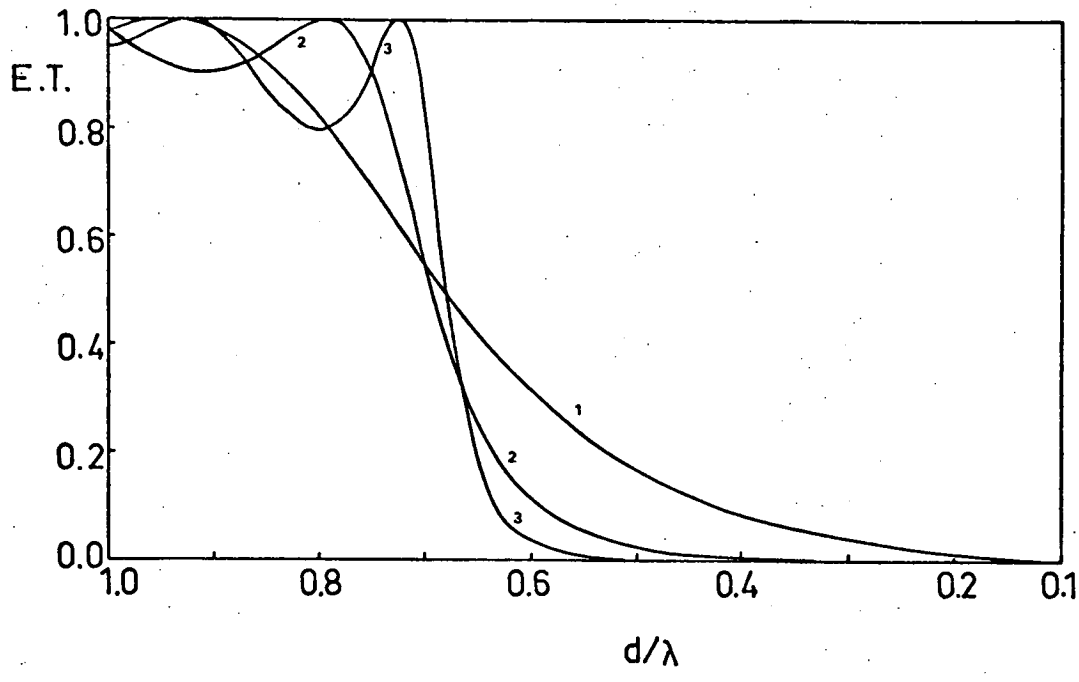

(a)

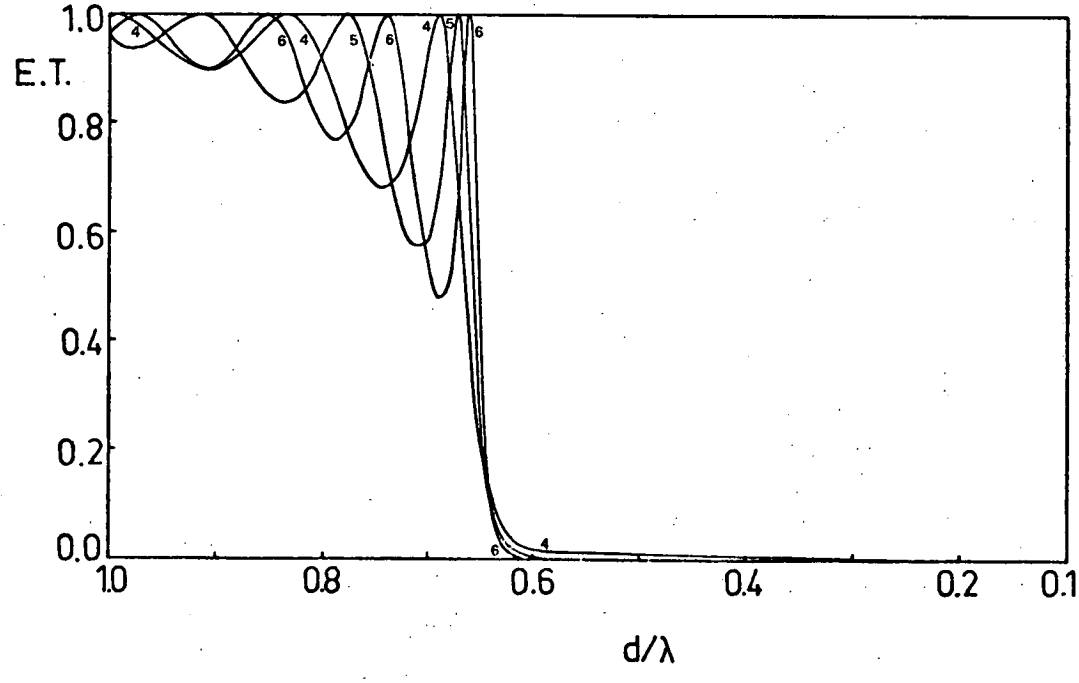

(b)

Figure 5.3 Normal incidence ($\phi = 0^{o}$) wavelength spectra for a multi-element grating composed of
(a) 1, 2 or 3 elements and
(b) 4, 5 or 6 elements
The grating parameters are: c/d = 0.7747, h/d = 0.2553, t_i/d = 0.1369 (for i = 1 to 5).
10 modes and 31 Rayleigh orders were used to specify the fields in each element and 9 Rayleigh orders were assumed to couple the elements.

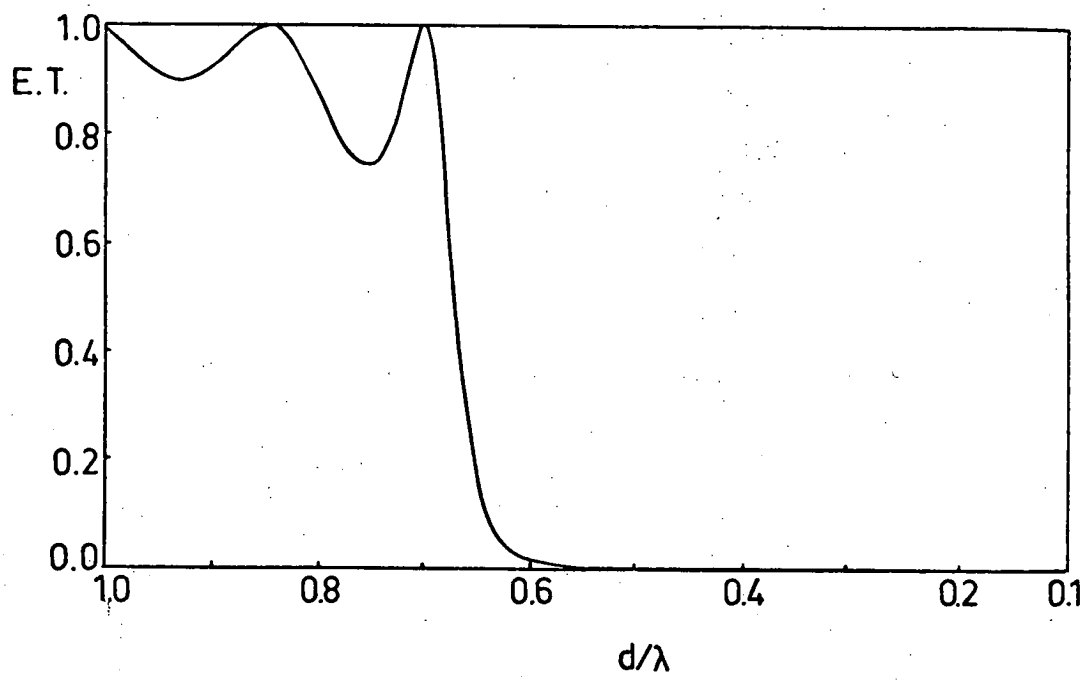

Figure 5.4 Normal incidence wavelength spectra for a 4-element grating stack, operated in P polarized radiation. The grating parameters are as given in figure 5.3, but $t_1/d = t_3/d = 0.1369$ and $t_2/d = 0.05$.

It has been suggested (see for example [5.12]) that the filtering characteristics of a four-element filter whose elements have a constant separation $t_1 = t_2 = t_3$ may be improved by the introduction of variable separation such that $t_1 = t_3$ and $t_2 \neq t_1$. These structures can be thought of as being composed of two subfilters (each having two elements). The subfilters act as the reflecting elements of the main interference filter and consequently the interference maxima of the subfilters can be positioned to optimise the transmission characteristics of the main filter. Such a structure has been considered and the results are shown in figure 5.4. This figure describes the diffraction properties of a four-element lamellar transmission grating, whose elements are identical to those of the gratings described in figure 5.3, but are now separated by normalised distances $t_1/d = t_3/d = 0.14$ and $t_2/d = 0.05$, operated in P polarized radiation. This structure demonstrates improved filtering performance compared with that given in figure 5.3b. The steepness of the cut-off is retained and the ripple in the passband is decreased.

Figure 5.5, showing the transmission properties of six-element lamellar transmission gratings operated in long wavelength S polarized radiation, demonstrates that this structure has application as a bandstop filter. The separations of the elements of each grating are constant, i.e. $t_n = t$ $(n = 1,2 \ldots .5)$ but the spectra represent gratings with different separations t.

The multi-element lamellar transmission grating also has application as a Fabry-Perot interferometer when operated in long wavelength P polarized radiation. This property has been previously demonstrated for a two-element lamellar grating by Adams and Botten [5.8] and for a multi-element lamellar grating by Botten [5.2]. In order that it may act as a Fabry-Perot interferometer, the structure must be operated in long

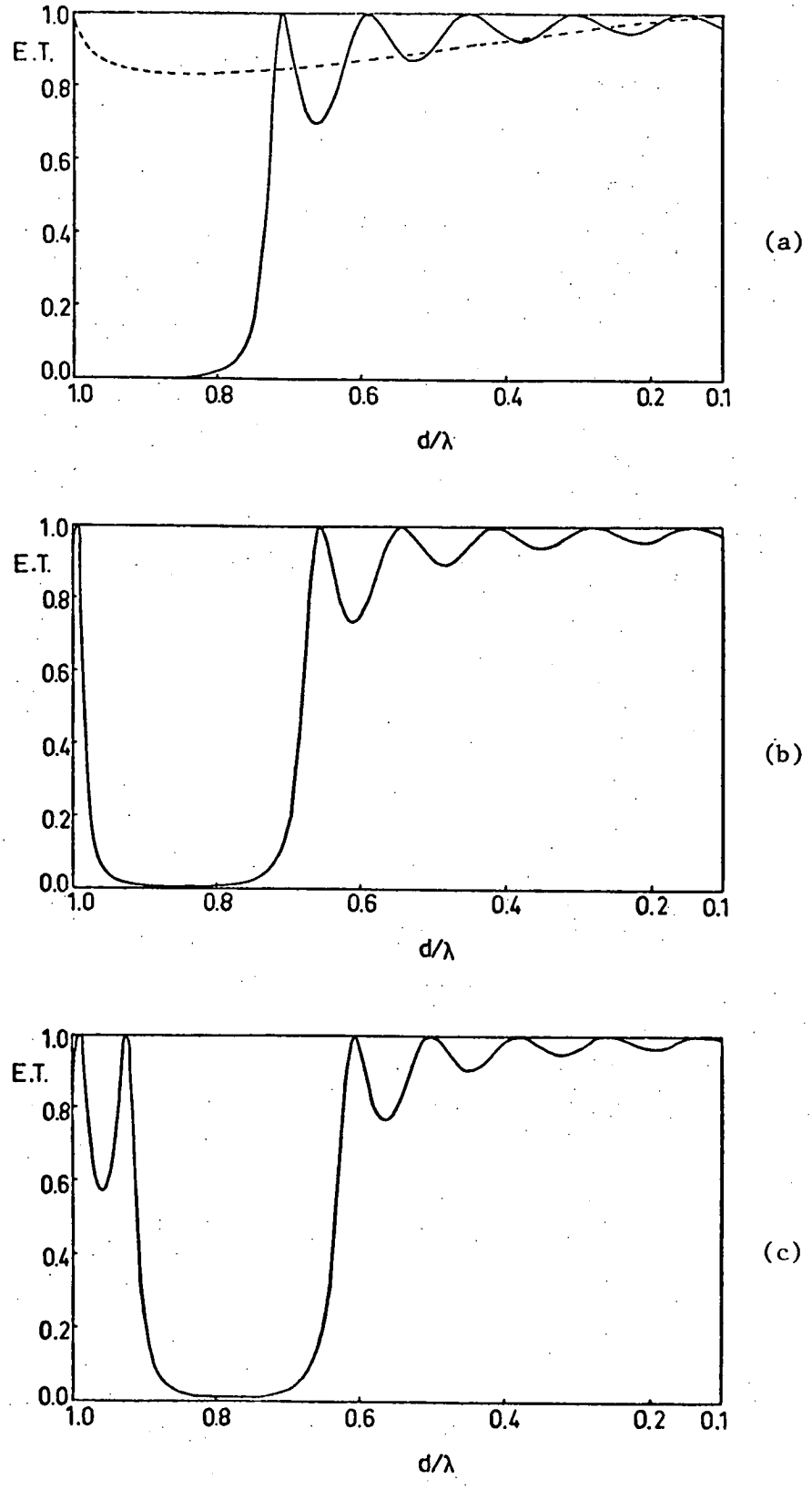

Figure 5.5 Normal incidence wavelength spectra for 6-element gratings operated in S polarized radiation. The grating parameters are: c/d = 0.7, h/d = 0.2 and
(a) $t_i/d = 0.3$
(b) $t_i/d = 0.35$
(c) $t_i/d = 0.4$
for i = 1 to 5. The transmission characteristics of the individual elements are represented by the broken curve.

wavelength radiation and the separation of the elements must be large compared with the period. Under these conditions the zeroth reflected and transmitted orders are the only orders coupling the elements of the grating. The analysis of Botten [5.2], which assumes the only coupling of the elements to occur through the zeroth diffracted orders, is therefore valid. Consequently, spectra obtained using the theory described in this chapter reproduce the earlier results given for this configuration and these will not be given here.

5.4 CONCLUSIONS

A recurrence relation for the scattering matrices of an up-down symmetric, lossless, multi-element grating has been derived in this chapter. This enables the diffraction properties of the grating to be inferred from those of a single element.

A series of conservation properties have been presented constraining the scattering matrices of this general profile multi-element grating. These relations not only ensure the well known [5.3, 5.6] property of unitarity of the "physical" submatrix of the scattering matrix, but also constrain the remaining elements of the scattering matrix. Here, the "physical" submatrix contains those elements of the scattering matrix corresponding to the propagating orders produced by waves incident in the propagating order channels. Thus, the complex amplitudes of the propagating and evanescent diffracted orders consequent upon waves incident in both propagating and evanescent order channels are now constrained. Furthermore, it has been shown that if the grating elements are also left-right symmetric, then the scattering matrices are symmetric. These constraints were shown to hold analytically (that is, independently of errors incurred in the field expansions when they are truncated for

the numerical implementation) for the multi-element lamellar transmission grating.

Sample numerical results have been presented illustrating the long wavelength filtering properties of the multi-element lamellar transmission grating. The slope of the spectral curve at the edge between passband and stopband regions was shown to increase as the number of elements in the grating was increased.

REFERENCES

[5.1] BOTTEN (L.C.), ADAMS (J.L.), DERRICK (G.H.). - Submitted to J. Optics (Paris).

[5.2] BOTTEN (L.C.). - Infrared Phys., 1979, 19, 659.

[5.3] URETSKY (J.L.). - Ann. Phys., 1965, 33, 400.

[5.4] NEVIÈRE (M.), VINCENT (P.). - Opt. Acta, 1976, 23, 557.

[5.5] VINCENT (P.), NEVIÈRE (M.). - Opt. Acta, 1979, 26, 889.

[5.6] FOX (J.R.). - Opt. Acta, 1980, 27, 289.

[5.7] BOTTEN (L.C.), ADAMS (J.L.), McPHEDRAN (R.C.), DERRICK (G.H.). - J. Optics (Paris), 1980, 11, 43.

[5.8] ADAMS (J.L.), BOTTEN (L.C.). - J. Optics (Paris), 1979, 10, 109.

[5.9] WIRGIN (A.), DELEUIL (R.). - J. Opt. Soc. Am., 1969, 59, 1348.

[5.10] MAYSTRE (D.), PETIT (R.). - Opt. Commun., 1972, 5, 90.

[5.11] BOTTEN (L.C.), COHEN (G.L.). - private communication.

[5.12] ULRICH (R.). - Appl. Opt., 1968, 7, 1987.

[5.13] HOLAH (G.D.). - International Journal of Infrared and Millimeter Waves, 1980, 1, 225.

CHAPTER 6

INTERFEROMETRIC PROPERTIES OF DOUBLE GRIDS

6.1 INTRODUCTION

The material presented in this chapter describes a rigorous investigation into the diffraction properties and interferometric application of a double inductive grid; that is, a structure consisting of two perfectly conducting rectangular-hole inductive grids lying in spatially separated parallel planes.

This study, which has been reported in a paper [6.1], published in the Journal of Optics (Paris), follows upon previous theoretical studies [6.2 - 6.6] of bi-periodic structures which are reviewed in detail in chapter 1. It was motivated by the need for a rigorous description of the properties of multi-element interference filters in the far infrared. During recent years numerous discussions of both a theoretical and an experimental nature have appeared (see section 1.4 of chapter 1). However, all but a few of the theoretical explanations of their characteristics were based on scalar optical theories describing the diffraction properties of single grids or gratings. All exceptions to this description [6.7 - 6.10] were studies on singly periodic multi-element diffraction grating configurations.

The results of this study confirm that the double inductive grid has the required interferometric properties to enable its use as a long wavelength Fabry-Perot interferometer. In general, the results obtained for the double grating interferometer [6.8] are shown to also apply to the double grid. That is, optimal interferometric properties are obtained for a symmetric grid having deep apertures of small cross-section and also the

aperture widths are the main factors determining the positions of the resonance maxima. One important feature, however, exhibited by the double grid but not by the double grating, is the independence of polarization for normally incident radiation. This is a considerable advantage when the interferometer is to be operated in unpolarized radiation.

Section 6.2 contains a description of the rigorous modal formalism derived to describe the action of the double grid. Since it is not easy to gain any physical insight into the interferometric properties of the double grid using this formalism, the long wavelength diffraction problem was solved using a multiple scattering technique. This analysis is given in section 6.3.

A detailed discussion of the features of the double grid spectra and the effects of the grid parameters on the interferometric properties of the structure are described in section 6.4. This section is divided into three parts. The first, section 6.4.1, discusses the numerical investigations which were carried out to determine the performance of the double grid as a long wavelength Fabry-Perot interferometer and consequently considers a symmetric double grid operated in normally incident radiation. The multiple scattering approach discussed in section 6.3 is used in conjunction with a monomodal approximation to understand the interference phenomenon associated with this problem. This monomodal and multiple scattering approach is extended in sections 6.4.2 and 6.4.3 to consider off-normal TE and TM polarized radiation and to analyse the features obtained under these incidence conditions. Although the latter diffracting configuration is not useful as an interferometer, the analysis is included here for completeness.

6.2 THEORETICAL TREATMENT OF THE DIFFRACTION PROBLEM

6.2.1 Notation and Description of the Diffraction Arrangement

Consider a plane wave of free space wavelength λ incident upon the double grid shown in figure 6.1. A conventional set of rectangular Cartesian coordinate axes (see figure 6.1) is defined with unit vectors $\hat{\underline{x}}$, $\hat{\underline{y}}$ and $\hat{\underline{z}}$ aligned with the OX, OY and OZ axes respectively. The double grid can then be specified as follows: Each perfectly conducting grid has period d along the OX axis with apertures of width $2c_1$ for the upper grid and $2c_2$ for the lower grid. The second periodicity axis is inclined at an angle η to the OZ axis and the projection of the grid periods along this axis onto the OZ axis is d', while the aperture widths along the OZ axis in the upper and lower grids are $2c_1'$ and $2c_2'$ respectively. The thicknesses of the upper and lower grids are $2h$ and $2h'$ respectively, while their centre to centre separation is $2s$. The lower grid is also displaced relative to the upper grid by distances of δx and δz as shown in figure 6.1. Also, S is defined by $S = 2s - h - h'$.

The direction of the plane wave which is incident upon the structure is specified by the angles ϕ and ψ shown in figure 6.2. The polarization of this incoming beam is described by the angle δ which is also defined in figure 6.2. Thus

$$\underline{k} = (\alpha_0, -\beta_{00}, \gamma_{00})$$

where $k = 2\pi/\lambda$ is the wavenumber of the incident wave and the direction cosines of this beam are given by

$$\left.\begin{aligned} \alpha_0 &= k \sin\phi \cos\psi \\ \beta_{00} &= k \cos\phi \\ \gamma_{00} &= k \sin\phi \sin\psi \end{aligned}\right\} \qquad (6.1)$$

Now, the electric and magnetic fields in both free space and

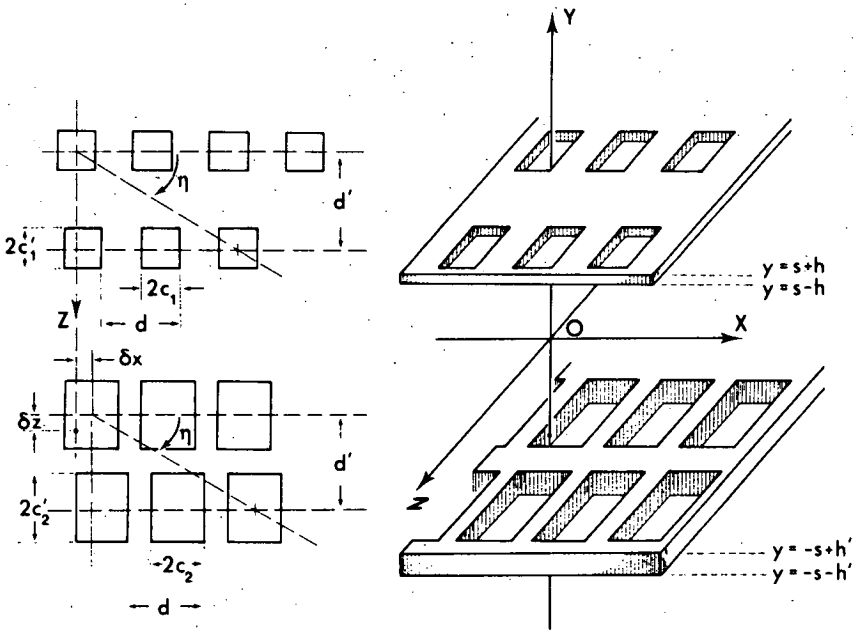

Figure 6.1

The geometry of the double grid.

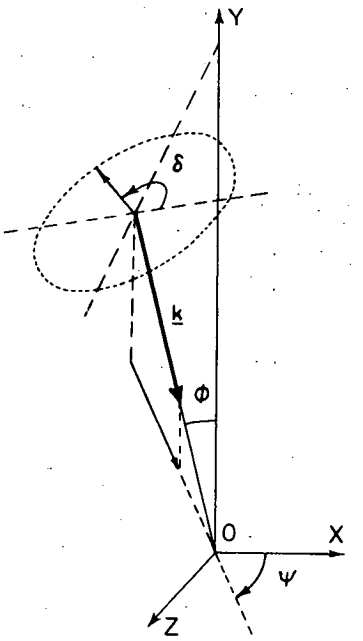

Figure 6.2

Specification of the incident field.

aperture regions may be described either by Cartesian vector modes or in terms of TE (transverse electric) or TM (transverse magnetic) orthogonal vector modes. Here TE implies no electric field component along the OY axis, while TM signifies no magnetic field component along this axis. The latter method of specifying the fields was adopted for the reasons given in section 1.5 of this thesis. That is, for certain incidence conditions no coupling occurs between the TE and TM fields. Also the amplitudes of an arbitrary polarized diffracted wave may be simply described in terms of the amplitudes corresponding to TE and TM polarized waves. This is exemplified by the analysis described in section 6.3 but is also advantageous in solving the diffraction problem for a double grid with dielectric plugs and films [6.11].

Throughout the analysis, the temporal dependence term $\exp(-i\omega t)$ will be suppressed.

In order to define the incident electric and magnetic fields several preliminary definitions must be made. The transverse electric and magnetic vector modes for the incident plane wave are introduced and are specified by

$$\underline{\hat{RTE}}_{00}(x,y,z) = \frac{1}{\zeta_{00}\sqrt{dd'}} \{\gamma_0 \underline{\hat{x}} - \alpha_0 \underline{\hat{z}}\} R^i(x,y,z) \tag{6.2}$$

$$\underline{\hat{RTM}}_{00}(x,y,z) = \frac{1}{\zeta_{00}\sqrt{dd'}} \{\alpha_0 \underline{\hat{x}} + \gamma_0 \hat{z}\} R^i(x,y,z) \tag{6.3}$$

where $$R^i(x,y,z) = \exp[i(\alpha_0 x - \beta_{00} y + \gamma_0 z)] \tag{6.4}$$

and $$\zeta_{00} = \sqrt{\alpha_0^2 + \gamma_0^2} \tag{6.5}$$

Then the transverse resolutes of the incident electric and magnetic fields are given by

$$\underline{E}_t^i = E_i \underline{\hat{RTE}}_{00} + F_i \underline{\hat{RTM}}_{00} \tag{6.6}$$

and

$$\hat{y} \times \underline{H}_t^i = \frac{1}{Z_0} \{ \frac{\beta_{00}}{k} E_i \underline{\hat{RTE}}_{00} + \frac{k}{\beta_{00}} F_i \underline{\hat{RTM}}_{00} \} \tag{6.7}$$

where

$$\left.\begin{aligned} E_i &= \cos \delta \\ F_i &= \beta_{00} \sin \delta / k \end{aligned}\right\} \tag{6.8}$$

and Z_0 is the free space impedance.

6.2.2 Free Space Fields

This plane wave incident upon the double grid produces a diffracted field which, in all semi-infinite free space regions, is composed of plane waves. The two dimensional periodicity of the structure constrains these waves to propagate along discrete lines, the directions of which are specified by integers p and q.

The free space fields can thus be expressed as a superposition of the following plane waves:

For upward going waves

$$R_{pq}(x,y,z) = \exp[i(\alpha_p x + \beta_{pq} y + \gamma_{pq} z)] \tag{6.9}$$

and for downward going waves

$$\hat{R}_{pq}(x,y,z) = \exp[i(\alpha_p x - \beta_{pq} y + \gamma_{pq} z)] \tag{6.10}$$

where the direction consines are given by [6.5]

$$\alpha_p = \alpha_0 + pK \quad , \tag{6.11}$$

where

$$K = \frac{2\pi}{d} \quad ,$$

$$\gamma_{pq} = \gamma_0 + qK' - \frac{pK}{\tan\eta} \quad , \tag{6.12}$$

where $K' = \frac{2\pi}{d'}$,

and
$$\left.\begin{aligned} \beta_{pq} &= \sqrt{k^2 - \alpha_p^2 - \gamma_{pq}^2} && \text{if } \alpha_p^2 + \gamma_{pq}^2 \leq k^2 \\ &= i\sqrt{\alpha_p^2 + \gamma_{pq}^2 - k^2} && \text{otherwise} \end{aligned}\right\} \quad (6.13)$$

The TE, TM vector modes for upward going waves in free space may then be written

$$\underline{RTE}_{pq}(x,y,z) = \frac{1}{\zeta_{pq}\sqrt{dd'}} \{\gamma_{pq}\, \hat{\underline{x}} - \alpha_p\, \hat{\underline{z}}\}\, R_{pq}(x,y,z) \quad (6.14)$$

$$\underline{RTM}_{pq}(x,y,z) = \frac{1}{\zeta_{pq}\sqrt{dd'}} \{\alpha_p\, \hat{\underline{x}} + \gamma_{pq}\, \hat{\underline{z}}\}\, R_{pq}(x,y,z) \quad (6.15)$$

where $\zeta_{pq} = \sqrt{\alpha_p^2 + \gamma_{pq}^2}$

The transverse vector modes for downward going plane waves $\hat{\underline{RTE}}_{pq}$ and $\hat{\underline{RTM}}_{pq}$ are defined similarly with $\hat{R}_{pq}(x,y,z)$ replacing $R_{pq}(x,y,z)$. The transverse resolutes of the reflected fields in $y > s + h$ are expressed by the following plane wave expansions

$$\underline{E}_t = \sum_{p=-\infty}^{\infty} \sum_{q=-\infty}^{\infty} [E_{pq}\, \underline{RTE}_{pq} + F_{pq}\, \underline{RTM}_{pq}] \quad (6.16)$$

$$\hat{\underline{y}} \times \underline{H}_t = \frac{-1}{Z_0} \sum_{p=-\infty}^{\infty} \sum_{q=-\infty}^{\infty} [\frac{\beta_{pq}}{k} E_{pq}\, \underline{RTE}_{pq} + \frac{k}{\beta_{pq}} F_{pq}\, \underline{RTM}_{pq}] \quad (6.17)$$

where the sets $\{E_{pq}\}$ and $\{F_{pq}\}$ designate the plane wave coefficients of the reflected fields. All following sums $\sum_{p,q}$ are over the same range as those specified in equations (6.16 - 17).

Similarly, the transverse resolutes of the transmitted fields in $y < -s-h'$ are

$$\underline{\hat{E}}_t = \sum_{p,q} [\hat{E}_{pq} \underline{\hat{RTE}}_{pq} + \hat{F}_{pq} \underline{\hat{RTM}}_{pq}] \tag{6.18}$$

$$\hat{\underline{y}} \times \underline{\hat{H}}_t = \frac{1}{Z_0} \sum_{p,q} [\frac{\beta_{pq}}{k} \hat{E}_{pq} \underline{\hat{RTE}}_{pq} + \frac{k}{\beta_{pq}} \hat{F}_{pq} \underline{\hat{RTM}}_{pq}] \tag{6.19}$$

while for the region $-s+h' < y < s-h$

$$\underline{E}_t^+ = \sum_{p,q} [E_{pq}^+ \underline{RTE}_{pq} + F_{pq}^+ \underline{RTM}_{pq}] \tag{6.20}$$

$$\hat{\underline{y}} \times \underline{H}_t^+ = -\frac{1}{Z_0} \sum_{p,q} [\frac{\beta_{pq}}{k} E_{pq}^+ \underline{RTE}_{pq} + \frac{k}{\beta_{pq}} F_{pq}^+ \underline{RTM}_{pq}] \tag{6.21}$$

$$\underline{E}_t^- = \sum_{p,q} [E_{pq}^- \underline{\hat{RTE}}_{pq} + F_{pq}^- \underline{\hat{RTM}}_{pq}] \tag{6.22}$$

$$\hat{\underline{y}} \times \underline{H}_t^- = \frac{1}{Z_0} \sum_{p,q} [\frac{\beta_{pq}}{k} E_{pq}^- \underline{\hat{RTE}}_{pq} + \frac{k}{\beta_{pq}} F_{pq}^- \underline{\hat{RTM}}_{pq}] \tag{6.23}$$

In the above, the sets $\{\hat{E}_{pq}\}$, $\{\hat{F}_{pq}\}$, $\{E_{pq}^+\}$, $\{F_{pq}^+\}$, $\{E_{pq}^-\}$ and $\{F_{pq}^-\}$ are the plane wave coefficients.

The region of validity of the Rayleigh expansions has been the subject of much discussion [6.12, 6.13] and it has been shown that different expansions must be used to specify the fields within the aperture regions.

6.2.3 Fields Within the Aperture Regions

The fields within the aperture regions are expanded in terms of waveguide modes. Consider firstly the appropriate form of the modes for Cartesian field components. The Cartesian modes for an inductive grid,

having rectangular apertures of widths $2c_1$ and $2c_1'$ along the OX and OZ axes respectively, are given by [6.14]

$$X_{nm}(x,z) = P_{nm} \cos[\frac{n\pi}{2c_1}(x + c_1)] \sin[\frac{m\pi}{2c_1'}(z + c_1')] \tag{6.24}$$

and $$Z_{nm}(x,z) = P_{nm} \sin[\frac{n\pi}{2c_1}(x + c_1)] \cos[\frac{m\pi}{2c_1'}(z + c_1')] \tag{6.25}$$

where $P_{nm} = \sqrt{\frac{\varepsilon_n \varepsilon_m}{4c_1 c_1'}}$

and $\varepsilon_j = 1 \qquad j = 0$

$= 2 \qquad$ otherwise

These modes thus characterise the field within the apertures of the upper grid. Similarly for the lower grid, the mode functions for Cartesian field components can be shown to be

$$\hat{X}_{nm}(x,z) = \hat{P}_{nm} \cos[\frac{n\pi}{2c_2}(x - \delta x + c_2)] \sin[\frac{m\pi}{2c_2'}(z - \delta z + c_2')] \tag{6.26}$$

$$\hat{Z}_{nm}(x,z) = \hat{P}_{nm} \sin[\frac{n\pi}{2c_2}(x - \delta x + c_2)] \cos[\frac{m\pi}{2c_2'}(z - \delta z + c_2')] \tag{6.27}$$

where $\hat{P}_{nm} = \sqrt{\frac{\varepsilon_n \varepsilon_m}{4c_2 c_2'}}$.

These modes explicitly satisfy the boundary conditions applying on the vertical walls of the apertures.

The TE and TM modes characterising the field within the upper grid apertures are then given by

$$\underline{MTEU}_{nm}(x,z) = g_{nm}[\frac{m\pi}{2c_1'} X_{nm}(x,z)\, \hat{\underline{x}} - \frac{n\pi}{2c_1} Z_{nm}(x,z)\, \hat{\underline{z}}] \tag{6.30}$$

and $$\underline{MTMU}_{nm}(x,z) = g_{nm}\left[\frac{n\pi}{2c_1} X_{nm}(x,z)\ \hat{\underline{x}} + \frac{m\pi}{2c_1'} Z_{nm}(x,z)\ \hat{\underline{z}}\right] \tag{6.31}$$

where $$g_{nm} = \left[\left(\frac{m\pi}{2c_1'}\right)^2 + \left(\frac{n\pi}{2c_1}\right)^2\right]^{-\frac{1}{2}} \tag{6.32}$$

Note that the modes $\underline{MTEU}_{00}$, $\underline{MTMU}_{n0}$ and $\underline{MTMU}_{0m}$ are trivial.

The transverse resolute of the electric field in the upper apertures is given by

$$\underline{E}_t = \sum_{(n,m)\in\Lambda} \{a_{nm} \sin[\mu_{nm}(y-s)] + b_{nm} \cos[\mu_{nm}(y-s)]\}\ \underline{MTEU}_{nm}(x,z)$$

$$+ \sum_{(n,m)\in\Lambda'} \{c_{nm} \sin[\mu_{nm}(y-s)] + d_{nm} \cos[\mu_{nm}(y-s)]\}\ \underline{MTMU}_{nm}(x,z) \tag{6.33}$$

where $\Lambda = \{(n,m) \mid n,m = 0, 1, 2 \ldots..;\ n + m \neq 0\}$

$\Lambda' = \{(n,m) \mid n,m = 1, 2, \ldots..\}$

and application of the Helmholtz equation constrains

$$\mu_{nm} = \left[k^2 - \left(\frac{n\pi}{2c_1}\right)^2 - \left(\frac{m\pi}{2c_1'}\right)^2\right]^{\frac{1}{2}} \quad . \tag{6.34}$$

Here the sets $\{a_{nm}\}$, $\{b_{nm}\}$, $\{c_{nm}\}$ and $\{d_{nm}\}$ designate the modal coefficients for the fields in the upper apertures.

The transverse resolute of the magnetic field in this region is given by

$$\hat{\underline{y}} \times \underline{H}_t = \frac{i}{Z_0}\Big\{ \sum_{(n,m)\in\Lambda} \left\{\frac{\mu_{nm}}{k}\left[a_{nm} \cos(\mu_{nm}(y-s)) - b_{nm} \sin(\mu_{nm}(y-s))\right]\right\} \times$$

$$\times\ \underline{MTEU}_{nm}(x,z)$$

$$+ \sum_{(n,m)\in\Lambda'} \left\{\frac{k}{\mu_{nm}}\left[c_{nm} \cos(\mu_{nm}(y-s)) - d_{nm} \sin(\mu_{nm}(y-s))\right]\right\} \times$$

$$\times\ \underline{MTMU}_{nm}(x,z)\Big\} \tag{6.35}$$

Similarly, the TE/TM modes specifying the field in the lower grid apertures, $\underline{MTEL}_{nm}(x,z)$ and $\underline{MTML}_{nm}(x,z)$ will be given by exactly the same expressions as equations (6.30) and (6.31), but with c_1 replaced by c_2, c_1' by c_2', X_{nm} by $\hat{X}_{nm}$ and Z_{nm} by $\hat{Z}_{nm}$. Then the transverse resolute of the electric field in the lower apertures is given by

$$\underline{E}_t = \sum_{(n,m)\epsilon\Lambda} \{\hat{a}_{nm} \sin[\hat{\mu}_{nm}(y+s)] + \hat{b}_{nm} \cos[\hat{\mu}_{nm}(y+s)]\} \underline{MTEL}_{nm}(x,z)$$

$$+ \sum_{(n,m)\epsilon\Lambda'} \{\hat{c}_{nm} \sin[\hat{\mu}_{nm}(y+s)] + \hat{d}_{nm} \cos[\hat{\mu}_{nm}(y+s)]\} \underline{MTML}_{nm}(x,z) \quad (6.36)$$

where $$\hat{\mu}_{nm} = [k^2 - (\frac{n\pi}{2c_2})^2 - (\frac{m\pi}{2c_2'})^2]^{\frac{1}{2}} \quad . \quad (6.37)$$

The transverse resolute of the magnetic field in the lower apertures can be expressed using an expansion similar to (6.35).

In order to relate these fields to the free space fields, continuity conditions are applied at the aperture-free space boundaries.

6.2.4 Application of Field Continuity Conditions

The relevant continuity conditions are that the transverse resolutes of the electric and magnetic fields be continuous across aperture-free space surfaces, i.e. at $y = s + h$, $s - h$, $-s + h'$, $-s - h'$. The Method of Moments is then employed to extract a system of linear equations whose unknowns are the modal field coefficients.

Consider firstly the continuity of $\underline{E}_t$ at $y = s + h$. This is expressed by

$$\sum_{p,q} [(E^*_{pq} + E^*_i \delta_{p0}\delta_{q0}) \underline{RTE}_{pq}(y=0) + (F^*_{pq} + F^*_i \delta_{p0}\delta_{q0}) \underline{RTM}_{pq}(y=0)]$$

$$= \sum_{(n,m)\epsilon\Lambda} [a^*_{nm} + b^*_{nm}] \underline{MTEU}_{nm}(x,z) + \sum_{(n,m)\epsilon\Lambda'} [c^*_{nm} + d^*_{nm}] \underline{MTMU}_{nm}(x,z)$$

$$\text{if } (x,z)\epsilon A$$

$$= 0 \qquad \text{otherwise} \quad (6.38)$$

Here A is the aperture region defined by $x \in [-c_1, c_1]$, $z \in [-c_1', c_1']$.

Also

$$\left.\begin{aligned} E^*_{pq} &= E_{pq}\, Y_{pq}(s+h) \quad , \\ E^*_i &= E_i\, Y_{pq}(-s-h) \quad , \\ F^*_{pq} &= F_{pq}\, Y_{pq}(s+h) \quad , \\ F^*_i &= F_i\, Y_{pq}(-s-h) \quad , \end{aligned}\right\} \tag{6.39}$$

$$Y_{pq}(y) = \exp[i\beta_{pq} y] \tag{6.40}$$

and

$$\left.\begin{aligned} a^*_{nm} &= a_{nm} \sin(\mu_{nm} h) \quad , \quad c^*_{nm} = c_{nm} \sin(\mu_{nm} h) \\ b^*_{nm} &= b_{nm} \cos(\mu_{nm} h) \quad , \quad d^*_{nm} = d_{nm} \cos(\mu_{nm} h) \end{aligned}\right\} \tag{6.41}$$

The Method of Moments is now applied by multiplying throughout by the complex conjugate of the $(r, s)^{th}$ plane wave term $\overline{\underline{RTE}}_{rs}(x,z)$ and integrating the resulting equation over the rectangle defined by $x \in [-c_1, d - c_1]$, $z \in [-c_1', d' - c_1']$ to give

$$E^*_{rs} + E^*_i\, \delta_{r0}\delta_{s0} = \sum_{(n,m)\in\Lambda} [a^*_{nm} + b^*_{nm}]\, J_{11}(rs;nm) + \sum_{(n,m)\in\Lambda'} [c^*_{nm} + d^*_{nm}]\, J_{12}(rs;nm) \quad . \tag{6.42}$$

Here, the modal inner products are defined by

$$J_{ij}(pq;nm) = \iint_A \overline{\underline{R}}_{i;pq} \cdot \underline{M}_{j;nm}\, dxdz \qquad i,j = 1,2. \tag{6.43}$$

In this expression, the following notation has been adopted in order to systematize the terminology,

$$\left.\begin{aligned} \underline{R}_{1;pq} &= \underline{\underline{RTE}}_{pq}\ (y=0) \quad , \\ \underline{R}_{2;pq} &= \underline{\underline{RTM}}_{pq}\ (y=0) \quad . \end{aligned}\right\} \tag{6.44}$$

$$\left.\begin{aligned} \underline{M}_{1;nm} &= \underline{\underline{MTEU}}_{nm}(x,z) \quad , \\ \text{and} \qquad \underline{M}_{2;nm} &= \underline{\underline{MTMU}}_{nm}(x,z) \quad . \end{aligned}\right\} \tag{6.45}$$

In the derivation of equation (6.42), the following orthogonality properties of the plane wave terms have also been used

$$\int_0^{d}\int_0^{d'} \underline{R}_{i;pq} \cdot \overline{\underline{R}}_{j;rs}\ dzdx = \delta_{pr}\ \delta_{qs}\ \delta_{ij} \qquad i,j = 1,2 \quad . \tag{6.46}$$

Similarly, by multiplying equation (6.38) by $\overline{\underline{\underline{RTM}}}_{rs}(y=0)$ and integrating over the area $x \in [-c_1, d-c_1]$, $z \in [-c_1', d'-c_1']$ the following equation is derived.

$$F_{rs}^* + F_i^*\ \delta_{r0}\ \delta_{s0} = \sum_{(n,m)\in\Lambda} [a_{nm}^* + b_{nm}^*]\ J_{21}(rs;nm) + \sum_{(n,m)\in\Lambda'} [c_{nm}^* + d_{nm}^*]\ J_{22}(rs;nm) \quad . \tag{6.47}$$

Equations (6.42) and (6.47) may be combined and written in the following matrix notation

$$P_0 V + P_0^{-1} A = J(e + f) \tag{6.48}$$

Here

$$P_0 = \begin{bmatrix} Y(s+h) & 0 \\ 0 & Y(s+h) \end{bmatrix} \tag{6.49}$$

where $\quad Y(s+h) = \text{diag}\ (Y_{pq}(s+h))$

$$J = \begin{bmatrix} [J_{11}(pq;nm)] & [J_{12}(pq;nm)] \\ [J_{21}(pq;nm)] & [J_{22}(pq;nm)] \end{bmatrix} \tag{6.50}$$

$$V = \begin{bmatrix} [E_{pq}] \\ [F_{pq}] \end{bmatrix}$$

$$e = \begin{bmatrix} [a^*_{nm}] \\ [c^*_{nm}] \end{bmatrix} , \qquad f = \begin{bmatrix} [b^*_{nm}] \\ [d^*_{nm}] \end{bmatrix}$$

and A is a partitioned vector $\begin{bmatrix} A_1 \\ A_2 \end{bmatrix}$ composed of elements

$$A_{1;pq} = E_i \, \delta_{p0} \, \delta_{q0} \qquad , \qquad A_{2;pq} = F_i \, \delta_{p0} \, \delta_{q0} \ .$$

In these definitions, the subscript pairs p,q and n,m should be regarded as compounded subscripts when filling the arrays. Here also the zeros in the array definition of P_0 represent the zero matrix of appropriate dimension.

Consider now the continuity of the transverse magnetic components at $y = s + h$.

$$-\frac{1}{Z_0} \sum_{p,q} \{ \frac{\beta_{pq}}{k} (E^*_{pq} - E^*_i \delta_{p0}\delta_{q0}) \underline{RTE}_{pq}(y=0) + \frac{k}{\beta_{pq}} (F^*_{pq} - F^*_i \delta_{p0}\delta_{q0}) \underline{RTM}_{pq}(y=0) \}$$

$$= \frac{i}{Z_0} \{ \sum_{(n,m)\in\Lambda} [D_{1;nm} \, a^*_{nm} - D_{2;nm} \, b^*_{nm}] \, \underline{MTEU}_{nm}(x,z)$$

$$+ \sum_{(n,m)\in\Lambda'} [D_{3;nm} \, c^*_{nm} - D_{4;nm} \, d^*_{nm}] \, \underline{MTMU}_{nm}(x,z) \} \quad (x,z) \in A \tag{6.51}$$

where $D_{1;nm} = \mu_{nm} \cot(\mu_{nm} h)/k$,

$D_{2;nm} = \mu_{nm} \tan(\mu_{nm} h)/k$,

$D_{3;nm} = k \cot(\mu_{nm} h)/\mu_{nm}$,

and $D_{4;nm} = k \tan(\mu_{nm} h)/\mu_{nm}$.

The Method of Moments is now applied by multiplying this equation by the complex conjugate of the modal basis function, $\overline{\underline{MTEU}}_{NM}(x,z)$ and integrating over the aperture region $(x,z) \in A$ to give

$$- \sum_{p,q} \{\frac{\beta_{pq}}{k} (E^*_{pq} - E^*_i \delta_{p0}\delta_{q0}) \overline{J_{11}}(pq;NM) + \frac{k}{\beta_{pq}} (F^*_{pq} - F^*_i \delta_{p0}\delta_{q0}) \overline{J_{21}}(pq;NM)\}$$

$$= i(D_{1;NM} a^*_{NM} - D_{2;NM} b^*_{NM}) \qquad N,M \in \Lambda \qquad (6.52)$$

where the mode orthogonality property is expressed by

$$\iint_A \underline{M}_{i;nm} \cdot \overline{\underline{M}}_{j;NM} \, dxdz = \delta_{nN}\delta_{mM}\delta_{ij} \qquad i,j = 1,2 \qquad (6.53)$$

Similarly, by multiplying equation (6.51) by $\overline{\underline{MTMU}}_{NM}(x,z)$ and integrating over the aperture region, an analogous equation is obtained which can be combined with (6.52) in the following matrix equation

$$J^H \chi [P_0 V - P_0^{-1} A] = - (D_o e - D_e f) \qquad (6.54)$$

where $$\chi = \begin{bmatrix} \beta & 0 \\ 0 & \beta^{-1} \end{bmatrix} \qquad (6.55)$$

$$D_o = \begin{bmatrix} D_1 & 0 \\ 0 & D_3 \end{bmatrix}$$

$$D_e = \begin{bmatrix} D_2 & 0 \\ 0 & D_4 \end{bmatrix}$$

and the following diagonal matrices have been defined

$$\beta = \text{diag}\ (\beta_{pq}/k)$$

$$D_j = \text{diag}\ (iD_{j;nm}) \qquad \text{for } j = 1, 2, 3, 4.$$

The remaining matrix equations follow from a consideration of the continuity of the transverse electric and magnetic fields at the previously mentioned surfaces. In equations derived from application of the continuity of the transverse electric field, the Method of Moments is applied by multiplying the resultant equations by the complex conjugate of a plane wave basis function and integrating over a unit period cell. However, for equations obtained from consideration of the continuity of the transverse magnetic field, the complex conjugate of a modal basis function is used and the integration is performed over the aperture region.

At $y = s - h$, the continuity of the transverse electric and magnetic fields are summarised respectively by the following matrix equation

$$P_1 V^+ + P_1^{-1} V^- = J(-e + f) \tag{6.56}$$

$$J^H \chi (P_1 V^+ - P_1^{-1} V^-) = - (D_o e + D_e f) \tag{6.57}$$

where P_1 is defined by equation (6.49) but $(s + h)$ is replaced by $(s - h)$,

$$V^+ = \begin{bmatrix} [E^+_{pq}] \\ [F^+_{pq}] \end{bmatrix}$$

and

$$V^- = \begin{bmatrix} [E^-_{pq}] \\ [F^-_{pq}] \end{bmatrix}$$

Similarly at $y = -s + h'$

$$P_2 V^+ + P_2^{-1} V^- = K (\hat{e} + \hat{f}) \tag{6.58}$$

$$K^H \chi (P_2 V^+ - P_2^{-1} V^-) = - (\hat{D}_o \hat{e} - \hat{D}_e \hat{f}) \tag{6.59}$$

where P_2 is defined by equation (6.49) but with $(s + h)$ replaced by $(-s + h')$,

$$\hat{D}_o = \begin{bmatrix} \hat{D}_1 & 0 \\ 0 & \hat{D}_3 \end{bmatrix} ,$$

$$\hat{D}_e = \begin{bmatrix} \hat{D}_2 & 0 \\ 0 & \hat{D}_4 \end{bmatrix}$$

where the diagonal matrices $\hat{D}_j = \text{diag}(i\hat{D}_{j;nm})$ $(j = 1,2,3,4)$ are composed of elements

$$\hat{D}_{1;nm} = \hat{\mu}_{nm} \cot(\hat{\mu}_{nm} h')/k$$

$$\hat{D}_{2;nm} = \hat{\mu}_{nm} \tan(\hat{\mu}_{nm} h')/k$$

$$\hat{D}_{3;nm} = k \cot(\hat{\mu}_{nm} h')/\hat{\mu}_{nm}$$

$$\hat{D}_{4;nm} = k \tan(\hat{\mu}_{nm} h')/\hat{\mu}_{nm} ,$$

$$\hat{e} = \begin{bmatrix} [\hat{a}_{nm} \sin(\hat{\mu}_{nm} h')] \\ [\hat{c}_{nm} \sin(\hat{\mu}_{nm} h')] \end{bmatrix} \qquad \hat{f} = \begin{bmatrix} [\hat{b}_{nm} \cos(\hat{\mu}_{nm} h')] \\ [\hat{d}_{nm} \cos(\hat{\mu}_{nm} h')] \end{bmatrix}$$

and

$$K = \begin{bmatrix} [K_{11}(pq;nm)] & [K_{12}(pq;nm)] \\ [K_{21}(pq;nm)] & [K_{22}(pq;nm)] \end{bmatrix} \tag{6.60}$$

The elements of this matrix are the modal inner products for the lower grid, given by

$$K_{ij}(pq;nm) = \iint_{A'} \underline{\bar{R}}_{i;pq} \cdot \underline{\hat{M}}_{j;nm} \; dxdz \qquad i,j = 1,2 \tag{6.61}$$

where A' is the region defined by $x \in [-c_2 + \delta x, c_2 + \delta x]$, $z \in [-c_2' + \delta z, c_2' + \delta z]$, $\underline{R}_{i;pq}$ $(i = 1,2)$ has been defined in equation (6.44) and

$$\left.\begin{aligned} \underline{\hat{M}}_{1;nm} &= \underline{\underline{MTEL}}_{nm}(x,z) \\ \underline{\hat{M}}_{2;nm} &= \underline{\underline{MTML}}_{nm}(x,z) \end{aligned}\right\} \tag{6.62}$$

Finally, the equations derived by field matching at $y = -s - h'$ may be written

$$P_3 \hat{V} = K(-\hat{e} + \hat{f}) \tag{6.63}$$

$$K^H \chi P_3 \hat{V} = \hat{D}_o \hat{e} + \hat{D}_e \hat{f} \tag{6.64}$$

where

$$\hat{V} = \begin{bmatrix} [\hat{E}_{pq}] \\ [\hat{F}_{pq}] \end{bmatrix}$$

and P_3 is given by equation (6.49) but $(s + h)$ is replaced by $(-s - h')$.

6.2.5 Elimination of the Rayleigh Field Coefficients

Substitution of equations (6.48) into (6.54) yields

$$(J^H \chi J + D_o)e + (J^H \chi J - D_e)f = 2 J^H \chi P_0^{-1} A \tag{6.65}$$

Simple manipulation of equations (6.56) and (6.58) leads to

$$L_1 V^+ = P_2^{-1} J(-e + f) - P_1^{-1} K(\hat{e} + \hat{f}) \tag{6.66}$$

$$-L_1 V^- = P_2 J(-e + f) - P_1 K(\hat{e} + \hat{f}) \tag{6.67}$$

where $$L_1 = 2i \begin{bmatrix} C_1 & 0 \\ 0 & C_1 \end{bmatrix}$$

and $$C_1 = \text{diag}[\sin(\beta_{pq} S)] \quad .$$

Substitution of equations (6.66) and (6.67) into equations (6.57) and (6.59) gives

$$J^H \chi L_3 J(-e + f) - J^H \chi L_2 K(\hat{e} + \hat{f}) = - (D_o e + D_e f) \tag{6.68}$$

and $$K^H \chi L_2 J(-e + f) - K^H \chi L_3 K(\hat{e} + \hat{f}) = - (\hat{D}_o \hat{e} - \hat{D}_e \hat{f}) \tag{6.69}$$

where $$L_2 = -i \begin{bmatrix} C_1^{-1} & 0 \\ 0 & C_1^{-1} \end{bmatrix}$$

and $$L_3 = i \begin{bmatrix} C_2 & 0 \\ 0 & C_2 \end{bmatrix}$$

where $$C_2 = \text{diag}[\cot(\beta_{pq} S)]$$

Finally, substitution of equation (6.63) into (6.64) yields

$$(K^H \chi K + \hat{D}_o)\hat{e} - (K^H \chi K - \hat{D}_e)\hat{f} = 0 \tag{6.70}$$

Equations (6.65,68,69,70) are the matrix equations which are used to determine the modal coefficients. Once these have been found, the

Rayleigh field quantities can be reconstructed using equations (6.48) and (6.63). The set of matrix equations is truncated to enable a solution to be obtained numerically and consequently the convergence properties of the numerical implementation need to be tested. The accuracy of the formalism was confirmed by the results of numerical tests of the Reciprocity Theorem, an example of which is contained in table 6.1, and also by using a series of symmetry constraints for doubly periodic structures, which are described in chapter 7.

Finally, the efficiencies of the real order (p,q) in reflection and transmission (ρ^R_{pq} and ρ^T_{pq} respectively) can be determined from a consideration of the Poynting vector and are given by

$$\rho^R_{pq} = \left(\frac{\beta_{pq}}{k} |E_{pq}|^2 + \frac{k}{\beta_{pq}} |F_{pq}|^2\right)/\rho_0 \tag{6.71}$$

$$\rho^T_{pq} = \left(\frac{\beta_{pq}}{k} |\hat{E}_{pq}|^2 + \frac{k}{\beta_{pq}} |\hat{F}_{pq}|^2\right)/\rho_0 \tag{6.72}$$

where $\rho_0 = \beta_{00}/k$. The expression describing the conservation of energy criterion is then given by

$$\sum_{(p,q)\in\Omega} (\rho^R_{pq} + \rho^T_{pq}) = 1 \tag{6.73}$$

where $$\Omega = \{(p,q) \mid \mathrm{Im}(\beta_{pq}) = 0 \} \quad .$$

6.3 RECONSTRUCTION OF THE LONG WAVELENGTH DIFFRACTION PROBLEM USING A MULTIPLE SCATTERING TECHNIQUE

In this section the amplitudes of propagating reflected and transmitted waves, for a double grid operated in long wavelength radiation

Table 6.1 Confirmation of the Reciprocity Theorem

Reciprocity results for a double grid specified by $d'/d = 1.5$, $c_1/d = 0.45$, $c_1'/d = 0.65$, $c_2/d = 0.7$, $c_2'/d = 0.8$, $\delta x/d = 0.2$, $\delta z/d = 0.3$, $S/d = 0.6$, $h/d = h'/d = 0.4$, $\eta = 70^\circ$ and operated in incident radiation of wavelength $\lambda/d = 0.95$.

The first diffraction problem was defined by incident angles $\phi = 30^\circ$, $\psi = 0^\circ$, $\delta = 90^\circ$. The (-1,-1) order was returned to give the second diffraction problem ($\phi = 32.28520^\circ$, $\psi = 32.57659^\circ$) and for this problem the polarization angle was chosen to be $\delta = 0^\circ$. In each problem the wave fields were specified by 4 modal indices and 11 Rayleigh orders.

	E_{-1-1}	F_{-1-1}	Energy Transmitted
Problem 1	(0.07795, 121.56°)	(0.02336, 105.71°)	0.22893
Problem 2	(0.29953, 45.14°)	(0.00998, 121.33°)	0.06197

The left and right hand sides of the Reciprocity relation [6.15] were calculated to be (0.06597, 121.33°) and (0.06590, 121.56°).

incident at arbitrary angles, are reconstructed using a multiple scattering technique. The individual elements of the double grids considered are assumed to be identical. The results of this reconstruction procedure will be used in the next section to analyse the properties of the double grid interferometer.

It is assumed that the wavelength of the incident radiation is sufficiently long so that only the zeroth orders in reflection and transmission propagate and also that the separation of the two grids is sufficiently large so that no evanescent coupling occurs between them. The diffracted complex field amplitudes of the double grid may then be obtained by considering all multiple reflections and transmissions of the zeroth order waves at each of the identical single grids.

The linear nature of the optical system enables the complex amplitude of a diffracted wave to be written as a linear combination of the amplitudes corresponding to $\delta=0^{\circ}$ and $\delta=90^{\circ}$ polarized waves. The following notation is introduced to facilitate the use of this property. If an incident wave having polarization angle $\delta=0^{\circ}$ (TE polarized) and unit amplitude strikes a single grid, let the amplitudes of the resulting zeroth order waves in reflection and transmission be given by (G^0, H^0) and $(\hat{G}^0, \hat{H}^0)$ respectively. Here G^0 is the complex amplitude of the TE component, while H^0 is the amplitude of the TM component, and the phase origin for all quantities is located at the centre of the single grid. Let the corresponding diffracted amplitude for a $TM(\delta=90^{\circ})$ polarized incident wave be (G^{90}, H^{90}) and $(\hat{G}^{90}, \hat{H}^{90})$.

An incident wave, with phase origin located at the centre of the double grid, is defined by the vector amplitudes

$$F_c = \begin{bmatrix} E_i \\ F_i \end{bmatrix} \tag{6.74}$$

Here the subscript "c" refers to the centred phase origin. Reflection and transmission matrices are defined respectively as follows:

$$\rho = \begin{bmatrix} G^0 & kG^{90}/\beta \\ H^0 & kH^{90}/\beta \end{bmatrix} \tag{6.75}$$

and

$$\tau = \begin{bmatrix} \hat{G}^0 & k\hat{G}^{90}/\beta \\ \hat{H}^0 & k\hat{H}^{90}/\beta \end{bmatrix} \tag{6.76}$$

Also, a transfer matrix, which is used to shift the phase origin of waves from the centre of the upper grid to the centre of the lower grid, is defined as

$$\sigma = \begin{bmatrix} \exp(i\eta) & 0 \\ 0 & \exp(i\eta) \end{bmatrix} \tag{6.77}$$

where $$\eta = 2\beta_{00}s = \beta_{00}(S + 2h) \tag{6.78}$$

The reflected and transmitted fields of the double grid (relative to the centre of the upper element and lower element respectively) are represented by the vectors

$$F_r = \exp(i\eta/2) \begin{bmatrix} E_{00} \\ F_{00} \end{bmatrix} \quad \text{and} \quad F_t = \exp(i\eta/2) \begin{bmatrix} \hat{E}_{00} \\ \hat{F}_{00} \end{bmatrix} \quad \text{respectively.}$$

Similarly, the upward and downward scattered fields shown in figure 6.3 are represented by vectors F_+ and F_- respectively. The incident field in this figure is specified by $F = \exp(-i\eta/2)\, F_c$. Then, these fields are related by the following expressions

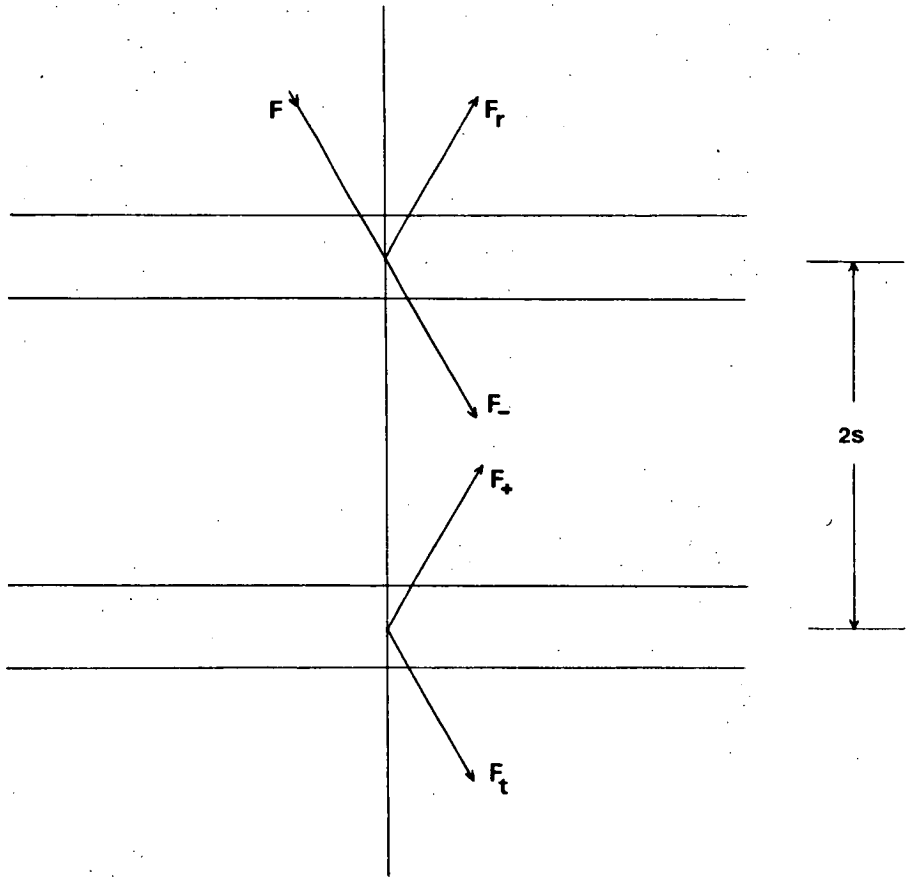

Figure 6.3 The notation used in the multiple scattering analysis.

$$\begin{bmatrix} F_r \\ F_- \end{bmatrix} = \begin{bmatrix} \rho & \tau \\ \tau & \rho \end{bmatrix} \begin{bmatrix} F \\ \sigma F_+ \end{bmatrix} \tag{6.79}$$

and

$$\begin{bmatrix} F_+ \\ F_t \end{bmatrix} = \begin{bmatrix} \rho & \tau \\ \tau & \rho \end{bmatrix} \begin{bmatrix} \sigma F_- \\ 0 \end{bmatrix} \tag{6.80}$$

Following an analysis similar to that given in section 5.2 of this thesis, the total reflected and transmitted complex amplitudes of the double grid (relative to the centre of the double grid) can be obtained from these equations and are given respectively by

$$\begin{bmatrix} E_{00} \\ F_{00} \end{bmatrix} = \exp(-i\eta)[\rho + \tau\sigma\rho\sigma(I - \rho\sigma\rho\sigma)^{-1}\tau] \begin{bmatrix} E_i \\ F_i \end{bmatrix} \tag{6.81}$$

and

$$\begin{bmatrix} \hat{E}_{00} \\ \hat{F}_{00} \end{bmatrix} = \exp(-i\eta)[\tau\sigma(I - \rho\sigma\rho\sigma)^{-1}\tau] \begin{bmatrix} E_i \\ F_i \end{bmatrix} \tag{6.82}$$

where I denotes the 2×2 identity matrix.

Equation (6.82) may be expanded to give

$$\begin{bmatrix} \hat{E}_{00} \\ F_{00} \end{bmatrix} = \exp(-i\eta)\tau\sigma[I + (\rho\sigma)^2 + (\rho\sigma)^4 + ...]\tau \begin{bmatrix} E_i \\ F_i \end{bmatrix} \tag{6.83}$$

which is just the sum of all the multiple reflections and transmissions of the double grid.

Equations (6.81) and (6.82) are the general expressions for the reflected and transmitted complex amplitudes of a double grid composed of identical elements, for arbitrary incidence parameters. However, these expressions may be much simplified for several specific incidence combinations and for a symmetric double grid, (that is, a double grid composed of two identical elements having square apertures, $\eta = 90^\circ$ and $d = d'$). McPhedran and Maystre [6.5] have shown that radiation satisfying the criterion

$$\phi \text{ arbitrary}, \quad \psi = 0^\circ, 45^\circ \text{ or } 90^\circ \tag{6.84}$$

incident on a symmetric grid, will produce diffracted fields satisfying

$$H^0 = \hat{H}^0 = 0 \qquad \text{and} \qquad G^{90} = \hat{G}^{90} = 0 \quad .$$

Under these conditions there is a "decoupling" of the field components and since

$$E_i = \cos\delta \quad , \qquad F_i = \beta_{00} \sin\delta/k$$

it can be seen that the polarization of the zeroth order wave is preserved upon interaction with the grid.

As an example, a $\delta = 0$ polarized wave satisfying equation (6.84), incident upon a symmetric double grid will give rise to a transmitted zeroth order wave whose amplitude is given by

$$\hat{E}_{00} = \frac{(\hat{G}^0)^2}{1 - (G^0)^2 \exp(2i\eta)} \tag{6.85}$$

and hence

$$|\hat{E}_{00}|^2 = \frac{1}{1 + f^0 \sin^2\xi^0} \tag{6.86}$$

where $$f^0 = \frac{4|G^0|^2}{(1 - |G^0|^2)^2} \tag{6.87}$$

and $$\xi^0 = \eta + \arg(G^0) \tag{6.88}$$

These can be recognised as giving the standard form of the transmitted intensity of a Fabry-Perot interferometer. Since there are no absorption losses, the transmission at the interference maxima is unity. Then using equation (6.72) it follows that expression (6.86) also gives the energy transmitted through the double grid structure.

The other important case which is of interest is that of a TM polarized ($\delta = 90^{\circ}$) wave also satisfying equation (6.84) incident on a symmetric double grid. Such a wave produces a transmitted wave whose complex amplitude is given by

$$\hat{F}_{00} = \frac{k(\hat{H}^{90})^2}{\beta_{00}[1-k^2\exp(2i\eta)(H^{90})^2/\beta_{00}^2]} \quad . \tag{6.89}$$

Thus the transmitted intensity can be written

$$|\hat{F}_{00}|^2 = \frac{\beta_{00}^2/k^2}{1 + f^{90}\sin^2(\xi^{90})} \tag{6.90}$$

where $$f^{90} = \frac{4\beta_{00}^2|H^{90}|^2}{k^2(\beta_{00}^2/k^2 - |H^{90}|^2)^2} \tag{6.91}$$

and $$\xi^{90} = \eta + \arg(H^{90}) \tag{6.92}$$

Thus the transmitted efficiency of the zeroth order is

$$\rho_{00}^{T} = \frac{1}{1 + f^{90}\sin^2(\xi^{90})} \quad . \tag{6.93}$$

These results were used to reconstruct the double grid performance and excellent agreement between the rigorous formalism and reconstruction procedure was found, provided the grid separation to period ratio was

$S/d \geq 1.5$. For values of S/d less than this, the rigorous formalism showed a noticeable dependence on the array phasing parameters δx and δz. Since the multiple scatter approach does not predict any dependence on these parameters, it can be deduced that the validity of the approach does not extend to separations smaller than this.

6.4 NUMERICAL INVESTIGATION OF THE INTERFEROMETRIC PROPERTIES OF THE DOUBLE GRID

As discussed in section 6.1, this section is primarily concerned with the operation of the double grid as a far infrared interferometer. The double grid is assumed to be composed of two identical symmetric single inductive grids (having $d = d'$, aperture widths $2c = 2c'$, aperture depths $2h$ and orthogonal axes of periodicity $\eta = 90^{o}$).

The multiple scattering approach discussed in section 6.3 is used, together with a monomodal approximation to describe the features of the spectra obtained for the double grid. Long wavelength radiation incident either normally or such that $\phi \neq 0$, $\psi = 0$, $\delta = 0$ or 90^{o} is considered. Such radiation satisfies the criterion given in equation (6.84) and as discussed in section 6.3, this leads to simplified expressions for the zeroth order diffracted efficiencies using the reconstruction procedure.

6.4.1 Application as a Fabry-Perot Interferometer

This section discusses the numerical investigations which were performed in order to assess the double grid as a long wavelength Fabry-Perot interferometer. In order to produce a high finesse interferometer, each element of the grid must be highly reflecting and since the grid is to be operated in unpolarized radiation, the structure must be polarization independent. This can be achieved with the

diffraction arrangement to be considered in this section, which consists of a symmetric double grid operated in long wavelength normally incident ($\phi = \psi = 0^{o}$) radiation. The reconstruction procedure discussed in section 6.3 is valid for this problem and in particular the transmitted intensity will be given by equation (6,86).

The curves depicted in figures 6.4a , 6.4c and 6.4d were obtained using the rigorous formalism, while that shown in figure 6.4b was computed using the reconstruction procedure and the results of a computer program that calculates the diffraction properties of a single grid (dashed curve). The excellent agreement shown by these curves confirms the validity of the reconstruction method.

In order to explain the interference phenomena shown in these curves, the results of the multiple scattering analysis will now be more closely investigated. Since the radiation is incident normally and the double grid is assumed totally symmetric (having aperture widths $2c$, thicknesses $2h$ and periods $d = d' = 1.0$), the grid will be polarization independent and conclusions drawn from the discussion for $\delta = 0^{o}$ polarized radiation will apply equally well to radiation polarized with $\delta = 90^{o}$.

The expression (6.86) shows that resonance maxima will occur for values of λ given by

$$\frac{2\pi}{\lambda}(S + 2h) + \arg(G^{0}) = \ell\pi \qquad \ell = 1, 2 \ldots\ldots \qquad (6.94)$$

Since this expression is dependent on G^{0} (the zeroth order reflected complex amplitude of the single grid), it can be seen that the grid parameters and the angles of incidence can provide mechanisms for displacing the interference maxima from the positions that would be

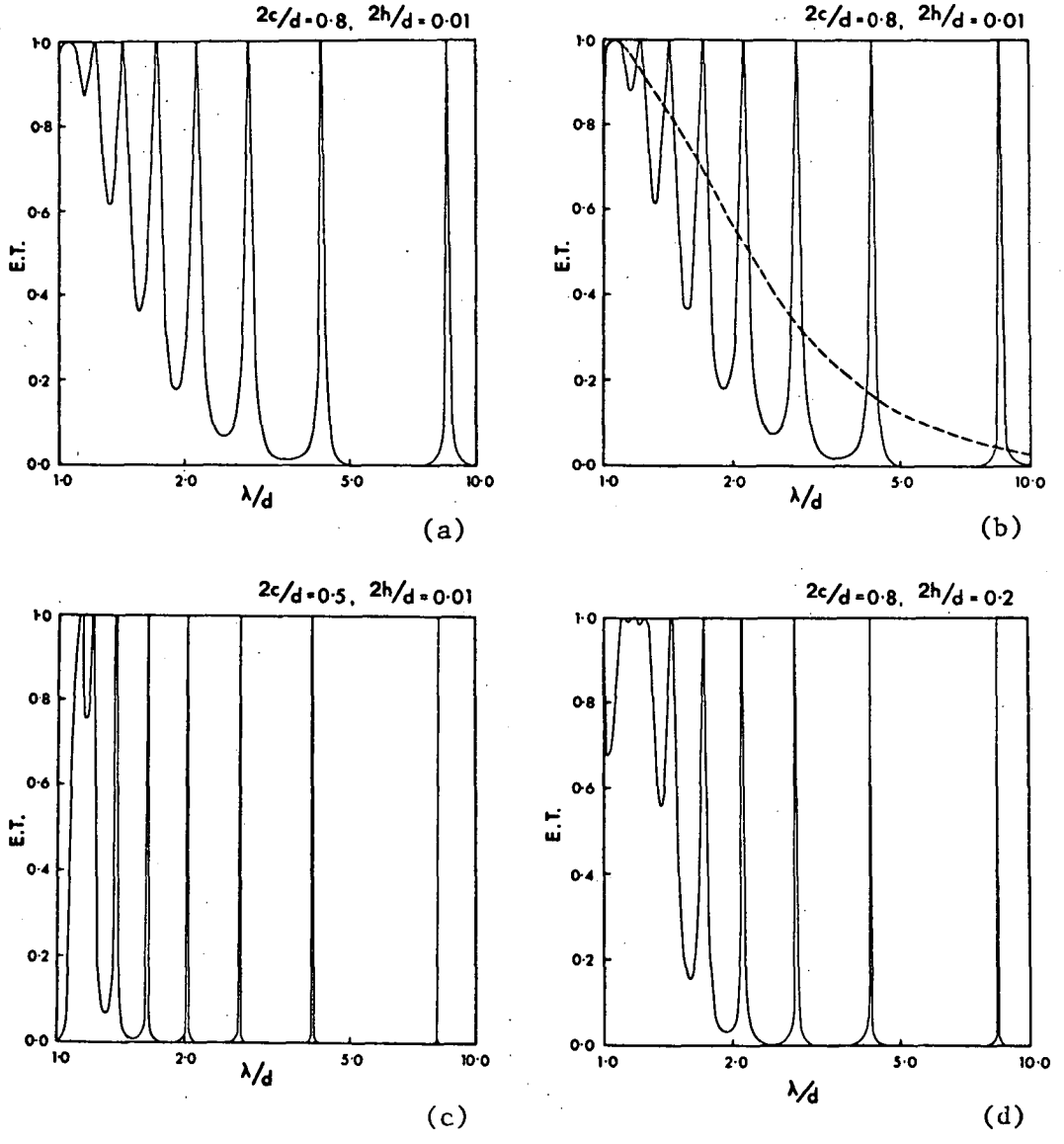

Figure 6.4 The transmission properties of a double grid operated in normally incident radiation with polarization angle $\delta = 0^{\circ}$, as a function of wavelength. The double grid is composed of a pair of identical symmetric grids ($d'/d = 1.0$) separated by $S/d = 4.0$ and aligned such that $\delta x/d = \delta z/d = 0.0$.

predicted geometrically,

$$\lambda_{max} = \frac{2S}{\ell} \tag{6.95}$$

Thus it is important to determine the relation between G^0 and the parameters specifying the grid and incident radiation. This information is extracted from the theory describing diffraction by a single grid by applying a monomodal approach. The analysis is similar to that described in chapter 3 and [6.8] and is based on work originally described by Chen [6.4] and later discussed by McPhedran and Maystre [6.5]. The crucial assumption in this approach is that a single mode carries the dominant fraction of the incident energy which passes through the grid. This assumption has been shown numerically to be justified for the diffraction problem under consideration.

Explicit expressions for G^0 and $\hat{G}^0$, the reflected and transmitted zeroth order complex amplitudes of a single symmetric grid (having aperture depth $2h$, groove widths $2c = 2c'$ and $d = d' = 1.0$) will now be derived.

Consider the modal expansion specifying the transverse resolute of the electric field applicable to a single grid (with phase origin located in the centre of the apertures). This will be given by

$$\underline{E}_t = \sum_{(n,m)\epsilon\Lambda} \{a^s_{nm}\sin(\mu_{nm}y) + b^s_{nm}\cos(\mu_{nm}y)\}\,\underline{MTEU}_{nm}(x,z)$$

$$+ \sum_{(n,m)\epsilon\Lambda'} \{c^s_{nm}\sin(\mu_{nm}y) + d^s_{nm}\cos(\mu_{nm}y)\}\,\underline{MTMU}_{nm}(x,z) \tag{6.96}$$

where $\underline{MTEU}_{nm}(x,z)$, $\underline{MTMU}_{nm}(x,z)$ and μ_{nm} have been defined in section 6.2.3. Here symbols with a superscript "s" refer to quantities

defined for the single grid.

Now for long wavelength radiation incident, such that ϕ is arbitrary but $\psi = 0^\circ$, $\delta = 0^\circ$, the dominant mode is that for which $n = 1$, $m = 0$. This is the only mode used in the description of fields within the apertures.

Then, by solving the single grid diffraction problem, it can be shown that

$$c_{10}^{s} = d_{10}^{s} = 0 \tag{6.97}$$

and

$$a_{10}^{s*} = a_{10}^{s} \sin(\nu_{10}h) = \frac{i\beta_{00}E_i^{s*}\bar{I}_{10}^{00}}{P(\lambda) - L\cot(Lh)} \tag{6.98}$$

$$b_{10}^{s*} = b_{10}^{s} \cos(\nu_{10}h) = \frac{i\beta_{00}E_i^{s*}\bar{I}_{10}^{00}}{P(\lambda) + L\tan(Lh)} \tag{6.99}$$

where

$$E_i^{s*} = \exp(-i\beta_{00}h)$$

$$L = \nu_{10}$$

$$P(\lambda) = \sum_{p,q} \frac{i}{\beta_{pq}} (k^2 - \alpha_p^2) \left|I_{10}^{pq}\right|^2$$

and

$$I_{10}^{pq} = \frac{1}{\sqrt{2}c} \int_{-c}^{c}\int_{-c}^{c} \sin\left[\frac{\pi}{2c}(x + c)\right] \exp[-i(\alpha_p x + \gamma_{pq} z)]\, dz dx$$

Using these results, the zeroth order reflected and transmitted amplitudes of the single grid can be shown to be

$$G^0 = -\exp(-i2\beta_{00}h)\left\{1 + i2\beta_{00}\left|I_{10}^{00}\right|^2 \left[\frac{L\cos(2Lh) - P(\lambda)\sin(2Lh)}{(P^2(\lambda) - L^2)\sin(2Lh) - 2P(\lambda)L\cos(2Lh)}\right]\right\}$$

(6.100)

and

$$\hat{G}^0 = -i2\beta_{00}\exp(-i2\beta_{00}h)|I_{10}^{00}|^2\left\{\frac{L}{(P^2(\lambda) - L^2)\sin(2Lh) - 2P(\lambda)L\cos(2Lh)}\right\} \tag{6.101}$$

These results apply to long wavelength radiation incident at arbitrary angles. Since this section is particularly concerned with properties of the double grid interferometer, radiation specified by the incident angles $\phi = \psi = \delta = 0^\circ$ will be considered. Under these conditions, careful consideration of the above results leads to the following conclusions:

$$\left.\begin{aligned} &(a)\quad |G^0| \to 1 \\ &\qquad \arg(G^0) \to \pi - 2\beta_{00}h \end{aligned}\right\} \quad \begin{aligned} &\text{as} \quad \lambda \to \infty \\ &\text{or} \quad c \to 0 \\ &\text{provided} \quad h \neq 0 \end{aligned} \tag{6.102}$$

Thus from equation (6.87) the finesse of the interferometer will increase as $\lambda \to \infty$ or $c \to 0$, and using equation (6.88)

$$\xi^0 \to \beta_{00}S + \pi ,$$

positioning the interference maxima at the geometrical positions (equation (6.95));

(b) for wavelengths in excess of twice the aperture width (i.e. $\lambda > 4c$, thus ensuring every mode is evanescent)

$$\left.\begin{aligned} &|G^0| \to 1 \\ &\arg(G^0) \to \pi - 2\beta_{00}h - \delta' \end{aligned}\right\} \quad \text{as} \quad h \to \infty \tag{6.103}$$

where $\delta' = \arg[(P(\lambda) - |L|)^2]$

Once again the finesse of the interferometer is increased as the

aperture depth is increased. However,

$$\xi^{0} \to \pi + \beta_{00}S + \delta'$$

where δ' is independent of h and depends only on the aperture width and incidence parameters. This result, also discovered for the double grating [6.8] shows that the grid depth does not govern the positions of the interference maxima, but that the aperture widths and parameters describing the incident field are the important features in determining the position of the resonances.

These results are illustrated in figure 6.4 . Consider finally the effects of polarization on the interferometric nature of the double grid, when the radiation is incident non-normally. Inspection of figures 6.5a,6.5b depicting wavelength spectra for a symmetric double grid operated in unpolarized, near-normally incident radiation shows that although the resonance half-widths are still small, total transmission of the incident energy at the resonance maxima is no longer assured. This can be attributed to the fact that under these conditions, the resonance maxima corresponding to the two fundamental polarizations ($\delta = 0^{\circ}$ and $\delta = 90^{\circ}$) may not occur at the same wavelength. Further discussion of these results is given in the following subsections.

6.4.2 Operation in Off-Normal ($\phi \neq 0^{\circ}$, $\psi = 0^{\circ}$) TE Polarized Radiation

Consider a symmetric grid having aperture widths $2c$ and depth $2h$, operated in long wavelength radiation with incidence angles specified by $\phi \neq 0^{\circ}$, $\psi = 0^{\circ}$ and $\delta = 0^{\circ}$. Again the radiation satisfies the criterion given in equation (6.84) and this leads to the simplified multiple scattering treatment. Figures 6.6a , c, d show spectra obtained for this diffraction arrangement using the rigorous formalism while figure 6.6b was obtained from the reconstruction process. The features of

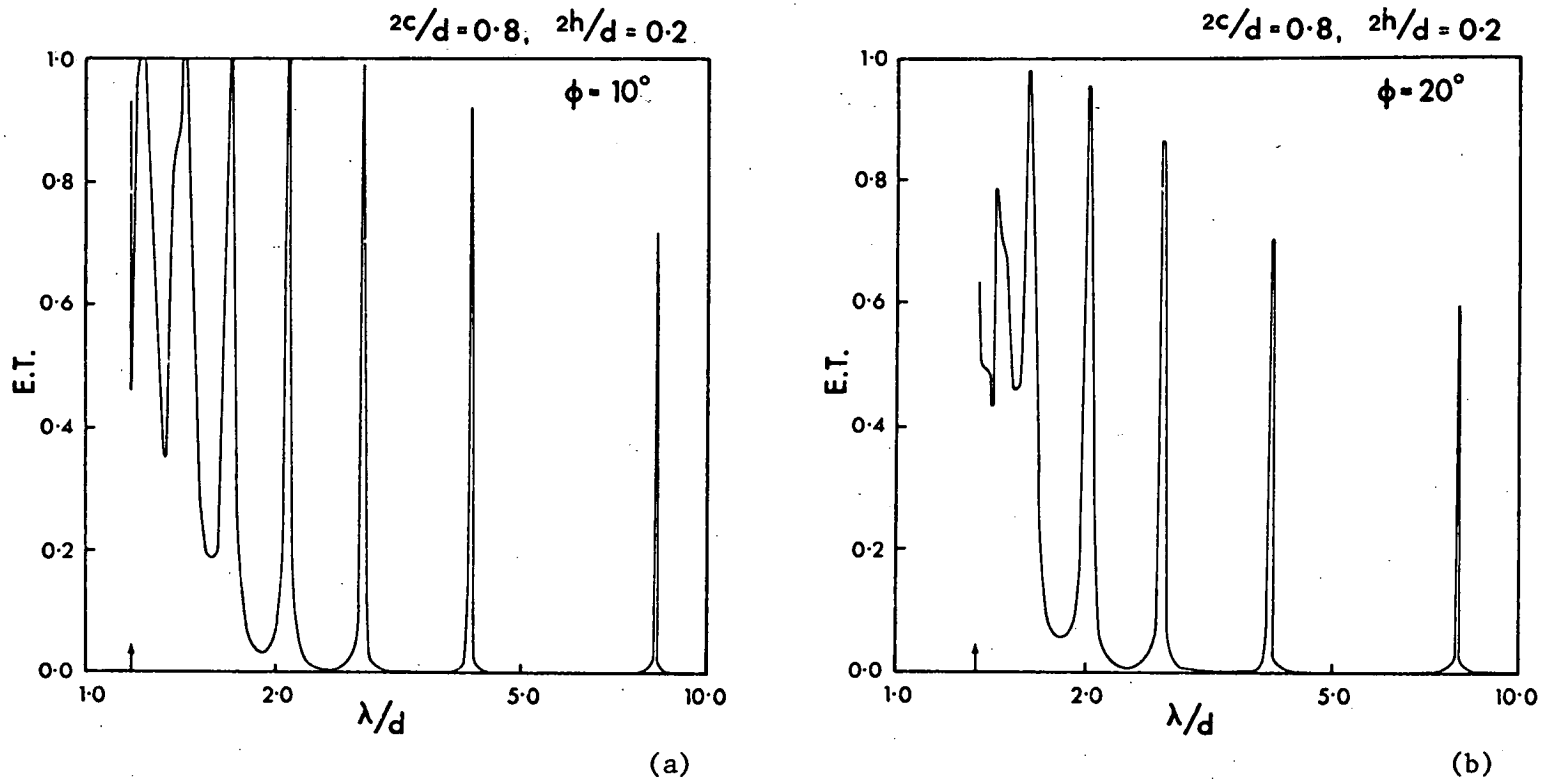

Figure 6.5 Wavelength spectra for a symmetric double grid operated in unpolarized, non-normally incident radiation having $\psi = 0^{o}$. The structure is specified by the parameters $d'/d = 1.0$, $S/d = 4.0$ and $\delta x/d = 0.0$.

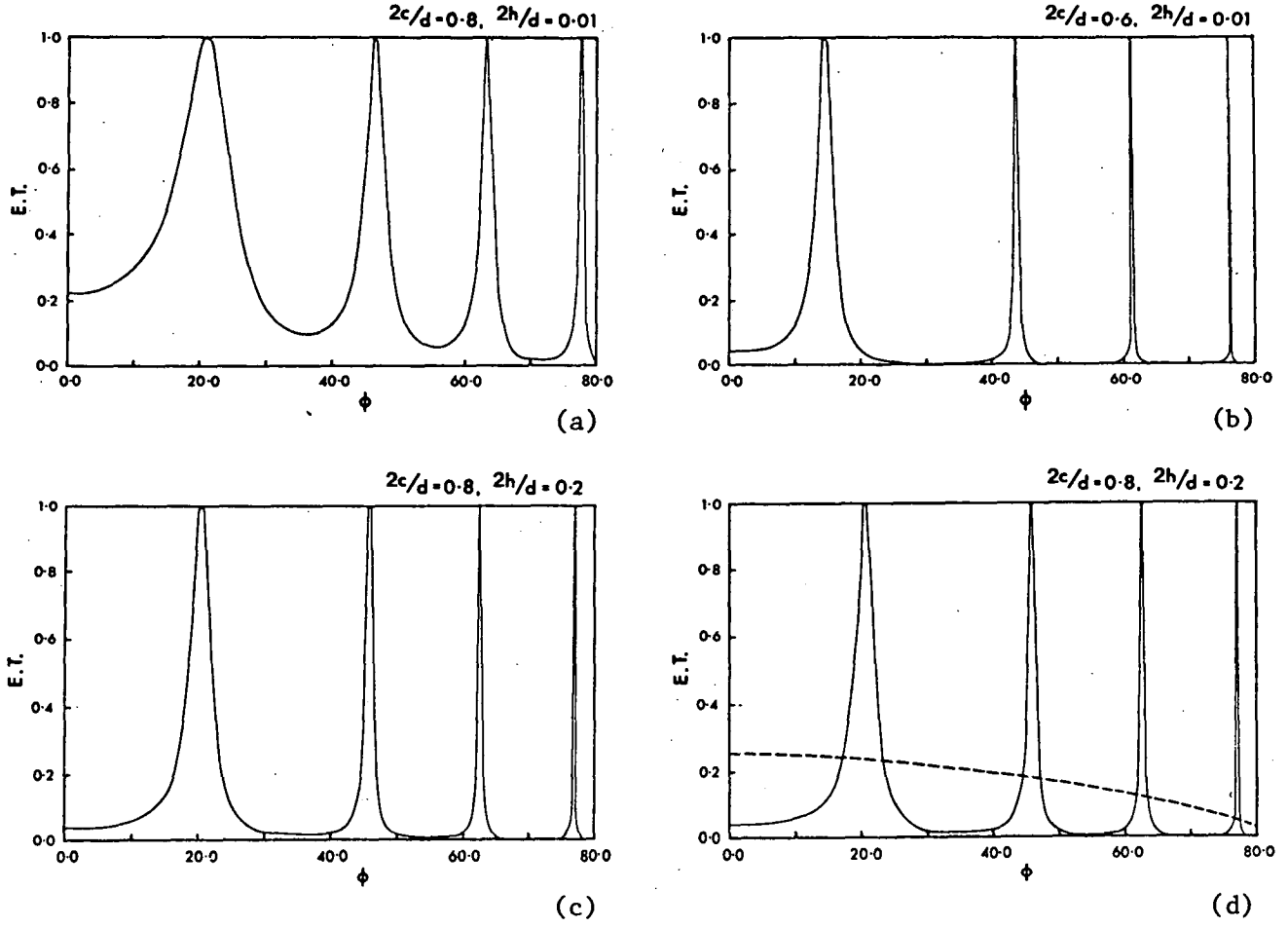

Figure 6.6 Angle of incidence spectra for a symmetric double grid specified by $d'/d = 1.0$, $S/d = 4.0$, $\delta x/d = \delta z/d = 0.0$ operated in TE ($\delta = 0^{\circ}$) polarized radiation of wavelength $\lambda/d = 2.0$ and having $\psi = 0^{\circ}$. Figure 6.6d was obtained using the reconstruction procedure and the broken curve represents the transmission properties of the single grid elements.

these curves to be noted immediately are that the finesse of the interferometer increases as $\phi \to 90^{o}$ and that decreasing aperture width and increasing grid depth again increase the finesse. These observations can be explained by making use of the results of the multiple scattering treatment and applying the monomodal approximation.

The complex reflected and transmitted amplitudes of the zeroth order waves diffracted by a single grid operated under these incidence conditions are again given by equations (6.100) and (6.101). Using these expressions the following properties can be deduced:

$$|G^{0}| \to 1 \quad , \quad \arg(G^{0}) \to \pi - 2\beta_{00}h \qquad \text{as} \quad \phi \to 90^{o} \tag{6.104}$$

$$\text{i.e.} \quad \xi^{0} \to \pi + \beta_{00}S \qquad \text{as} \quad \phi \to 90^{o} \quad .$$

Thus as $\phi \to 90^{o}$, the finesse of the interferometer increases and the positions of the interference maxima tend to the positions obtained geometrically:

$$\phi_{max} = \arccos\left(\frac{\ell\lambda}{2S}\right) \tag{6.105}$$

The aperture width and grid depth dependence described for normally incident radiation in section 6.4.1 can be shown to also apply to this case. These results are confirmed in figure 6.6 for the symmetric double grid.

6.4.3 Operation in Off-Normal ($\phi \neq 0^{o}$, $\psi = 0^{o}$) TM Polarized Radiation

The wavelength of radiation is assumed sufficiently long so that only the zeroth orders in reflection and transmission propagate, and that the double grid is symmetric, having aperture widths $2c$, grid depths $2h$ and periods $d = d' = 1$. Firstly, expressions will be derived for the

reflected (H^{90}) and transmitted ($\hat{H}^{90}$) complex amplitudes of the zeroth orders diffracted by a single grid by adopting a monomodal approximation. The double grid performance is then reconstructed using equations (6.89 - 93).

The waveguide modal expansion given in equation (6.96) will again describe the transverse resolute of the electric field in the aperture region of the single grid. In this case, however, the dominant mode is that for which $n = 0$, $m = 1$. Then by solving the single grid diffraction problem, the following results can be derived:

$$c_{01}^{s} = d_{01}^{s} = 0$$

$$a_{01}^{s*} = a_{01}^{s}\sin(\nu_{01}h) = \frac{ik^2 F_i^{s*} \bar{I}_{01}^{00}}{\beta_{00}(S(\lambda) - L'\cot(L'h))} \tag{6.106}$$

$$b_{01}^{s*} = b_{01}^{s}\cos(\nu_{01}h) = \frac{ik^2 F_i^{s*} \bar{I}_{01}^{00}}{\beta_{00}(S(\lambda) + L'\tan(L'h))} \tag{6.107}$$

where $F_i^{s*} = \beta_{00}\exp(-i\beta_{00}h)/k$

$$L' = \nu_{01}$$

$$S(\lambda) = \sum_{p,q} \frac{i}{\beta_{pq}}(k^2 - \gamma_{pq}^2)|I_{01}^{pq}|^2$$

and $$I_{01}^{pq} = \frac{1}{\sqrt{2}c}\int_{-c}^{c}\int^{c} \sin[\tfrac{\pi}{2c}(z + c)]\exp[-i(\alpha_p x + \gamma_{pq} z)]\,dzdx$$

This inner product can be evaluated analytically. Then

$$H^{90} = -\exp(-i2\beta_{00}h)\{\frac{\beta_{00}}{k} + i2k\,|I_{01}^{00}|^2\,[\frac{L'\cos(2L'h) - S(\lambda)\sin(2L'h)}{(S^2(\lambda)-L'^2)\sin(2L'h)-2S(\lambda)L'\cos(2L'h)}]\} \tag{6.108}$$

and

$$\hat{H}^{90} = -i2k \exp(-i2\beta_{00}h)|I_{01}^{00}|^2\left\{\frac{L'}{(S^2(\lambda)-L'^2)\sin(2L'h)-2S(\lambda)L'\cos(2L'h)}\right\} . \tag{6.109}$$

At this stage it is worth reiterating that for radiation incident such that $\phi = \psi = 0^o$, the results described for TE polarized ($\delta = 0^o$) radiation are exactly the same as for TM polarized ($\delta = 90^o$) radiation. Explicit consideration of the above results confirms this comment.

Now consider radiation such that ϕ is arbitrary, $\psi = 0^o$ and $\delta = 90^o$, and in particular what happens as $\phi \to 90^o$. The expression for the finesse, equation (6.91) is dependent on $\cos\phi$ not only through the term (H^{90}) but also from the quantity β_{00}. Using expressions (6.108), (6.109) it may be shown that

$$\hat{H}^{90} \to \frac{2iL'\cos\phi}{k|I_{01}^{00}|^2 \sin(2L'h)} \exp(-2i\beta_{00}h) \qquad \text{as} \quad \phi \to 90^o \tag{6.110}$$

and

$$H^{90} \to \cos\phi \exp(-2i\beta_{00}h) \qquad \text{as} \quad \phi \to 90^o . \tag{6.111}$$

Thus, for h sufficiently large so that $\sin(2Lh)$ is not negligible and c large enough so that the inner product is non-zero, the finesse

$$\mathcal{F}^{90} = \frac{4\cos^2\phi|H^{90}|^2}{|\hat{H}^{90}|^2}$$

increases as $\phi \to 90^o$. Also from equation (6.92)

$$\xi^{90} \to \beta_{00}S + \pi \qquad \text{as} \quad \phi \to 90^o .$$

In other words, the positions of the resonance maxima should tend to the geometric limit as the angle of incidence becomes more oblique.

It is also noted that the single grid zeroth order reflected efficiency

$$\frac{k^2}{\beta_{00}^2} |H^{90}|^2 \to 1 \qquad \text{as} \quad \phi \to 90^\circ \quad .$$

The broken curves given in figures 6.7a and 6.7b depict angle of incidence spectra for single grids having deep apertures of large cross-section and confirm the above predictions for the single grid. These curves show that the transmittance of the single grid operated in TM polarized radiation rises from the value at normal incidence ($\phi = 0^\circ$), reaches a maximum and then rapidly approaches the limiting value of zero at $\phi = 90^\circ$. Consequently, the half-widths of the resonances in the double grid angle of incidence spectra, which are shown by the solid curves in figure 6.7, would be expected to decrease only for maxima located very close to $\phi = 90^\circ$.

Finally, the dependence of these curves on c and h are considered. For radiation incident near normal, it can be shown that

(a) $|H^{90}| \to \cos\phi$ as $c \to 0$

$\arg(H^{90}) \to \pi - 2\beta_{00}h$.

From equation (6.91), the finesse improves as the aperture width decreases and

$$\xi^{90} \to \beta_{00}S + \pi$$

which implies that the positions of the resonance maxima tend to the geometric limit given by equation (6.105) as $c \to 0$, and

(b) $|H^{90}| \to \cos\phi$ as $h \to \infty$ $(\lambda > 4c)$

$\arg(H^{90}) \to \pi - 2\beta_{00}h - \delta''$

where $\delta'' = \arg[S(\lambda) - |L'|]^2$

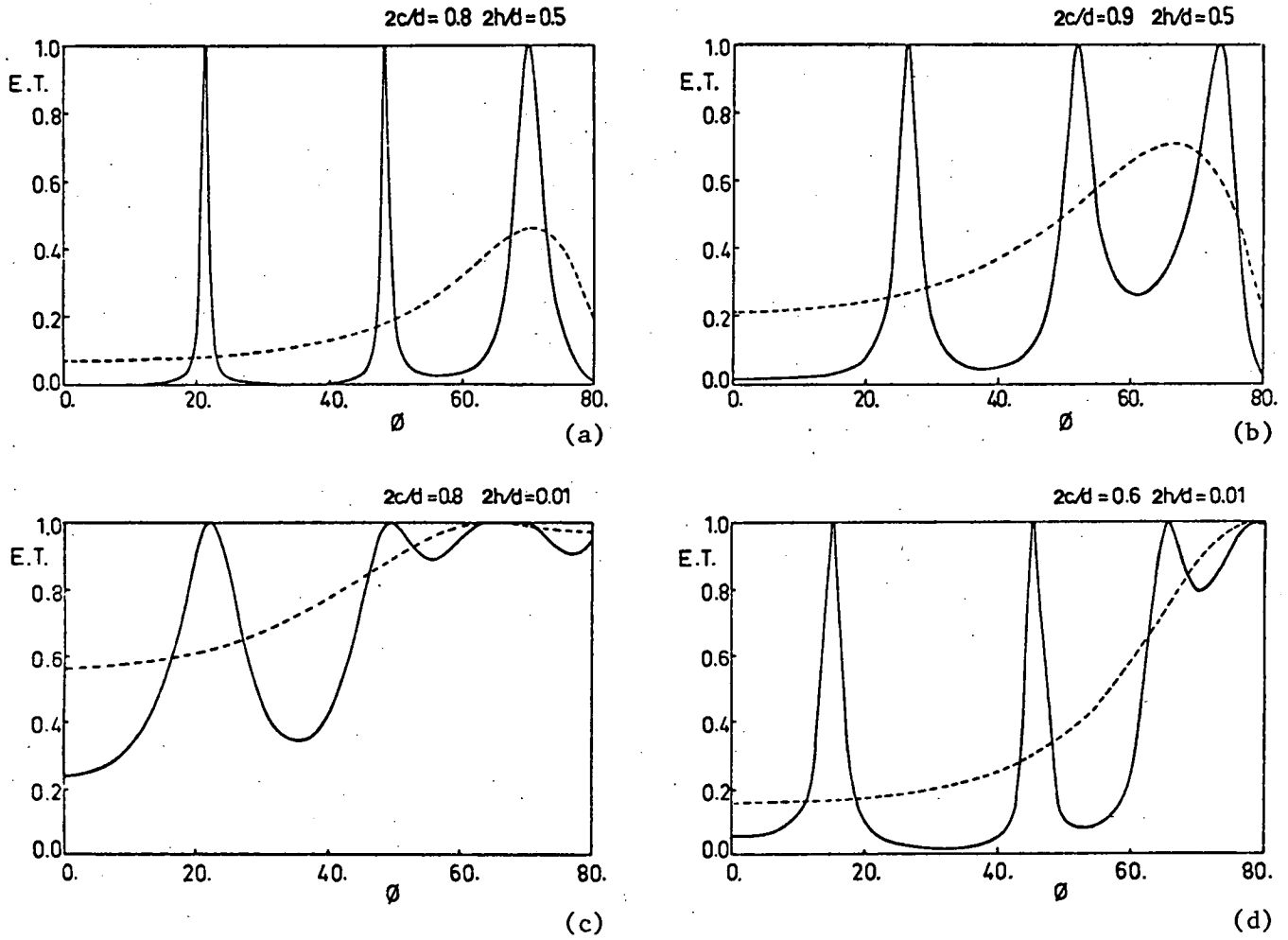

Figure 6.7 As for figure 6.6, but operated in TM ($\delta = 90^{\circ}$) polarized radiation. All broken curves represent the transmission properties of the single grid elements.

This shows that the finesse again increases as the aperture depth increases.

6.5 CONCLUSIONS

This chapter has discussed a rigorous formalism describing the diffraction properties of the infinitely conducting double grid shown in figure 6.1. The theory has been verified by numerical experiments and the results obtained are in excellent agreement with the Reciprocity Theorem and the symmetry constraints discussed in chapter 7.

The investigations concentrated on the applications as Fabry-Perot interferometers of symmetric double grids operated in long wavelength radiation. A multiple scattering, monomodal approach was used to optimise the performance of the double grid for the interferometric application and it was confirmed that high finesse interferometers could be constructed from grids having deep apertures of narrow cross-section. The positions of the interference maxima were also found to be chiefly governed by the aperture widths and incidence parameters. Thus, in general, the properties discovered for the double grating interferometer [6.8] were found to apply to the double grid. However, in contrast with the double grating, the symmetric double grid interferometer is effective when operated in normally incident unpolarized radiation due to the polarization independence exhibited by this structure under these incidence conditions.

The multiple scattering approach was also used in conjunction with the monomodal treatment to investigate the properties of the double grid operated in non-normally incident ($\phi \neq 0^{o}, \psi = 0^{o}$) radiation. Again the interferometric action of the double grid is improved with decreasing aperture width and increasing depth for both TE and TM polarized incident waves.

REFERENCES

[6.1] ADAMS (J.L.). - J. Optics (Paris), accepted.

[6.2] CHEN (C.-C.). - I.E.E.E. Trans. MTT-18, 1970, 627.

[6.3] CHEN (C.-C.). - I.E.E.E. Trans. MTT-19, 1971, 475.

[6.4] CHEN (C.-C.). - I.E.E.E. Trans. MTT-21, 1973, 1.

[6.5] McPHEDRAN (R.C.), MAYSTRE (D.). - Appl. Phys., 1977, 14, 1; University of Sydney Research Report SP 76/1.

[6.6] ADAMS (J.L.), BOTTEN (L.C.), McPHEDRAN (R.C.). - J. Optics (Paris), 1978, 8, 87; chapter 8, this thesis.

[6.7] BLOK (H.), MUR (G.). - Appl. Sci. Res., 1972, 26, 389.

[6.8] ADAMS (J.L.), BOTTEN (L.C.). - J. Optics (Paris), 1979, 10, 109; chapter 3, this thesis.

[6.9] BOTTEN (L.C.). - Infrared Phys., 1979, 19, 659.

[6.10] BOTTEN (L.C.), ADAMS (J.L.), DERRICK (G.H.). - J. Optics (Paris) submitted.

[6.11] ADAMS (J.L.). - University of Tasmania Research Report, DGRG 79/1.

[6.12] NEVIERE (M.), CADILHAC (M.). - Opt. Commun., 1970, 2, 235.

[6.13] PETIT (R.). - Rev. Opt., 1966, 45, 249.

[6.14] MARCUVITZ (N.). - "Waveguide Handbook" McGraw-Hill, New York, 1951.

[6.15] PETIT (R.). - Topics in Current Physics, Vol. 22, section 2.2, "Electromagnetic Theory of Gratings", Springer-Verlag, Heidelberg, 1980.

CHAPTER 7

SYMMETRY RELATIONS OF THE MULTI-ELEMENT INDUCTIVE GRID

7.1 INTRODUCTION

The investigations [7.1] presented in this chapter describe the diffraction properties of multi-element grids, which are structures composed of a stack of an arbitrary number of identical grids. Each grid element is assumed to be perfectly conducting and up-down symmetric.

This study represents a generalisation to doubly periodic structures of the investigations reported in chapter 5, which analysed the properties of multi-element gratings. Since the relevant introductory material for this chapter has already been presented in section 5.1, it will not be repeated here. The multiple scattering approach used in chapter 5, which incorporated the interaction of all orders (both propagating and evanescent) between the elements, is also adopted in this chapter to analyse the multi-element grid diffraction problem. A matrix recurrence relation is derived in section 7.2.2 for the reflected and transmitted complex amplitudes of the multi-element grid.

In particular, a multi-element grid, whose components are perfectly conducting, rectangular-holed inductive grids, is considered. The scattering properties of the individual elements of this grid are described in detail in section 7.2.3 and are determined using the technique developed by Chen [7.2, 7.3] and McPhedran and Maystre [7.4].

A series of new conservation relations are derived in section 7.3 for the individual up-down symmetric, perfectly conducting, rectangular-holed, inductive grid elements. These properties are shown to hold analytically (that is, independently of errors introduced by truncating

the field expansions) for this structure. The constraints are analogous to those presented in chapter 5 for singly periodic structures and provide a comprehensive and very useful check on the numerical implementation of the formalism. All orders, both propagating and evanescent, are constrained whether the orders are produced by waves incident in the propagating order or evanescent order channels. In addition, the same conservation properties are shown in section 7.4, to hold analytically for the entire grid stack.

A short description of the long wavelength filtering properties of the multi-element, rectangular-holed inductive grid is given in section 7.5 and the effect of the number of elements in the structure on the filtering characteristics is discussed. These results incorporate and generalise those presented in chapter 6, which described the diffraction properties of a two-element grid interferometer.

7.2 THE THEORETICAL FORMALISM

7.2.1 Notation and Description of the Diffraction Arrangement

The structure considered in this chapter is composed of $(n + 1)$ identical, up-down symmetric, perfectly conducting grids, as shown in figure 7.1. (Here n is an arbitrary positive integer). A Cartesian coordinate system, with unit vectors $\hat{x}$, $\hat{y}$ and $\hat{z}$ aligned with the OX, OY and OZ axes respectively, is introduced with the OY axis orthogonal to each element of the grid. Each individual grid element has period $d = 2\pi/K$ along the OX axis and period $d' = 2\pi/K'$ along the second periodicity axis OZ. (Here it is assumed for simplicity that the two axes of periodicity are perpendicular, but a similar analysis can be applied for an arbitrary inclination of the two axes).

A plane wave of wavelength $\lambda = 2\pi/k$ is assumed to be incident on

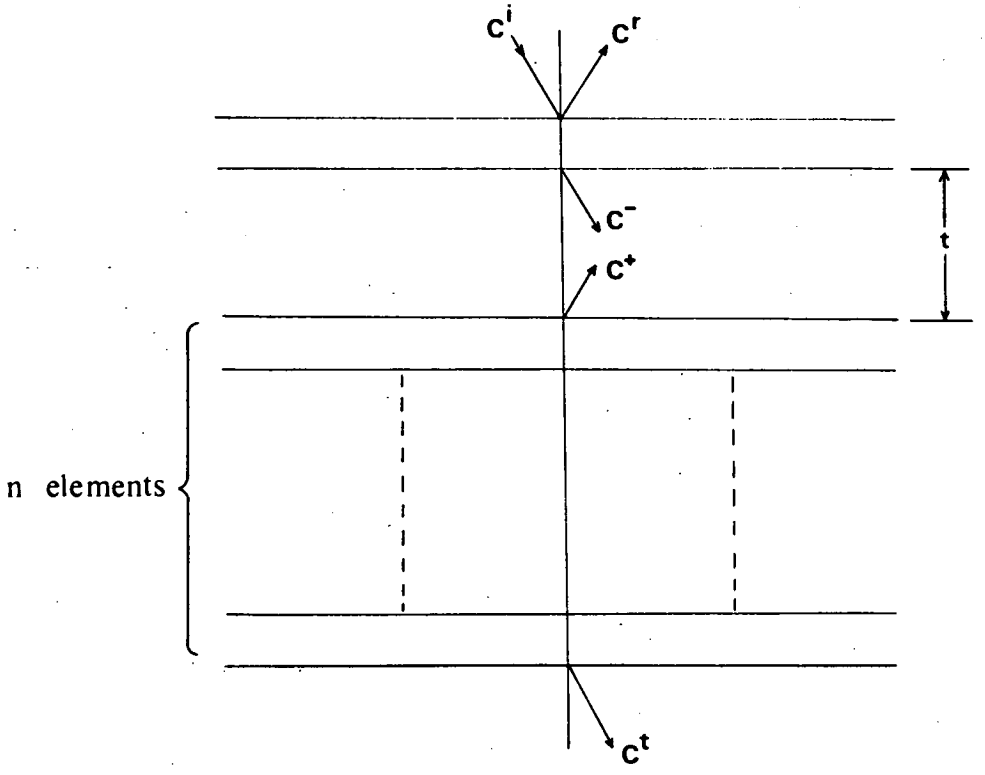

Figure 7.1 Side view of the (n + 1) -element grid stack and specification of the fields considered in the multiple scattering analysis.

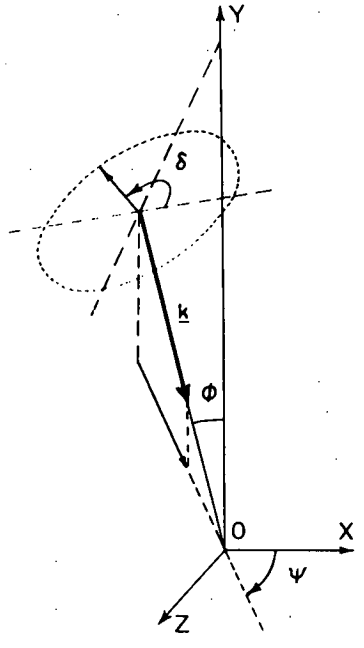

Figure 7.2 Specification of the incident field.

the structure, with direction specified by the angles ϕ and ψ depicted in figure 7.2. The polarization of the incoming wave is specified by the angle δ shown in this figure. Thus, the direction of the incident plane wave is specified by the direction sines and cosines

$$\left.\begin{aligned} \alpha_0 &= k \sin\phi \cos\psi \\ \gamma_0 &= k \sin\phi \sin\psi \\ \beta_{00} &= k \cos\phi \end{aligned}\right\} \qquad (7.1)$$

The fields in all regions are specified in terms of TE (transverse electric) and TM (transverse magnetic) vector modes, already introduced in chapter 6. Thus the transverse resolute of the incident electric field is given by

$$\underline{E}_t^i = \sqrt{\frac{k}{\beta_{00}}}\, E^i\, \underline{\hat{RTE}}_{00}(x,y,z) + \sqrt{\frac{\beta_{00}}{k}}\, F^i\, \underline{\hat{RTM}}_{00}(x,y,z) \qquad (7.2)$$

where $E^i = \cos\delta$

and $F^i = \sin\delta$

and the other quantities are defined in equations (6.2) to (6.5). The scaling factors $\sqrt{\frac{k}{\beta_{00}}}$ and $\sqrt{\frac{\beta_{00}}{k}}$ are introduced to normalise the energy properties of the system and reduce the complexity of the mathematical representation of the conservation relations described in section 7.3.

The field incident upon the multi-element grid produces a diffracted field which in free space is composed of a discrete set of plane waves whose direction sines and cosines are given by

$$\alpha_p = \alpha_0 + pK \qquad (-\infty < p < \infty) \quad , \qquad (7.3a)$$

$$\gamma_q = \gamma_0 + qK' \qquad (-\infty < q < \infty) \tag{7.3b}$$

and

$$\left.\begin{aligned} \beta_{pq} &= \sqrt{k^2 - \alpha_p^2 - \gamma_q^2} && \text{if } |\alpha_p^2 + \gamma_q^2| \le k \\ &= i\sqrt{\alpha_p^2 + \gamma_q^2 - k^2} && \text{if } |\alpha_p^2 + \gamma_q^2| > k \end{aligned}\right\} \tag{7.4}$$

As discussed in section 5.2.1, it is important to note that the set of direction series for the problem is closed.

The recurrence relations for the scattering matrices of the multi-element grid stack are derived by considering the $(n + 1)$-element stack as being composed of a single grid element placed above the remaining n-elements as shown in figure 7.1. Alternatively, recurrence relations can be derived by considering the n-element grid placed above the remaining grid element. The response of both the single element and n-element stacks to fields incident in all channels (p,q) (that is, with direction sines α_p and γ_q) must be determined in order to apply the multiple scattering treatment. The scattering properties of the single element are written as reflection and transmission scattering matrices ρ_1 and τ_1 respectively. The matrix ρ_1 has the following partitioned form

$$\rho_1 = \begin{bmatrix} E(0) & E(90) \\ F(0) & F(90) \end{bmatrix} \tag{7.5}$$

Here the following notation has been adopted. The submatrix $E(\delta)$ (for $\delta = 0^o$ or 90^c) is composed of elements $E^{\delta}_{rs,pq}$ where $\sqrt{\frac{k}{\beta_{rs}}}\, E^{\delta}_{rs,pq}$ is the complex amplitude of the TE component of the wave reflected into the (r,s) channel, corresponding to either a TE polarized $(\delta = 0^o)$ wave of amplitude $\sqrt{\frac{k}{\beta_{pq}}}\, E^i$ or a TM polarized

($\delta = 90^{\circ}$) wave of amplitude $\sqrt{\frac{\beta_{pq}}{k}}\, F^{i}$, incident in the (p,q) channel. $F(\delta)$ contains the corresponding amplitudes $\sqrt{\frac{\beta_{rs}}{k}}\, F^{\delta}_{rs,pq}$ of the TM component of the diffracted waves. Again the scaling factors $\sqrt{\frac{k}{\beta_{rs}}}$ and $\sqrt{\frac{\beta_{rs}}{k}}$ are introduced to normalise the energy properties of the system. Similar definitions apply to the elements of the matrix τ_1 but all amplitudes have a superscript $\hat{}$, denoting transmission. The phase origins for the elements of ρ_1 and τ_1 are the upper and lower surfaces respectively of the single grid element in the centre of a nominated aperture.

Similarly, the reflection and transmission scattering matrices for the remaining n-element grid are designated by ρ_n and τ_n respectively. The phase origin for the elements of these matrices are taken to be the upper and lower surfaces respectively of the n-element grid.

7.2.2 The Recurrence Relation for the Scattering Matrices

This derivation follows closely that given in section 5.2.2 of this thesis. However, the theoretical and numerical complexity of the problem is much greater when considering multi-element grids since both the TE and TM field amplitudes must be incorporated in the scattering matrices.

The following partitioned column vector is introduced to represent the complex amplitudes of the TE and TM components of the various channels of the incident field.

$$C^{i} = \begin{bmatrix} [E^{i}_{pq}] \\ \\ [F^{i}_{pq}] \end{bmatrix} \tag{7.6}$$

where $[E^{i}_{pq}]$ and $[F^{i}_{pq}]$ are column vectors.

Note that the subscripts pq and rs should be regarded as compounded subscripts when considering the numerical implementation of the theory. That is, when filling the arrays the subscript pair pq is taken as a single entity.

In a similar manner, the overall reflected and transmitted fields are represented by C^r and C^t respectively while the upward and downward scattered fields shown in figure 7.1 are represented by the vectors C^+ and C^-. In order to relate the fields on either side of the free space regions separating the grid elements, a matrix P

$$P = \begin{bmatrix} [p_{pq}] & [p_{pq}] \\ [p_{pq}] & [p_{pq}] \end{bmatrix}$$

is introduced, where p is a diagonal submatrix

$$p = \text{diag}(\exp(i\beta_{pq}t)).$$

Using exactly the derivation given in section 5.2.2, the following constraints are obtained.

$$C^r = \rho_1 C^i + \tau_1 P C^+ \tag{7.7}$$

$$C^- = \tau_1 C^i + \rho_1 P C^+ \tag{7.8}$$

and

$$C^+ = \rho_n P C^- \tag{7.9}$$

$$C^t = \tau_n P C^- \tag{7.10}$$

Equations (7.7 - 7.10) reduce very simply to

$$C^r = \rho_{n+1} C^i \tag{7.11}$$

and

$$C^t = \tau_{n+1} C^i \tag{7.12}$$

where

$$\rho_{n+1} = \rho_1 + \tau_1 P \rho_n P (J - \rho_1 P \rho_n P)^{-1} \tau_1 \qquad (7.13)$$

and

$$\tau_{n+1} = \tau_n P (J - \rho_1 P \rho_n P)^{-1} \tau_1 \qquad (7.14)$$

denote the reflection and transmission scattering matrices of the (n+1)-element grid. Here $J = \begin{bmatrix} I & 0 \\ 0 & I \end{bmatrix}$, where I denotes the standard identity matrix of appropriate dimension. Equations (7.13) and (7.14) are best rewritten in the more compact form

$$A_{n+1} = A_1 + B_1 A_n (J - A_1 A_n)^{-1} B_1 \qquad (7.15)$$

and

$$B_{n+1} = B_n (J - A_1 A_n)^{-1} B_1 \qquad (7.16)$$

where

$$A_k = \rho_k P \qquad (7.17)$$

and

$$B_k = \tau_k P \qquad k = 1, \ldots\ldots n+1 \qquad (7.18)$$

The matrix recurrence relations (7.15) and (7.16) may be used to determine the scattering properties of a multi-element grid having an arbitrary number of elements. These relations have exactly the same form as those derived for the multi-element grating (equations (5.13) and (5.14)). Obviously these recurrence relations may be generalised as in section 5.2.2 to encompass multi-element grids having arbitrary separations between the individual elements.

7.2.3 Scattering Matrices for a Single Rectangular-Holed Inductive Grid

The elements of the scattering matrices for a single rectangular-holed inductive grid are explicitly determined in this section. The motivations for choosing this structure as the reflecting elements of the multi-element grid were the same as those discussed in section 5.2.3 of this thesis when rationalising the choice of lamellar gratings as the

components of multi-element gratings. That is, the theory describing the diffraction properties of perfectly conducting, rectangular-hole inductive grids is well known [7.2 - 7.4], and it has been shown [7.4] that constraints such as conservation of energy are analytically satisfied by the single grid formalism. Also the system is lossless and possesses both up-down and left-right symmetries, thus permitting the derivation of certain conservative properties (section 7.3) of the diffracting system.

A plane wave is now considered to be incident upon the perfectly conducting inductive grid shown in figure 7.3, in the channel (p,q). In the free space regions, the fields are expressed in terms of Rayleigh expansions. The transverse resolutes of the reflected fields in $y > h$ are thus described by

$$\underline{E}_t = \sum_{r,s} \{\sqrt{\frac{k}{\beta_{rs}}} [E^i_{pq} \exp(-i\beta_{pq} y') \delta_{rs,pq} + E_{rs,pq} \exp(i\beta_{rs} y')] \underline{RTE}_{rs}(x,0,z)$$

$$+ \sqrt{\frac{\beta_{rs}}{k}} [F^i_{pq} \exp(-i\beta_{pq} y') \delta_{rs,pq} + F_{rs,pq} \exp(i\beta_{rs} y')] \underline{RTM}_{rs}(x,0,z)\} \tag{7.19}$$

and

$$\hat{y} \times \underline{H}_t = -\frac{1}{Z_0} \sum_{r,s} \{\sqrt{\frac{\beta_{rs}}{k}} [E_{rs,pq} \exp(i\beta_{rs} y') - E^i_{pq} \exp(-i\beta_{pq} y') \delta_{rs,pq}] \times$$

$$\times \underline{RTE}_{rs}(x,0,z)$$

$$+ \sqrt{\frac{k}{\beta_{rs}}} [F_{rs,pq} \exp(i\beta_{rs} y') - F^i_{pq} \exp(-i\beta_{pq} y') \delta_{rs,pq}] \underline{RTM}_{rs}(x,0,z)\} \tag{7.20}$$

where $y' = y - h$, Z_0 is the free space impedence, $\underline{RTE}_{rs}(x,y,z)$ and $\underline{RTM}_{rs}(x,y,z)$ are defined by equations (6.14) and (6.15) and the sums $\sum_{r,s}$ are over the range $r \in (-\infty, \infty)$, $s \in (-\infty, \infty)$.

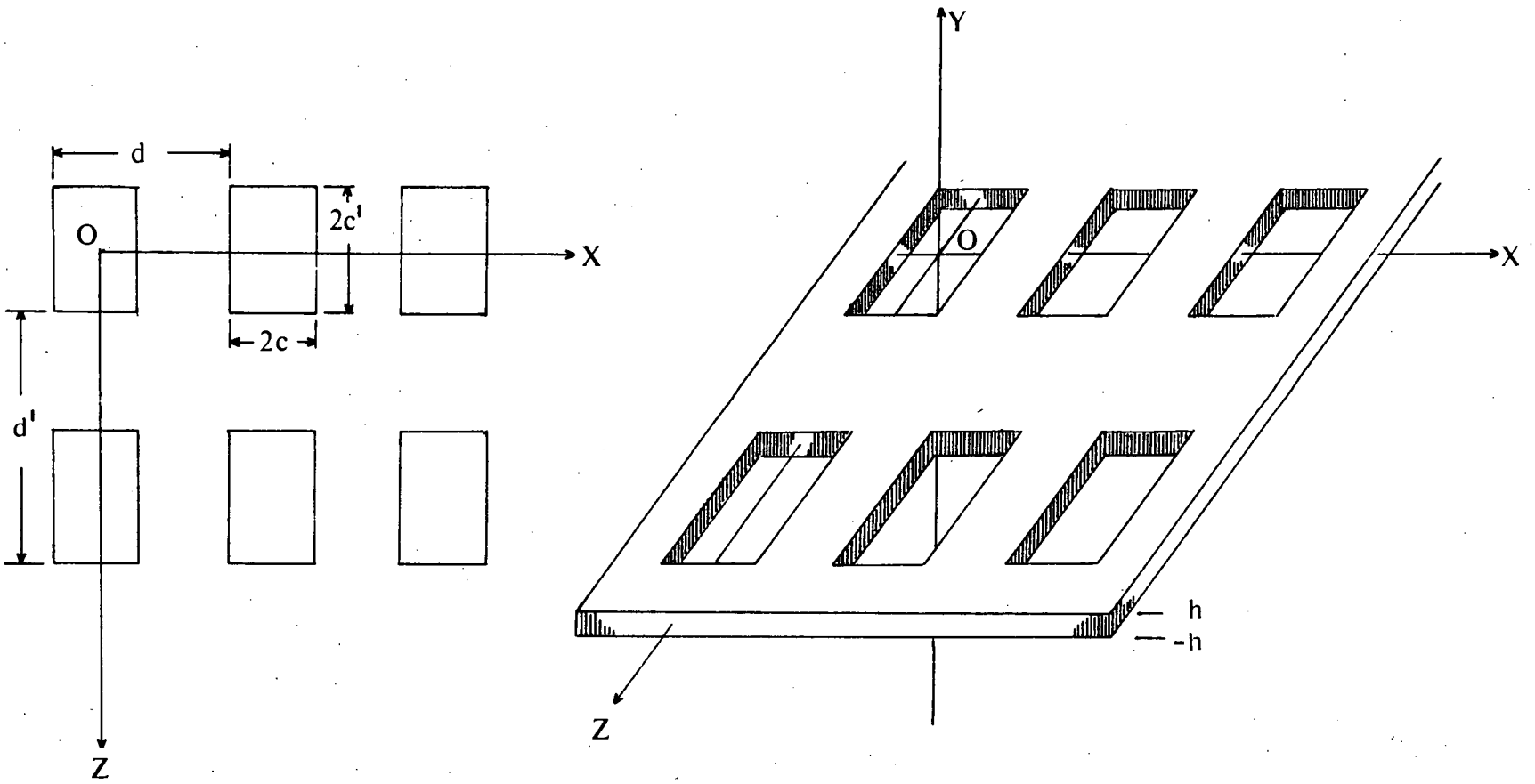

Figure 7.3 Geometry of the inductive grid elements.

The elements are assumed infinite in extent.

Similarly the transverse resolutes of the fields in the free space region $y < -h$ are expressed by the following plane wave expansions

$$\underline{E}_t = \sum_{r,s} \{\sqrt{\frac{k}{\beta_{rs}}}\, \hat{E}_{rs,pq} \exp(-i\beta_{rs} y'')\underline{RTE}_{rs}(x,0,z) + \sqrt{\frac{\beta_{rs}}{k}}\, \hat{F}_{rs,pq} \exp(-i\beta_{rs} y'')\underline{RTM}_{rs}(x,0,z)\} \tag{7.21}$$

and

$$\hat{y} \times \underline{H}_t = \frac{1}{Z_0} \sum_{r,s} \{\sqrt{\frac{\beta_{rs}}{k}}\, \hat{E}_{rs,pq} \exp(-i\beta_{rs} y'')\underline{RTE}_{rs}(x,0,z) + \sqrt{\frac{k}{\beta_{rs}}}\, \hat{F}_{rs,pq} \exp(-i\beta_{rs} y'')\underline{RTM}_{rs}(x,0,z)\} \tag{7.22}$$

where $y'' = y + h$

Within the aperture region ($|x| \le c$, $|z| \le c'$, $|y| \le h$) the field is expanded as a sum of waveguide modes. Thus, the transverse resolutes of the fields in this region are given by

$$\underline{E}_t = \sum_{n,m\in\Lambda} \{[b_{1;nm,pq}\cos(\mu_{nm} y) + b_{2;nm,pq}\sin(\mu_{nm} y)]\underline{MTEU}_{nm}(x,z)\} + \sum_{n,m\in\Lambda'} \{[d_{1;nm,pq}\cos(\mu_{nm} y) + d_{2;nm,pq}\sin(\mu_{nm} y)]\underline{MTMU}_{nm}(x,z)\} \tag{7.23}$$

and

$$\hat{y} \times \underline{H}_t = -\frac{i}{Z_0} \Big\{ \sum_{n,m\in\Lambda} \{\frac{\mu_{nm}}{k}[b_{1;nm,pq}\sin(\mu_{nm} y) - b_{2;nm,pq}\cos(\mu_{nm} y)]\}\underline{MTEU}_{nm}(x,z) + \sum_{n,m\in\Lambda'} \{\frac{k}{\mu_{nm}}[d_{1;nm,pq}\sin(\mu_{nm} y) - d_{2;nm,pq}\cos(\mu_{nm} y)]\}\underline{MTMU}_{nm}(x,z)\} \tag{7.24}$$

where $\Lambda = \{(n,m) \mid n,m = 0,1,2.....;\ n+m \neq 0\}$,

$\Lambda' = \{(n,m) \mid n,m = 1,2,.....\}$.

and $\underline{\underline{MTEU}}_{nm}(x,z)$ and $\underline{\underline{MTMU}}_{nm}(x,z)$ are defined by equations (6.30) and (6.31) respectively, with c_1 being replaced by c, and c_1' by c'. Also μ_{nm} is defined by equation (6.34).

Now that the fields within all regions of space have been specified, the continuity conditions appropriate to the problem are applied. These are that the transverse resolutes of the electric and magnetic fields are continuous across aperture-free space interfaces.

Following an analysis similar to that presented in chapter 6, the equations derived from the continuity of the transverse component of the electric field, after application of the Method of Moments, can be written

$$\sqrt{\frac{k}{\beta_{RS}}}\,[E^i_{pq}\delta_{RS,pq} + E_{RS,pq}] = \sum_{n,m\epsilon\Lambda}\{[b^*_{1;nm,pq} + b^*_{2;nm,pq}]\,L_{11}(RS;nm)\} + \sum_{n,m\epsilon\Lambda'}\{[d^*_{1;nm,pq} + d^*_{2;nm,pq}]\,L_{12}(RS;nm)\} \tag{7.25}$$

$$\sqrt{\frac{\beta_{RS}}{k}}\,[F^i_{pq}\delta_{RS,pq} + F_{RS,pq}] = \sum_{n,m\epsilon\Lambda}\{[b^*_{1;nm,pq} + b^*_{2;nm,pq}]\,L_{21}(RS;nm)\} + \sum_{n,m\epsilon\Lambda'}\{[d^*_{1;nm,pq} + d^*_{2;nm,pq}]\,L_{22}(RS;nm)\} \tag{7.26}$$

$$\sqrt{\frac{k}{\beta_{RS}}}\,\hat{E}_{RS,pq} = \sum_{n,m\epsilon\Lambda}\{[b^*_{1;nm,pq} - b^*_{2;nm,pq}]\,L_{11}(RS,nm) + \sum_{n,m\epsilon\Lambda'}\{[d^*_{1;nm,pq} - d^*_{2;nm,pq}]\,L_{12}(RS;nm)\} \tag{7.27}$$

and

$$\sqrt{\frac{\beta_{RS}}{k}}\,\hat{F}_{RS,pq} = \sum_{n,m\epsilon\Lambda}\{[b^{*}_{1;nm,pq} - b^{*}_{2;nm,pq}]\,L_{21}(RS;nm)\}$$

$$+ \sum_{n,m\epsilon\Lambda'}\{[d^{*}_{1;nm,pq} - d^{*}_{2;nm,pq}]\,L_{22}(RS;nm)\} \tag{7.28}$$

Here

$$b^{*}_{1;nm,pq} = b_{1;nm,pq}\cos(\mu_{nm}h) \tag{7.29}$$

$$b^{*}_{2;nm,pq} = b^{*}_{2;nm,pq}\sin(\mu_{nm}h) \tag{7.30}$$

and similar definitions apply to $d^{*}_{1;nm,pq}$ and $d^{*}_{2;nm,pq}$.

The following modal inner products have also been defined.

$$L_{ij}(pq;nm) = \iint_{A} \underline{\bar{R}}_{i;pq} \cdot \underline{M}_{j;nm}\,dxdz \qquad i,j = 1,2 \tag{7.31}$$

In this definition, the symbols $\underline{R}$ and $\underline{M}$ are specified by equations (6.44) and (6.45) and A is the aperture region defined by $x \in [-c,c]$, $z \in [-c',c']$.

The up-down symmetry of the grid element is now used to decouple the diffraction problem into its y-symmetric and y-anti-symmetric parts. The solution of the y-symmetric problem is considered firstly. Addition of equations (7.25) and (7.27) yields

$$\sqrt{\frac{k}{\beta_{RS}}}\,[E^{i}_{pq}\delta_{RS,pq} + S_{1E}(RS,pq)] = 2\sum_{n,m\epsilon\Lambda}[b^{*}_{1;nm,pq}L_{11}(RS;nm)]$$

$$+ 2\sum_{n,m\epsilon\Lambda'}[d^{*}_{1;nm,pq}L_{12}(RS;nm)] \tag{7.32}$$

where

$$S_{1E}(RS,pq) = E_{RS,pq} + \hat{E}_{RS,pq}\ . \tag{7.33}$$

Similarly equations (7.26) and (7.28) may be combined and written

$$\sqrt{\frac{\beta_{RS}}{k}}\,[F^{i}_{pq}\delta_{RS,pq} + S_{1F}(RS,pq)] = 2\sum_{n,m\epsilon\Lambda}[b^{*}_{1;nm,pq}L_{21}(RS;nm)]$$

$$+ 2\sum_{n,m\epsilon\Lambda'}[d^{*}_{1;nm,pq}L_{22}(RS;nm)] \qquad (7.34)$$

where $$S_{1F}(RS,pq) = F_{RS,pq} + \hat{F}_{RS,pq} \qquad (7.35)$$

The continuity of the transverse resolute of the magnetic fields at $y = \pm h$ is now considered. Equations derived by applying this continuity condition are projected onto the orthogonal waveguide modal basis and integrated over the aperture region $(x,z)\ \epsilon\ A$. The following equations are obtained for the y-symmetric parts.

$$\sum_{r,s}\{\sqrt{\frac{\beta_{rs}}{k}}\,[S_{1E}(rs,pq) - E^{i}_{pq}\delta_{rs,pq}]\,\bar{L}_{11}(rs;NM)$$

$$+ \sqrt{\frac{k}{\beta_{rs}}}\,[S_{1F}(rs,pq) - F^{i}_{pq}\delta_{rs,pq}]\,\bar{L}_{21}(rs;NM)\}$$

$$= 2i\,\frac{\mu_{NM}}{k}\,b^{*}_{1;NM,pq}\tan(\mu_{NM}h) \qquad (7.36)$$

and

$$\sum_{r,s}\{\sqrt{\frac{\beta_{rs}}{k}}\,[S_{1E}(rs,pq) - E^{i}_{pq}\delta_{rs,pq}]\,\bar{L}_{12}(rs;NM)$$

$$+ \sqrt{\frac{k}{\beta_{rs}}}\,[S_{1F}(rs,pq) - F^{i}_{pq}\delta_{rs,pq}]\,\bar{L}_{22}(rs;NM)\}$$

$$= 2i\,\frac{k}{\mu_{NM}}\,d^{*}_{1;NM,pq}\tan(\mu_{NM}h) \qquad (7.37)$$

Equations (7.32) and (7.34) may be combined and written in the following matrix notation

$$\chi^{-\frac{1}{2}}(V_1 + A) = 2Le \qquad (7.38)$$

where

$$V_1 = \begin{bmatrix} [S_{1E}(rs,pq)] \\ \\ [S_{1F}(rs,pq)] \end{bmatrix} , \tag{7.39}$$

$$L = \begin{bmatrix} [L_{11}(rs;nm)] & [L_{12}(rs;nm)] \\ \\ [L_{21}(rs;nm)] & [L_{22}(rs;nm)] \end{bmatrix} , \tag{7.40}$$

$$e = \begin{bmatrix} [b^*_{1;nm,pq}] \\ \\ [d^*_{1;nm,pq}] \end{bmatrix} , \tag{7.41}$$

and

$$\chi = \begin{bmatrix} \beta & 0 \\ \\ 0 & \beta^{-1} \end{bmatrix} . \tag{7.42}$$

Here β is a diagonal matrix defined by

$$\beta = \text{diag}(\beta_{rs}/k) \tag{7.43}$$

and A is a partitioned vector $\begin{bmatrix} A_1 \\ A_2 \end{bmatrix}$ composed of elements

$$A_{1;rs} = E^i_{pq}\delta_{rs,pq} , \qquad A_{2;rs} = F^i_{pq}\delta_{rs,pq} . \tag{7.44}$$

In a similar manner, equations (7.36) and (7.37) are written

$$L^H \chi^{\frac{1}{2}} [V_1 - A] = -2iD_e e \tag{7.45}$$

where

$$D_e = \begin{bmatrix} D_1 & 0 \\ \\ 0 & D_2 \end{bmatrix} \tag{7.46}$$

and

$$\left.\begin{aligned} D_1 &= \text{diag}\left(-\frac{\mu_{nm}}{k}\tan(\mu_{nm}h)\right) \\ D_2 &= \text{diag}\left(-\frac{k}{\mu_{nm}}\tan(\mu_{nm}h)\right) \end{aligned}\right\} \tag{7.47}$$

Here it is noted that the elements of the matrix D_e are purely real. Again in these definitions, the subscript pairs r,s and n,m should be regarded as compounded subscripts when filling the arrays.

Substitution of equations (7.38) in (7.45) leads to the following equation constraining the modal field quantities corresponding to the y-symmetric problem

$$(L^H \chi L + iD_e)e = L^H \chi^{\frac{1}{2}} A \tag{7.48}$$

Since this section is concerned with determining a scattering matrix composed of amplitudes corresponding to diffraction problems with incident waves of polarization $\delta = 0^\circ$ and $\delta = 90^\circ$ (see equation (7.5)), equation (7.48) is rewritten in the form

$$(L^H \chi L + iD_e)B_1 = L^H \chi^{\frac{1}{2}} V_i \tag{7.49}$$

where

$$B_1 = \begin{bmatrix} [b^*_{1;nm,pq}(0)] & [b^*_{1;nm,pq}(90)] \\ [d^*_{1;nm,pq}(0)] & [d^*_{1;nm,pq}(90)] \end{bmatrix} \tag{7.50}$$

and

$$V_i = \begin{bmatrix} A_1(0) & A_1(90) \\ A_2(0) & A_2(90) \end{bmatrix} \tag{7.51}$$

Here the vectors A_1 and A_2 are defined in equation (7.44). In these definitions the "0" and "90" refer to the quantities corresponding to an incident field having polarization angle $\delta = 0^\circ$ and $\delta = 90^\circ$

respectively. Also, since

$$E^i = \cos\delta \qquad \text{and} \qquad F^i = \sin\delta \ ,$$

then

$$A_1(0) = I, \quad A_2(0) = 0, \quad A_1(90) = 0 \quad \text{and} \quad A_2(90) = I$$

and hence $V_i = J$.

Here J has been defined in section 7.2.2. Thus equation (7.38) may be written

$$S_1 = - J + 2\chi^{\frac{1}{2}} L B_1 \tag{7.52}$$

where $S_1 = \left[\, [V_1(0)] \quad [V_1(90)] \, \right]$

or $$S_1 = - J + 2\chi^{\frac{1}{2}} L (L^H \chi L + iD_e)^{-1} L^H \chi^{\frac{1}{2}} \ . \tag{7.53}$$

The set of linear equations (7.49) is solved numerically and equation (7.52) is then used to reconstruct the scattering matrix elements. This process must be followed for fields incident in each channel (p,q).

The y-antisymmetric problem is solved in an analogous manner, but in equations (7.32) to (7.53) the subscript "1" is replaced by the subscript "2", "tan" is replaced by "-cot" and D_e is replaced by D_o. Also the following definitions are made

$$S_{2E}(RS,pq) = E_{RS,pq} - \hat{E}_{RS,pq} \tag{7.54}$$

$$S_{2F}(RS,pq) = F_{RS,pq} - \hat{F}_{RS,pq} \tag{7.55}$$

Then for the y-antisymmetric problem, the system of equations (7.49) is written

$$(L^H \chi L + iD_o) B_2 = L^H \chi^{\frac{1}{2}} V_i \tag{7.56}$$

while the reconstruction equation is

$$S_2 = -J + \chi^{\frac{1}{2}} L B_2$$

$$= -J + 2\chi^{\frac{1}{2}} L (L^H \chi L + iD_o)^{-1} L^H \chi^{\frac{1}{2}} \quad . \qquad (7.57)$$

In these equations, it is noted, that the matrices S_1 and S_2 are related to the scattering matrices ρ_1 and τ_1 introduced in section 7.2.1, as follows

$$S_1 = \rho_1 + \tau_1 \qquad (7.58)$$

$$S_2 = \rho_1 - \tau_1 \qquad (7.59)$$

Thus, the response of each grid element to waves incident in each channel (p,q) has been determined and the scattering matrices ρ_1 and τ_1 have been characterised. This analysis, together with the multiple scattering formalism presented in section 7.2.2, enables the diffraction properties of a multi-element, rectangular-holed inductive grid to be obtained.

7.3 CONSTRAINTS ON THE SCATTERING MATRICES OF THE SINGLE GRID ELEMENTS

In this section, the properties constraining the scattering matrices of the inductive grid element considered in section 7.2.3 will be derived. These properties, which provide constraints on all elements of the scattering matrices, are used to check the numerical implementation of the single element grid formalism.

The conservation relation constraining the scattering matrices of the single rectangular-holed inductive grid may be written

$$S^{\dagger} J_r S = J_r - i J_e S + i S^{\dagger} J_e \tag{7.60}$$

where S denotes the scattering matrices S_1 or S_2 introduced in section 7.2.3, J_r and J_e are partitioned matrices defined by

$$J_r = \begin{bmatrix} I_r & 0 \\ 0 & I_r \end{bmatrix} , \tag{7.61}$$

$$J_e = \begin{bmatrix} I_e & 0 \\ 0 & -I_e \end{bmatrix} , \tag{7.62}$$

$$(I_r)_{rs,pq} = \varepsilon_{rs} \delta_{rs,pq} ,$$

$$(I_e)_{rs,pq} = (1 - \varepsilon_{rs}) \delta_{rs,pq} ,$$

and

$$\varepsilon_{rs} = 1 \quad \text{if} \quad \beta_{rs}^2 \geq 0$$

$$= 0 \quad \text{if} \quad \beta_{rs}^2 < 0 .$$

It should be noted that $J \neq J_r + J_e$.

Equation (7.60) is the analogous relation to equation (5.41) given in section 5.2.4.1, which constrains the scattering matrices of an up-down symmetric, lossless, singly periodic element. The similarities between these equations is obvious. However, it is to be noted that J_e takes a different form for the conservation relation applying to the grid. The negative sign is introduced to take into account the differing scaling factors, $\sqrt{\frac{k}{\beta_{rs}}}$ and $\sqrt{\frac{\beta_{rs}}{k}}$, multiplying the TE and TM amplitudes, respectively.

As discussed in section 5.2.4.2, by pre-multiplying and post-

multiplying equation (7.60) by the matrices J_r or J_e, a series of relations constraining both the propagating and evanescent orders is derived. In particular, the following relation can be obtained

$$J_r S^H J_r S J_r = J_r \tag{7.63}$$

since $J_r J_r = J_r$ and $J_r J_e = J_e J_r = 0$.

Equation (7.63) ensures the unitarity of the submatrix of the scattering matrix S, containing the elements of S corresponding to the diffracted propagating waves produced by waves incident in the propagating order channels.

Equation (7.60) is now derived for the scattering matrix S_1 defined by equation (7.53) which is rewritten

$$S_1 = -J + 2\chi^{\frac{1}{2}} U \chi^{\frac{1}{2}} \tag{7.64}$$

where

$$U = L Q^{-1} L^H \tag{7.65}$$

and

$$Q = L^H \chi L + iD_e \quad . \tag{7.66}$$

Consider

$$\begin{aligned} S_1^H J_r S_1 &= (-J + 2\chi^{\frac{1}{2}} U \chi^{\frac{1}{2}})^H J_r (-J + 2\chi^{\frac{1}{2}} U \chi^{\frac{1}{2}}) \\ &= 4(\bar{\chi})^{\frac{1}{2}} U^H (\bar{\chi})^{\frac{1}{2}} J_r \chi^{\frac{1}{2}} U \chi^{\frac{1}{2}} - 2(\bar{\chi})^{\frac{1}{2}} U^H (\bar{\chi})^{\frac{1}{2}} J_r \\ &\quad - 2 J_r \chi^{\frac{1}{2}} U \chi^{\frac{1}{2}} + J_r \\ &= 4(\bar{\chi})^{\frac{1}{2}} L (Q^{-1})^H L^H (\bar{\chi})^{\frac{1}{2}} J_r \chi^{\frac{1}{2}} L Q^{-1} L^H \chi^{\frac{1}{2}} \\ &\quad - 2(\bar{\chi})^{\frac{1}{2}} L (Q^{-1})^H L^H (\bar{\chi})^{\frac{1}{2}} J_r - 2 J_r \chi^{\frac{1}{2}} L Q^{-1} L^H \chi^{\frac{1}{2}} + J_r \end{aligned} \tag{7.67}$$

In order to simplify this equation, it is necessary to show that

$$Q + Q^H = 2L^H J_r \chi J_r L \tag{7.68}$$

Using equation (7.66),

$$Q + Q^H = L^H \chi L + iD_e + L^H \bar{\chi} L - i\bar{D}_e$$

$$= L^H (\chi + \bar{\chi}) L \quad , \tag{7.69}$$

since D_e is purely real.

The matrix

$$(\chi + \bar{\chi}) = \begin{bmatrix} \beta + \bar{\beta} & 0 \\ 0 & \beta^{-1} + (\bar{\beta})^{-1} \end{bmatrix}$$

is now evaluated, where β is the diagonal matrix defined by equation (7.43).

$$\beta + \bar{\beta} = \sum_{(r,s)\in\Omega_r} \beta_{rs}/k + i \sum_{(r,s)\in\Omega_e} |\beta_{rs}|/k$$

$$+ \sum_{(r,s)\in\Omega_r} \beta_{rs}/k - i \sum_{(r,s)\in\Omega_e} |\beta_{rs}|/k$$

where $\Omega_r = \{(r,s) \mid \beta_{rs}^2 \geq 0 \}$

and $\Omega_e = \{(r,s) \mid \beta_{rs}^2 < 0 \}$.

Then $$\beta + \bar{\beta} = 2 \sum_{(r,s)\in\Omega_r} \beta_{rs}/k \quad .$$

Similarly,

$$\beta^{-1} + (\bar{\beta})^{-1} = 2 \sum_{(r,s)\in\Omega_r} k/\beta_{rs} \quad .$$

Hence, the proposition (7.68) is established.

Then equation (7.67) is written

$$S_1^H J_r S_1 = 2(\bar{\chi})^{\frac{1}{2}} L(Q^{-1})^H (Q+Q^H) Q^{-1} L^H \chi^{\frac{1}{2}} - 2(\bar{\chi})^{\frac{1}{2}} L(Q^{-1})^H L^H (\bar{\chi})^{\frac{1}{2}} J_r$$

$$- 2J_r \chi^{\frac{1}{2}} L Q^{-1} L^H \chi^{\frac{1}{2}} + J_r$$

$$= 2(\bar{\chi})^{\frac{1}{2}} L(Q^{-1})^H L^H (\chi^{\frac{1}{2}} - (\bar{\chi})^{\frac{1}{2}} J_r) + 2((\bar{\chi})^{\frac{1}{2}} - J_r \chi^{\frac{1}{2}}) L Q^{-1} L^H \chi^{\frac{1}{2}} + J_r . \qquad (7.70)$$

By noting that

$$(\bar{\beta})^{\frac{1}{2}} I_e = -i\beta^{\frac{1}{2}} I_e \quad ,$$

it follows that

$$\chi^{\frac{1}{2}} - (\bar{\chi})^{\frac{1}{2}} J_r = i(\bar{\chi})^{\frac{1}{2}} J_e$$

and

$$(\bar{\chi})^{\frac{1}{2}} - J_r \chi^{\frac{1}{2}} = - iJ_e \chi^{\frac{1}{2}} \quad .$$

Hence equation (7.70) becomes

$$S_1^H J_r S_1 = 2i(\bar{\chi})^{\frac{1}{2}} U^H (\bar{\chi})^{\frac{1}{2}} J_e - 2iJ_e \chi^{\frac{1}{2}} U \chi^{\frac{1}{2}} + J_r$$

$$= J_r - iJ_e S_1 + iS_1^H J_e$$

confirming equation (7.60) analytically for the scattering matrix S_1. The same result may be similarly derived for the scattering matrix S_2 defined by equation (7.57).

Thus a new relation has been derived constraining both the propagating and evanescent waves diffracted by the single inductive grid when waves are incident in either the propagating or evanescent order channels. The conservation relation therefore provides a thorough means of testing the numerical implementation of the grid formalism presented

in section 7.2.3.

Confirmation of the conservation properties was obtained from the numerical solution of this grid problem and sample results are presented in table 7.1. The numerical calculations have also demonstrated that the scattering matrices of the inductive grid element are symmetric. This property is a consequence of both the left-right symmetry of the element and reciprocity. It should be possible to show that the scattering matrices of this structure are analytically constrained to be symmetric as demonstrated for the single lamellar grating in section 5.2.4.4. This will be the subject of future investigation.

7.4 CONSTRAINTS ON THE SCATTERING MATRICES OF THE MULTI-ELEMENT GRID

The process of mathematical induction is used in this section to establish the conservation properties of the scattering matrices of an evenly spaced ($t_n = t$ for all n) multi-element grid, whose elements are rectangular-holed inductive grids. These derivations are very similar to those given in section 5.2.5.

Since $S_1 = \rho + \tau$, the conservation relation (7.60) may be rewritten in terms of the following two equations

$$A_1^H J_r A_1 = J_r - iP^H J_e A_1 + iA_1^H J_e P$$

and

$$B_1^H J_r B_1 = - iP^H J_e B_1 + iB_1^H J_e P$$

where the definitions of A_k and B_k given in equations (7.17) and (7.18) have also been recalled. The relations to be established by induction can thus be written

$$A_k^H J_r A_k = J_r - iP^H J_e A_k + iA_k^H J_e P \tag{7.71}$$

and

1 1-1.43514E-01 3.69306E-01	2 1 6.96534E-02 1.21609E-02	3 1 1.71809E-01-5.13215E-02	4 1 6.96534E-02 1.21609E-02
1 2 6.96534E-02 1.21609E-02	2 2-6.13647E-01-4.23203E-01	3 2 6.96534E-02 1.21609E-02	4 2-2.49749E-02 1.21463E-02
1 3 1.71809E-01-5.13215E-02	2 3 6.96534E-02 1.21609E-02	3 3-1.43514E-01 3.69306E-01	4 3 1.38955E-01-6.63427E-02
1 4 6.96534E-02 1.21609E-02	2 4-2.49749E-02 1.21463E-02	3 4 1.38955E-01-6.63427E-02	4 4-5.13647E-01-4.23203E-01
1 5 1.19630E-01-1.35515E-01	2 5-5.61452E-01-1.57937E-01	3 5 1.19630E-01-1.35515E-01	4 5 1.81780E-14 4.69715E-13
1 6 1.38955E-01-6.63427E-02	2 6-2.49749E-02 1.21463E-02	3 6 6.96534E-02 1.21609E-02	4 6 1.76964E-01-4.94696E-01
1 7 1.71809E-01-5.13215E-02	2 7 1.38955E-01-6.63427E-02	3 7-4.84571E-01-1.74440E-01	4 7 6.96534E-02 1.21609E-02
1 8 1.38955E-01-6.63427E-02	2 8 1.76964E-01-4.94696E-01	3 8 1.38955E-01-6.63427E-02	4 8-2.49749E-02 1.21463E-02
1 9-4.84571E-01-1.74440E-01	2 9 1.38955E-01-6.63427E-02	3 9 1.71809E-01-5.13215E-02	4 9 1.38955E-01-6.63427E-02
1 10-1.58056E-12 2.29756E-12	2 10 3.02077E-02 1.88071E-01	3 10 4.15414E-01-4.73377E-01	4 10-3.02077E-02-1.88071E-01
1 11 2.81621E-01-1.93234E-01	2 11-1.05543E-11-7.14705E-12	3 11-2.81621E-01 1.93234E-01	4 11 1.17653E-01 1.59734E-03
1 12-4.15414E-01 4.73377E-01	2 12-3.02077E-02-1.88071E-01	3 12-2.91532E-12 9.25485E-12	4 12 1.56544E-02 3.98795E-02
1 13-2.81621E-01 1.93234E-01	2 13-1.17653E-01-1.59734E-03	3 13 1.71918E-02 4.37788E-01	4 13-1.03362E-11-7.24490E-12
1 14 1.19630E-01-1.35515E-01	2 14-6.17161E-12-2.75095E-12	3 14-1.19630E-01 1.35515E-01	4 14-3.61452E-01-1.57937E-01
1 15-1.71918E-02-4.37788E-01	2 15 1.17653E-01 1.59734E-03	3 15 2.81621E-01-1.93234E-01	4 15 2.71230E-12-8.69826E-12
1 16 4.15414E-01-4.73377E-01	2 16-1.56544E-02-3.98795E-02	3 16-9.34539E-12-3.75537E-12	4 16 3.02077E-02 1.88071E-01
1 17 1.71918E-02 4.37788E-01	2 17 2.82332E-12-8.43599E-12	3 17-1.71918E-02-4.37788E-01	4 17-1.17653E-01-1.59734E-03
1 18-8.71067E-12 1.92705E-12	2 18 1.56544E-02 3.98795E-02	3 18-4.15414E-01 4.73377E-01	4 18-1.56544E-02-3.98795E-02

5 1 1.19630E-01-1.35515E-01	6 1 1.38955E-01-6.63427E-02	7 1 1.71809E-01-5.13215E-02	8 1 1.38955E-01-6.63427E-02
5 2-3.61452E-01-1.57937E-01	6 2-2.49749E-02 1.21463E-02	7 2 1.38955E-01-6.63427E-02	8 2 1.76964E-01-4.94696E-01
5 3 1.19630E-01-1.35515E-01	6 3 6.96534E-02 1.21609E-02	7 3-4.84571E-01-1.74440E-01	8 3 1.38955E-01-6.63427E-02
5 4 1.47372E-13 3.35082E-13	6 4 1.76964E-01-4.94696E-01	7 4 6.96534E-02 1.21609E-02	8 4-2.49749E-02 1.21463E-02
5 5 2.47897E-01 5.45269E-01	6 5 5.65423E-14 4.26086E-13	7 5-1.19630E-01 1.35515E-01	8 5 3.61452E-01 1.57937E-01
5 6 1.85564E-13 3.62544E-13	6 6-6.13647E-01-4.23203E-01	7 6 1.38955E-01-6.63427E-02	8 6-2.49749E-02 1.21463E-02
5 7-1.19632E-01 1.35515E-01	6 7 1.38955E-01-6.63427E-02	7 7-1.43514E-01 3.69989E-01	8 7 6.96534E-02 1.21609E-02
5 8 3.61452E-01 1.57937E-01	6 8-2.49749E-02 1.21463E-02	7 8 6.96534E-02 1.21609E-02	8 8-6.13647E-01-4.23203E-01
5 9-1.19630E-01 1.35515E-01	6 9 6.96534E-02 1.21609E-02	7 9 1.71809E-01-5.13215E-02	8 9 5.96534E-02 1.21609E-02
5 10-2.51224E-02-2.55811E-01	6 10-1.56544E-02-3.98795E-02	7 10-4.15414E-01 4.73377E-01	8 10 1.56544E-02 3.98795E-02
5 11-6.35813E-12-2.68971E-12	6 11-1.17653E-01-1.59734E-03	7 11-1.71918E-02-4.37788E-01	8 11 2.88236E-12-6.72520E-12
5 12 2.51224E-02 2.55811E-01	6 12 3.02077E-02 1.88071E-01	7 12-8.37229E-12-3.47809E-12	8 12-1.56544E-02-3.98795E-02
5 13 4.86192E-01 5.51473E-03	6 13 3.02947E-12-8.92275E-12	7 13 2.81621E-01-1.93234E-01	8 13 1.17653E-01 1.59734E-03
5 14 4.38879E-12 9.38169E-12	6 14 3.61452E-01 1.57937E-01	7 14 1.19634E-01-1.35515E-01	8 14 5.23930E-12 2.64385E-12
5 15-4.86192E-01-5.51473E-03	6 15-1.26118E-11-6.60119E-12	7 15 1.71910E-02 4.37788E-01	8 15-1.17653E-01-1.59734E-03
5 16-2.51224E-02-2.55811E-01	6 16 1.56544E-02 3.98795E-02	7 16-2.43366E-12 9.75219E-12	8 16-3.02077E-02-1.88071E-01
5 17 6.37492E-12 2.72993E-12	6 17 1.17653E-01 1.59734E-03	7 17-2.81621E-01 1.93234E-01	8 17-1.05996E-11-6.85455E-12
5 18 2.51224E-02 2.55811E-01	6 18-3.02077E-02-1.88071E-01	7 18 4.15414E-01-4.73377E-01	8 18 3.02077E-02 1.88071E-01

9 1-4.84571E-01-1.74440E-01	10 1 2.77520E-12-5.65005E-12	11 1 2.81621E-01-1.93234E-01	12 1-4.15414E-01 4.73377E-01
9 2 1.38955E-01-6.63427E-02	10 2 3.02077E-02 1.88071E-01	11 2-5.87717E-14-2.97224E-13	12 2-3.02077E-02-1.88071E-01
9 3 1.71809E-01-5.13215E-02	10 3 4.15414E-01-4.73377E-01	11 3-2.81621E-01 1.93234E-01	12 3-2.75263E-12-3.73169E-12
9 4 1.38955E-01-6.63427E-02	10 4-3.02077E-02-1.88071E-01	11 4 1.17653E-01 1.59734E-03	12 4 1.56544E-02 3.98795E-02
9 5-1.19630E-01 1.35515E-01	10 5-2.51224E-02-2.55811E-01	11 5-1.64392E-13 2.74205E-14	12 5 2.51224E-02 2.55811E-01
9 6 6.96534E-02 1.21609E-02	10 6-1.56544E-02-3.98795E-02	11 6-1.17653E-01-1.59734E-03	12 6 3.02077E-02 1.88071E-01
9 7 1.71809E-01-5.13215E-02	10 7-4.15414E-01 4.73377E-01	11 7-1.71918E-02-4.37788E-01	12 7 2.13167E-12-2.84345E-12
9 8 6.96534E-02 1.21609E-02	10 8 1.56544E-02 3.98795E-02	11 8-1.46804E-13-2.81320E-13	12 8-1.56544E-02-3.98795E-02
9 9-1.43514E-01 3.69989E-01	10 9-1.32587E-12 2.34291E-12	11 9 1.71918E-02 4.37788E-01	12 9 4.15414E-01-4.73377E-01
9 10-8.40217E-12 1.66544E-12	10 10-8.56734E-01-7.94785E-01	11 10 7.11686E-01 7.95620E-02	12 10-1.76892E-01-5.46576E-02
9 11 1.71918E-02 4.37788E-01	10 11 7.11686E-01 7.95622E-02	11 11 1.94773E-01 4.28645E-01	12 11 7.11686E-01 7.95622E-02
9 12 4.15414E-01-4.73377E-01	10 12-1.76892E-01-5.46576E-02	11 12 7.11686E-01 7.95620E-02	12 12-8.66734E-01-7.94785E-01
9 13-1.19632E-01 1.35515E-01	10 13 2.51224E-02 2.55811E-01	11 13-4.86192E-01-5.51473E-03	12 13 2.51224E-02 2.55811E-01
9 14-2.81621E-01 1.93234E-01	10 14 2.51224E-02 2.55811E-01	11 14-4.86192E-01-5.51473E-03	12 14 2.51224E-02 2.55811E-01
9 15 2.81621E-01 1.93234E-01	10 15-3.42986E-01-2.45212E-01	11 15-5.81517E-02 2.15459E-01	12 15 7.11686E-01 7.95622E-02
9 16-4.15414E-01 4.73377E-01	10 16-1.76892E-01-5.46576E-02	11 16-3.42986E-01-2.45212E-01	12 16 3.44685E-01 5.77340E-01
9 17 2.81621E-01-1.93234E-01	10 17-3.42986E-01-2.45212E-01	11 17 6.69178E-01-1.95468E-01	12 17-3.42986E-01-2.45212E-01
9 18-1.88946E-12 1.81756E-12	10 18 3.44685E-01 5.77340E-01	11 18-3.42986E-01-2.45212E-01	12 18-1.76892E-01-5.46576E-02

13 1-2.81621E-01 1.93234E-01	14 1 1.19630E-01-1.35515E-01	15 1-1.71918E-02-4.37788E-01	16 1-4.15414E-01-4.73377E-01
13 2-1.17653E-01-1.59734E-03	14 2 3.27521E-14-9.35217E-14	15 2 1.17653E-01 1.59734E-03	16 2-1.56544E-02-3.98795E-02
13 3 1.71918E-02 4.37788E-01	14 3-1.19630E-01 1.35515E-01	15 3 2.81621E-01-1.93234E-01	16 3 2.70434E-12-2.86223E-12
13 4 2.13924E-13 5.44284E-13	14 4-3.61452E-01-1.57937E-01	15 4-1.09416E-13 1.28933E-13	16 4 3.02077E-02 1.88071E-01
13 5 4.86192E-01 5.51473E-03	14 5 6.62280E-14 4.53480E-14	15 5-4.86192E-01-5.51473E-03	16 5-2.51224E-02-2.55811E-01
13 6-1.21179E-13-1.82823E-13	14 6 3.61452E-01 1.57937E-01	15 6-1.53369E-13-5.61666E-14	16 6 1.56544E-02 3.98795E-02
13 7 2.81621E-01-1.93234E-01	14 7 1.19632E-01-1.35515E-01	15 7 1.71918E-02 4.37788E-01	16 7-5.58267E-12 3.97776E-12
13 8 1.17653E-01 1.59734E-03	14 8 7.11178E-14-6.72312E-14	15 8-1.17653E-01-1.59734E-03	16 8-3.02077E-02-1.88071E-01
13 9-1.71918E-02-4.37788E-01	14 9-1.19630E-01 1.35515E-01	15 9-2.81621E-01 1.93234E-01	16 9-4.15414E-01 4.73377E-01
13 10 7.11686E-01 7.95622E-02	14 10 2.51224E-02 2.55811E-01	15 10-3.42986E-01-2.45212E-01	16 10-1.76892E-01-5.46576E-02
13 11-5.81517E-02 2.15459E-01	14 11-4.86192E-01-5.51473E-03	15 11-5.81517E-02 2.15459E-01	16 11-3.42986E-01-2.45212E-01
13 12-3.42986E-01-2.45212E-01	14 12 2.51224E-02 2.55811E-01	15 12 7.11686E-01 7.95622E-02	16 12 3.44685E-01 5.77340E-01
13 13 1.94773E-01 4.28645E-01	14 13-6.47286E-12-2.69631E-12	15 13 6.69178E-01-1.95468E-01	16 13 7.11686E-01 7.95622E-02
13 14 6.37363E-12-2.27158E-13	14 14 2.47497E-01 5.45269E-01	15 14-6.87521E-12-4.15634E-13	16 14-2.51224E-02-2.55811E-01
13 15 6.69178E-01-1.95468E-01	14 15 6.54441E-12 2.53265E-12	15 15 1.94773E-01 4.28645E-01	16 15-3.42986E-01-2.45212E-01
13 16 7.11686E-01 7.95622E-02	14 16-2.51224E-02-2.55811E-01	15 16-3.42986E-01-2.45212E-01	16 16-8.66734E-01-7.94785E-01
13 17-5.81517E-02 2.15459E-01	14 17 4.86192E-01 5.51473E-03	15 17-5.81517E-02 2.15459E-01	16 17 7.11686E-01 7.95622E-02
13 18-3.42986E-01-2.45212E-01	14 18-2.51224E-02-2.55811E-01	15 18 7.11686E-01 7.95622E-02	16 18-1.76892E-01-5.46576E-02

17 1 1.71918E-02 4.37788E-01	18 1-2.60177E-12 2.76277E-12		
17 2-2.12344E-13 7.53632E-14	18 2 1.56544E-02 3.98795E-02		
17 3-1.71918E-02-4.37788E-01	18 3-4.15414E-01 4.73377E-01		
17 4-1.17653E-01-1.59734E-03	18 4-1.56544E-02-3.98795E-02		
17 5 1.69168E-13 1.82651E-14	18 5 2.51224E-02 2.55811E-01		
17 6 1.17653E-01 1.59734E-03	18 6-3.02077E-02-1.88071E-01		
17 7-2.81621E-01 1.93234E-01	18 7 4.15414E-01-4.73377E-01		
17 8-1.82754E-13 4.59442E-14	18 8 3.02077E-02 1.88071E-01		
17 9 2.81621E-01-1.93234E-01	18 9 3.52412E-12-5.69729E-12		
17 10-3.42986E-01-2.45212E-01	18 10 3.44685E-01 5.77340E-01		
17 11 6.69178E-01-1.95468E-01	18 11-3.42986E-01-2.45212E-01		
17 12-3.42986E-01-2.45212E-01	18 12-1.76892E-01-5.46576E-02		
17 13-5.81517E-02 2.15459E-01	18 13-3.42986E-01-2.45212E-01		
17 14 4.86192E-01 5.51473E-03	18 14-2.51224E-02-2.55811E-01		
17 15-5.81517E-02 2.15459E-01	18 15 7.11686E-01 7.95620E-02		
17 16 7.11686E-01 7.95620E-02	18 16-1.76892E-01-5.46576E-02		
17 17 1.94773E-01 4.28645E-01	18 17 7.11686E-01 7.95620E-02		
17 18 7.11686E-01 7.95620E-02	18 18-8.66734E-01-7.94785E-01		

Matrix $\rho_1 + \tau_1$

Table 7.1a Confirmation of the symmetry of the single grid scattering matrix $\rho_1 + \tau_1$
Grid parameters: d'/d = 1.0, 2c/d = 2c'/d = 0.8, 2h/d = 0.1
Incidence parameters: $\lambda/d = 0.95$, $\phi = \psi = \delta = 0^o$
The two integers i,j indicate the matrix element (i,j).

1 1	1.00000E+00	0.	2 1	2.80714E-13	0.	3 1	6.69137E-12	0.	4 1	1.23332E-13	0.
1 2	2.80714E-13	0.	2 2	1.00000E+00	0.	3 2	1.50654E-13	0.	4 2	3.09808E-12	0.
1 3	6.69137E-12	0.	2 3	1.50654E-13	0.	3 3	1.00000E+00	0.	4 3	1.72269E-13	0.
1 4	1.23332E-13	0.	2 4	3.09808E-12	0.	3 4	1.72269E-13	0.	4 4	1.00000E+00	0.
1 5	2.55795E-12	0.	2 5	1.41406E-13	0.	3 5	6.43889E-12	0.	4 5	1.96152E-13	0.
1 6	1.72681E-11	0.	2 6	1.52527E-12	0.	3 6	7.41576E-13	0.	4 6	2.27374E-12	0.
1 7	4.13812E-12	0.	2 7	1.74225E-11	0.	3 7	5.43999E-12	0.	4 7	1.42109E-13	0.
1 8	2.60671E-14	0.	2 8	3.58161E-12	0.	3 8	1.71132E-11	0.	4 8	3.58161E-12	0.
1 9	3.51447E-12	0.	2 9	3.42243E-13	0.	3 9	5.50900E-12	0.	4 9	1.68541E-11	0.
1 10	3.33635E-13	0.	2 10	2.59246E-12	0.	3 10	7.60936E-13	0.	4 10	1.38306E-12	0.

---

5 1	2.55795E-12	0.	6 1	1.70681E-11	0.	7 1	4.13812E-12	0.	8 1	2.60671E-14	0.
5 2	1.41406E-13	0.	6 2	1.52527E-12	0.	7 2	1.74225E-11	0.	8 2	3.58161E-12	0.
5 3	6.43889E-12	0.	6 3	7.41576E-13	0.	7 3	5.43999E-12	0.	8 3	1.71132E-11	0.
5 4	1.96152E-13	0.	6 4	2.27374E-12	0.	7 4	1.42109E-13	0.	8 4	3.58161E-12	0.
5 5	1.00000E+00	0.	6 5	2.66348E-13	0.	7 5	3.83998E-12	0.	8 5	5.27361E-14	0.
5 6	2.66348E-13	0.	6 6	1.00000E+00	0.	7 6	1.36424E-12	0.	8 6	8.96037E-12	0.
5 7	3.83998E-12	0.	6 7	1.36424E-12	0.	7 7	1.00000E+00	0.	8 7	5.08423E-13	0.
5 8	5.27361E-14	0.	6 8	8.96037E-12	0.	7 8	5.08423E-13	0.	8 8	1.00000E+00	0.
5 9	4.15104E-12	0.	6 9	3.88536E-12	0.	7 9	1.75329E-11	0.	8 9	4.54747E-13	0.
5 10	1.71275E-11	0.	6 10	1.61435E-11	0.	7 10	3.70138E-12	0.	8 10	7.87974E-12	0.

---

9 1	3.51447E-12	0.	10 1	3.33635E-13	0.
9 2	3.42243E-13	0.	10 2	2.59246E-12	0.
9 3	5.50900E-12	0.	10 3	7.60936E-13	0.
9 4	1.68541E-11	0.	10 4	1.38306E-12	0.
9 5	4.15104E-12	0.	10 5	1.71275E-11	0.
9 6	3.88536E-12	0.	10 6	1.61435E-11	0.
9 7	1.75329E-11	0.	10 7	3.70138E-12	0.
9 8	4.54747E-13	0.	10 8	7.87974E-12	0.
9 9	1.00000E+00	0.	10 9	2.09628E-12	0.
9 10	2.09628E-12	0.	10 10	1.00000E+00	0.

Table 7.1b Confirmation of the conservation property $J_r S^H J_r S J_r = J_r$ for the single grid specified in table 7.1a. Here $S = \rho_1 + \tau_1$.

1 1 1.69138E-11 0.	2 1 2.95709E-12 0.	3 1 5.68434E-12 0.	4 1 1.01685E-12 0.
1 2 2.95709E-12 0.	2 2 9.09495E-13 0.	3 2 1.28449E-12 0.	4 2 2.88714E-13 0.
1 3 5.68434E-12 0.	2 3 1.28449E-12 0.	3 3 9.09495E-12 0.	4 3 2.27374E-12 0.
1 4 1.01685E-12 0.	2 4 2.88714E-13 0.	3 4 2.27374E-12 0.	4 4 7.27596E-12 0.
1 5 5.10959E-12 0.	2 5 6.69137E-12 0.	3 5 5.10959E-12 0.	4 5 1.58654E-13 0.
1 6 3.27923E-12 0.	2 6 1.23332E-13 0.	3 6 1.53819E-12 0.	4 6 3.09808E-12 0.
1 7 8.33876E-12 0.	2 7 2.50111E-12 0.	3 7 1.81899E-12 0.	4 7 1.68073E-12 0.
1 8 2.27374E-12 0.	2 8 2.55795E-12 0.	3 8 2.03369E-12 0.	4 8 1.41406E-13 0.
1 9 3.63798E-12 0.	2 9 2.24536E-12 0.	3 9 8.33876E-12 0.	4 9 3.09262E-12 0.
1 10 1.27640E-11 0.	2 10 2.03369E-12 0.	3 10 5.75215E-12 0.	4 10 9.09495E-13 0.
1 11 1.81899E-12 0.	2 11 1.70681E-11 0.	3 11 3.63798E-12 0.	4 11 1.12527E-12 0.
1 12 9.09495E-12 0.	2 12 2.41702E-12 0.	3 12 9.16968E-12 0.	4 12 2.77545E-12 0.
1 13 8.13477E-12 0.	2 13 4.13812E-12 0.	3 13 2.27374E-13 0.	4 13 1.74225E-11 0.
1 14 4.98669E-12 0.	2 14 2.68671E-14 0.	3 14 4.06738E-12 0.	4 14 3.58161E-12 0.
1 15 4.54747E-13 0.	2 15 3.51447E-12 0.	3 15 4.06738E-12 0.	4 15 3.42243E-13 0.
1 16 1.28622E-11 0.	2 16 4.59835E-12 0.	3 16 1.67810E-11 0.	4 16 3.66629E-12 0.
1 17 4.54747E-12 0.	2 17 3.33635E-13 0.	3 17 4.83403E-12 0.	4 17 2.59246E-12 0.
1 18 9.40827E-12 0.	2 18 3.85054E-12 0.	3 18 2.57244E-12 0.	4 18 3.92508E-12 0.

5 1 5.10959E-12 0.	6 1 3.27923E-12 0.	7 1 8.33876E-12 0.	8 1 2.27374E-12 0.
5 2 6.69137E-12 0.	6 2 1.23332E-13 0.	7 2 2.50111E-12 0.	8 2 2.55795E-12 0.
5 3 5.10959E-12 0.	6 3 1.53819E-12 0.	7 3 1.81899E-12 0.	8 3 2.03369E-12 0.
5 4 1.58654E-13 0.	6 4 3.29808E-12 0.	7 4 1.68073E-12 0.	8 4 1.41406E-13 0.
5 5 1.45519E-11 0.	6 5 1.72269E-13 0.	7 5 4.68743E-12 0.	8 5 6.43889E-12 0.
5 6 1.72269E-13 0.	6 6 7.27596E-12 0.	7 6 4.06738E-12 0.	8 6 1.96152E-13 0.
5 7 4.68743E-12 0.	6 7 4.06738E-12 0.	7 7 1.09139E-11 0.	8 7 1.01685E-12 0.
5 8 6.43889E-12 0.	6 8 1.96152E-13 0.	7 8 1.01685E-12 0.	8 8 9.09495E-12 0.
5 9 4.68743E-12 0.	6 9 1.13829E-12 0.	7 9 6.13909E-12 0.	8 9 9.16573E-13 0.
5 10 7.87974E-12 0.	6 10 3.69261E-12 0.	7 10 1.81899E-12 0.	8 10 3.09262E-12 0.
5 11 7.41576E-13 0.	6 11 2.27374E-12 0.	7 11 3.86535E-12 0.	8 11 2.66348E-13 0.
5 12 9.23316E-12 0.	6 12 3.74994E-12 0.	7 12 1.72819E-11 0.	8 12 4.79645E-12 0.
5 13 5.43999E-12 0.	6 13 1.42109E-13 0.	7 13 4.06738E-12 0.	8 13 3.63998E-12 0.
5 14 1.71132E-11 0.	6 14 3.58161E-12 0.	7 14 3.66629E-12 0.	8 14 5.27361E-14 0.
5 15 5.50900E-12 0.	6 15 1.68541E-11 0.	7 15 4.06738E-12 0.	8 15 4.15184E-12 0.
5 16 9.27506E-12 0.	6 16 2.65161E-12 0.	7 16 1.05398E-11 0.	8 16 1.13687E-12 0.
5 17 7.60936E-13 0.	6 17 1.38306E-12 0.	7 17 5.75215E-12 0.	8 17 1.71275E-11 0.
5 18 8.21382E-12 0.	6 18 1.36424E-12 0.	7 18 7.49989E-12 0.	8 18 1.87497E-12 0.

9 1 3.63798E-12 0.	10 1 1.27640E-11 0.	11 1 1.81899E-12 0.	12 1 9.13477E-12 0.
9 2 2.84636E-12 0.	10 2 2.83369E-12 0.	11 2 1.76681E-11 0.	12 2 2.41702E-12 0.
9 3 8.33876E-12 0.	10 3 5.75215E-12 0.	11 3 3.63798E-12 0.	12 3 9.16968E-12 0.
9 4 3.09262E-12 0.	10 4 9.09495E-13 0.	11 4 1.52527E-12 0.	12 4 2.77545E-12 0.
9 5 4.68743E-12 0.	10 5 7.87974E-12 0.	11 5 7.41576E-13 0.	12 5 9.23316E-12 0.
9 6 1.13829E-12 0.	10 6 3.69261E-12 0.	11 6 2.27374E-12 0.	12 6 3.74994E-12 0.
9 7 6.13909E-12 0.	10 7 1.81899E-12 0.	11 7 3.86535E-12 0.	12 7 1.72819E-11 0.
9 8 9.16573E-13 0.	10 8 3.09262E-12 0.	11 8 2.66348E-13 0.	12 8 4.79645E-12 0.
9 9 1.27329E-11 0.	10 9 1.65583E-11 0.	11 9 7.85345E-12 0.	12 9 9.27506E-12 0.
9 10 1.65583E-11 0.	10 10 3.63798E-12 0.	11 10 1.21533E-11 0.	12 10 1.99468E-11 0.
9 11 7.85345E-12 0.	10 11 1.21533E-11 0.	11 11 1.45519E-11 0.	12 11 1.29762E-11 0.
9 12 9.27526E-12 0.	10 12 1.99468E-11 0.	11 12 1.29762E-11 0.	12 12 3.63798E-12 0.
9 13 3.86535E-12 0.	10 13 7.40275E-12 0.	11 13 1.36424E-12 0.	12 13 2.00914E-11 0.
9 14 4.29008E-12 0.	10 14 2.27374E-12 0.	11 14 8.96037E-12 0.	12 14 1.01303E-11 0.
9 15 5.14488E-12 0.	10 15 4.06738E-12 0.	11 15 3.86536E-12 0.	12 15 3.18323E-12 0.
9 16 7.71732E-12 0.	10 16 2.33122E-11 0.	11 16 5.75215E-12 0.	12 16 1.81899E-12 0.
9 17 2.57244E-12 0.	10 17 2.57244E-11 0.	11 17 1.61435E-11 0.	12 17 6.55846E-12 0.
9 18 1.59598E-11 0.	10 18 1.28622E-11 0.	11 18 2.30086E-11 0.	12 18 2.64380E-11 0.

13 1 8.13477E-12 0.	14 1 4.98669E-12 0.	15 1 4.54747E-13 0.	16 1 1.28522E-11 0.
13 2 4.13812E-12 0.	14 2 2.68671E-14 0.	15 2 3.51447E-12 0.	16 2 4.59835E-12 0.
13 3 2.27374E-13 0.	14 3 4.06738E-12 0.	15 3 4.06738E-12 0.	16 3 1.67810E-11 0.
13 4 1.74225E-11 0.	14 4 3.58161E-12 0.	15 4 3.42243E-13 0.	16 4 3.66629E-12 0.
13 5 5.43999E-12 0.	14 5 1.71132E-11 0.	15 5 5.50900E-12 0.	16 5 9.27506E-12 0.
13 6 1.42129E-13 0.	14 6 3.58161E-12 0.	15 6 1.68541E-11 0.	16 6 2.65161E-12 0.
13 7 4.06738E-12 0.	14 7 3.66629E-12 0.	15 7 4.06738E-12 0.	16 7 1.05398E-11 0.
13 8 3.63998E-12 0.	14 8 5.27361E-14 0.	15 8 4.15184E-12 0.	16 8 1.13687E-12 0.
13 9 3.86535E-12 0.	14 9 4.29008E-12 0.	15 9 5.14488E-12 0.	16 9 7.71732E-12 0.
13 10 7.40275E-12 0.	14 10 2.27374E-12 0.	15 10 4.06738E-12 0.	16 10 2.33122E-11 0.
13 11 1.36424E-12 0.	14 11 8.96037E-12 0.	15 11 3.86536E-12 0.	16 11 5.75215E-12 0.
13 12 2.00914E-11 0.	14 12 1.01303E-11 0.	15 12 3.18323E-12 0.	16 12 1.81899E-12 0.
13 13 1.45519E-11 0.	14 13 5.08423E-13 0.	15 13 1.75329E-11 0.	16 13 2.27374E-13 0.
13 14 5.08423E-13 0.	14 14 9.09495E-12 0.	15 14 4.54747E-13 0.	16 14 9.97339E-12 0.
13 15 1.75329E-11 0.	14 15 4.54747E-13 0.	15 15 1.45519E-11 0.	16 15 1.81899E-11 0.
13 16 2.27374E-13 0.	14 16 9.97339E-12 0.	15 16 1.81899E-11 0.	16 16 3.63798E-12 0.
13 17 3.70138E-12 0.	14 17 7.87974E-12 0.	15 17 2.89528E-12 0.	16 17 1.48491E-11 0.
13 18 5.75215E-12 0.	14 18 3.97091E-12 0.	15 18 9.09495E-12 0.	16 18 1.92718E-11 0.

17 1 4.54747E-12 0.	18 1 9.40827E-12 0.	
17 2 3.33635E-13 0.	18 2 3.85054E-12 0.	
17 3 4.83403E-12 0.	18 3 2.57244E-12 0.	
17 4 2.59245E-12 0.	18 4 3.92508E-12 0.	
17 5 7.60936E-13 0.	18 5 8.21382E-12 0.	
17 6 1.38306E-12 0.	18 6 1.36424E-12 0.	
17 7 5.75215E-12 0.	18 7 7.49989E-12 0.	
17 8 1.71275E-11 0.	18 8 1.87497E-12 0.	
17 9 2.57244E-12 0.	18 9 1.59598E-11 0.	
17 10 2.57244E-11 0.	18 10 1.28622E-11 0.	
17 11 1.61435E-11 0.	18 11 2.30086E-11 0.	
17 12 6.55846E-12 0.	18 12 2.64380E-11 0.	
17 13 3.70138E-12 0.	18 13 5.75215E-12 0.	
17 14 7.87974E-12 0.	18 14 3.97091E-12 0.	
17 15 2.89628E-12 0.	18 15 9.09495E-12 0.	
17 16 1.48491E-11 0.	18 16 1.92718E-11 0.	
17 17 1.45519E-11 0.	18 17 1.15043E-11 0.	
17 18 1.15043E-11 0.	18 18 1.81899E-11 0.	

Table 7.1c Confirmation of the conservation property $S^H J_r S + i J_e S - i S^H J_e - J_r = 0$ for the single grid specified in table 7.1a. Here $S = \rho_1 + \tau_1$.

$$B_k^H J_r B_k = - iP^H J_e B_k + iB_k^H J_e P \tag{7.72}$$

Again, as in section 5.2.5.1, it is necessary to introduce alternate expressions for equations (7.15) and (7.16) in order to establish the proposition (7.72) for all k. By considering the $(n+1)$-element grid as being composed of an n-element grid above the remaining element, the following equations are derived according to section 7.2.2.

$$A_{n+1} = A_n + B_n A_1 (J - A_n A_1)^{-1} B_n \tag{7.73}$$

and

$$B_{n+1} = B_1 (J - A_n A_1)^{-1} B_n \tag{7.74}$$

Equations (7.71) and (7.72) have been shown to hold for $k = 1$. If it is assumed that they are satisfied for $k = n$, then the proof that these relations hold for $k = n+1$ follows exactly that given in section 5.2.5.1, where I_r, I_e and I are now replaced by J_r, J_e and J respectively. It should be noted that this direct comparison is possible since nowhere in the proof is the relation $J_r + J_e = J$ (which is the generalised expression of $I_r + I_e = I$) used. From the definitions of J_r and J_e it is obvious that this relation does not hold.

Thus the multi-element grid has been shown to possess the same conservation properties as the individual elements composing it. These results have been numerically confirmed using the computer program describing the diffraction properties of a perfectly-conducting, rectangular-holed, multi-element inductive grid and a sample result is given in table 7.2.

7.5 NUMERICAL INVESTIGATION OF THE FILTERING CHARACTERISTICS OF THE MULTI-ELEMENT INDUCTIVE GRID

The long wavelength filtering characteristics of the multi-element

1 1	1-4.621844E-01 1.700441E-01	2 1	9.749062E-02-1.725421E-02	3 1	9.833944E-02-2.719256E-02	4 1	9.749062E-02-1.725421E-02
1 2	8.749062E-02-1.725421E-02	2 2	-6.563666E-01-4.630785E-01	3 2	9.749062E-02-1.725421E-02	4 2	-6.563666E-01-4.630785E-01
1 3	9.833944E-02-2.719256E-02	2 3	9.749062E-02-1.725421E-02	3 3	-4.621844E-01 1.700441E-01	4 3	9.833944E-02-2.719256E-02
1 4	9.749062E-02-1.725421E-02	2 4	-6.563666E-01-4.630785E-01	3 4	1.355639E-01-3.861955E-01	4 4	-6.563666E-01-4.630785E-01
1 5	1.355639E-01-3.861955E-01	2 5	-1.402566E-03 2.447055E-05	3 5	1.355639E-01-3.861955E-01	4 5	-1.402566E-03 2.447055E-05
1 6	1.355639E-01-3.861955E-01	2 6	-6.563666E-01-4.630785E-01	3 6	9.749062E-02-1.725421E-02	4 6	9.749062E-02-1.725421E-02
1 7	9.833944E-02-2.719256E-02	2 7	1.355639E-01-3.861955E-01	3 7	-1.979066E-01-3.591566E-02	4 7	9.749062E-02-1.725421E-02
1 8	1.355639E-01-3.861955E-01	2 8	9.749062E-02-1.725421E-02	3 8	1.355639E-01-3.861955E-01	4 8	-6.563666E-01-4.630785E-01
1 9	-1.979066E-01-3.591566E-02	2 9	1.355639E-01-3.861955E-01	3 9	9.833944E-02-2.719256E-02	4 9	1.355639E-01-3.861955E-01
1 10	-7.333733E-12 1.990336E-13	2 10	2.745987E-02 1.476384E-01	3 10	1.658961E-01-2.162465E-01	4 10	2.745987E-02-1.476384E-01
1 11	2.773287E-01-1.698883E-01	2 11	-1.446347E-11-3.416125E-12	3 11	-2.773287E-01 1.698883E-01	4 11	-4.482305E-03-2.023605E-02
1 12	-1.658911E-01 2.162465E-01	2 12	-2.745987E-02-1.476384E-01	3 12	-8.514921E-12 4.971536E-12	4 12	-1.146405E-02 1.292495E-01
1 13	-2.773287E-01 1.698883E-01	2 13	4.482305E-03 2.023605E-02	3 13	3.288666E-02 2.192291E-01	4 13	-1.288622E-11-2.541168E-12
1 14	1.356394E-02-3.688136E-02	2 14	5.733591E-12 3.917777E-13	3 14	-1.356394E-02 3.688136E-02	4 14	-1.146405E-02 2.447055E-05
1 15	-3.288666E-02-2.192291E-01	2 15	-4.482305E-03-2.023605E-02	3 15	2.773287E-01-1.698883E-01	4 15	4.884044E-12-2.343407E-12
1 16	1.658911E-01-2.162465E-01	2 16	1.146405E-02-1.292495E-01	3 16	-6.641394E-12 4.879485E-13	4 16	2.745987E-02 1.476384E-01
1 17	3.288666E-02 2.192291E-01	2 17	6.752556E-12-2.331156E-13	3 17	-3.288666E-02-2.192291E-01	4 17	4.482305E-03 2.023605E-02
1 18	-2.236254E-13 2.277421E-12	2 18	-1.146405E-02 1.292495E-01	3 18	-1.658911E-01 2.162465E-01	4 18	1.146405E-02-1.292495E-01

5 1	1.356639E-02-3.688136E-02	6 1	1.655354E-01-3.861955E-02	7 1	9.833944E-02-2.719256E-02	8 1	1.655354E-01-3.861955E-02
5 2	-1.487595E-03 2.447055E-05	6 2	-9.922295E-02 3.359666E-02	7 2	1.655354E-01-3.861955E-02	8 2	3.427725E-01-4.630785E-01
5 3	1.356639E-02-3.688136E-02	6 3	9.749062E-02-1.725421E-02	7 3	-1.979066E-01-3.591566E-02	8 3	1.655354E-01-3.861955E-02
5 4	5.325795E-12 9.494136E-13	6 4	3.427727E-01-4.630785E-01	7 4	9.749062E-02-1.725421E-02	8 4	-9.922295E-02 3.359666E-02
5 5	-9.948064E-01-8.448432E-05	6 5	5.166935E-13 8.651860E-13	7 5	-1.356639E-02 3.688136E-02	8 5	1.487595E-03-2.447055E-05
5 6	-5.680208E-12 3.262228E-13	6 6	-6.563666E-01-4.630785E-01	7 6	1.655354E-01-3.861955E-02	8 6	-9.922295E-02 3.359666E-02
5 7	-1.356639E-02 3.688136E-02	6 7	1.655354E-01-3.861955E-02	7 7	-4.621844E-01 1.700441E-01	8 7	9.749062E-02-1.725421E-02
5 8	1.487595E-03-2.447055E-05	6 8	-9.922295E-02 3.359666E-02	7 8	9.749062E-02-1.725421E-02	8 8	-6.563666E-01-4.630785E-01
5 9	-1.356639E-02 3.688136E-02	6 9	9.749062E-02-1.725421E-02	7 9	9.833944E-02-2.719256E-02	8 9	9.749062E-02-1.725421E-02
5 10	-6.718953E-02-3.174437E-02	6 10	1.146405E-02-1.292495E-01	7 10	-1.658911E-01 2.162465E-01	8 10	-1.146405E-02 1.292495E-01
5 11	7.485768E-12-7.972882E-13	6 11	4.482305E-03 2.023605E-02	7 11	-3.288666E-02-2.192291E-01	8 11	6.859868E-12-2.744688E-12
5 12	6.718953E-02 3.174437E-02	6 12	2.745987E-02 1.476384E-01	7 12	-8.976635E-12 4.269208E-13	8 12	1.146405E-02-1.292495E-01
5 13	-1.547495E-02-6.986437E-02	6 13	5.277285E-12-2.750355E-13	7 13	2.773287E-01-1.698831E-01	8 13	-4.482305E-03-2.023605E-02
5 14	-3.627209E-11-5.459167E-13	6 14	1.487595E-03-2.447055E-05	7 14	1.356639E-02-3.688136E-02	8 14	-5.343665E-12 1.642525E-13
5 15	1.547495E-02 6.986437E-02	6 15	-1.291653E-11-2.175508E-12	7 15	3.288666E-02 2.192291E-01	8 15	4.482305E-03 2.023605E-02
5 16	-6.718953E-22-3.174437E-02	6 16	-1.146405E-02 1.292495E-01	7 16	-8.911457E-12 5.098297E-12	8 16	-2.745871E-02-1.476385E-01
5 17	-6.946355E-12 4.547223E-13	6 17	-4.482305E-03-2.023605E-02	7 17	-2.773287E-01 1.698831E-01	8 17	-1.143963E-11-1.954065E-12
5 18	6.718953E-02 3.174437E-02	6 18	-2.745871E-02-1.476385E-01	7 18	1.658911E-01-2.162465E-01	8 18	2.745871E-02 1.476385E-01

9 1	-1.979884E-01-3.591566E-02	10 1	1.207345E-12-4.272777E-12	11 1	2.773287E-01-1.698831E-01	12 1	-1.658911E-01 2.162465E-01
9 2	1.655354E-01-3.861955E-02	10 2	2.745977E-02 1.476384E-01	11 2	5.836626E-13-3.332927E-13	12 2	-2.745871E-02-1.476385E-01
9 3	9.833944E-02-2.719256E-02	10 3	1.658961E-01-2.162465E-01	11 3	-2.773287E-01 1.698831E-01	12 3	-1.363955E-12 1.877197E-12
9 4	1.655354E-01-3.861955E-02	10 4	-2.745987E-02-1.476384E-01	11 4	-4.482305E-03-2.023605E-02	12 4	-1.146405E-02 1.292495E-01
9 5	-1.356639E-02 3.688136E-02	10 5	-5.718933E-02-3.174377E-02	11 5	-2.045277E-12 8.741437E-15	12 5	5.718935E-02 3.174377E-02
9 6	9.749062E-02-1.725421E-02	10 6	1.146405E-02-1.292495E-01	11 6	4.482305E-03 2.023605E-02	12 6	2.745871E-02 1.476385E-01
9 7	9.833944E-02-2.719256E-02	10 7	-1.658911E-01 2.162465E-01	11 7	-3.288666E-02-2.192291E-01	12 7	-2.372677E-12-1.756339E-12
9 8	9.749062E-02-1.725421E-02	10 8	-1.146405E-02 1.292495E-01	11 8	-8.734421E-13-2.242525E-13	12 8	1.146405E-02-1.292495E-01
9 9	-4.621844E-01 1.700441E-01	10 9	2.938557E-12 6.791288E-14	11 9	3.288666E-02 2.192291E-01	12 9	1.658911E-01-2.162465E-01
9 10	-5.346801E-13 2.589211E-12	10 10	-8.164209E-01-3.822663E-01	11 10	4.434365E-01 2.717055E-02	12 10	-1.367535E-01-5.490915E-02
9 11	3.268666E-02 2.192291E-01	10 11	4.434365E-01 2.717055E-02	11 11	-1.235532E-01-4.528841E-02	12 11	4.434365E-01 2.717055E-02
9 12	1.658911E-01-2.162465E-01	10 12	-1.367535E-01-5.490915E-02	11 12	4.434365E-01 2.717055E-02	12 12	-9.164209E-01-3.822663E-01
9 13	-3.288666E-02-2.192291E-01	10 13	4.434365E-01 2.717055E-02	11 13	1.718066E-01 2.201091E-01	12 13	-1.487911E-01-3.432791E-01
9 14	-1.356639E-02 3.688136E-02	10 14	6.718933E-02 3.174377E-22	11 14	1.547495E-02 6.986437E-02	12 14	6.718933E-02 3.174377E-02
9 15	-2.773287E-21 1.698883E-01	10 15	-1.487911E-01-3.432791E-01	11 15	1.718066E-01 2.201091E-01	12 15	4.434365E-01 2.717055E-02
9 16	-1.658911E-01 2.162465E-01	10 16	-1.367535E-01-5.490915E-02	11 16	-1.487911E-01-3.432791E-01	12 16	7.668961E-02 1.186011E-01
9 17	2.773287E-01-1.698831E-01	10 17	-1.487911E-01-3.432791E-01	11 17	7.774533E-01-4.651302E-01	12 17	-1.487911E-01-3.432791E-01
9 18	-7.850268E-12-6.119768E-13	10 18	7.680968E-02 1.186011E-01	11 18	-1.487911E-01-3.432791E-01	12 18	-1.367535E-01-5.490915E-02

13 1	-2.773287E-01 1.698831E-01	14 1	1.356639E-02-3.688136E-02	15 1	-3.288666E-02-2.192291E-01	16 1	1.658911E-01-2.162465E-01
13 2	4.482305E-03 2.023605E-02	14 2	-5.849211E-13 2.568195E-13	15 2	-4.482305E-03-2.023605E-02	16 2	1.146405E-02-1.292495E-01
13 3	3.288666E-02 2.192291E-01	14 3	-1.356639E-02 3.688136E-02	15 3	2.773287E-01-1.698831E-01	16 3	-1.201953E-12-1.363205E-12
13 4	1.594225E-12-2.243795E-13	14 4	-1.487595E-03 2.447055E-05	15 4	-1.721359E-12 3.484447E-14	16 4	2.745871E-02 1.476385E-01
13 5	-1.547495E-02-6.986437E-02	14 5	3.277095E-12 1.299887E-13	15 5	1.547495E-02 6.986437E-02	16 5	-5.718935E-02-3.174377E-02
13 6	-2.098495E-12 3.247935E-13	14 6	1.487595E-03-2.447055E-05	15 6	1.445577E-12 9.855021E-15	16 6	-1.146405E-02 1.292495E-01
13 7	2.773287E-01-1.698831E-01	14 7	1.356639E-02-3.688136E-02	15 7	3.288666E-02 2.192291E-01	16 7	-1.962882E-12 1.568575E-12
13 8	-4.482305E-03-2.023605E-02	14 8	1.309665E-12 5.543975E-13	15 8	4.482305E-03 2.023605E-02	16 8	2.745871E-02-1.476385E-01
13 9	-3.288666E-02-2.192291E-01	14 9	-1.356639E-02 3.688136E-02	15 9	-2.773287E-01 1.698831E-01	16 9	-1.658911E-01 2.162465E-01
13 10	4.434365E-01 2.717055E-02	14 10	5.718933E-02 3.174377E-02	15 10	-1.487911E-01-3.432791E-01	16 10	-1.367535E-01-5.490915E-02
13 11	1.718686E-01 2.201091E-01	14 11	1.547495E-02 6.986437E-02	15 11	1.718066E-01 2.201091E-01	16 11	-1.487911E-01-3.432791E-01
13 12	-1.487911E-01-3.432791E-01	14 12	6.718933E-02 3.174377E-02	15 12	4.434365E-01 2.717055E-02	16 12	7.680961E-02 1.186011E-01
13 13	-1.235532E-01-4.528841E-02	14 13	1.622555E-12-1.254424E-13	15 13	7.774533E-01-4.651302E-01	16 13	4.434365E-01 2.717055E-02
13 14	-7.422435E-12-1.222355E-13	14 14	-9.949464E-01-8.448432E-05	15 14	5.866531E-13 1.081921E-12	16 14	-6.719935E-02-3.174377E-02
13 15	7.774533E-01-4.651302E-01	14 15	-1.528668E-12 4.697898E-13	15 15	-1.235532E-01-4.528841E-02	16 15	-1.487911E-01-3.432791E-01
13 16	4.434365E-01 2.717055E-02	14 16	-6.718935E-02-3.174377E-02	15 16	-1.487911E-01-3.432791E-01	16 16	-9.164209E-01-3.822663E-01
13 17	1.718686E-01 2.201091E-01	14 17	-1.547495E-02-6.986437E-02	15 17	1.718066E-01 2.201091E-01	16 17	4.434365E-01 2.717055E-02
13 18	-1.487911E-01-3.432791E-01	14 18	-6.718935E-02-3.174377E-02	15 18	4.434365E-01 2.717055E-02	16 18	-1.367535E-01-5.490915E-02

17 1	3.288666E-02 2.192291E-01	18 1	1.229027E-12-3.269311E-13				
17 2	6.848424E-14 2.336777E-13	18 2	-1.146405E-02 1.292495E-01				
17 3	-3.288666E-02-2.192291E-01	18 3	-1.658911E-01 2.162465E-01				
17 4	4.482305E-03 2.023605E-02	18 4	1.146405E-02-1.292495E-01				
17 5	-3.805648E-13-1.854258E-13	18 5	6.718935E-02 3.174377E-02				
17 6	-4.482305E-03-2.023605E-02	18 6	-2.745871E-02-1.476385E-01				
17 7	-2.773287E-01 1.698831E-01	18 7	1.658911E-01-2.162465E-01				
17 8	-8.637718E-14 1.736279E-13	18 8	2.745987E-02 1.476384E-01				
17 9	2.773287E-01-1.698831E-01	18 9	2.253933E-12-4.611277E-12				
17 10	-1.487911E-01-3.432791E-01	18 10	7.680961E-02 1.186011E-01				
17 11	7.774533E-01-4.651302E-01	18 11	-1.487911E-01-3.432791E-01				
17 12	-1.487911E-01-3.432791E-01	18 12	-1.367535E-01-5.490915E-02				
17 13	1.718066E-01 2.201091E-01	18 13	-1.487911E-01-3.432791E-01				
17 14	-1.547495E-02-6.986437E-02	18 14	-6.718935E-02-3.174377E-02				
17 15	1.718066E-01 2.201091E-01	18 15	4.434365E-01 2.717055E-02				
17 16	4.434365E-01 2.717055E-02	18 16	-1.367535E-01-5.490915E-02				
17 17	-1.235532E-01-4.528841E-02	18 17	1.434265E-01 2.717055E-02				
17 18	4.434365E-01 2.717055E-02	18 18	-9.164209E-01-3.822663E-01				

Array $\rho_3 + \tau_3$

Table 7.2a Confirmation of the symmetry of the 3-element grid scattering matrix $\rho_3 + \tau_3$. The individual elements are specified in table 7.1a and are separated by $t_1/d=t_2/d=1.0$.

1	1	1.00000E+00	0.	2	1	2.23344E-13	0.	3	1	9.76131E-12	0.	4	1	2.06799E-12	0.
1	2	2.23344E-13	0.	2	2	1.00000E+00	0.	3	2	5.09757E-12	0.	4	2	1.26275E-13	0.
1	3	9.76131E-12	0.	2	3	5.09757E-12	0.	3	3	1.00000E+00	0.	4	3	4.19434E-12	0.
1	4	2.06799E-12	0.	2	4	1.26275E-13	0.	3	4	4.19434E-12	0.	4	4	1.00000E+00	0.
1	5	7.60650E-12	0.	2	5	1.82313E-12	0.	3	5	1.65184E-11	0.	4	5	4.31379E-13	0.
1	6	1.45618E-11	0.	2	6	4.22060E-12	0.	3	6	7.50897E-12	0.	4	6	1.56938E-12	0.
1	7	3.75591E-12	0.	2	7	1.13162E-11	0.	3	7	9.52878E-12	0.	4	7	4.81746E-12	0.
1	8	5.84406E-12	0.	2	8	4.79648E-12	0.	3	8	3.32848E-11	0.	4	8	5.73954E-12	0.
1	9	8.10220E-12	0.	2	9	3.91653E-12	0.	3	9	1.45434E-11	0.	4	9	1.07804E-11	0.
1	10	6.63618E-12	0.	2	10	3.72598E-12	0.	3	10	5.55599E-12	0.	4	10	6.41462E-12	0.

5	1	7.60650E-12	0.	6	1	1.45618E-11	0.	7	1	3.75591E-12	0.	8	1	5.84406E-12	0.
5	2	1.82313E-12	0.	6	2	4.22060E-12	0.	7	2	1.13162E-11	0.	8	2	4.79648E-12	0.
5	3	1.65184E-11	0.	6	3	7.50897E-12	0.	7	3	9.52878E-12	0.	8	3	3.32848E-11	0.
5	4	4.31379E-13	0.	6	4	1.56938E-12	0.	7	4	4.81746E-12	0.	8	4	5.73954E-12	0.
5	5	1.00000E+00	0.	6	5	6.86681E-12	0.	7	5	7.78858E-12	0.	8	5	3.43435E-12	0.
5	6	6.86681E-12	0.	6	6	1.00000E+00	0.	7	6	1.12888E-11	0.	8	6	3.38015E-12	0.
5	7	7.78858E-12	0.	6	7	1.12888E-11	0.	7	7	1.00000E+00	0.	8	7	4.92221E-12	0.
5	8	3.43435E-12	0.	6	8	3.38015E-12	0.	7	8	4.92221E-12	0.	8	8	1.00000E+00	0.
5	9	3.38326E-12	0.	6	9	2.03369E-11	0.	7	9	1.37350E-11	0.	8	9	5.47478E-12	0.
5	10	1.38112E-11	0.	6	10	3.84369E-11	0.	7	10	1.82126E-11	0.	8	10	4.58463E-12	0.

9	1	8.10220E-12	0.	10	1	6.63618E-12	0.
9	2	3.91653E-12	0.	10	2	3.72598E-12	0.
9	3	1.45434E-11	0.	10	3	5.55599E-12	0.
9	4	1.07804E-11	0.	10	4	6.41462E-12	0.
9	5	3.38326E-12	0.	10	5	1.38112E-11	0.
9	6	2.03369E-11	0.	10	6	3.84369E-11	0.
9	7	1.37350E-11	0.	10	7	1.82126E-11	0.
9	8	5.47478E-12	0.	10	8	4.58463E-12	0.
9	9	1.00000E+00	0.	10	9	1.15961E-11	0.
9	10	1.15961E-11	0.	10	10	1.00000E+00	0.

Table 7.2b Confirmation of the conservation property $J_r S^H J_r S J_r = J_r$ for the 3-element grid specified in table 7.2a. Here $S = \rho_3 + \tau_3$.

1 1 1.81899E-12 0.	2 1 1.87497E-12 0.	3 1 1.56167E-12 0.	4 1 2.[illegible] 0.
1 2 1.87497E-12 0.	2 2 7.27596E-12 0.	3 2 4.10216E-12 0.	4 2 2.23544E-13 0.
1 3 1.56167E-12 0.	2 3 4.10216E-12 0.	3 3 9.09495E-12 0.	4 3 3.76139E-12 0.
1 4 2.50111E-12 0.	2 4 2.23544E-13 0.	3 4 3.76139E-12 0.	4 4 5.45697E-12 0.
1 5 2.38075E-12 0.	2 5 9.76131E-12 0.	3 5 2.41702E-12 0.	4 5 5.89759E-12 0.
1 6 2.14504E-12 0.	2 6 2.86799E-12 0.	3 6 2.89399E-12 0.	4 6 1.26975E-13 0.
1 7 5.84851E-12 0.	2 7 3.15878E-12 0.	3 7 6.82121E-13 0.	4 7 2.73794E-12 0.
1 8 1.22444E-12 0.	2 8 7.60658E-12 0.	3 8 2.59246E-12 0.	4 8 1.82313E-12 0.
1 9 1.94268E-12 0.	2 9 3.27923E-12 0.	3 9 5.08423E-12 0.	4 9 2.34096E-12 0.
1 10 1.36789E-11 0.	2 10 2.57244E-12 0.	3 10 8.13477E-12 0.	4 10 3.97091E-12 0.
1 11 5.75215E-12 0.	2 11 1.45618E-11 0.	3 11 9.27586E-12 0.	4 11 4.22760E-12 0.
1 12 0. 0.	2 12 2.03369E-12 0.	3 12 4.59762E-12 0.	4 12 4.85279E-12 0.
1 13 4.86738E-12 0.	2 13 3.75591E-12 0.	3 13 7.49989E-12 0.	4 13 1.13162E-11 0.
1 14 2.14372E-12 0.	2 14 5.84466E-12 0.	3 14 2.14504E-12 0.	4 14 4.79648E-12 0.
1 15 2.41702E-12 0.	2 15 8.10220E-12 0.	3 15 5.14488E-12 0.	4 15 3.91653E-12 0.
1 16 1.10645E-11 0.	2 16 2.33058E-12 0.	3 16 7.39973E-12 0.	4 16 2.03369E-12 0.
1 17 5.53224E-12 0.	2 17 6.63618E-12 0.	3 17 3.63798E-12 0.	4 17 3.72598E-12 0.
1 18 4.67529E-12 0.	2 18 5.12482E-12 0.	3 18 1.81899E-12 0.	4 18 1.82099E-12 0.

---

5 1 2.38075E-12 0.	6 1 2.14504E-12 0.	7 1 5.84851E-12 0.	8 1 1.22444E-12 0.
5 2 9.76131E-12 0.	6 2 2.86799E-12 0.	7 2 3.15878E-12 0.	8 2 7.60658E-12 0.
5 3 2.41702E-12 0.	6 3 2.89399E-12 0.	7 3 6.82121E-13 0.	8 3 2.59246E-12 0.
5 4 5.89757E-12 0.	6 4 1.26275E-13 0.	7 4 2.73794E-12 0.	8 4 1.82313E-12 0.
5 5 4.36557E-11 0.	6 5 4.19434E-12 0.	7 5 3.57357E-12 0.	8 5 1.65184E-11 0.
5 6 4.19434E-12 0.	6 6 3.63798E-12 0.	7 6 2.96459E-12 0.	8 6 4.31379E-13 0.
5 7 3.57357E-12 0.	6 7 2.96459E-12 0.	7 7 1.81899E-12 0.	8 7 6.24347E-12 0.
5 8 1.65184E-11 0.	6 8 4.31379E-13 0.	7 8 6.24347E-12 0.	8 8 3.63798E-12 0.
5 9 4.33839E-13 0.	6 9 2.73794E-12 0.	7 9 2.95586E-12 0.	8 9 6.82121E-13 0.
5 10 2.28508E-12 0.	6 10 2.65974E-12 0.	7 10 1.81899E-12 0.	8 10 5.57427E-12 0.
5 11 7.50897E-12 0.	6 11 1.55938E-12 0.	7 11 2.14504E-12 0.	8 11 9.86681E-12 0.
5 12 8.08688E-12 0.	6 12 9.09495E-13 0.	7 12 1.06821E-11 0.	8 12 4.20641E-12 0.
5 13 9.52878E-12 0.	6 13 4.81746E-12 0.	7 13 4.06738E-12 0.	8 13 7.78858E-12 0.
5 14 3.32846E-11 0.	6 14 5.73954E-12 0.	7 14 1.27106E-12 0.	8 14 3.43435E-12 0.
5 15 1.45434E-11 0.	6 15 1.07804E-11 0.	7 15 7.55825E-12 0.	8 15 3.38326E-12 0.
5 16 8.66196E-12 0.	6 16 1.76215E-12 0.	7 16 3.61521E-12 0.	8 16 9.09495E-13 0.
5 17 5.55569E-12 0.	6 17 6.41462E-12 0.	7 17 7.27596E-12 0.	8 17 1.35112E-11 0.
5 18 1.81899E-12 0.	6 18 2.73794E-12 0.	7 18 4.06738E-12 0.	8 18 3.89262E-12 0.

---

9 1 1.94268E-12 0.	10 1 1.36789E-11 0.	11 1 5.75215E-12 0.	12 1 0. 0.
9 2 3.27923E-12 0.	10 2 2.57244E-12 0.	11 2 1.45618E-11 0.	12 2 2.03369E-12 0.
9 3 5.08423E-12 0.	10 3 8.13477E-12 0.	11 3 9.27586E-12 0.	12 3 4.59762E-12 0.
9 4 2.34096E-12 0.	10 4 3.97091E-12 0.	11 4 4.22760E-12 0.	12 4 4.85279E-12 0.
9 5 4.33839E-13 0.	10 5 2.28508E-12 0.	11 5 7.50897E-12 0.	12 5 8.08688E-12 0.
9 6 2.73794E-12 0.	10 6 2.65974E-12 0.	11 6 1.56938E-12 0.	12 6 9.09495E-13 0.
9 7 2.95586E-12 0.	10 7 1.81899E-12 0.	11 7 2.14504E-12 0.	12 7 1.06821E-11 0.
9 8 6.82121E-13 0.	10 8 6.57427E-12 0.	11 8 6.86681E-12 0.	12 8 4.20641E-12 0.
9 9 3.63798E-12 0.	10 9 6.55631E-12 0.	11 9 1.94268E-12 0.	12 9 5.45697E-12 0.
9 10 6.55631E-12 0.	10 10 1.81899E-12 0.	11 10 1.83315E-12 0.	12 10 1.29922E-11 0.
9 11 1.94268E-12 0.	10 11 1.83315E-12 0.	11 11 4.36557E-11 0.	12 11 1.09234E-11 0.
9 12 5.45697E-12 0.	10 12 1.29922E-11 0.	11 12 1.09234E-11 0.	12 12 5.45697E-12 0.
9 13 8.18545E-12 0.	10 13 9.88226E-12 0.	11 13 1.12888E-11 0.	12 13 1.09135E-11 0.
9 14 2.20740E-12 0.	10 14 4.14918E-12 0.	11 14 3.38215E-12 0.	12 14 2.73794E-12 0.
9 15 3.63798E-12 0.	10 15 7.49989E-12 0.	11 15 2.03369E-11 0.	12 15 7.77873E-12 0.
9 16 5.75215E-12 0.	10 16 1.32444E-11 0.	11 16 1.16472E-11 0.	12 16 1.09163E-11 0.
9 17 5.75215E-12 0.	10 17 2.27919E-11 0.	11 17 3.94369E-11 0.	12 17 1.22822E-11 0.
9 18 1.61311E-11 0.	10 18 8.41283E-12 0.	11 18 2.36469E-11 0.	12 18 1.04121E-11 0.

---

13 1 4.86738E-12 0.	14 1 2.14372E-12 0.	15 1 2.41702E-12 0.	16 1 1.10645E-11 0.
13 2 3.75591E-12 0.	14 2 5.84466E-12 0.	15 2 8.10220E-12 0.	16 2 2.33058E-12 0.
13 3 7.49989E-12 0.	14 3 2.14504E-12 0.	15 3 5.14488E-12 0.	16 3 7.39973E-12 0.
13 4 1.13162E-11 0.	14 4 4.79648E-12 0.	15 4 3.91653E-12 0.	16 4 2.03369E-12 0.
13 5 9.52878E-12 0.	14 5 3.32846E-11 0.	15 5 1.45434E-11 0.	16 5 8.66198E-12 0.
13 6 4.81746E-12 0.	14 6 5.73954E-12 0.	15 6 1.07804E-11 0.	16 6 1.76215E-12 0.
13 7 4.06738E-12 0.	14 7 1.27106E-12 0.	15 7 7.55825E-12 0.	16 7 3.61521E-12 0.
13 8 7.78858E-12 0.	14 8 3.43435E-12 0.	15 8 3.38326E-12 0.	16 8 9.09495E-13 0.
13 9 8.18545E-12 0.	14 9 2.20743E-12 0.	15 9 3.63798E-12 0.	16 9 5.75215E-12 0.
13 10 9.88226E-12 0.	14 10 4.14918E-12 0.	15 10 7.49989E-12 0.	16 10 1.32444E-11 0.
13 11 1.12888E-11 0.	14 11 3.38015E-12 0.	15 11 2.03369E-11 0.	16 11 1.16472E-11 0.
13 12 1.09139E-11 0.	14 12 2.73794E-12 0.	15 12 7.77873E-12 0.	16 12 1.09163E-11 0.
13 13 1.45519E-11 0.	14 13 4.92221E-12 0.	15 13 1.37350E-11 0.	16 13 1.13687E-12 0.
13 14 4.92221E-12 0.	14 14 1.45519E-11 0.	15 14 5.47478E-12 0.	16 14 3.53710E-12 0.
13 15 1.37350E-11 0.	14 15 5.47478E-12 0.	15 15 2.91036E-11 0.	16 15 1.15043E-11 0.
13 16 1.13687E-12 0.	14 16 3.53712E-12 0.	15 16 1.15043E-11 0.	16 16 1.09139E-11 0.
13 17 1.02126E-11 0.	14 17 4.58463E-12 0.	15 17 1.15961E-11 0.	16 17 1.21022E-11 0.
13 18 1.81899E-12 0.	14 18 2.95586E-12 0.	15 18 1.55962E-11 0.	16 18 8.21382E-12 0.

---

17 1 5.53224E-12 0.	18 1 4.67529E-12 0.
17 2 6.63618E-12 0.	18 2 5.12482E-12 0.
17 3 3.63798E-12 0.	18 3 1.81899E-12 0.
17 4 3.72598E-12 0.	18 4 1.82099E-12 0.
17 5 5.55569E-12 0.	18 5 1.81800E-12 0.
17 6 6.41462E-12 0.	18 6 2.73794E-12 0.
17 7 7.27596E-12 0.	18 7 3.63798E-12 0.
17 8 1.35112E-11 0.	18 8 3.89262E-12 0.
17 9 5.75215E-12 0.	18 9 1.61311E-11 0.
17 10 2.27919E-11 0.	18 10 8.41283E-12 0.
17 11 3.94369E-11 0.	18 11 2.36469E-11 0.
17 12 1.22822E-11 0.	18 12 1.04121E-11 0.
17 13 1.82126E-11 0.	18 13 1.81899E-12 0.
17 14 4.58463E-12 0.	18 14 2.95586E-12 0.
17 15 1.15961E-11 0.	18 15 1.55962E-11 0.
17 16 1.21022E-11 0.	18 16 8.21382E-12 0.
17 17 4.36557E-11 0.	18 17 5.57413E-12 0.
17 18 5.57413E-12 0.	18 18 1.81899E-12 0.

Table 7.2c Confirmation of the conservation property $S^H J_r S + iJ_e S - iS^H J_e - J_r = 0$ for the 3-element grid specified in table 7.2a. Here $S = \rho_3 + \tau_3$.

rectangular-holed inductive grid were numerically investigated using a computer program relying upon the recurrence relation derived in section 7.2.2 and upon the formalism described in section 7.2.3 for the scattering matrices of this inductive grid element. Sample results of these investigations are presented in this section.

Figure 7.4 depicts low pass transmission characteristics of three multi-element inductive grids operated in normally-incident TE polarized radiation. It should be noted that under these conditions, the square-holed (c = c') grids are polarization independent and the results given in this figure therefore apply to radiation incident with any polarization angle. The curves given in figures 7.4a, 7.4b and 7.4c correspond to grids with one, two or three elements, having varying aperture widths and depths. The elements of each grid are separated by a constant separation $t = t_1 = t_2 = 0.25$.

It is seen from figures 7.4a and 7.4b and figures 7.4b and 7.4c, that decreasing the aperture width and increasing the aperture depth leads to sharper cut-off between the transmission and rejection regions. The edge steepness is also observed to increase as the number of elements in the filter is increased and under these conditions the interference ripple in the passband also becomes more significant. These observations were noted for the multi-element grating in section 5.3, a feature also observed by Ulrich [7.5] and Holah [7.6] for grids.

Figure 7.5 shows in detail the resonances occurring at $\lambda/d \simeq 8.5$ for a multi-element grid Fabry-Perot interferometer operated in normal incidence. This arrangement was considered in chapter 6 when investigating the filtering properties of the double grid and the two-element curve given in figure 7.5a reproduces that given in figure 6.2a. The splitting of this

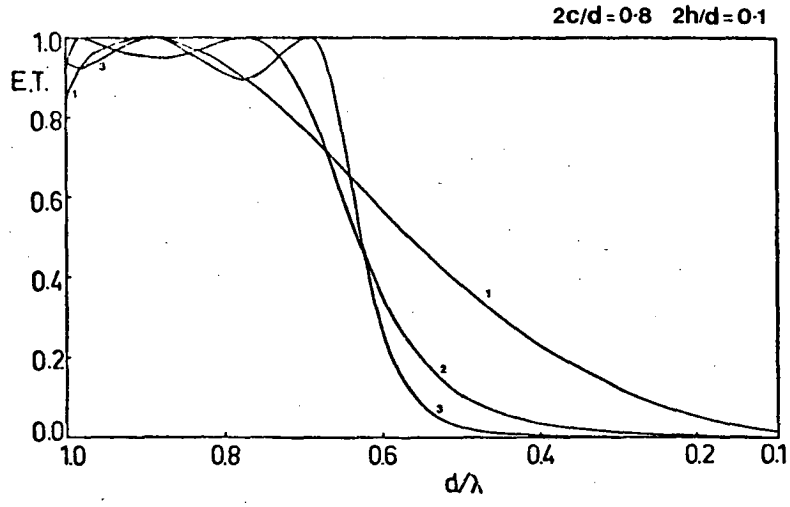

(a)

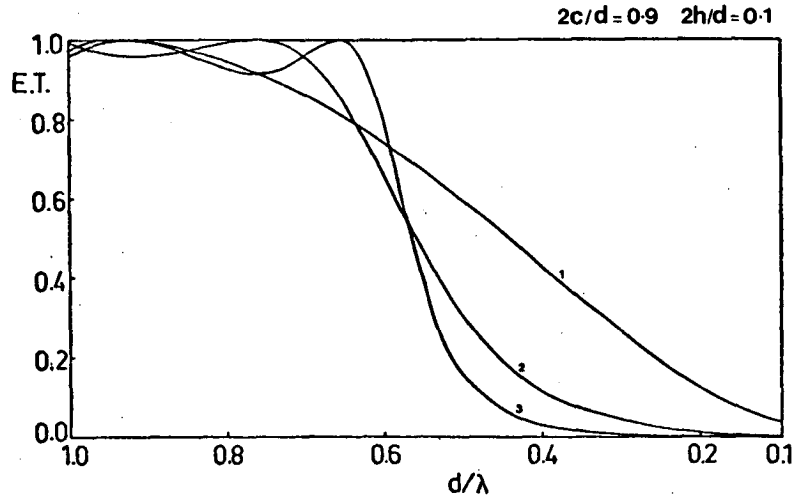

(b)

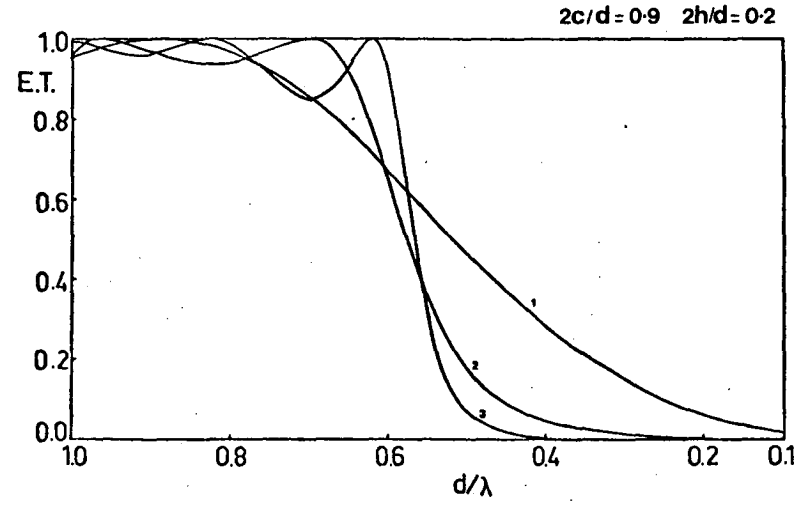

(c)

Figure 7.4 Normal incidence ($\phi = \psi = 0^{\circ}$) wavelength spectra for a 1, 2 or 3 element square-holed inductive grid, operated in TE($\delta = 0^{\circ}$) polarized radiation. In each case, the elements are separated by t/d = 0.25 and 9 Rayleigh orders are used to couple the elements.

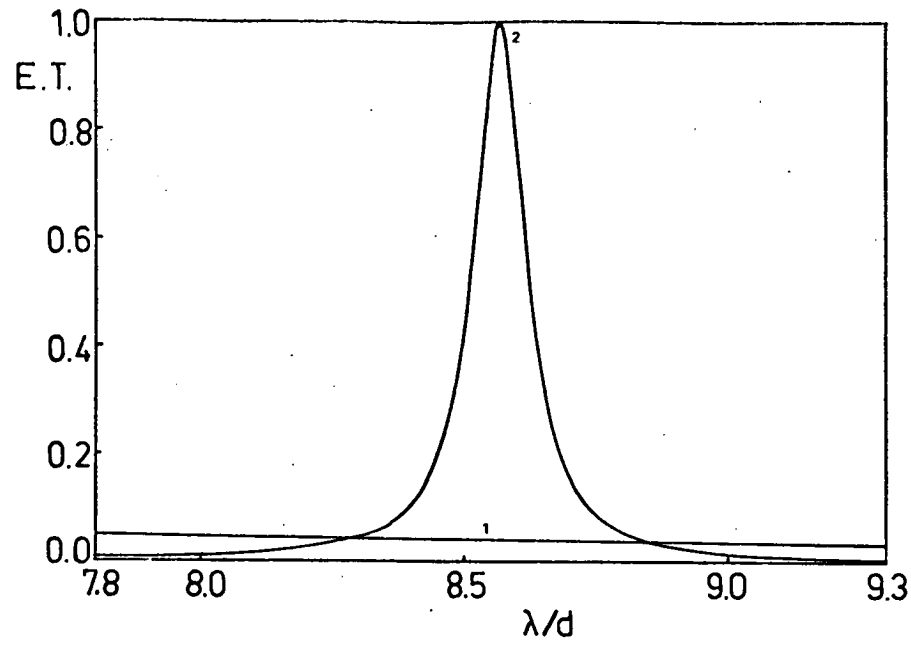

(a)

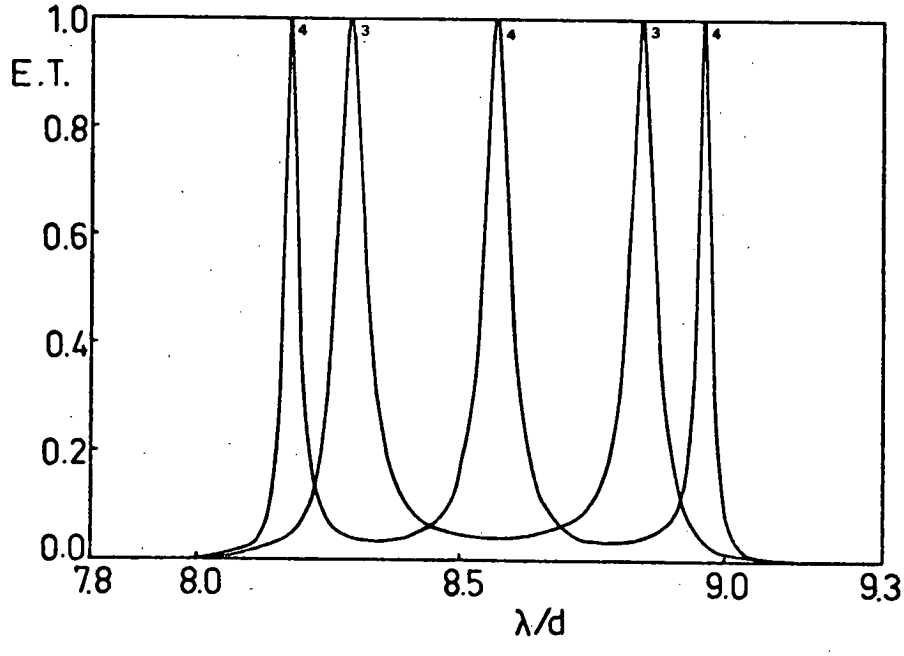

(b)

Figure 7.5 Normal incidence ($\phi = \psi = 0^{o}$) wavelength spectra for a multi-element square-holed inductive grid composed of
(a) 1 or 2 elements and
(b) 3 or 4 elements,
operated in TE ($\delta = 0^{o}$) polarized radiation. The grid parameters are $d'/d = 1.0$, $c/d = 0.8$, $h/d = 0.01$ and the separation of each element is $t/d = 4.0$.

resonance for three and four-element grids, shown in figure 7.5b, is noted. These curves also demonstrate that the finesse of the resonances increases as the number of elements in the filter increases. These results are similar to those obtained by Botten [7.7] for the multi-element grating.

7.6 CONCLUSIONS

A rigorous multiple scattering approach has been used in this chapter to describe the diffraction properties of multi-element grids having an arbitrary number of up-down symmetric elements. A matrix recurrence relation for the scattering matrices of this structure was derived using this procedure.

A rectangular-holed, perfectly conducting inductive grid was considered in detail. The scattering matrices associated with both the individual elements as well as the entire grid stack were shown to be analytically constrained by a series of conservation properties. These properties rely upon the lossless nature and the up-down symmetry of the elements. In particular, the sub-matrix containing the elements of the scattering matrix corresponding to the diffracted propagating waves arising from propagating incident waves, was shown to be constrained to be unitary.

A brief description of the long wavelength filtering properties of the rectangular-holed multi-element inductive grid was presented. It was demonstrated numerically that increasing the number of elements in the filters causes an increase in the steepness of the edge between passband and stopband regions of low pass filters. It also increases the finesse of resonances occurring in the transmission spectra of multi-element grid interferometers.

REFERENCES

[7.1] ADAMS (J.L.), BOTTEN (L.C.). - J. Optics (Paris), to be submitted.

[7.2] CHEN (C.-C.). - I.E.E.E. Trans., 1970, MTT-18, 627.

[7.3] CHEN (C.-C.). - I.E.E.E. Trans., 1973, MTT-21, 1.

[7.4] McPHEDRAN (R.C.), MAYSTRE (D.). - Appl. Phys., 1977, 14, 1.

[7.5] ULRICH (R.). - Appl. Opt., 1968, 7, 1987.

[7.6] HOLAH (G.D.). - International Journal of Infrared and Millimeter Waves, 1980, 1, 225.

[7.7] BOTTEN (L.C.). - Infrared Phys., 1979, 19, 659.

CHAPTER 8

THE CROSSED LAMELLAR TRANSMISSION GRATING

8.1 INTRODUCTION

The investigations discussed in this chapter were motivated by a suggestion of Horwitz [8.1] that doubly periodic diffracting structures could provide an effective solar selective surface. Herein, the structure considered is termed the crossed lamellar transmission grating and it consists of two singly periodic, perfectly conducting lamellar gratings arranged in spatially separated parallel planes. The two axes of periodicity of the structure may be inclined at any non-zero angle and consequently the grating is doubly periodic.

Firstly, a brief review of the literature relevant to investigations of doubly periodic structures whose two non-parallel axes of periodicity lie in separated parallel planes, is given. One of the earliest studies of this type was undertaken in 1953 by Groves [8.2], who investigated both theoretically and experimentally the transmission properties of a pair of parallel wire gratings, the wires of which formed some arbitary angle with each other. This study, which was restricted to gratings having periods much smaller than the wavelength of the incident radiation, was based on the formalism derived by Wessel [8.3] .

Wessel's theory, derived for a grating composed of perfectly conducting wires of circular cross-section, is developed by determining the currents induced in the wires by the electric field (parallel to the wires). The radius of the wires was assumed to be much smaller than the wavelength of the incident radiation and thus it was possible to apply a scalar optics approach to the problem.

Adonina et al [8.4] in 1969, adopted a substantially different approach to determine the diffraction properties of a grating composed of two lamellar gratings, whose axes of periodicity formed an arbitrary angle to each other, (that is, the crossed lamellar transmission grating with inclined axes). They considered radiation incident normally on the structure and solved the diffraction problem using a multiple scattering approach. In their analysis, however, the wavelength was assumed greater than the grating period, so that the specularly reflected and transmitted orders were the sole propagating orders. Furthermore, they assumed that the separation of the two component gratings was sufficiently large so that the evanescent fields did not contribute to the coupling between the gratings.

In 1974, Hill and Wait [8.5] considered the diffraction of plane waves by a structure consisting of a pair of wire gratings arranged in separated planes with orthogonal axes of periodicity. Again the wire radius was assumed much smaller than the wavelength of the incident radiation so that there was no spatial variation of the current distribution across the wires. They then determined the current induced on the wires of the grating by the incident field.

This was the stage at which research on structures of this type had reached when the investigations described in this chapter were undertaken. The lack of a rigorous description of the diffraction properties of the crossed lamellar transmission grating and the earlier success of McPhedran and Maystre [8.6] when determining the diffraction properties of perfectly conducting inductive grids, provided further motivation for this study.

In section 8.2, two theoretical formalisms for the crossed lamellar transmission grating are derived. The first of these is described in

section 8.2.2 and considers in detail a grating with orthogonal axes of periodicity. Investigations of the properties of this structure were originally undertaken as the author's project [8.7] for an Honours degree in Science, and are the subject of a paper [8.8]. The analysis is performed by describing the fields in the grooves of each grating by a modal expansion and specifying the fields in each free space region, above, between and below the gratings by Rayleigh expansions. These expansions are then matched by applying the field continuity conditions and the Method of Moments [8.9] to derive a system of linear equations for the unknown modal coefficients. The modifications to this procedure, which are necessary when considering gratings with inclined axes of periodicity, are indicated. The formalism for this structure is not given in detail, since the crossed lamellar transmission grating is shown to have application as a solar selective surface only if the periodicity axes are orthogonal. Thus it is not thought necessary to complicate the discussion by the introduction of this parameter.

Bearing in mind the cumbersome nature of this formalism, an alternative, less involved technique is given in section 8.2.3 for solving the diffraction problem of the crossed lamellar transmission grating with orthogonal axes of periodicity. This approach is based on a multiple scattering analysis, valid for arbitrary angles of incidence and incorporating all plane wave interactions between the upper and lower gratings of the structure. The analysis described is somewhat similar to that used in chapters 5 and 7 in the study of multiple-element gratings and grids. This formalism is shown to be computationally more efficient than that given in section 8.2.2, provided the wavelength to period ratio is sufficiently large.

Since the plane wave and modal expansions describing the fields must

be truncated to determine a numerical solution to the diffraction problem, it is necessary to test the formalism against theoretical constraints, such as those imposed by conservation of energy and reciprocity. A new theoretical test is derived in this chapter, which constrains the complex amplitudes of the fields diffracted by square symmetric, doubly periodic structures operated in a Littrow mount. This is an extension to doubly periodic structures of an earlier result derived by Botten [8.10] for singly periodic gratings.

A detailed discussion of the spectral characteristics of the crossed lamellar transmission grating with orthogonal periodicity axes is given in section 8.3. The structure is shown to have filtering characteristics comparable with those of the inductive grids widely used in infrared spectroscopy [8.11]. However, the crossed lamellar transmission grating has an additional feature, the array separation parameter, which may be used to tune the transmission bandwidth. In particular, the grating is shown to have application as a solar heat mirror.

Previous theoretical studies of the application of doubly periodic structures as solar heat mirrors have been undertaken by McPhedran and Maystre [8.6], McPhedran and Botten [8.12] and Bliek et al [8.13]. McPhedran and Maystre showed that perfectly conducting inductive grids, having square apertures, are capable of providing high absorptance to emittance ratios if they are used in direct illumination and employ diurnal tracking. Subsequently, the theory was extended [8.12, 8.13] to consider an inductive grid with circular apertures, dielectric layers above and below the grid and dielectric plugs in the apertures.

Finally, in section 8.4, the multiple scattering analysis described in section 8.2.3 is used to study the effect of the grating separation

parameter on the behaviour of the structure. In particular, the extent of the evanescent coupling between the component gratings as a function of their separation is investigated.

8.2 THEORETICAL FORMULATIONS OF THE DIFFRACTION PROBLEM

8.2.1 Notation and Description of the Diffraction Arrangement

The doubly periodic structure considered in this chapter consists of two perfectly conducting lamellar transmission gratings arranged in free space as shown in figure 8.1. The lamellar gratings are placed in spatially separated parallel planes, a distance S apart and are arranged so that the two axes of periodicity are orthogonal.

The OY axis of a rectangular Cartesian coordinate system is chosen to be orthogonal to both sets of grooves such that $y = s + h$ and $y = s - h$ correspond to the top and bottom surfaces respectively of the upper set of grooves, and $y = -s + h'$ and $y = -s - h'$ correspond respectively to the top and bottom surfaces of the lower set of grooves. The OX axis of the coordinate system is chosen to be in the direction of periodicity of the upper grating and the OZ axis then lies in the direction of periodicity of the lower grating. The apertures of the upper grating are all identical in shape, are of width $2c$ and have spatial period d. Similarly, the apertures in the lower grating are all identical in shape but are chosen to have width $2c'$ and a period d'. The unit vectors aligned with the OX, OY and OZ axes are designated $\hat{\underline{x}}$, $\hat{\underline{y}}$ and $\hat{\underline{z}}$ respectively.

The structure may be generalised to allow for an arbitrary inclination of the two axes of periodicity. This grating is termed the crossed lamellar transmission grating with inclined axes and is depicted in figure 8.2. The upper array is chosen to be inclined at an angle

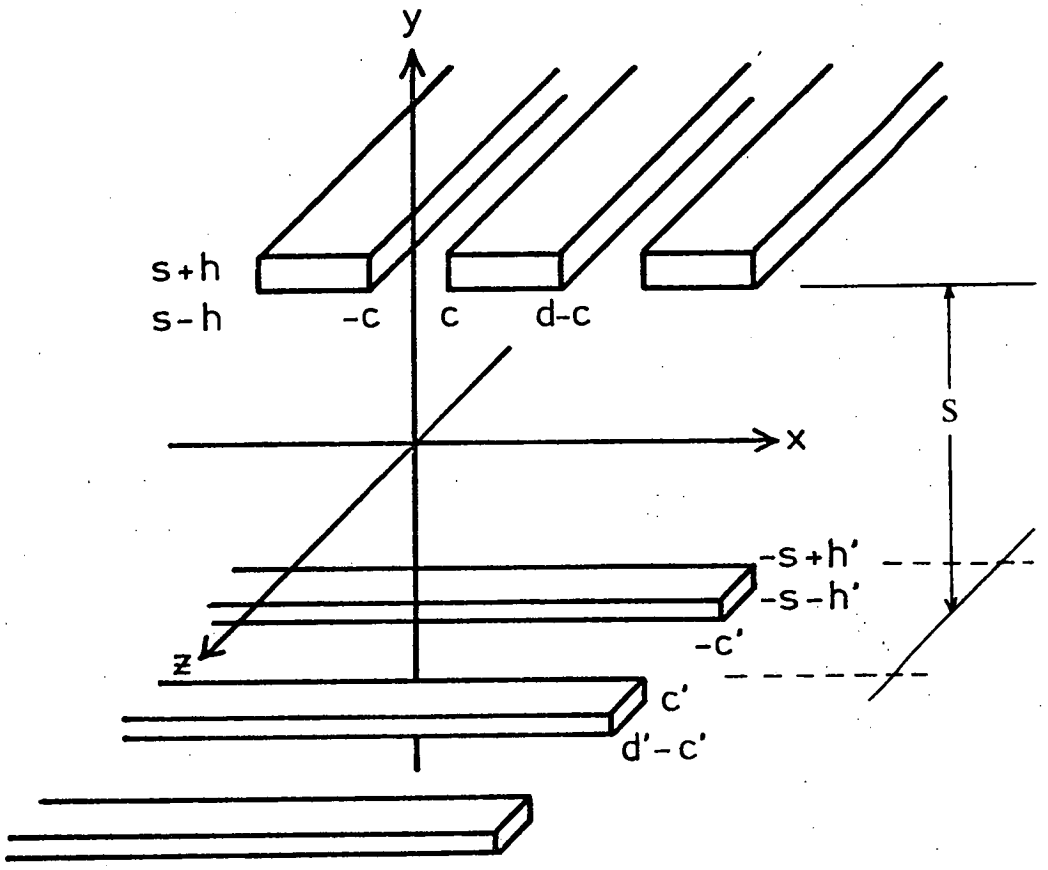

Figure 8.1 The geometry of the crossed lamellar transmission grating with orthogonal axes of periodicity.

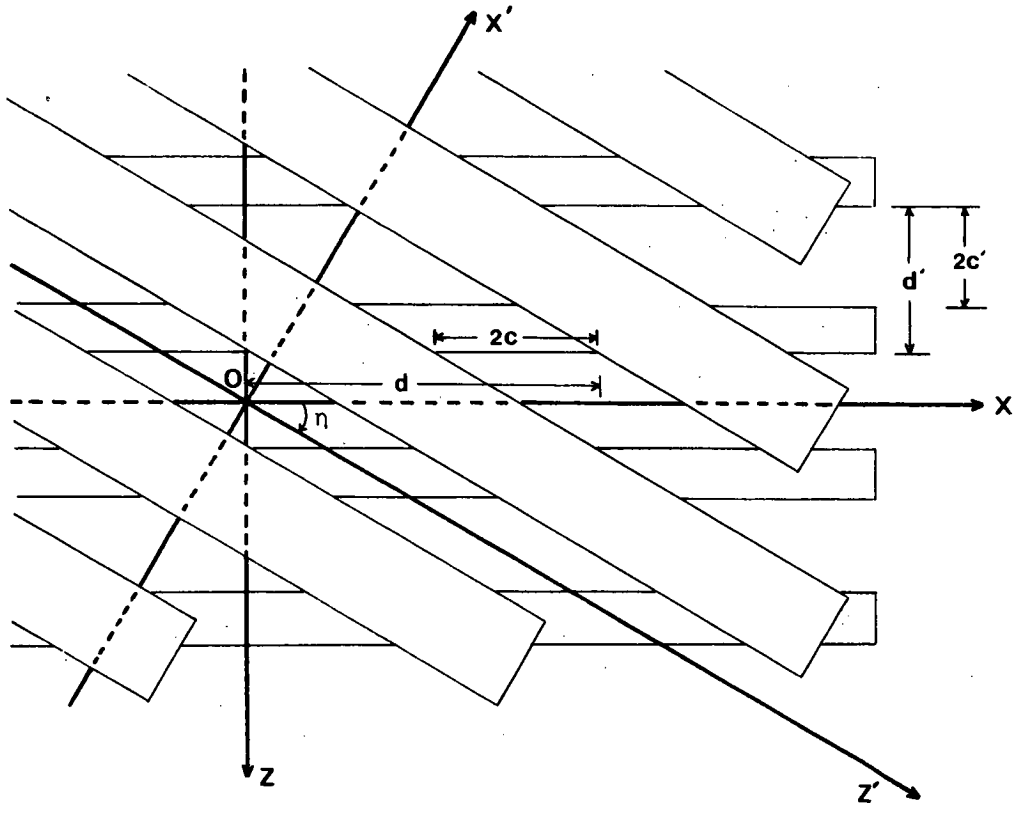

Figure 8.2 The geometry of the crossed lamellar transmission grating with inclined axes.

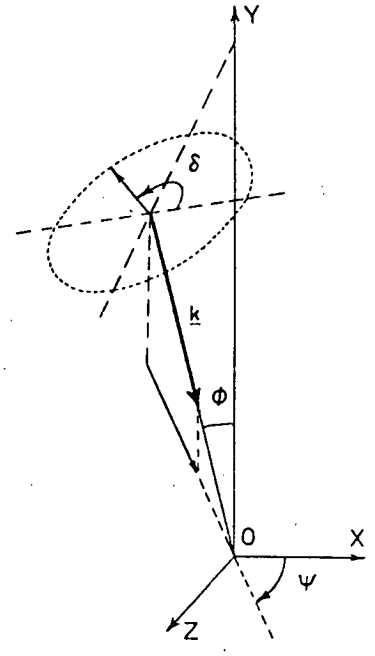

Figure 8.3 Specification of the incident field.

η ($\eta \neq 0^{(0)}$) to the OX axis. This notation is adopted in order to preserve the periodicity directions and consequently preserve the notation introduced in chapter 6, when discussing the properties of inductive grids. An additional coordinate system, distinguished by superscripted primes, is introduced for this problem, as shown in figure 8.2.

Thus

$$\begin{bmatrix} x' \\ z' \end{bmatrix} = \begin{bmatrix} \sin\eta & -\cos\eta \\ \cos\eta & \sin\eta \end{bmatrix} \begin{bmatrix} x \\ z \end{bmatrix} \tag{8.1}$$

A plane wave of wavelength $\lambda = 2\pi/k$ is assumed to be incident upon the structure with direction specified in figure 8.3. The wavevector of this wave therefore is specified by

$$\underline{k} = (\alpha_0, -\beta_{00}, \gamma_{00})$$

where the direction sines and cosines are given in equation (6.1).

As in chapter 6, the fields in all grating regions are specified in terms of TE and TM orthogonal vector modes and throughout the analysis, the temporal dependence term $\exp(-i\omega t)$ is suppressed.

The transverse resolutes of the incident electric and magnetic fields are given by

$$\underline{E}_t^i = E_i \, \underline{\hat{RTE}}_{00} + F_i \, \underline{\hat{RTM}}_{00} \tag{8.2}$$

and

$$\hat{\underline{y}} \times \underline{H}_t = \frac{1}{Z_0} \{ \frac{\beta_{00}}{k} E_i \, \underline{\hat{RTE}}_{00} + \frac{k}{\beta_{00}} F_i \, \underline{\hat{RTM}}_{00} \} \tag{8.3}$$

where all symbols are defined in equations (6.2 - 6.5) and (6.8).

8.2.2 The Modal Formulation of the Diffraction Problem

In this formalism, the fields in all free space regions are described in terms of plane wave expansions, while the fields within the

aperture regions are specified by waveguide modal expansions. The continuity conditions at each grating surface are applied and the field problem is explicitly solved in terms of the modal coefficients by applying the Method of Moments [8.9]. The formalism is presented for the crossed lamellar transmission grating with orthogonal axes of periodicity, but modifications required in considering the inclined axes case will be indicated.

8.2.2.1 *Free Space Fields*

The crossed lamellar transmission grating is doubly-periodic, and so gives rise to doubly-infinite series of diffracted plane waves in the three free-space regions. Each diffracted wave is numbered by two integers p and q, with its direction of propagation being specified by the direction cosines α_p, β_{pq} and γ_q given by

$$\alpha_p = \alpha_0 + pK \tag{8.4}$$

$$\gamma_q = \gamma_0 + qK' \tag{8.5}$$

$$\left.\begin{aligned} \beta_{pq} &= \sqrt{k^2 - \alpha_p^2 - \gamma_q^2} && \text{if } |\alpha_p^2 + \gamma_q^2| \geq k^2 \\ &= i\sqrt{k^2 - \alpha_p^2 - \gamma_q^2} && \text{if } |\alpha_p^2 + \gamma_q^2| < k^2 \end{aligned}\right\} \tag{8.6}$$

where $K = 2\pi/d$ and $K' = 2\pi/d'$.

It is to be noted that for an arbitrary inclination of the periodicity axes, η , the direction sine γ is a function of the two integers p and q

$$\gamma_{pq} = \gamma_0 + qK' - pK/\tan\eta \quad . \tag{8.7}$$

Using the notation of chapter 6, the transverse resolute of the electric and magnetic free space diffracted fields in the region $y > s + h$ are given respectively by the following plane wave expansions

$$\underline{E}_t = \sum_{p=-\infty}^{\infty} \sum_{q=-\infty}^{\infty} [E_{pq} \underline{RTE}_{pq}(x,y,z) + F_{pq} \underline{RTM}_{pq}(x,y,z)] \tag{8.8}$$

and

$$\hat{y} \times \underline{H}_t = -\frac{1}{Z_0} \sum_{p=-\infty}^{\infty} \sum_{q=-\infty}^{\infty} [\frac{\beta_{pq}}{k} E_{pq} \underline{RTE}_{pq}(x,y,z) + \frac{k}{\beta_{pq}} F_{pq} \underline{RTM}_{pq}(x,y,z)] \tag{8.9}$$

where for later convenience the following definitions are made:

$$\underline{RTE}_{pq}(x,y,z) = \underline{R}_{1;pq}(x) \exp i(\beta_{pq} y + \gamma_q z) \quad , \tag{8.10}$$

$$\underline{RTM}_{pq}(x,y,z) = \underline{R}_{2;pq}(x) \exp i(\beta_{pq} y + \gamma_q z) \quad , \tag{8.11}$$

and
$$\left.\begin{aligned} \underline{R}_{1;pq} &= \underline{V}_1 \exp(i\alpha_p x) \\ \underline{R}_{2;pq} &= \underline{V}_2 \exp(i\alpha_p x) \end{aligned}\right\} \quad . \tag{8.12}$$

Here
$$\left.\begin{aligned} \underline{V}_1 &= \frac{1}{\zeta_{pq}\sqrt{dd'}} \{\gamma_q \hat{x} - \alpha_p \hat{z}\} \\ \underline{V}_2 &= \frac{1}{\zeta_{pq}\sqrt{dd'}} \{\alpha_p \hat{x} + \gamma_q \hat{z}\} \end{aligned}\right\} \tag{8.13}$$

and
$$\zeta_{pq} = \sqrt{\alpha_p^2 + \gamma_q^2} \quad . \tag{8.14}$$

The transverse resolutes of the transmitted fields in the region $y < -s - h'$ and of the upward and downward going fields in the region $-s + h' < y < s - h$ are given by equations (6.18) to (6.23).

At this stage it is worth confirming that the direction sines of the diffracted waves are indeed given by equations (8.4) and (8.7) if the axes of the grating are inclined. Consider a plane wave with direction sines $(\alpha_0, -\beta_0, \gamma_0)$ incident upon the upper grating. In the primed coordinate system, these direction sines are given by $(\alpha_0', -\beta_0, \gamma_0')$ where using equation (8.1) ,

$$\alpha_0' = \alpha_0 \sin \eta - \gamma_0 \cos \eta$$

and $$\gamma_0' = \alpha_0 \cos \eta + \gamma_0 \sin \eta \quad .$$

The field upon interaction with this grating, is diffracted in the OX' direction only and hence the direction of the p^{th} diffracted wave is specified by $(\alpha_p', \beta_{p0}', \gamma_0')$

where $$\alpha_p' = \alpha_0' + \frac{2\pi p}{d \sin \eta} \quad .$$

In the original reference frame, the direction cosines of this diffracted wave are

$$\alpha_p = \alpha_p' \sin \eta + \gamma_0' \cos \eta$$

$$\gamma_p = - \alpha_p' \cos \eta + \gamma_0' \sin \eta \quad .$$

This wave, incident upon the lower grating, is then diffracted only in the OZ direction. Thus the waves diffracted by the lower grating have direction cosines $(\alpha_p, \beta_{pq}, \gamma_{pq})$ where

$$\gamma_{pq} = \gamma_p + \frac{2\pi q}{d'}$$

$$= - \alpha_p' \cos \eta + \gamma_0' \sin \eta + \frac{2\pi q}{d'} \quad .$$

That is, $$\gamma_{pq} = \gamma_0 - p\frac{2\pi}{d} \cot \eta + q\frac{2\pi}{d'}$$

Also $$\alpha_p = \alpha_p' \sin \eta + \gamma_0' \cos \eta$$

$$= \alpha_0 + \frac{2\pi p}{d} \quad .$$

Thus the direction cosines given in chapter 6 for the grid problem are recovered.

8.2.2.2 *Fields Within the Groove Regions*

Firstly the crossed lamellar transmission grating with orthogonal

axes of periodicity is considered. Adams et al [8.8] have shown that the relevant Cartesian modes for the upper grating are given by the functions

$$MEXU_{mq}(x,z) = P_m \cos\frac{m\pi}{2c}(x + c) \exp i\gamma_q z \tag{8.15}$$

$$MEZU_{mq}(x,z) = P_m \sin\frac{m\pi}{2c}(x + c) \exp i\gamma_q z \tag{8.16}$$

where $$P_m = \sqrt{\frac{\varepsilon_m}{2cd'}}$$

and
$$\left.\begin{aligned} \varepsilon_m &= 1 \qquad \text{if} \quad m = 0 \\ &= 2 \qquad \text{otherwise} \end{aligned}\right\} \tag{8.17}$$

It is worthwhile to note that the form of the mode functions given in equations (8.15) and (8.16) for the grooves of the upper grating, can be qualitatively explained as follows. Firstly, the x-dependent functions are those of a lamellar transmission grating operated in a classical mount. Secondly, since the grooves are open-ended in the z-direction, the field has a z-dependence characterised by the pseudo-periodicity of the Rayleigh expansions.

The TE and TM modes for the fields within this region can be shown (see appendix 8.1) to be given by

$$\underline{MTEU}_{mq}(x,z) = \underline{M}_{1;mq} \exp i\gamma_q z \tag{8.18}$$

and
$$\underline{MTMU}_{mq}(x,z) = \underline{M}_{2;mq} \exp i\gamma_q z \tag{8.19}$$

where
$$\underline{M}_{1;mq} = g_{mq}\{i\gamma_q \cos\frac{m\pi}{2c}(x + c)\hat{\underline{x}} + \frac{m\pi}{2c} \sin\frac{m\pi}{2c}(x + c)\hat{\underline{z}}\} \tag{8.20}$$

$$\underline{M}_{2;mq} = g_{mq}\{\frac{m\pi}{2c} \cos\frac{m\pi}{2c}(x + c)\hat{\underline{x}} + i\gamma_q \sin\frac{m\pi}{2c}(x + c)\hat{\underline{z}}\} \tag{8.21}$$

and
$$g_{mq} = P_m[(\frac{m\pi}{2c})^2 + \gamma_q^2]^{-\frac{1}{2}} \tag{8.22}$$

The transverse resolutes of the electric and magnetic fields in the upper grooves are then given respectively by

$$\underline{E}_t = \sum_{m=0}^{\infty}\sum_{q=-\infty}^{\infty}\{[a_{mq}\sin(\mu_{mq}(y-s)) + b_{mq}\cos(\mu_{mq}(y-s))]\underline{MTEU}_{mq}(x,z)\}$$
$$+ \sum_{m=1}^{\infty}\sum_{q=-\infty}^{\infty}\{[c_{mq}\sin(\mu_{mq}(y-s)) + d_{mq}\cos(\mu_{mq}(y-s))]\underline{MTMU}_{mq}(x,z)\} \tag{8.23}$$

and

$$\hat{y}\times\underline{H}_t = \frac{i}{Z_0}\{\sum_{m=0}^{\infty}\sum_{q=-\infty}^{\infty}\{\frac{\mu_{mq}}{k}[a_{mq}\cos(\mu_{mq}(y-s)) - b_{mq}\sin(\mu_{mq}(y-s))]\underline{MTEU}_{mq}(x,z)\}$$
$$+ \sum_{m=1}^{\infty}\sum_{q=-\infty}^{\infty}\frac{k}{\mu_{mq}}[c_{mq}\cos(\mu_{mq}(y-s)) - d_{mq}\sin(\mu_{mq}(y-s))]\underline{MTMU}_{mq}(x,z)\}\} \tag{8.24}$$

where
$$\mu_{mq} = \sqrt{k^2 - \gamma_q^2 - (\frac{m\pi}{2c})^2} \tag{8.25}$$

is obtained upon application of the Helmholtz equation.

Similarly, the mode functions appropriate to the lower grooves, expressed in TE/TM coordinates are given by

$$\underline{MTEL}_{mp}(x,z) = \underline{\hat{M}}_{1;mp}\exp(i\alpha_p x) \tag{8.26}$$

and

$$\underline{MTML}_{mp}(x,z) = \underline{\hat{M}}_{2;mp}\exp(i\alpha_p x) \tag{8.27}$$

where
$$\underline{\hat{M}}_{1;mp} = \hat{g}_{mp}\{\frac{m\pi}{2c'}\sin[\frac{m\pi}{2c'}(z+c')]\hat{x} + i\alpha_p\cos[\frac{m\pi}{2c'}(z+c')]\hat{z}\} \tag{8.28}$$

$$\underline{\hat{M}}_{2;mp} = \hat{g}_{mp}\{i\alpha_p\sin[\frac{m\pi}{2c'}(z+c')]\hat{x} + \frac{m\pi}{2c'}\cos[\frac{m\pi}{2c'}(z+c')]\hat{z}\} \tag{8.29}$$

and
$$\hat{g}_{mp} = \sqrt{\frac{\varepsilon_m}{2c'd}}\,[(\frac{m\pi}{2c'})^2 + \alpha_p^2]^{-\frac{1}{2}} \tag{8.30}$$

is the normalisation factor.

Then the transverse resolutes of the electric and magnetic fields in the grooves of the lower grating are given respectively by

$$\underline{E}_t = \sum_{m=0}^{\infty} \sum_{p=-\infty}^{\infty} \{[\hat{a}_{mp}\sin(\hat{\mu}_{mp}(y+s)) + \hat{b}_{mp}\cos(\hat{\mu}_{mp}(y+s))]\underline{\underline{MTEL}}_{mp}(x,z)$$

$$+ \sum_{m=1}^{\infty} \sum_{p=-\infty}^{\infty} [\hat{c}_{mp}\sin(\mu_{mp}(y+s)) + \hat{d}_{mp}\cos(\hat{\mu}_{mp}(y+s))]\underline{\underline{MTML}}_{mp}(x,z)\} \tag{8.31}$$

and

$$\hat{y} \times \underline{H}_t = \frac{i}{Z_0}\{\sum_{m=0}^{\infty} \sum_{p=-\infty}^{\infty} \{\frac{\hat{\mu}_{mp}}{k}[\hat{a}_{mp}\cos(\hat{\mu}_{mp}(y+s)) - \hat{b}_{mp}\sin(\hat{\mu}_{mp}(y+s))]\underline{\underline{MTEL}}_{mp}(x,z)\}$$

$$+ \sum_{m=1}^{\infty} \sum_{q=-\infty}^{\infty} \{\frac{k}{\hat{\mu}_{mp}}[\hat{c}_{mp}\cos(\hat{\mu}_{mp}(y+s)) - \hat{d}_{mp}\sin(\hat{\mu}_{mp}(y+s))]\underline{\underline{MTML}}_{mp}(x,z)\}\} \tag{8.32}$$

where

$$\hat{\mu}_{mp} = \sqrt{k^2 - \alpha_p^2 - (\frac{m\pi}{2c'})^2} \tag{8.33}$$

When considering the crossed lamellar transmission grating with inclined axes, the modal fields in the grooves of the upper grating are defined with respect to the primed coordinate system. In this case

$$\underline{\underline{MTEU}}_{mq}(x',z') = g'_{mq}\{i\gamma'_q MEXU_{mq}(x',z')\hat{\underline{x}}' + \frac{m\pi}{2c\sin\eta} MEZU_{mq}(x',z')\hat{\underline{z}}'\} \tag{8.34}$$

and

$$\underline{\underline{MTMU}}_{mq}(x',z') = g'_{mq}\{\frac{m\pi}{2c\sin\eta} MEXU_{mq}(x',z')\hat{\underline{x}}' + i\gamma'_q MEXU_{mq}(x',z')\hat{\underline{z}}'\} \tag{8.35}$$

where

$$MEXU_{mq}(x',z') = P_m \cos[\frac{m\pi(x' + c\sin\eta)}{2c\sin\eta}] \exp(i\gamma'_q z') \quad ,$$

$$MEZU_{mq}(x',z') = P_m \sin[\frac{m\pi(x' + c\sin\eta)}{2c\sin\eta}] \exp(i\gamma'_q z') \quad ,$$

$$g'_{mq} = P_m[(\frac{m\pi}{2c \sin\eta})^2 + \gamma'^2_q]^{-\frac{1}{2}}$$

and $\hat{x}'$ and $\hat{z}'$ are unit vectors aligned with the OX' and OZ' axes respectively. Appropriate continuity conditions must now be applied at all grating surfaces to relate the free space and modal fields.

8.2.2.3 *Application of the Continuity Conditions*

The continuity conditions applying to this problem are that the transverse electric and magnetic fields are continuous across all aperture-free space boundaries. Again, the crossed lamellar transmission grating with orthogonal axes of periodicity is considered.

The continuity of the transverse electric field at $y = s + h$ for this structure can be written

$$\sum_{p,q} \{[E_{pq}Y_{pq}(s+h) + E_iY_{00}(-s-h)\delta_{p0}\delta_{q0}]\underline{RTE}_{pq}(x,0,z)$$

$$+ [F_{pq}Y_{pq}(s+h) + F_iY_{00}(-s-h)\delta_{p0}\delta_{q0}]\underline{RTM}_{pq}(x,0,z)\}$$

$$= \sum_{m\epsilon\Lambda}\sum_{q}[a^*_{mq} + b^*_{mq}]\underline{MTEU}_{mq}(x,z) + \sum_{m\epsilon\Lambda'}\sum_{q}[c^*_{mq} + d^*_{mq}]\underline{MTMU}_{mq}(x,z)$$

$$\text{if} \quad x \in [-c,c]$$

$$= 0 \qquad \text{otherwise} \qquad (8.36)$$

Here $$Y_{pq}(y) = \exp(i\beta_{pq}y) \qquad (8.37)$$

$$\left.\begin{aligned} \begin{Bmatrix} a^*_{mq} \\ c^*_{mq} \end{Bmatrix} &= \begin{Bmatrix} a_{mq} \\ c_{mq} \end{Bmatrix} \sin(\mu_{mq}h) \\ \begin{Bmatrix} b^*_{mq} \\ d^*_{mq} \end{Bmatrix} &= \begin{Bmatrix} b_{mq} \\ d_{mq} \end{Bmatrix} \cos(\mu_{mq}h) \end{aligned}\right\} \qquad (8.38)$$

and $$\Lambda = \{ m \mid m = 0,1,2,.....\}$$

$$\Lambda' = \{ m \mid m = 1,2,.....\}$$

In this equation and hereafter summations over the integers p, q are understood to run from $-\infty$ to ∞ unless otherwise stated.

The Method of Moments is applied to equation (8.36) by multiplying throughout by $\overline{RTE}_{rs}(y=0)$ and integrating the resulting equation over the region $x \in [-c,c]$, $z \in [0,d']$. This procedure leads to the following equation:

$$E_{rs}Y_{rs}(s+h) + E_iY_{00}(-s-h)\delta_{r0}\delta_{s0}$$

$$= \sum_{m\in\Lambda} [a^*_{ms} + b^*_{ms}]J_{11}(rs;ms) + \sum_{m\in\Lambda'} [c^*_{ms} + d^*_{ms}]J_{12}(rs;ms) \qquad (8.39)$$

$$r,s \in (-\infty,\infty)$$

Here the modal inner products are defined by

$$J_{ij}(rs;ms) = d' \int_{-c}^{c} \underline{\overline{R}}_{i;rs} \cdot \underline{M}_{j;ms}\, dx \qquad i,j = 1,2 \qquad (8.40)$$

where $\underline{R}$ and $\underline{M}$ are defined by equations (8.12), (8.13) and (8.20), (8.21) respectively. Analytic expressions for these inner products are given in appendix 8.2. It is also to be noted that in deriving equation (8.39), the following relation has been used

$$\int_0^{d'}\int_{-c}^{c} \underline{\overline{R}}_{i;rs} \cdot \underline{M}_{j;mq} \exp[i(\gamma_q - \gamma_s)z]\, dxdz = J_{ij}(rs;mq)\, \delta_{sq}$$

Furthermore, the orthogonality properties of the plane wave terms have also been applied in the derivation of equation (8.39).

A second equation may be derived from equation (8.36) by multiplying throughout by the orthogonal plane wave term $\overline{\underline{RTM}}_{rs}(y=0)$ and integrating over the region $x \in [-c,c]$, $z \in [0,d']$ to yield

$$F_{rs}Y_{rs}(s+h) + F_iY_{00}(-s-h)\delta_{r0}\delta_{s0}$$

$$= \sum_{m=0}^{\infty}[a^*_{ms} + b^*_{ms}]J_{21}(rs;ms) + \sum_{m=1}^{\infty}[c^*_{ms} + d^*_{ms}]J_{22}(rs;ms)$$

$$r,s \in (-\infty,\infty) \qquad (8.41)$$

Consider briefly how this procedure is modified for the case of the crossed lamellar transmission grating with inclined axes. Equation (8.36) is replaced by

$$\sum_{p,q}\{[E_{pq}Y_{pq}(s+h) + E_iY_{00}(-s-h)\delta_{p0}\delta_{q0}]\underline{\underline{RTE'}}_{pq}(x',0,z')$$

$$+ [F_{pq}Y_{pq}(s+h) + F_iY_{00}(-s-h)\delta_{p0}\delta_{q0}]\underline{\underline{RTM'}}_{pq}(x',0,z')\}$$

$$= \sum_{m\in\Lambda}\sum_{q}[a^*_{mq} + b^*_{mq}]\underline{\underline{MTEU}}_{mq}(x',z') + \sum_{m\in\Lambda'}\sum_{q}[c^*_{mq} + d^*_{mq}]\underline{\underline{MTMU}}_{mq}(x',z')$$

$$\text{for } x' \in [-c\sin\eta, c\sin\eta]$$

$$= 0 \qquad \text{otherwise} \quad . \qquad (8.42)$$

Here $\underline{\underline{MTEU}}_{mq}(x',z')$ and $\underline{\underline{MTMU}}_{mq}(x',z')$ are given by equations (8.34) and (8.35) and $\underline{\underline{RTE'}}_{pq}(x',z')$ and $\underline{\underline{RTM'}}_{pq}(x',z')$ are given by equations (8.10) and (8.11), but α_p, γ_{pq} are replaced by α'_p, γ'_{pq}. In this case, the Method of Moments is applied by multiplying equation (8.42) by $\overline{\underline{\underline{RTE'}}}_{rs}(x',z')$ or $\overline{\underline{\underline{RTM'}}}_{rs}(x',z')$ and integrating the resulting equation over the region $x' \in [-c\sin\eta, c\sin\eta]$, $z' \in [0, d'/\sin\eta]$. Relations similar to equations (8.39) and (8.41) are derived, but naturally the inner products are different.

Attention is now returned to the crossed lamellar transmission grating with orthogonal axes of periodicity and the continuity of the transverse magnetic field is considered.

$$-\frac{1}{Z_0}\{\sum_{p,q}\{\frac{\beta_{pq}}{k}(E_{pq}Y_{pq}(s+h) - E_iY_{00}(-s-h)\delta_{p0}\delta_{q0})\underline{RTE}_{pq}(x,0,z)$$

$$+\frac{k}{\beta_{pq}}(F_{pq}Y_{pq}(s+h) - F_iY_{00}(-s-h)\delta_{p0}\delta_{q0})\underline{RTM}_{pq}(x,0,z)\}$$

$$=\frac{i}{Z_0}\{\sum_{m\epsilon\Lambda}\sum_{q}[(D_{1;mq}a^*_{mq} - D_{2;mq}b^*_{mq})\underline{MTEU}_{mq}(x,z)]$$

$$+\sum_{m\epsilon\Lambda'}\sum_{q}[(D_{3;mq}c^*_{mq} - D_{4;mq}d^*_{mq})\underline{MTMU}_{mq}(x,z)]\}$$

$$\text{if } x\epsilon[-c,c]$$

$$z\epsilon[0,d'] \qquad (8.43)$$

where
$$\left.\begin{aligned} D_{1;mq} &= \mu_{mq}\cot(\mu_{mq}h)/k \\ D_{2;mq} &= \mu_{mq}\tan(\mu_{mq}h)/k \\ D_{3;mq} &= k\cot(\mu_{mq})/\mu_{mq} \\ \text{and}\quad D_{4;mq} &= k\tan(\mu_{mq}h)/\mu_{mq}\ . \end{aligned}\right\} \qquad (8.44)$$

The Method of Moments is applied to this equation by multiplying throughout by the conjugate of either modal basis function $\overline{\underline{MTEU}}_{MQ}$ or $\overline{\underline{MTMU}}_{MQ}$ and integrating over the region $x\epsilon[-c,c]$, $z\epsilon[0,d']$ to yield

$$-\sum_{p}\{\frac{\beta_{pQ}}{k}[E_{pQ}Y_{pQ}(s+h) - E_iY_{00}(-s-h)\delta_{p0}\delta_{Q0}]\bar{J}_{11}(pQ;MQ)$$

$$+\frac{k}{\beta_{pQ}}[F_{pQ}Y_{pQ}(s+h) - F_iY_{00}(-s-h)\delta_{p0}\delta_{Q0}]\bar{J}_{21}(pQ;MQ)\}$$

$$=i(D_{1;MQ}a^*_{MQ} - D_{2;MQ}b^*_{MQ}) \qquad \text{for each } M\epsilon\Lambda,\ Q\epsilon(-\infty,\infty) \qquad (8.45)$$

and

$$- \sum_p \{ \frac{\beta_{pQ}}{k} [E_{pQ} Y_{pQ}(s+h) - E_i Y_{00}(-s-h)\delta_{p0}\delta_{Q0}] \bar{J}_{12}(pQ;MQ)$$

$$+ \frac{k}{\beta_{pQ}} [F_{pQ} Y_{pQ}(s+h) - F_i Y_{00}(-s-h)\delta_{p0}\delta_{Q0}] \bar{J}_{22}(pQ;MQ)\}$$

$$= i(D_{3;MQ} c^*_{MQ} - D_{4;MQ} d^*_{MQ})$$

$$\text{for each} \quad M \in \Lambda', \; Q \in (-\infty,\infty) \qquad (8.46)$$

Similarly, twelve equations may be derived from application of the Method of Moments to equations derived from applying the continuity conditions at the remaining grating surfaces. Integrations are performed over the rectangular apertures

(i) $z \in [0,d']$, $x \in [-c,c]$ for equations derived from continuity conditions at $y = s-h$ and

(ii) $z \in [-c',c']$, $x \in [0,d]$ for those derived from continuity conditions at $y = -s+h'$, $-s-h'$.

It is to be noted that for the case of the crossed lamellar transmission grating with inclined axes integrations for case (i) are performed over the region $z' \in [0,d'/\sin\eta]$, $x' \in [-c\sin\eta, c\sin\eta]$ and that the analysis is unchanged for the second grating.

Naturally, in the derivation of equations obtained from applying the continuity conditions at the lower grating surfaces, a new set of modal inner products must be defined and these are specified by

$$K_{ij}(rs;mr) = d \int_{-c'}^{c'} \bar{\hat{R}}_{i;rs} \cdot \hat{M}_{j;mr} \, dz \qquad i,j = 1,2 \qquad (8.47)$$

where $\hat{M}$ is given by equations (8.28) and (8.29)

$$\hat{R}_{j;pq} = V_j \exp(i\gamma_q z) \qquad j = 1,2 \qquad (8.48)$$

where the V_j are defined by equation (8.13).

Also, to simplify the equation, the following notation is introduced

$$\left.\begin{aligned} \left.\begin{matrix} \hat{a}^*_{mp} \\ \hat{c}^*_{mp} \end{matrix}\right\} &= \left.\begin{matrix} \hat{a}_{mp} \\ \hat{c}_{mp} \end{matrix}\right\} \sin(\hat{\mu}_{mp}h') \\ \left.\begin{matrix} \hat{b}^*_{mp} \\ \hat{d}^*_{mp} \end{matrix}\right\} &= \left.\begin{matrix} \hat{b}_{mp} \\ \hat{d}_{mp} \end{matrix}\right\} \cos(\hat{\mu}_{mp}h') \end{aligned}\right\} \qquad (8.49)$$

Then following an exactly analogous treatment to that described in chapter 6, the following matrix equations are obtained constraining the unknown modal coefficients. In these equations the integers P,Q take values in the range $(-\infty,\infty)$.

$$\begin{aligned} 2[\frac{\beta_{00}}{k}E_i\bar{J}_{11}(00;M0) + \frac{k}{\beta_{00}}F_i\bar{J}_{21}(00;M0)]Y_{00}(-s-h) \\ = \sum_{m\epsilon\Lambda} a^*_{mQ}[\sum_p L_{11}(pQ;mM) + iD_{1;MQ}\delta_{Mm}] \\ + \sum_{m\epsilon\Lambda} b^*_{mQ}[\sum_p L_{11}(pQ;mM) - iD_{2;MQ}\delta_{Mm}] \\ + \sum_{m\epsilon\Lambda'} (c^*_{mQ} + d^*_{mQ})[\sum_p L_{12}(pQ;mM)] \end{aligned}$$

$$M \epsilon \Lambda \qquad (8.50)$$

where $$L_{ij}(pQ;mM) = \sum_{n=1,2} \bar{J}_{ni}(pQ;MQ)\chi_{nn}(p,Q)J_{nj}(pQ;mQ) \qquad (8.51)$$

and χ is a 2×2 matrix given by

$$\chi(p,Q) = \begin{bmatrix} \beta_{pQ}/k & 0 \\ 0 & k/\beta_{pQ} \end{bmatrix} \qquad (8.52)$$

$$2\left[\frac{\beta_{00}}{k}E_i\bar{J}_{12}(00;M0) + \frac{k}{\beta_{00}}F_i\bar{J}_{22}(00;M0)\right]Y_{00}(-s-h)$$

$$= \sum_{m\in\Lambda}[a^*_{mQ} + b^*_{mQ}]\left[\sum_p L_{21}(pQ;mM)\right] + \sum_{m\in\Lambda'} c^*_{mQ}\left[\sum_p L_{22}(pQ;mM) + iD_{3;mQ}\delta_{mM}\right]$$

$$+ \sum_{m\in\Lambda'} d^*_{mQ}\left[\sum_p L_{22}(pQ;mM) - iD_{4;mQ}\delta_{mM}\right] \qquad M\in\Lambda' \tag{8.53}$$

$$\sum_{m\in\Lambda} a^*_{mQ}\left[\sum_p T_{pQ}L_{11}(pQ;mM) + iD_{1;mQ}\delta_{mM}\right] + \sum_{m\in\Lambda} b^*_{mQ}\left[-\sum_p T_{pQ}L_{11}(pQ;mM) + iD_{2;mQ}\delta_{mM}\right]$$

$$+ \sum_{m\in\Lambda'}(c^*_{mQ} - d^*_{mQ})\left(\sum_p T_{pQ}L_{12}(pQ;mM)\right] + \sum_{m\in\Lambda}\sum_p(\hat{a}^*_{mp} + \hat{b}^*_{mp})[-T'_{pQ}N_{11}(pQ;mM)]$$

$$+ \sum_{m\in\Lambda'}\sum_p(\hat{c}^*_{mp} + \hat{d}^*_{mp})[-T'_{pQ}N_{12}(pQ;mM)] = 0 \qquad M\in\Lambda' \tag{8.54}$$

where
$$\left.\begin{aligned} T_{pq} &= i\cot(\beta_{pq}S) \\ T'_{pq} &= \frac{1}{i\sin(\beta_{pq}S)} \end{aligned}\right\} \tag{8.55}$$

and
$$N_{ij}(pQ,mM) = \sum_{n=1,2}\bar{J}_{ni}(pQ;MQ)\chi_{nn}(pQ)K_{nj}(pQ;mp) \tag{8.56}$$

$$\sum_{m\in\Lambda}(a^*_{mQ} - b^*_{mQ})\left[\sum_p T_{pQ}L_{21}(pQ;mM)\right] + \sum_{m\in\Lambda'} c^*_{mQ}\left[\sum_p T_{pQ}L_{22}(pQ;mM) + iD_{3;mQ}\delta_{mM}\right]$$

$$+ \sum_{m\in\Lambda'} d^*_{mQ}\left[-\sum_p T_{pQ}L_{22}(pQ;mM) + iD_{4;mQ}\delta_{mM}\right]$$

$$+ \sum_{m\in\Lambda}\sum_p(\hat{a}^*_{mp} + \hat{b}^*_{mp})[-T'_{pQ}N_{21}(pQ;mM)]$$

$$+ \sum_{m\in\Lambda'}\sum_p(\hat{c}^*_{mp} + \hat{d}^*_{mp})[-T'_{pQ}N_{22}(pQ;mM)] = 0 \qquad M\in\Lambda' \tag{8.57}$$

$$\sum_{m\in\Lambda}\sum_{q}(-a^{*}_{mq}+b^{*}_{mq})[T'_{Pq}\hat{N}_{11}(Pq;mM)]+\sum_{m\in\Lambda'}\sum_{q}(-c^{*}_{mq}+d^{*}_{mq})[T'_{Pq}\hat{N}_{12}(Pq;mM)]$$

$$+\sum_{m\in\Lambda}\hat{a}^{*}_{mP}[\sum_{q}T_{Pq}\hat{L}_{11}(Pq;mM)+i\hat{D}_{1;mP}\delta_{mM}]$$

$$+\sum_{m\in\Lambda}\hat{b}^{*}_{mP}[\sum_{q}T_{Pq}\hat{L}_{11}(Pq;mM)-i\hat{D}_{2;mP}\delta_{mM}]$$

$$+\sum_{m\in\Lambda'}(\hat{c}^{*}_{mP}+\hat{d}^{*}_{mP})[\sum_{q}T_{Pq}\hat{L}_{12}(Pq;mM)]=0 \qquad M\in\Lambda \tag{8.58}$$

where $$\hat{N}_{ij}(Pq;mM)=\sum_{n=1,2}\overline{K}_{ni}(Pq;MP)\chi_{nn}(Pq)J_{nj}(Pq;mq) \tag{8.59}$$

$$\hat{L}_{ij}(Pq;mM)=\sum_{n=1,2}\overline{K}_{ni}(Pq;MP)\chi_{nn}(Pq)K_{nj}(Pq;mP) \tag{8.60}$$

and $\hat{D}_{i;mp}$ (for $i = 1,4$) are given by equations (8.44) but μ_{mq} and h are replaced by $\hat{\mu}_{mp}$ and h' respectively.

$$\sum_{m\in\Lambda}\sum_{q}(-a^{*}_{mq}+b^{*}_{mq})[T'_{Pq}\hat{N}_{21}(Pq;mM)]+\sum_{m\in\Lambda'}\sum_{q}(-c^{*}_{mq}+d^{*}_{mq})[T'_{Pq}\hat{N}_{22}(Pq;mM)]$$

$$+\sum_{m\in\Lambda}(\hat{a}^{*}_{mP}+\hat{b}^{*}_{mP})[\sum_{q}T_{Pq}\hat{L}_{21}(Pq;mM)]$$

$$+\sum_{m\in\Lambda'}\hat{c}^{*}_{mP}[\sum_{q}T_{Pq}\hat{L}_{22}(Pq;mM)+i\hat{D}_{3;mP}\delta_{Mm}]$$

$$+\sum_{m\in\Lambda'}\hat{d}^{*}_{mP}[\sum_{q}T_{Pq}\hat{L}_{22}(Pq;mM)-i\hat{D}_{4;mP}\delta_{Mm}]=0 \qquad M\in\Lambda' \tag{8.61}$$

$$\sum_{m\in\Lambda}\hat{a}^{*}_{mP}[-\sum_{q}\hat{L}_{11}(Pq;mM)-i\hat{D}_{1;mP}\delta_{Mm}]+\sum_{m\in\Lambda}\hat{b}^{*}_{mP}[\sum_{q}\hat{L}_{11}(Pq;mM)-i\hat{D}_{2;mP}\delta_{mM}]$$

$$+\sum_{m\in\Lambda'}(-\hat{c}^{*}_{mP}+\hat{d}^{*}_{mP})[\sum_{q}\hat{L}_{12}(Pq;mM)]=0 \qquad M\in\Lambda \tag{8.62}$$

and finally,

$$\sum_{m\in\Lambda}(-\hat{a}^{*}_{mP}+\hat{b}^{*}_{mP})\Big[\sum_{q}\hat{L}_{21}(Pq;mM)\Big]+\sum_{m\in\Lambda'}\hat{c}^{*}_{mP}\Big[-\sum_{q}\hat{L}_{22}(Pq;mM)-i\hat{D}_{3;mP}\delta_{mM}\Big]$$

$$+\sum_{m\in\Lambda'}\hat{d}^{*}_{mP}\Big[\sum_{q}\hat{L}_{22}(Pq;mM)-i\hat{D}_{4;mP}\delta_{mM}\Big]=0 \qquad M\in\Lambda' \tag{8.63}$$

Thus eight matrix equations (8.50, 53, 54, 57, 58, 61-63) which are functions of the eight infinite sets of modal coefficients have been derived. Solution of this set of relations and reconstruction of the Rayleigh coefficients permits evaluation of the reflected and transmitted energies associated with each order and mode as a function of wavelength and grating parameters.

8.2.2.5 *Numerical Solution of the Equations*

The matrix equations derived in the previous section involve infinite summations over the Rayleigh orders p,q and the modal index m. Since these summations must be truncated to obtain a numerical solution, reciprocity and conservation of energy tests are needed to verify the accuracy of the numerical results. The numerical implementation of the formalism was also tested against a new constraint derived in appendix 8.3. This result constrains the complex amplitudes of the diffracted field quantities of a doubly periodic structure having rectangular axes of symmetry, operated in a Littrow mount. For a (f,g) order Littrow mount, the result is expressed simply by

$$\mathrm{Re}\Big\{\sum_{p,q}\Big[\frac{\beta_{pq}}{k}\big(E_{pq}\bar{E}_{f-p,g-q}+\hat{E}_{pq}\bar{\hat{E}}_{f-p,g-q}\big)$$

$$+\frac{k}{\beta_{pq}}\big(F_{pq}\bar{F}_{f-p,g-q}+\hat{F}_{pq}\bar{\hat{F}}_{f-p,g-q}\big)\Big]\Big\}=0 \tag{8.64}$$

Numerical confirmations of this test and the Reciprocity Theorem are given in tables 8.2 and 8.1 respectively.

Table 8.1 Numerical Confirmation of the Reciprocity Theorem

Grating Parameters: $d = 1.0$, $d' = 1.2$, $2c = 0.25$, $2c' = 0.4$, $S = 0.4$, $2h = 2h' = 0.6$ (all lengths in arbitrary units).

Wavelength: $\lambda/d = 1.1$

Incidence Parameters: Problem 1 - $\phi = 30^\circ$, $\psi = 35^\circ$, $\delta = 90^\circ$
Problem 2 - $\phi = 48.46421^\circ$, $\psi = -22.52765^\circ$, $\delta = 90^\circ$ (return of (-1,0) order)

Method Parameters: 4 modal indices and 5 Rayleigh orders to describe the diffracted fields in both arrays.

	E_{-10}	F_{-10}	E.T.
Problem 1	$(0.10428, -7.710^\circ)$	$(0.34942, -168.887^\circ)$	0.00287
Problem 2	$(0.22526, -172.764^\circ)$	$(0.34979, -168.887^\circ)$	0.00457

This table confirms the reciprocity relation:

$$\beta_{pq}\cos\delta' E_{pq} + k\sin\delta' F_{pq} = \beta_{00}\cos\delta E'_{pq} + k\sin\delta F'_{pq} \quad \text{(see [8.17])}$$

Table 8.2 Demonstration of the Properties of the Littrow Expression for a (-1, -1) order Littrow Mount

Grating Parameters: $d/d' = 1.0$, $2c/d = 2c'/d = 0.9$, $S/d = 0.6$, $2h/d = 2h'/d = 0.3$

Wavelength: $\lambda/d = 1.2$

Incidence Parameters: $\phi = 58.0596^\circ$, $\psi = 45^\circ$, $\delta = 0^\circ$.

In each case, the same set of Rayleigh orders and waveguide modes were used to describe the diffracted fields in the two arrays.

Rayleigh orders	0, -1,1	0, -1,1, -2,2	0, -1,1, -2
Waveguide modes	0,1,2	0,1,2	0,1,2
L.H.S. of Littrow expression	3.83×10^{-3}	3.78×10^{-4}	5.96×10^{-11}

It should be noted that these equations cannot be decoupled as was possible for the inductive grid [8.6] and numerical solution for N modal indices and Q Rayleigh orders in both arrays involves inversion of a matrix with $2 \times Q \times (4N - 2)$ complex elements. For $N = 3$ and $Q = 5$, this solution requires 176 seconds of central processor time on the Burroughs B6700 computer. Thus, machine computation time and array storage limit the number of modal quantities which can be determined. If too many orders are propagating the matrices to be generated become too large and consequently the numerical solution has been restricted to normalised wavelengths (λ/d and λ/d') in excess of 0.5.

8.2.3 A Multiple-Scattering Theory for the Crossed Lamellar Transmission Grating with Orthogonal Periodicity Axes

In this section a rigorous multiple scattering approach is used to analyse the diffraction properties of the crossed lamellar transmission grating with orthogonal axes of periodicity.

8.2.3.1 *The Multiple Scattering Analysis*

The notations introduced in section 8.2.1 will be used in this section. Again the analysis is simplified if the electric and magnetic fields are expressed in terms of TE and TM components.

The diffracted fields in the three free space regions are composed of plane waves propagating in directions $(\alpha_p, \beta_{pq}, \gamma_q)$ where the direction cosines are again specified by equations (8.4) to (8.6).

The complex amplitudes of the TE and TM components of the incident field are denoted by E_i and F_i as in section 8.2.1, with the phase origin of these amplitudes being the centre of the grating. The complex amplitudes of the incident field with respect to the centre of the upper grating are denoted by E^i and F^i. The response of the upper grating to this incident field is now considered. The TE/TM

amplitudes for the $(p,q)^{th}$ order diffracted by this grating in reflection and transmission are written respectively as E_{pq}, F_{pq}, E^{-}_{pq} and F^{-}_{pq}. Here the phase origin of these quantities is taken to be the centre of the upper grating and thus the amplitudes E_{pq}, F_{pq} are different in phase to those introduced in section 8.2.2.

The amplitude E_{pq} is determined not only by the TE coefficient E^i in the incident field, but also by F^i, and similarly for F_{pq}. The linearity of the diffraction process enables E_{pq}, F_{pq} to be related to E^i, F^i by a matrix expression,

$$\begin{bmatrix} E_{pq} \\ F_{pq} \end{bmatrix} = \begin{bmatrix} E^{ee}_{pq} & kE^{em}_{pq} / \beta_{pq} \\ F^{me}_{pq} & kF^{mm}_{pq} / \beta_{pq} \end{bmatrix} \begin{bmatrix} E^i \\ F^i \end{bmatrix} \tag{8.65}$$

where E^{ee}_{pq} and F^{me}_{pq} are the amplitudes of waves reflected by the upper grating when a TE polarized wave $(\delta = 0^o)$ is incident upon it, while E^{em}_{pq} and F^{mm}_{pq} are the corresponding quantities for a TM polarized incident wave.

In order to perform the multiple scattering analysis, the response of the upper grating not only to this incident wave, but also to a wave incident in the general channel (r,s) needs to be characterised. The corresponding scattering matrix elements are written with subscripts $pq;rs$ where (r,s) denotes the incident channel and (p,q) the diffracted channel. It is to be noted that the diffraction process by the first grating changes only the first subscript, so that a typical non-zero matrix element for it has subscripts $ps;rs$.

A vector C^i describing the most general incident field is introduced:

$$C^i = \begin{bmatrix} [E^i_{rs}] \\ [F^i_{rs}] \end{bmatrix} \tag{8.66}$$

where the TE coefficients in all possible channels (r,s) are listed, followed by the TM coefficients in all incident channels. A similar notation is used for the vector C^r characterising the field diffracted by the upper grating into the region $y > s + h$:

$$C^r = \begin{bmatrix} [E_{pq}] \\ [F_{pq}] \end{bmatrix} . \tag{8.67}$$

The vectors C^r and C^i are linked by the matrix equation

$$C^r = \rho C^i \tag{8.68}$$

where ρ is the reflection scattering matrix for the upper grating:

$$\rho = \begin{bmatrix} [E^{ee}_{pq;rs}] & [kE^{em}_{pq;rs} / \beta_{pq}] \\ [F^{me}_{pq;rs}] & [kF^{mm}_{pq;rs} / \beta_{pq}] \end{bmatrix} . \tag{8.69}$$

Similar notations describe the setting up of a field transmitted by the upper grating

$$C^- = \begin{bmatrix} [E^-_{pq}] \\ [F^-_{pq}] \end{bmatrix} \tag{8.70}$$

and

$$C^- = \tau C^i \tag{8.71}$$

The transmitted field C^- from the upper grating travels downward through a distance (2s) from the phase origin at $y = s$ to that for the

lower grating at $y = -s$. A transfer matrix P is used to calculate the amplitude modifications resulting from this propagation:

$$P = \begin{bmatrix} [p_{pq;rs}] & [p_{pq;rs}] \\ [p_{pq;rs}] & [p_{pq;rs}] \end{bmatrix} \tag{8.72}$$

where $$p_{pq;rs} = \delta_{pr}\delta_{qs}\exp(2i\beta_{pq}s) \tag{8.73}$$

The incident field vector for the lower grating is then PC^-. The diffraction by this grating is characterised by scattering matrices ρ' and τ' (for the reflected and transmitted fields respectively). Thus, the reflected and transmitted field vectors are respectively

$$C^+ = \rho' PC^- \tag{8.74}$$

and $$C^t = \tau' PC^- \tag{8.75}$$

The reflected field vector C^+ of (8.74) gives, after multiplication by P, the vector characterising a field incident from below on the upper grating. This is shown in figure 8.4. By utilizing the up-down symmetry of the individual grating elements and the principle of linear superposition, the following relations constraining the scattered fields are derived;

$$\begin{bmatrix} C^r \\ C^- \end{bmatrix} = \begin{bmatrix} \rho & \tau \\ \tau & \rho \end{bmatrix} \begin{bmatrix} C^i \\ PC^+ \end{bmatrix} \tag{8.76}$$

$$\begin{bmatrix} C^+ \\ C^t \end{bmatrix} = \begin{bmatrix} \rho' & \tau' \\ \tau' & \rho' \end{bmatrix} \begin{bmatrix} PC^- \\ 0 \end{bmatrix} \tag{8.77}$$

Upon elimination of C^- and C^+ from equations (8.76) and (8.77),

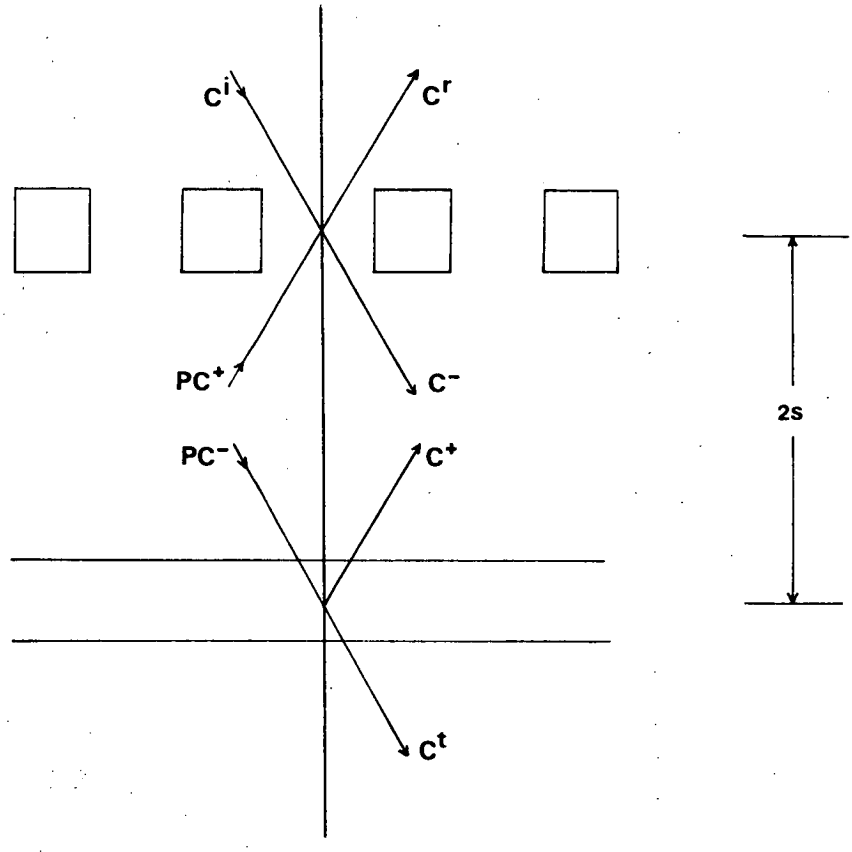

Figure 8.4 The fields considered in the multiple scattering analysis.

It follows that

$$C^r = [\rho + \tau P\rho' P(I - \rho P\rho' P)^{-1}\tau]C^i \tag{8.78}$$

and

$$C^t = \tau' P(I - \rho P\rho' P)^{-1}\tau C^i \tag{8.79}$$

where I denotes the identity matrix of appropriate dimension. Equations (8.78) and (8.79) could be derived by noting that

$$(I - \rho P\rho' P)^{-1} = (I + \rho P\rho' P + (\rho P\rho' P)^2 + ...) \quad .$$

Thus, for example, equation (8.78) is

$$C^r = \rho C^i + \tau P\rho' P(I + \rho P\rho' P + (\rho P\rho' P)^2 + ...)\tau C^i$$

which represents the steps of a multiple scattering analysis.

Although this alternative equation makes the analysis easy to comprehend, it is difficult to use this representation to derive equation (8.78) since it is not easy to establish the necessary and sufficient condition that the spectral radius of $\rho P\rho' P$ be less than 1, and hence show the existence of the inverse.

Given the four scattering matrices ρ, τ, ρ' and τ', the reflected and transmitted fields for the structure may be obtained from equations (8.78) and (8.79).

8.2.3.2 *The Lamellar Grating in Conical Diffraction*

This section considers the evaluation of the scattering matrices for the two lamellar gratings composing the structure. It is noted that the response of each grating is required not only for all possible propagating incident waves, but also for all evanescent waves, which are capable of providing significant coupling between the two gratings. Also, it is noted that some waves strike each grating out of their principal plane. That is, they give rise to conical diffraction effects.

For a propagating incident wave in conical diffraction, a theorem due to Maystre [8.14] permits the evaluation of the reflected and transmitted fields, knowing only how the grating responds to waves incident in the classical diffraction mounts. However, Maystre's Theorem does not apply to evanescent waves incident in conical diffraction. For this reason, the formalism described in this section has been developed for perfectly conducting lamellar gratings utilised in conical diffraction.

The upper element of the crossed lamellar transmission grating is considered in this derivation. A plane wave is assumed to be approaching the upper grating from above in the channel (r,s). The polarization of the plane wave is specified by the TE/TM complex amplitudes E^i_{rs} and F^i_{rs} respectively. In the region $y > s + h$, the electric field is written, where $y' = y - s$

$$\underline{E}_t = \sum_p \{ [E_{ps;rs}\exp(i\beta_{ps}y') + E^i_{rs}\exp(-i\beta_{rs}y')\delta_{pr}]\underline{RTE}_{ps}(x,0,z)$$

$$+ [F_{ps,rs}\exp(i\beta_{ps}y') + F^i_{rs}\exp(-i\beta_{rs}y')\delta_{pr}]\underline{RTM}_{ps}(x,0,z)\} \qquad (8.80)$$

The vector bases functions are defined by equations (8.10) to (8.13). Similarly for the transmitted field in $y < s - h$

$$\hat{\underline{E}}_t = \sum_p [\hat{E}_{ps;rs}\exp(-i\beta_{ps}y')\underline{RTE}_{ps}(x,0,z) + \hat{F}_{ps;rs}\exp(-i\beta_{ps}y')\underline{RTM}_{ps}(x,0,z)] \qquad (8.81)$$

The following modal expansion is used to specify the field in the groove region of the upper grating, $s - h < y < s + h$

$$\underline{E}_t = \sum_m \{ [a_m\sin(\mu_{ms}y') + b_m\cos(\mu_{ms}y')]\underline{M}_{1;ms} +$$

$$+ [c_m\sin(\mu_{ms}y') + d_m\cos(\mu_{ms}y')]\underline{M}_{2;ms}\} \exp(i\gamma_s z) \qquad (8.82)$$

where $\underline{M}_1$ and $\underline{M}_2$ are defined by equations (8.20) and (8.21) respectively, and μ_{ms} is defined by equation (8.25).

The use of Maxwell's equation permits the deduction of the transverse resolutes of the magnetic fields in all three regions. As in section 8.2.2.3, the diffraction problem is solved by applying the continuity conditions on the electric and magnetic fields at the aperture boundaries $y' = \pm h$, and the boundary conditions on the electric field in the metallic region of the planes $y' = \pm h$. The structure, however, in this case is up-down symmetric and this permits a decoupling of the field problem into its y-symmetric and y-antisymmetric parts.

Consider the y-antisymmetric problem firstly. The equations derived from the continuity of $\underline{E}_t$ at $y' = \pm h$ may be written, after multiplying by $\overline{\underline{RTE}}_{ps}(x,z)$ and integrating over the aperture region $x \in [-c,c]$

$$E_{ps;rs}Y_{ps}(h) + E^{i}_{rs}Y_{rs}(-h)\delta_{pr} = \sum_{m\epsilon\Lambda} (a^{*}_{m} + b^{*}_{m})J'_{11}(ps;ms) + \sum_{m\epsilon\Lambda'} (c^{*}_{m} + d^{*}_{m})J'_{12}(ps;ms) \quad (8.83)$$

and

$$\hat{E}_{ps;rs}Y_{ps}(-h) = \sum_{m\epsilon\Lambda} (-a^{*}_{m} + b^{*}_{m})J'_{11}(ps,ms) + \sum_{m\epsilon\Lambda'} (-c^{*}_{m} + d^{*}_{m})J'_{12}(ps;ms) \quad (8.84)$$

Here the inner products J'_{ij} are given by

$$J'_{ij} = J_{ij}/d'$$

where J_{ij} is defined in equation (8.40), and a^{*}_{m}, b^{*}_{m}, c^{*}_{m} and d^{*}_{m} are

defined by equation (8.38). Also $Y_{rs}(y)$ is defined by equation (8.37).

The y-symmetric modes may now be eliminated from equations (8.83) and (8.84) by taking their difference:

$$E_{ps;rs}Y_{ps}(h) - \hat{E}_{ps;rs}Y_{ps}(-h) + E^{i}_{rs}Y_{rs}(-h)\delta_{pr}$$

$$= 2\{ \sum_{m\epsilon\Lambda} a^{*}_{m}J'_{11}(ps;ms) + \sum_{m\epsilon\Lambda'} c^{*}_{m}J'_{12}(ps;ms) \qquad (8.85)$$

Using a similar analysis, it follows that

$$F_{ps;rs}Y_{ps}(h) - \hat{F}_{ps;rs}Y_{ps}(-h) + F^{i}_{rs}Y_{rs}(h)\delta_{pr}$$

$$= 2\{ \sum_{m\epsilon\Lambda} a^{*}_{m}L'_{21}(ps;ms) + \sum_{m\epsilon\Lambda'} c^{*}_{m}L'_{22}(ps;ms)\} \qquad (8.86)$$

The magnetic field continuity conditions may be derived in a similar manner to that described in section 8.2.2.3. These can be written for the y-antisymmetric problem as

$$\sum_{p} \{\frac{\beta_{ps}}{k} [E_{ps;rs}Y_{ps}(h) - \hat{E}_{ps;rs}Y_{ps}(-h) - E^{i}_{rs}Y_{rs}(-h)\delta_{pr}] \bar{J}'_{11}(ps;Ms)$$

$$+ \frac{k}{\beta_{ps}} [F_{ps;rs}Y_{ps}(h) - \hat{F}_{ps;rs}Y_{ps}(-h) - F^{i}_{rs}Y_{rs}(-h)\delta_{pr}] \bar{J}'_{21}(ps;Ms)$$

$$= -2i \frac{\mu_{Ms}}{k} a^{*}_{M}\cot(\mu_{Ms}h) \qquad M \epsilon \Lambda \qquad (8.87)$$

and

$$\sum_{p} \{ \frac{\beta_{ps}}{k} [E_{ps;rs}Y_{ps}(h) - \hat{E}_{ps;rs}Y_{ps}(-h) - E^{i}_{rs}Y_{rs}(-h)\delta_{pr}] \bar{J}'_{12}(ps;Ms)$$

$$+ \frac{k}{\beta_{ps}} [F_{ps;rs}Y_{ps}(h) - \hat{F}_{ps;rs}Y_{ps}(-h) - F^{i}_{rs}(-h)\delta_{pr}] \bar{J}'_{22}(ps;Ms)$$

$$= -2i \frac{k}{\mu_{Ms}} c^{*}_{M}\cot(\mu_{Ms}h) \qquad M \epsilon \Lambda' \qquad (8.88)$$

Substitution of equations (8.85) and (8.86) in equations (8.87) and (8.88) leads to the following equations:

$$\sum_{m\epsilon\Lambda} \Big\{ a_m^* \Big\{ \sum_p \Big[\frac{\beta_{ps}}{k} J'_{11}(ps;ms)\bar{J}'_{11}(ps;Ms) + \frac{k}{\beta_{ps}} J'_{21}(ps;ms)\,\bar{J}'_{21}(ps;ms)\Big] + i\,\frac{\mu_{Ms}}{k}\cot(\mu_{Ms}h)\delta_{mM}\Big\}\Big\}$$

$$+ \sum_{m\epsilon\Lambda'} \Big\{ c_m^* \Big\{\sum_p \Big[\frac{\beta_{ps}}{k} J'_{12}(ps;Ms)\bar{J}'_{11}(ps;Ms) + \frac{k}{\beta_{ps}} J'_{22}(ps;ms)\bar{J}'_{21}(ps;Ms)\Big]\Big\}\Big\}$$

$$= \delta_{pr}\Big[\frac{\beta_{ps}}{k} E^i_{ps}\bar{J}'_{11}(ps;Ms) + \frac{k}{\beta_{ps}} F^i_{ps}\bar{J}'_{21}(ps;Ms)\Big]\, Y_{ps}(-h)$$

$$M \in \Lambda \qquad (8.89)$$

and

$$\sum_{m\epsilon\Lambda} \Big\{ a_m^* \Big\{\sum_p \Big[\frac{\beta_{ps}}{k} J'_{11}(ps;ms)\,\bar{J}'_{12}(ps;Ms) + \frac{k}{\beta_{ps}} J'_{21}(ps;ms)\,\bar{J}'_{22}(ps;Ms)\Big]\Big\}\Big\}$$

$$+ \sum_{m\epsilon\Lambda'} \Big\{ c_m^* \Big\{\sum_p \Big[\frac{\beta_{ps}}{k} J'_{12}(ps;ms)\,\bar{J}'_{12}(ps;Ms) + \frac{k}{\beta_{ps}} J'_{22}(ps;ms)\,\bar{J}'_{22}(ps;Ms)\Big] + i\,\frac{k}{\mu_{Ms}}\cot(\mu_{Ms}h)\delta_{mM}\Big\}\Big\}$$

$$= \delta_{pr}\Big[\frac{\beta_{ps}}{k} E^i_{ps}\,\bar{J}'_{12}(ps;Ms) + \frac{k}{\beta_{ps}} F^i_{ps}\,\bar{J}'_{22}(ps;Ms)\Big]\, Y_{ps}(-h)$$

$$M \in \Lambda' \qquad (8.90)$$

Corresponding equations for the y-symmetric modal amplitudes b_m^* and d_m^* may be derived by replacing "cot" by "-tan" in equations (8.89) and (8.90).

A set of linear equations has thus been derived, which permits the evaluation of the modal amplitudes and through them, the plane wave

coefficients. Although attention has been restricted to the upper grating, analogous methods enable the evaluation of the scattering matrices for the lower grating. In this case, however, the plane wave coefficients are subscripted by (rq;rs) and the mode functions are given by equations (8.28) and (8.29).

8.2.3.3 *Numerical Considerations*

The multiple scattering formalism presented in section 8.2.3.1, in conjunction with the single lamellar grating formalism described in section 8.2.3.2 was implemented numerically. A flow chart for this problem is given in figure 8.5.

Numerical solution for this problem thus involves solving each single lamellar diffraction problem for each order (p,q) (with the integers p and q taking values $-(Q-1)/2$ to $(Q-1)/2$) chosen to couple the arrays and then evaluating the multiple scatter expressions (8.78) and (8.79). If N modal indices and R Rayleigh orders are used to describe the fields for each single lamellar grating problem, then the matrices to be inverted are of dimension N and are thus independent of the number of Rayleigh orders. However, the matrix to be inverted in the expression (8.78) is of dimension $2 \times Q^2$. Thus most of the processor time is expended in the evaluation of the multiple scattering expressions.

This procedure is therefore more computationally efficient than the method described in section 8.2.2, provided that the wavelength to period ratio and the separation of the elements is sufficiently large so that few orders couple the arrays. As the wavelength to period ratio becomes smaller and more orders propagate, the size of the scattering matrices becomes prohibitively large and the computational efficiency of the method drops rapidly.

Figure 8.5 Flow chart for the multiple scattering program

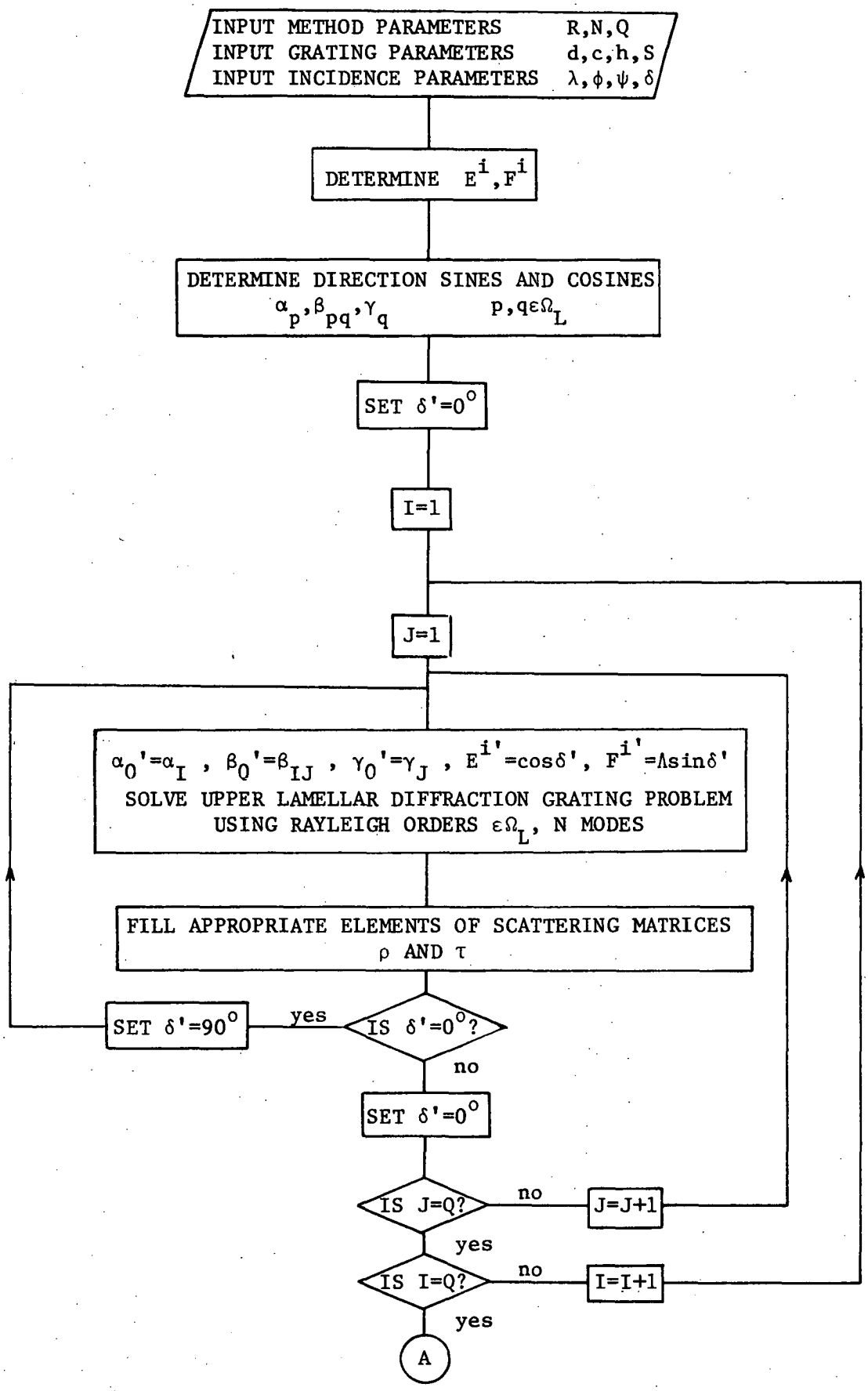

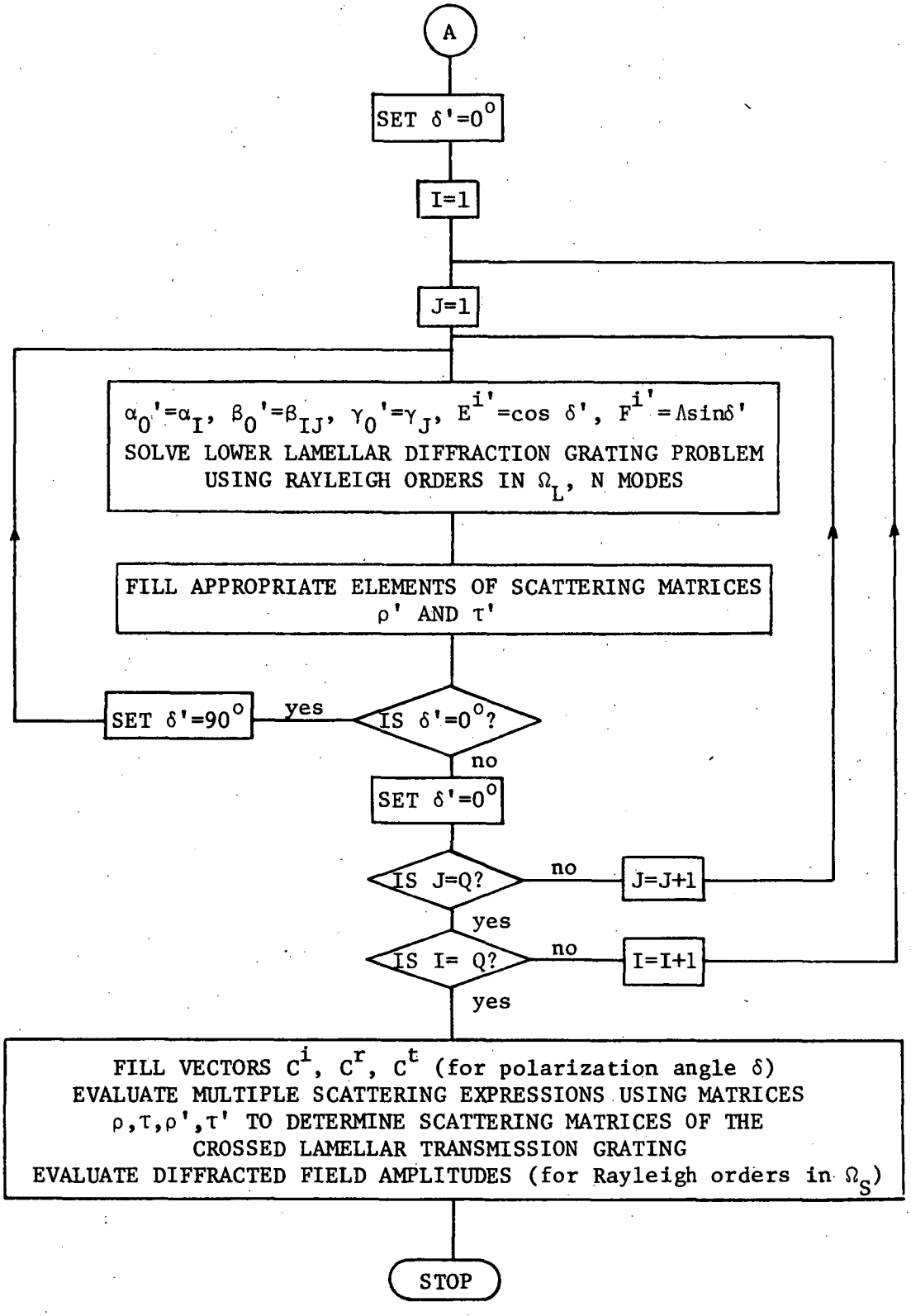

Note: $\Omega_L = \{(p,q) \mid p=1,\ldots R,\ q=1,\ldots R\}$

$\Omega_S = \{(p,q) \mid p=1,\ldots Q,\ q=1,\ldots Q\}$

$\Lambda = \beta_0' / k$

This formalism was verified numerically using the well-known constraints of conservation of energy and reciprocity. Results of a test confirming the Reciprocity Theorem is given in table 8.3.

8.3 SPECTRAL PROPERTIES AND SOLAR SELECTIVITY

In this section, the performance of the crossed lamellar transmission grating with orthogonal axes of periodicity is discussed and in particular, the grating parameters are optimised for the application of the structure as a solar selective surface. This investigation is carried out using the formalism described in section 8.2.2.

8.3.1 Spectral Characteristics

The diffraction properties of the crossed lamellar transmission grating have been extensively studied in the area where the grating periods are comparable with the wavelength of the incident radiation. Figure 8.6 shows the spectral characteristics of a typical grating used in normally incident radiation. This curve, characterising the behaviour of this class of gratings, can be divided into three main regions

- the transmission region $\lambda/d \leq 1.0$,
- the transition region $1.0 \leq \lambda/d \leq 2.5$,
- the long wavelength filtering region $\lambda/d \geq 2.5$.

In this figure, the broken curve designates the energy transmitted through the grating by the (0,0) order E.T.(0,0), while the total energy transmitted through the grating is indicated by the solid curve. It is seen that the (0,0) order no longer carries the total energy below the Wood anomaly when the higher orders begin to propagate. This anomaly separates the transmission and transition regions of the spectrum. For the grating discussed in figure 8.6, five orders in both reflection and transmission propagate immediately below the Wood anomaly, whereas only

Table 8.3 Confirmation of the Reciprocity Theorem Using the Multiple Scattering Formalism

Grating Parameters: $d = 1.0$, $c/d = 0.8$, $h/d = 0.2$, $S/d = 1.0$, $\eta = 90^{\circ}$

Wavelength: $\lambda/d = 0.95$

Incidence Parameters: Problem 1 - $\phi = 10^{\circ}$, $\psi = 20^{\circ}$, $\delta = 90^{\circ}$
Problem 2 - $\phi = 10^{\circ}$, $\psi = 20^{\circ}$, $\delta = 0^{\circ}$
Problem 3 - $\phi = 52.11^{\circ}$, $\psi = -4.32^{\circ}$, $\delta = 0^{\circ}$
(return (-1,0) order)

Method Parameters: 15 Rayleigh orders, 6 modes for each single lamellar diffraction problem.

3 orders in multiple scattering analysis.

Problem	E_{-10}	F_{-10}	E.T.
1	(0.223723 ,-46.2539°)	(0.212196 ,106.9350°)	0.7720
2	(0.556825 ,136.3660°)	(0.109583 ,108.8331°)	0.7354
3	(0.347288 ,136.3808°)	(0.137408 ,-46.2537°)	0.2708

The left and right hand sides of the Reciprocity relation

$$\beta_{pq}\cos\delta' E_{pq} + k\sin\delta' F_{pq} = \beta_{00}\cos\delta E'_{pq} + k\sin\delta F'_{pq} \quad \text{(see [8.17])}$$

are calculated to be

(0.908700, -46.2539°) and (0.908705, -46.2537°) for problems 1 and 3,

(2.261664, 136.3660°) and (2.261787, 136.3808°) for problems 2 and 3.

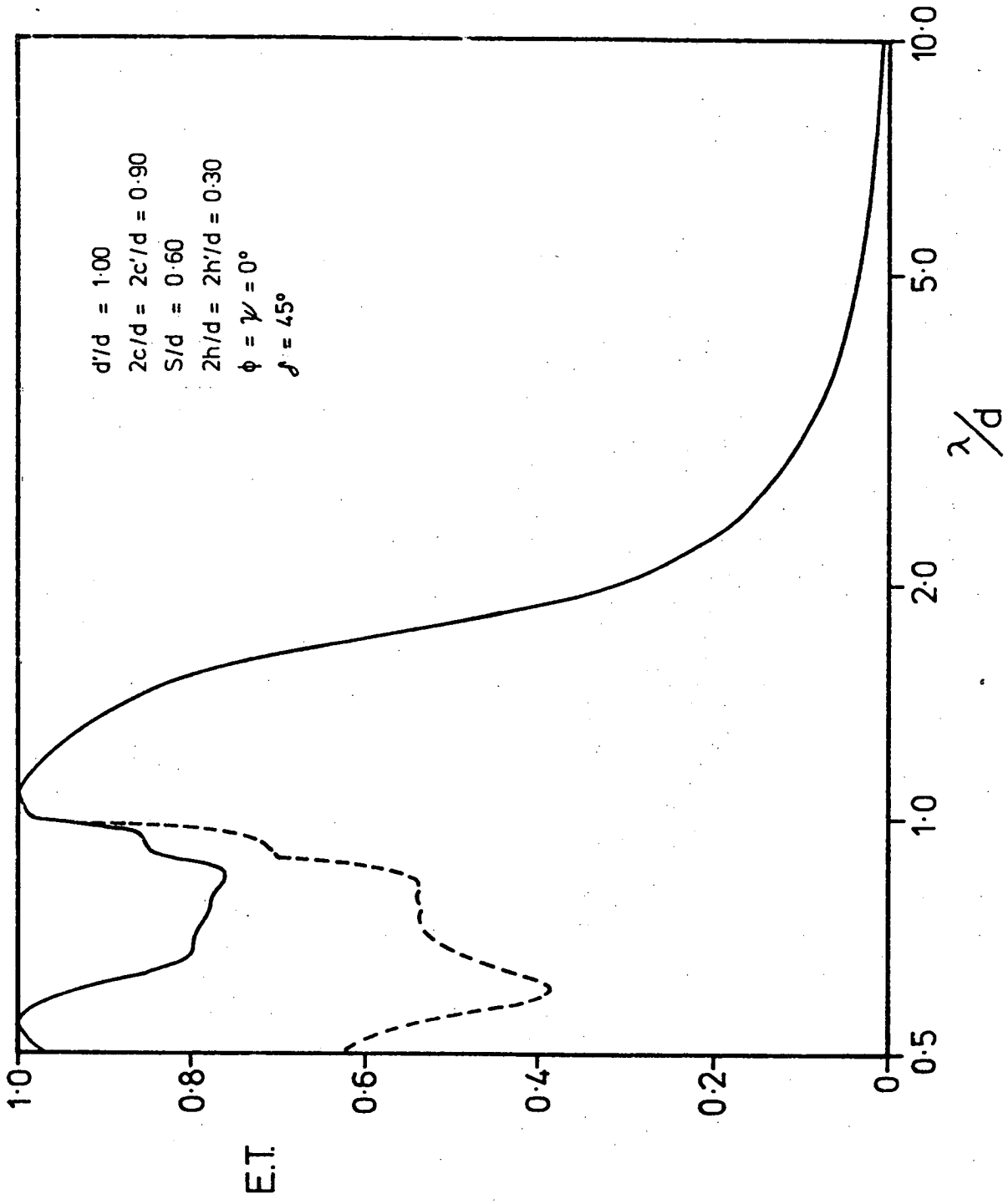

Figure 8.6 A typical spectrum of a crossed lamellar transmission grating with orthogonal axes of periodicity. The broken curve denotes the transmissivity of the (0,0) order, E.T.(0,0).

the specularly reflected and transmitted orders propagate above it.

This figure also shows that most of the energy is reflected in the long wavelength filtering region. This high reflectance is due to the fact that strong and unperturbed current flows can be set up. Either or both of the spatially separated gratings composing the structure can contribute to behaviour characteristic of a singly periodic lamellar transmission grating operated in P polarized radiation. In this configuration the electric vector is aligned with the grooves and the induced currents flow unperturbed along the length of the grooves.

It is to be noted that in all efficiency curves, the abscissae represent the normalised wavelength (λ/d). This choice is appropriate since the grating is perfectly conducting and consequently the formalism has no absolute wavelength dependence. Predictions made from the curves, therefore, will apply equally well to any wavelength range if the grating period is rescaled suitably.

8.3.2 Effect of the Grating Parameters and Incident Radiation on the Spectral Characteristics

The numerical investigations have shown that gratings, having square symmetry ($d = d'$ and $c = c'$), have a transmissivity which does not depend greatly upon the polarization of the incident radiation. This property is not analytically assured as was the case for the inductive grid discussed by McPhedran and Maystre [8.6].

Figure 8.7 confirms that the transmission properties of gratings, which do not possess square symmetry are dependent on the polarization of the incident beam. Departures from square symmetry cause detrimental effects on the transmittance of gratings operated in unpolarized radiation. All subsequent curves shown will therefore correspond to gratings having square symmetry.

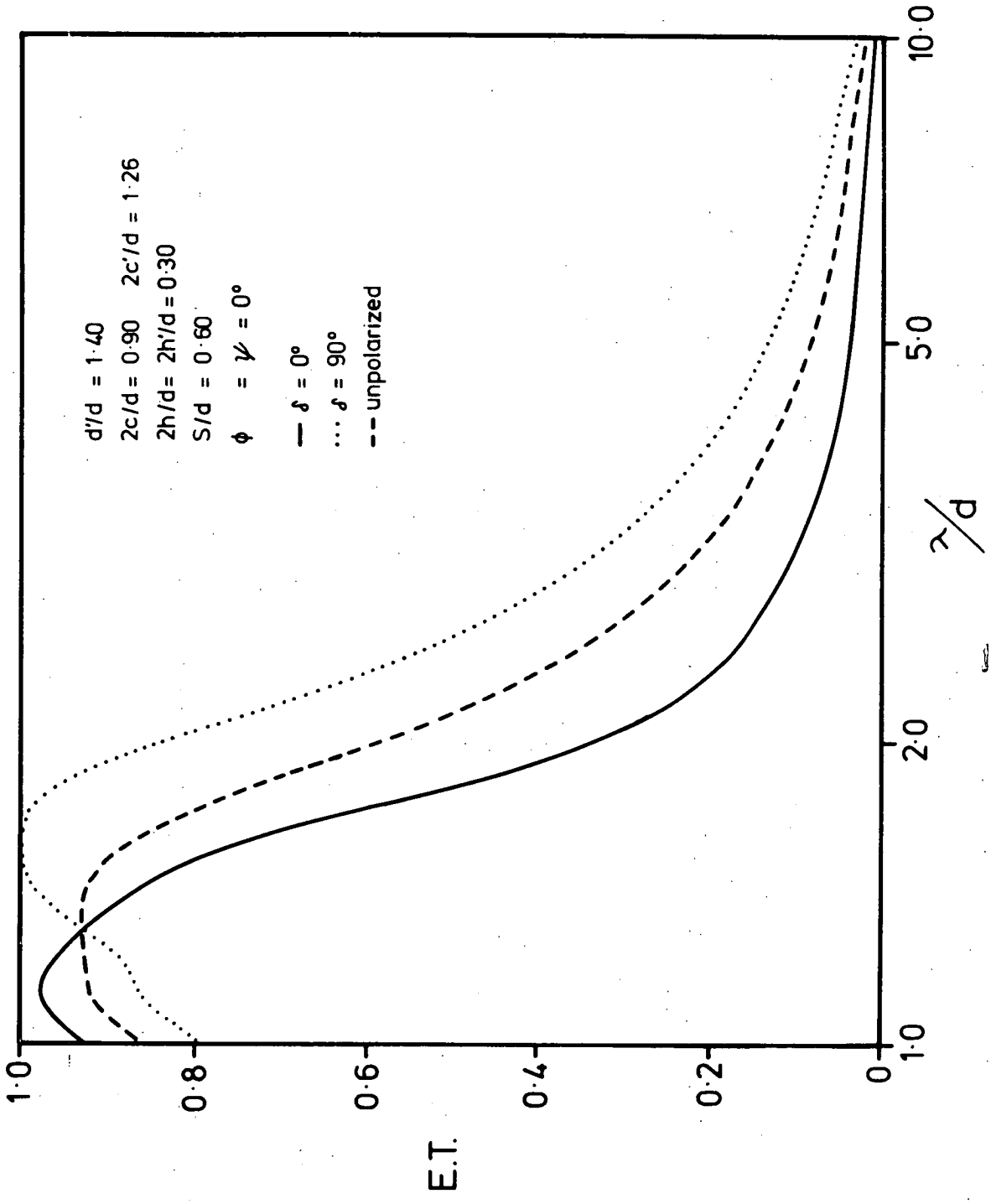

Figure 8.7 Effect of the grating symmetry on the transmission characteristics of a crossed lamellar transmission grating ($\eta = 90^{o}$).

The effects of altering the angle of incidence ϕ of the incident radiation are illustrated in figures 8.8a to 8.8f. Again the broken curves depict the transmission characteristics of the (0,0) order. The curves show that the transmissivity decreases as the angle of incidence increases. This is to be expected since, as ϕ tends to 90°, the incident wave propagates almost parallel to the grating surface and thus cannot adequately couple to the modal field to produce a significant transmitted energy component. Thus to obtain maximum transmissivity, it is imperative to operate the grating at near normal incidence (that is, $\phi < 30^{\circ}$).

An examination of the curves in figure 8.9 shows that the larger grating apertures produce greater transmissivity in the transition region. This property is also observed to hold in the transmission region.

The effect of increasing the groove thickness in the transmission curves is demonstrated in figure 8.10. This parameter can be increased to tune the long wavelength filtering tail without substantial effect on the transmission peak at shorter wavelengths. The deeper grooves produce a sharper fall-off from the transmission peak. This effect is produced by an enhanced guiding of the waves through the grooves. For example, if the groove depth is of the order of a few wavelengths, the longer wavelengths will be rejected, whereas the shorter wavelengths will only be slightly attenuated. This effect can also be explained by close examination of the formalism presented in section 8.2.2. In the limit as $h \to \infty$, the y-symmetric and y-antisymmetric modal coefficients become identical in amplitude and differ in phase by $\pi/2$, thereby reducing the total flux of energy to zero.

Some interesting properties have been observed by altering the groove separation and transmission features similar to those encountered

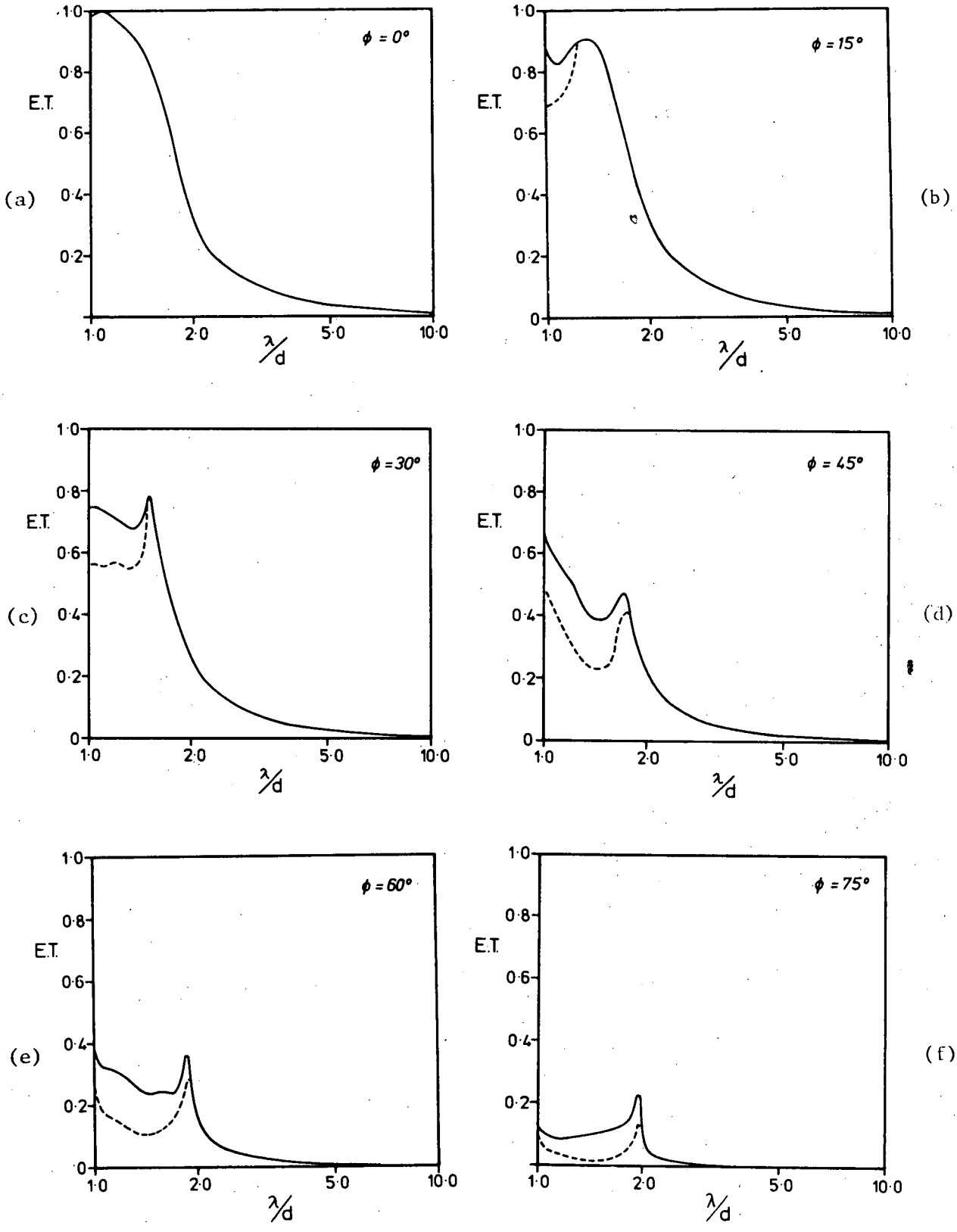

Figure 8.8 The effect of angle of incidence on transmissivity for a grating having square symmetry, $2c/d = 0.9$, $S/d = 0.6$, $2h/d = 2h'/d = 0.3$ and $\psi = 0^{o}$.

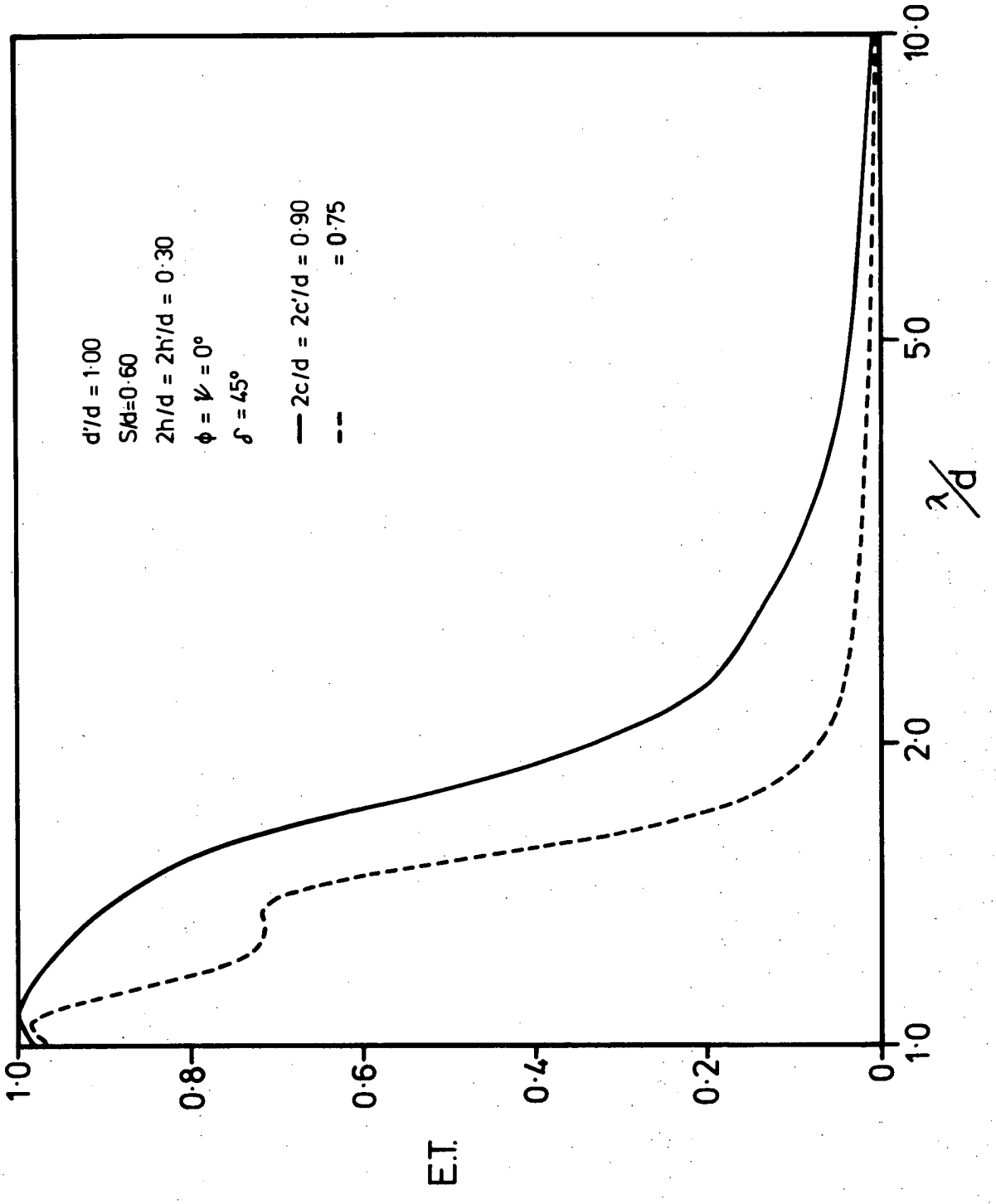

Figure 8.9 The transmissivity as a function of wavelength for different grating apertures.

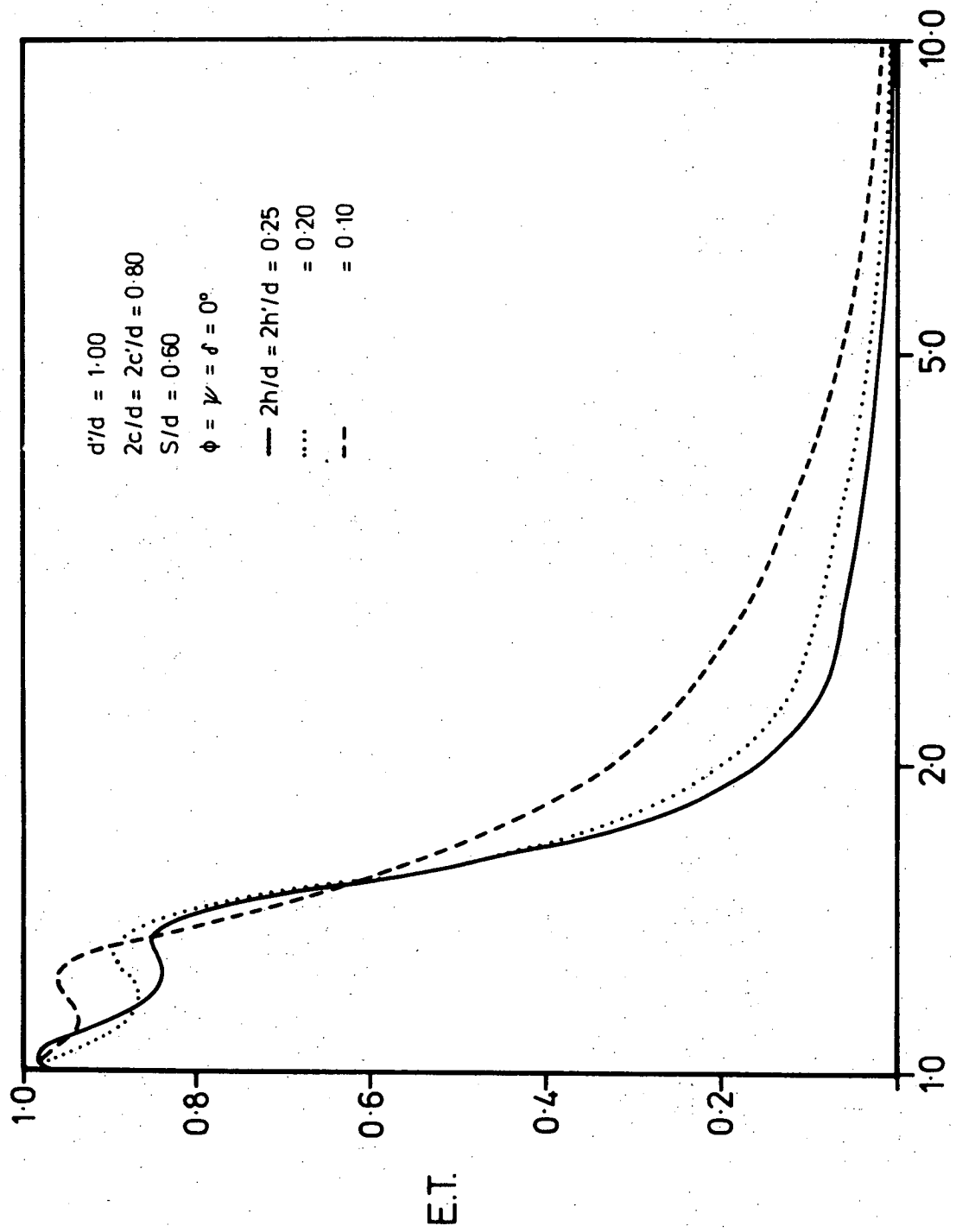

Figure 8.10 The effect of groove thickness on transmissivity.

in Fabry-Perot interferometers (see chapters 3 and 6) are demonstrated. For the classical interferometer, resonance maxima caused by constructive interference occur at wavelengths defined by

$$\lambda = 2 \times [\text{optical distance}]/n \qquad n = 1,2,3 \ldots\ldots \qquad (8.91)$$

Hence for a grating used in normally incident radiation with an array separation $S/d = 1.25$, resonance maxima in the vicinity of wavelengths of $\lambda/d = 2.5$, 1.25, etc. are expected. Figure 8.11 shows that resonances do occur in these regions. Similarly, resonances are seen occurring in the region of $\lambda/d = 1.8$ for $S/d = 0.9$ and $\lambda/d = 1.2$ for $S/d = 0.6$. The resonances are moved slightly from the predicted positions because of a phase term introduced by each grating. Normalised separations in the range 0.5 to 0.6 will produce resonances in the transition region and consequently produce enhanced transmission there. Further discussion of the effect of the array separation is given in section 8.4.

These observations are used in the following section to optimise the crossed lamellar transmission grating for its application as a solar selective surface.

8.3.3 Application to Solar Selective Systems

Figure 8.12 demonstrates that over 50% of the incident solar flux is either reflected by or absorbed within the atmosphere. It is therefore necessary to minimise any further losses within the absorbing system to maximise the efficiency. Although convection and conduction losses may be significantly reduced by thermal insulation, the third loss mechanism, radiation, is more difficult to control.

Thus it is necessary to introduce a device, in this case a solar selective surface, which ideally is totally transmitting in the solar spectrum ($0.2 < \lambda < 1.5$ μm), yet totally reflecting in the infrared.

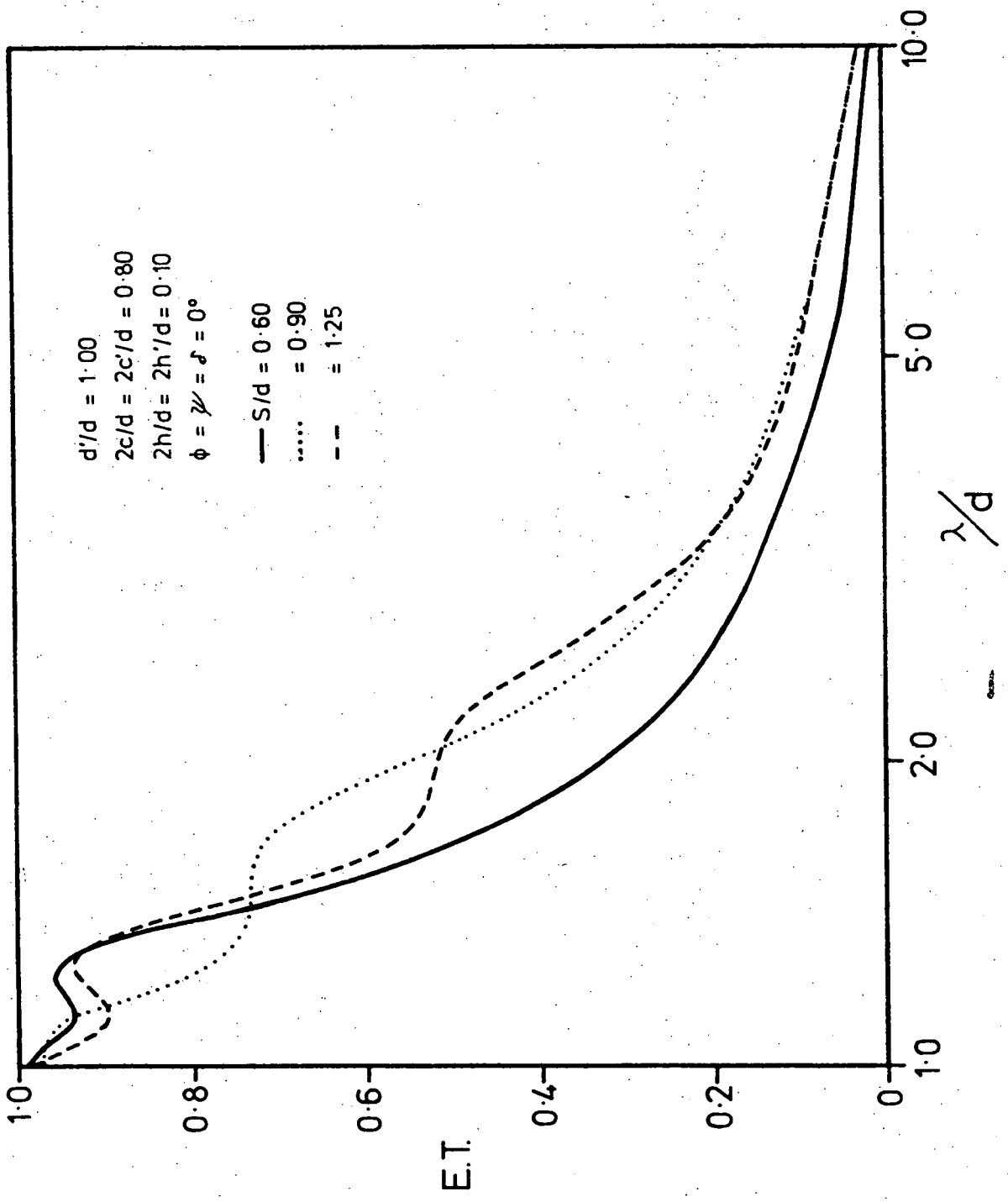

Figure 8.11 The transmission properties of a crossed lamellar transmission grating ($\eta = 90^{o}$) for several array separations.

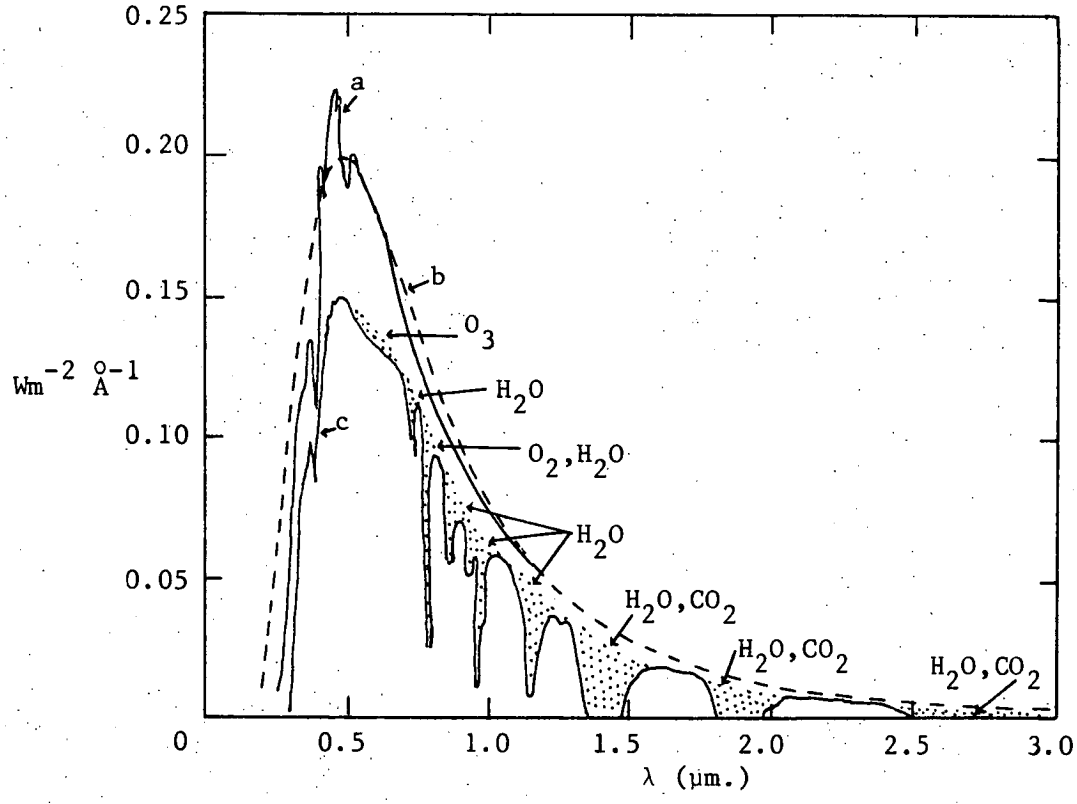

Figure 8.12 Spectral distribution curves related to the sun; shaded areas indicate absorption, at sea level, due to the atmospheric constituents shown. (Ref. [8.15]).

a. Solar irradiation curve outside atmosphere
b. Curve for black body at 5900K
c. Solar irradiation curve at sea level.

The aim of this section is to discuss the design of the crossed lamellar transmission grating to fit this ideal as closely as possible, and to determine its viability as a solar selective surface.

The system under consideration consists of a grating placed in front of a perfect black body which absorbs all the solar energy transmitted through the grating, heats up to some equilibrium temperature ($\simeq$ 700 K) and re-emits infrared radiation characteristic of this temperature, isotropically through the hemisphere of all possible directions. The grating then must inhibit the escape of this energy radiated at infrared wavelengths.

Since incident solar radiation is largely unpolarized and since large bandwidth selectivity is required, the grating should not act as a polarizer for normal incidence and hence the grating must possess square symmetry. The preceding section leads to the conclusion that optimal filtering and passband characteristics for solar selective surfaces are obtained for a grating having deep grooves ($2h/d \gtrsim 0.3$) with thin groove ($2c/d \gtrsim 0.9$) walls and a normalised separation in the vicinity of $S/d = 0.6$. Figure 8.8 shows that tracking of the sun would maximise the integrated absorptivity, since if the sun's centre lies at large angles to the grating normal, the grating will reflect the short wavelengths.

An a/e (absorptivity/emissivity) ratio was calculated for a system consisting of the grating referred to in figure 8.6 placed in front of a black body absorber which reaches an equilibrium temperature of 700 K. This was undertaken using the procedure reviewed by McPhedran and Maystre [8.16]. Table 8.4 lists the calculated absorptivity, "a(0,0)" for energy passing undeviated through the grating and "a" for all energy passing through the grating, and emittance "e" as a function

Table 8.4

d μm	Case 1 a(0,0)%	Case 1 a%	Case 2 a(0,0)%	Case 2 a%	Case 3 a(0,0)%	Case 3 a%	e%
0.5	58	64	25	32	20	26	0.6
0.6	61	71	28	35	23	30	0.8
0.7	61	75	29	38	24	32	1.0
0.8	61	78	30	40	25	34	1.2
0.9	61	79	31	41	26	35	1.5
1.0	61	81	31	42	26	36	1.8
1.5	59	84	32	44	28	38	4.6
2.0	52	86	32	45	28	39	9.2

Absorptivity and emissivity as a function of period for a grating having square symmetry, $2c/d = 0.9$, $S/d = 0.6$ and $2h/d = 2h'/d = 0.3$.

of grating period for the following three cases:

(1) a steered grating in direct illumination,

(2) an unsteered grating in direct illumination, and

(3) an unsteered grating in diffuse illumination.

This table shows that optimal solar selectivity is obtained for grating periods in the range 0.8 - 1.0 μm. Weighted absorptivities of around 80% are possible if the system is tracked to follow the sun, but in the absence of tracking or in diffuse illumination this value is approximately halved. The emissivity was derived for a perfectly conducting grating and is in the range 1 - 2%. However, this assumption is not necessarily valid for many metal coatings used in the visible and conductivity effects would probably raise this value of emittance to 3 - 4%.

8.4 NUMERICAL INVESTIGATION OF THE EVANESCENT COUPLING BETWEEN THE ARRAYS

In this section, the multiple scattering formalism described in section 8.2.3 is used to investigate numerically the extent of evanescent coupling between the individual arrays of the crossed lamellar transmission grating.

Figures 8.13a to 8.13e are spectra obtained for a square symmetric grating with normalised separations (S/d) varying from 0.1 to 4.0. The curves are limited to wavelengths longer than the grating period so that the zeroth orders are the sole propagating orders. The solid curves were obtained assuming the zeroth propagating order and five evanescent orders couple the individual gratings, whereas the broken curves were computed assuming zeroth order coupling only. Figure 8.13c should be compared with figure 8.11, which was obtained using the formalism

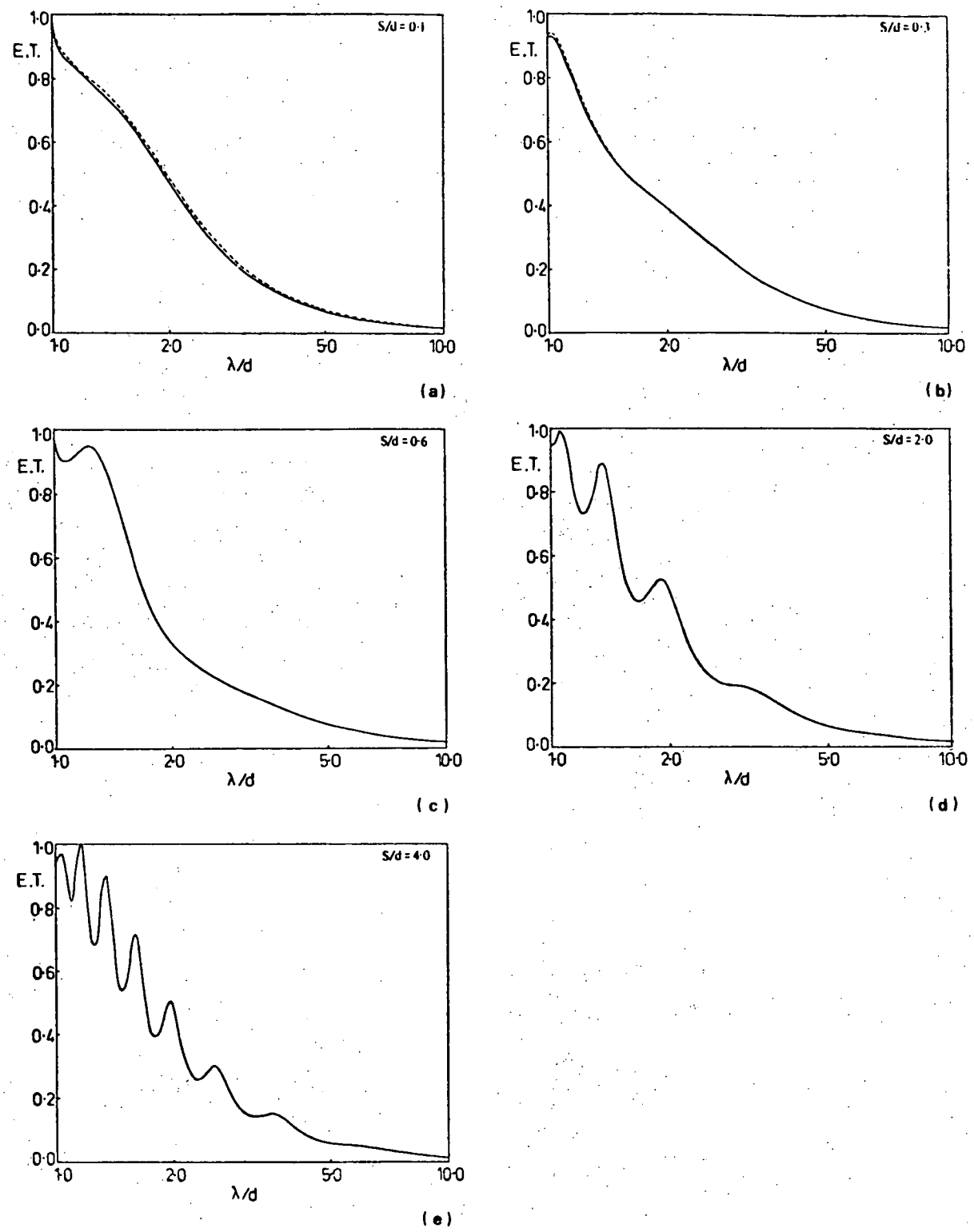

Figure 8.13 Transmission spectra for a crossed lamellar transmission grating ($\eta = 90^{o}$) specified by $d'/d = 1.0$, $2c/d = 2c'/d = 0.8$, $2h/d = 2h'/d = 0.1$, operated in normally incident radiation $\phi = \psi = \delta = 0^{o}$, for varying array separations S/d. The solid curve was obtained assuming 9 orders couple the individual arrays, whereas the broken curve corresponds to zeroth order coupling only.

described in section 8.2.2. The agreement between the two methods is excellent.

The evanescent orders which most strongly couple the arrays are considered (that is, those orders $(p,q) \in \Omega_e$ for which $|\beta_{pq}|^2$ is closest to zero). Here $\Omega_e = \{(p,q) | \mathrm{Re}(\beta_{pq}) = 0\}$. It appears empirically that the evanescent coupling by these orders becomes negligible for values of the normalised wavelength (λ/d) and separation (s/d) such that at the point halfway between the two component gratings, the evanescent field has fallen to $\frac{1}{e}$ of its value at the centre of the individual grating. That is, the values of λ and S such that

$$\exp[i\beta_{pq}(\frac{S}{2} + h)] = \exp(-1)$$

or

$$|\beta_{pq}|(\frac{S}{2} + h) = 1 \qquad (8.92)$$

For the gratings described in figure 8.13, the orders (0,-1), (-1,0), (0,1) and (1,0) should provide the strongest evanescent coupling between the gratings for normalised wavelengths $\lambda/d > 1$. For $\lambda/d < 1$, the orders are propagating and must interact between the gratings. Then using equation (8.92), it follows that these evanescent orders couple the component gratings of the structures considered in figure 8.13, as indicated below:

(1) $S/d = .1$, $h/d = .1$ - noticeable coupling for all $\lambda/d > 1$.

(2) $S/d = .3$, $h/d = .1$ - negligible coupling for $\lambda/d > 1.3$

(3) $S/d = .6$, $h/d = .1$ - negligible coupling for $\lambda/d > 1$.

These predictions are confirmed by inspection of figure 8.13.

The separations for which the components of the crossed lamellar transmission grating are no longer coupled by the evanescent orders are in accordance with those suggested for the double grating (see

chapter 3), but are much smaller than those obtained for the double grid (see chapter 6). That is, the double grid appears to be coupled much more strongly by the evanescent fields than either the crossed lamellar transmission grating or the double grating. This is a matter requiring more investigation.

Finally, figures 8.13d and 8.13e confirm the suggestion proposed in section 8.3.2, that resonance maxima occur at wavelengths in the vicinity of those specified by equation (8.91).

8.5 CONCLUSIONS

Two new formalisms describing the diffraction of a plane wave by a perfectly conducting lamellar transmission grating have been detailed. The first theory was formulated by using Rayleigh expansions to describe the fields in the three free space regions and applying the continuity conditions and the Method of Moments to match these fields to the modal expansions describing the fields in both groove regions. This necessitates the solution of eight series of matrix equations for the unknown modal coefficients. The second theory was derived using a rigorous multiple scattering technique incorporating the interaction of both propagating and evanescent orders between the two gratings.

Although the formalisms are appropriate for any wavelength range, the numerical implementation has been restricted to wavelengths greater than 0.5 due to limitations imposed by currently available computing resources. The multiple scattering formalism was shown to be the more computationally efficient, for wavelength to period ratios sufficiently large.

A new amplitude constraint for doubly periodic structures with rectangular symmetry, operated in a Littrow mount has been derived (see

appendix 8.3) and has been shown to be a valuable check on the accuracy of the numerical implementation of the crossed lamellar transmission grating formalism. This test was used in conjunction with the constraints of conservation of energy and reciprocity to confirm the validity and physical accuracy of the two methods.

The numerical simulations described in this chapter have shown that the crossed lamellar transmission grating with orthogonal axes of periodicity has potential use as a solar selective surface, capable of providing a/e ratios of the order of 30. Its performance is very similar to that of the optimised grid investigated by McPhedran and Maystre [8.6]. However, the separation parameter is an additional feature possessed by the crossed lamellar transmission grating, which may be used to optimise the transmission bandwidth for this solar energy application. It is stressed that the assumption of perfect conductivity made in this study is not necessarily valid for many metal coatings used in the visible and further investigations are necessary to include the effects of finite conductivity into the formalisms. The modal formalism presented in chapter 2 for finitely conducting lamellar gratings represents the first step towards the realisation of this aim.

REFERENCES

[8.1] HORWITZ (C.M.). - Opt. Commun., 1974, 11, 210.

[8.2] GROVES (W.E.). - J. Appl. Phys., 1953, 24, 845.

[8.3] WESSEL (W.). - Hoch. Elekt. Akust., 1939, 54, 62.

[8.4] ADONINA (A.I.), ANDRUSENKO (A.M.), KOMISSAROV (Y.S.), PAVLYUK (V.A.). - Izvestiyavuz Radiofizika, 1969, 12, 1213.

[8.5] HILL (D.A.), WAIT (J.R.). - Can. J. Phys., 1974, 52, 227.

[8.6] McPHEDRAN (R.C.), MAYSTRE (D.). - Appl. Phys., 1977, 14, 1.

[8.7] ADAMS (J.L.). - University of Tasmania, Honours Thesis, 1976.

[8.8] ADAMS (J.L.), BOTTEN (L.C.), McPHEDRAN (R.C.). - J. Optics (Paris), 1978, 9, 91.

[8.9] HARRINGTON (R.F.). - "Field Computation by Moment Methods", (London: Collier-Macmillan), 1968.

[8.10] BOTTEN (L.C.). - Opt. Acta, 1978, 25, 481.

[8.11] ULRICH (R.). - Infrared Phys., 1967, 7, 65.

[8.12] McPHEDRAN (R.C.), BOTTEN (L.C.). - University of Sydney, Report SP77/5, 1977.

[8.13] BLIEK (P.), BOTTEN (L.C.), DELEUIL (R.), McPHEDRAN (R.C.), MAYSTRE (D.). - I.E.E.E. Trans. MTT, 1980, 28, 1119.

[8.14] MAYSTRE (D.). - Thèse No. A09545, L'Université d'Aix-Marseille III, France, 1974.

[8.15] Report on the Committee on Solar Energy Research in Australia, Report No. 17, 1973.

[8.16] McPHEDRAN (R.C.), MAYSTRE (D.). - University of Sydney, Report SP76/1, 1976.

[8.17] Ed. PETIT (R.). - Topics in Current Physics, Vol. 22, "Electromagnetic Theory of Gratings", Springer-Verlag, Heidelberg, 1980.

APPENDIX 8.1 DERIVATION OF THE TE/TM MODAL BASIS FUNCTIONS

In this appendix, an orthonormal set of TE/TM modes characterising the fields within the upper groove region are derived.

In Cartesian components, it has been shown [8.8] that the x and z variations of the modal fields are given respectively by $MEXU_{mq}(x,z)$ and $MEZU_{mq}(x,z)$, which are defined by equations (8.15) and (8.16).

The following vectors are introduced to describe the transverse components of the electric and magnetic fields

$$\underline{MTEU}_{mq}(x,z) = A_{mq} MEXU_{mq} \hat{\underline{x}} + B_{mq} MEZU_{mq} \hat{\underline{z}} \tag{A1.1}$$

and

$$\underline{MTMU}_{mq}(x,z) = C_{mq} MEXU_{mq} \hat{\underline{x}} + D_{mq} MEZU_{mq} \hat{\underline{z}} \tag{A1.2}$$

(These are vector fields whose y-components are zero). The unknown coefficients are now determined.

Using Maxwell's equations, it follows that

$$\text{div } (\underline{MTEU}_{mq}) = 0 \tag{A1.3}$$

and

$$\hat{\underline{y}} . \text{curl } (\underline{MTMU}_{mq}) = 0 \tag{A1.4}$$

It can easily be shown using equations (A1.1) and (A1.3) that

$$B_{mq} = - \frac{i}{\gamma_q} \frac{m\pi}{2c} A_{mq} \tag{A1.5}$$

Similarly, using equations (A1.2) and (A1.4), it follows that

$$D_{mq} = i\gamma_q \frac{2c}{m\pi} C_{mq} \quad . \tag{A1.6}$$

In order to normalise the modes according to

$$\int_{-c}^{c} \int_{0}^{d'} \underline{MTIU}_{mq}(x,z) \cdot \overline{\underline{MTIU}}_{MQ}(x,z) \, dzdx = \delta_{mM} \delta_{qQ} \tag{A1.7}$$

where l may take the values E and M, the vector functions are written

$$\underline{MTEU}_{mq}(x,z) = g_{mq}\{i\gamma_q MEXU_{mq}(x,z)\hat{\underline{x}} + \frac{m\pi}{2c} MEZU_{mq}(x,z)\hat{\underline{z}}\} \tag{A1.8}$$

and

$$\underline{MTMU}_{mq}(x,z) = g_{mq}\{\frac{m\pi}{2c} MEXU_{mq}(x,z)\hat{\underline{x}} + i\gamma_q MEZU_{mq}(x,z)\hat{\underline{z}}\} \tag{A1.9}$$

where g_{mq} is given by equation (8.22).

It is readily seen that the vector modal fields $\underline{MTEU}_{mq}(x,z)$ and $\underline{MTMU}_{mq}(x,z)$ are orthogonal.

APPENDIX 8.2 ANALYTIC EXPRESSIONS FOR THE INNER PRODUCTS FOR THE UPPER GRATING

In order to detail expressions for the inner products, two integrals are evaluated.

$$I_1 = \int_{-c}^{c} \sin[\frac{m\pi}{2c}(x+c)]\exp(-i\alpha_p x)\, dx$$

$$= -i\,\frac{m\pi}{c}\,\frac{\sin(\alpha_p c)}{b} \qquad m \text{ even or } 0$$

$$= -\,\frac{m\pi}{c}\,\frac{\cos(\alpha_p c)}{b} \qquad m \text{ odd}$$

$$= \mp\, ic\, \exp(\mp\, i\,\frac{m\pi}{2}) \qquad \frac{m\pi}{2c} = \mp\,\alpha_p$$

where

$$b = \alpha_p^2 - (\frac{m\pi}{2c})^2$$

and $$I_2 = \int_{-c}^{c} \cos[\frac{m\pi}{2c}(x+c)]\, \exp(-i\alpha_p x)\, dx$$

$$= 2\alpha_p\,\frac{\sin(\alpha_p c)}{b} \qquad m \text{ even or } 0$$

$$= -\,2i\alpha_p\,\frac{\cos(\alpha_p c)}{b} \qquad m \text{ odd}$$

$$= \frac{2c}{\varepsilon_m} \exp(\pm i \frac{m\pi}{2}) \qquad \frac{m\pi}{2c} = \pm \alpha_p \ .$$

Then

$$J_{11}(pq;mq) = \Gamma \left[i\gamma_q{}^2 I_2 - \frac{m\pi}{2c} \alpha_p I_1 \right]$$

$$J_{12}(pq;mq) = \Gamma \left[\gamma_q \frac{m\pi}{2c} I_2 - i\gamma_q \alpha_p I_1 \right]$$

$$J_{21}(pq;mq) = \Gamma \left[i\gamma_q \alpha_p I_2 + \frac{m\pi}{2c} \gamma_q I_1 \right]$$

$$J_{22}(pq;mq) = \Gamma \left[\frac{m\pi}{2c} \alpha_p I_2 + i\gamma_q{}^2 I_1 \right]$$

where

$$\Gamma = \frac{g_{mq}}{\zeta_{pq}} \sqrt{\frac{d'}{d}}$$

and ζ_{pq}, g_{mq} are given by equations (8.14) and (8.22) respectively.

Similar evaluations may be made for the inner products appropriate to the lower grating.

APPENDIX 8.3 AN AMPLITUDE CONSTRAINT FOR THE LITTROW MOUNT

The search for this property, which applies to doubly periodic structures having rectangular axes of symmetry, operated in a Littrow configuration, was motivated by the derivation by Botten [8.10] of a constraint on the diffracted field quantities of a symmetric, singly periodic grating operated in a (-1) order Littrow mount.

In the following derivation, it is assumed that field quantities represent the physical fields, in contrast to those used in the numerical implementation, which are represented by truncated expansions. It is also assumed that the coordinate axes are symmetrically located within the grating apertures.

In the space $y \geq (s+h)$ the transverse resolutes of the electric and magnetic fields are given by

$$\underline{E}_t = \sum_{p,q} \{[E_{pq}\exp(i\beta_{pq}y) + E_i\exp(-i\beta_{00}y)\delta_{p0}\delta_{q0}]\underline{\underline{RTE}}_{pq}(x,0,z)$$

$$+ [F_{pq}\exp(i\beta_{pq}y) + F_i\exp(-i\beta_{00}y)\delta_{p0}\delta_{q0}]\underline{\underline{RTM}}_{pq}(x,0,z)\} \qquad \text{(A3.1)}$$

and

$$\hat{y} \times \underline{H}_t = -\frac{1}{Z_0}\sum_{p,q} \{\frac{\beta_{pq}}{k}[E_{pq}\exp(i\beta_{pq}y) - E_i\exp(-i\beta_{00}y)\delta_{p0}\delta_{q0}]\underline{\underline{RTE}}_{pq}(x,0,z)$$

$$+ \frac{k}{\beta_{pq}}[F_{pq}\exp(i\beta_{pq}y) - F_i\exp(-i\beta_{00}y)\delta_{p0}\delta_{q0}]\underline{\underline{RTM}}_{pq}(x,0,z)\} \qquad \text{(A3.2)}$$

If the case of an (f,g) order Littrow mount is considered, then the values of α_p and γ_q are given by

$$\left.\begin{aligned} \alpha_p &= -\alpha_{f-p} = (p - f/2)\,K \qquad \text{and} \\ \gamma_q &= -\gamma_{g-q} = (q - g/2)\,K' \qquad . \end{aligned}\right\} \qquad \text{(A3.3)}$$

By now operating the grating in a $(-f,-g)$ order Littrow mount, the corresponding transverse resolute of the electric field is

$$\underline{E}_t^{\dagger} = \sum_{p,q} \{[E_{pq}^{\dagger}\exp(i\beta_{pq}^{\dagger}y) + E_i^{\dagger}\exp(-i\beta_{00}^{\dagger}y)\delta_{p0}\delta_{q0}]\underline{\underline{RTE}}_{pq}^{\dagger}(x,0,z)$$

$$+ [F_{pq}^{\dagger}\exp(i\beta_{pq}^{\dagger}y) + F_i^{\dagger}\exp(-i\beta_{00}^{\dagger}y)\delta_{p0}\delta_{q0}]\underline{\underline{RTM}}_{pq}^{\dagger}(x,0,z)\} \qquad \text{(A3.4)}$$

where

$\alpha_p^{\dagger} = (p + f/2)\,K = -\alpha_{-p}$ and

$\gamma_q^{\dagger} = (q + g/2)\,K' = -\gamma_{-q}$

and $\underline{\underline{RTE}}_{pq}^{\dagger}$ and $\underline{\underline{RTM}}_{pq}^{\dagger}$ are given by equations (8.10) and (8.11) respectively, but α_p, β_{pq} and γ_q are replaced by $\alpha_p^{\dagger}$, $\beta_{pq}^{\dagger}$ and $\gamma_q^{\dagger}$ respectively.

The symmetry of the optical arrangement implies that $E^{\dagger}_{pq} = E_{-p-q}$ and $F^{\dagger}_{pq} = F_{-p-q}$ and thus equation (A3.4) becomes

$$\underline{E}^{\dagger}_t = \sum_{p,q} \{[E_{f-p,g-q}\exp(i\beta_{f-p,g-q}y) + E_i\exp(-i\beta_{00}y)\delta_{pf}\delta_{qg}]\underline{RTE}_{pq}(x,0,z) + [F_{f-p,g-q}\exp(i\beta_{f-p,g-q}y) + F_i\exp(-i\beta_{00}y)\delta_{pf}\delta_{qg}]\underline{RTM}_{pq}(x,0,z)\} \tag{A3.5}$$

A similar relation is derived for the transverse resolute $(\hat{y} \times \underline{H}_t)^{\dagger}$ of this field.

If these two fields are superposed, the total electric and magnetic field quantities, given by $\underline{E}^T_t$ and $(\hat{y} \times \underline{H}_t)^T$, can be written

$$\underline{E}^T_t = \underline{E}_t + \underline{E}^{\dagger}_t$$

and $$(\hat{y} \times \underline{H}_t)^T = (\hat{y} \times \underline{H}_t) + (\hat{y} \times \underline{H}_t)^{\dagger} .$$

The total flux of energy through the surface T, defined in figure 8.14 is given by

$$\iint_T S_y \, dzdx = -\tfrac{1}{2}\mathrm{Re}\left\{ \iint_T \underline{E}^T_t \cdot \overline{(\hat{y} \times \underline{H}_t)^T} \, dzdx \right.$$

$$= T_1 + T_2 . \tag{A3.6}$$

where $$T_1 = \frac{1}{2Z_0}\mathrm{Re}\left\{ \sum_{p,q} \{[E_{pq}\exp(i\beta_{pq}y) + E_i\exp(-i\beta_{00}y)\delta_{p0}\delta_{q0} + E_{PQ}\exp(i\beta_{PQ}y) + E_i\exp(-i\beta_{00}y)\delta_{pf}\delta_{qg}] \times \left[\frac{\overline{\beta}_{pq}}{k}\overline{E}_{pq}\exp(-i\overline{\beta}_{pq}y) - \frac{\beta_{00}}{k}E_i\exp(i\beta_{00}y)\delta_{p0}\delta_{q0} + \frac{\overline{\beta}_{PQ}}{k}\overline{E}_{PQ}\exp(-i\overline{\beta}_{PQ}y) - \frac{\beta_{00}}{k}E_i\exp(i\beta_{00}y)\delta_{pf}\delta_{qg}\right]\}\right\}$$

and T_2 is given by exactly the same expression, but throughout E is

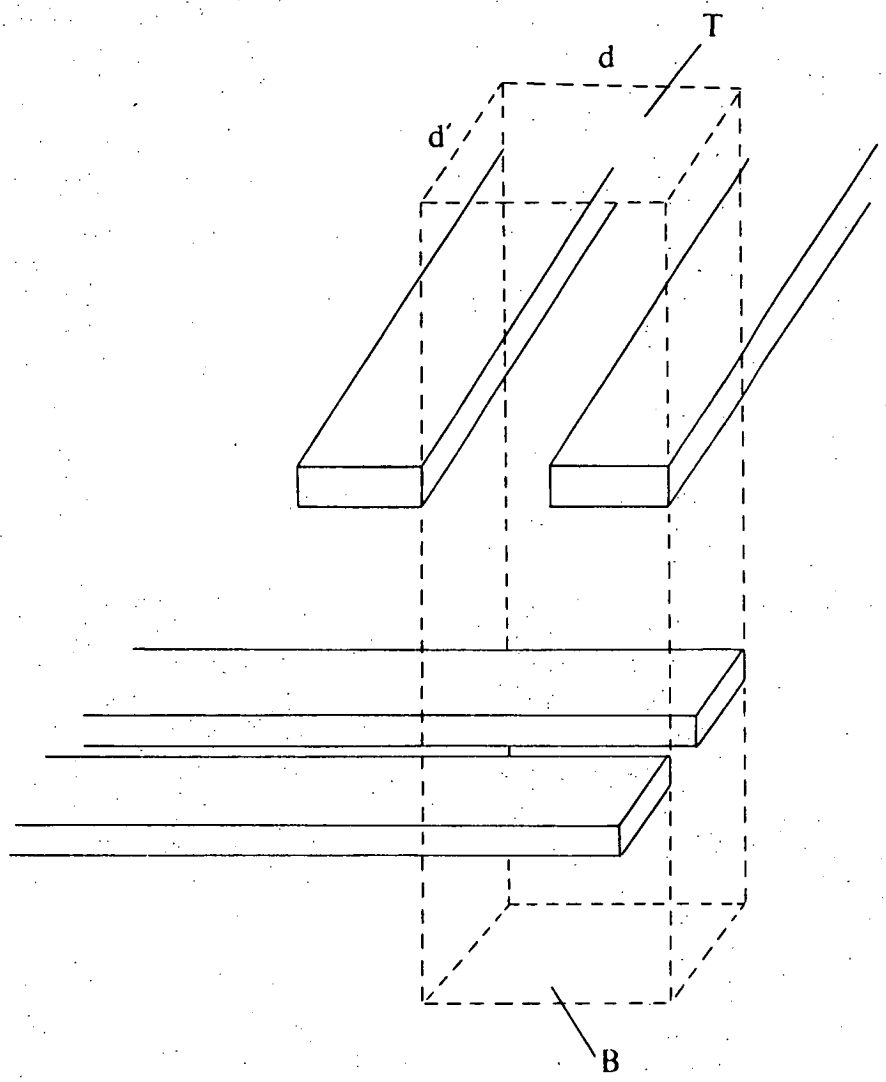

Figure 8.14 The surfaces of integration used in the derivation of the amplitude constraint for the Littrow mount.

replaced by F and $\frac{\beta_{pq}}{k}$ by $\frac{k}{\beta_{pq}}$. Here the definitions $P = f-p$, $Q = g-q$ have been made.

The expression for T_1 can be expanded to the form

$$T_1 = \frac{1}{2Z_0} \mathrm{Re} \{ \sum_{p,q} [\frac{\overline{\beta}_{pq}}{k}|E_{pq}|^2 \exp(-2\mathrm{Im}(\beta_{pq})y) + \frac{\overline{\beta}_{pq}}{k}|E_{PQ}|^2 \exp(-2\mathrm{Im}(\beta_{pq})y)$$

$$+ 2\frac{\overline{\beta}_{pq}}{k} \mathrm{Re}(E_{pq}\overline{E}_{PQ}) \exp(-2\mathrm{Im}(\beta_{pq})y)$$

$$- 4i \frac{\beta_{00}}{k} E_i \mathrm{Im}(E_{00}\exp(2i\beta_{00}y)) - 4i \frac{\beta_{00}}{k} E_i \mathrm{Im}(E_{fg}\exp(2i\beta_{00}y))$$

$$- 2E_i^2 \frac{\beta_{00}}{k}] \} \quad .$$

So T_1 reduces to

$$T_1 = \sum_{p,q\in\Omega_r} [\frac{\beta_{pq}}{k}(|E_{pq}|^2 + |E_{PQ}|^2 - 2E_i^2\delta_{p0}\delta_{q0} + 2\mathrm{Re}(E_{pq}\overline{E}_{PQ}))]$$

where $\Omega_r = \{(p,q) \mid \mathrm{Im}(\beta_{pq}) = 0\}$.

Similarly,

$$T_2 = \sum_{p,q\in\Omega_r} [\frac{k}{\beta_{pq}}(|F_{pq}|^2 + |F_{PQ}|^2 - 2F_i^2\delta_{p0}\delta_{q0} + 2\mathrm{Re}(F_{pq}\overline{F}_{PQ}))] \quad .$$

A similar result can be derived for the total flux of energy through the surface B shown in figure 8.14. Since $\iint_T S_y \, dzdx = \iint_B S_y \, dzdx$ physically within the formalism and since conservation of energy imposes the constraint

$$\sum_{p,q\in\Omega_r} \{\frac{\beta_{pq}}{k} [|E_{pq}|^2 + |E_{PQ}|^2 + |\hat{E}_{pq}|^2 + |\hat{E}_{PQ}|^2 - 2E_i^2\delta_{p0}\delta_{q0}]$$

$$+ \frac{k}{\beta_{pq}} [|F_{pq}|^2 + |F_{PQ}|^2 + |\hat{F}_{pq}|^2 + |\hat{F}_{PQ}|^2 - 2F_i^2\delta_{p0}\delta_{q0}]\} \quad ,$$

the following relation can be derived

$$\sum_{p,q\in\Omega_r} \left[\frac{\beta_{pq}}{k} \mathrm{Re}(E_{pq}\overline{E}_{f-p,g-q} + \hat{E}_{pq}\overline{\hat{E}}_{f-p,g-q}) + \frac{k}{\beta_{pq}} \mathrm{Re}(F_{pq}\overline{F}_{f-p,g-q} + \hat{F}_{pq}\overline{\hat{F}}_{f-p,g-q})\right] = 0 \qquad \text{(A3.7)}$$

This relation, the Littrow expression, for a general Littrow mount is the two dimensional analogue of the expression derived for lossless, singly periodic transmission gratings [8.10]. The Littrow expression is in general not precisely satisfied by the computed field amplitudes and thus it can be used as a convergence check for the algorithm. However, if the truncated set of Rayleigh orders is chosen in the following field symmetrical fashion:

$$\Omega_1 = \{(p,q) \mid \begin{array}{lll} f - n \le p \le n & \text{if} & f \le 0; \\ -n \le p \le f + n & & f > 0; \\ g - m \le q \le m & & g \le 0; \\ -m \le q \le g + m & & g > 0\} \end{array}$$

where n and m are arbitrary positive integers, then the constraint is analytically satisfied, as demonstrated in [8.8].